Investigation on long-term safety aspects of a radioactive waste repository in a diagenetic clay formation

– Final Report –

GRS BGR DBETEC

PROJ	PSP	OBJ	FUNK	KOMP	BAUG	AG	UA	LFNR	RV
FE						BE	BY	0008	00

DOKID: 11780526
ULV-Nr.: 659482

Investigation on long-term safety aspects of a radioactive waste repository in a diagenetic clay formation

– Final Report –

Authors:

[1]Jobmann, M.
[2]Flügge, J.
[1]Gazul, R.
[3]Hammer, J.
[1]Herold, P.
[1]Krone, J.
[1]Kuate Simo, E.
[3]Kühnlenz, T.
[2]Laggiard, E.
[1]Lommerzheim, A.
[2]Meleshyn, A.
[1]Müller, C.
[2]Rübel, A.
[2]Wolf, J.
[2]Zhao, H.

[1]DBE TECHNOLOGY GmbH, Eschenstraße 55, D-31224 Peine.
[2]Gesellschaft für Anlagen- und Reaktorsicherheit (GRS) gGmbH, Theodor-Heuss-Straße 4, D-38122 Braunschweig.
[3]Bundesanstalt für Geowissenschaften und Rohstoffe (BGR), Stilleweg 2, D-30655 Hannover.

This report was produced during the R&D project: **SANTOS**
(Sicherheitsanalytische Untersuchungen für ein Endlager für radioaktive Abfälle in einer diagenetisch überprägten Tonformation in der Nachbetriebsphase)

Auftraggeber: KIT FKZ: 02E11182A/B

Berichtsnummer: TEC-32-2016-AB

Stand 28.03.2017

The research work that is the basis of this report was funded by the German Federal Ministry for Economic Affairs and Energy (BMWi = Bundesministerium für Wirtschaft und Energie)) represented by the Project Management Agency Karlsruhe (Karlsruhe Institute of Technology, KIT) under the contract numbers FKZ 02E11182 B (DBETEC) and 02E11182 A (GRS). The authors alone, however, are responsible for the contents of this study.

Table of Contents

Acknowledgements

The authors would like to thank our Russian partners for supporting our studies and the constructive discussions about the investigated issues. In particular we would like to thank the Russian national operator FGUP NO.RAO, the team from the St. Petersburg branch of the IGE RAN in person of Prof. V. Rumynin and Dr. A. Nikulenkov, the colleagues of the former FGUP LI VNIPIET (now: Atomprojekt), FGUP RADON and the Radium Institute V.G. Khlopin.

Abbreviations and acronyms

AEA Technology	Atomic Energy Authority, UK
ANDRA	Agence nationale pour la gestion des déchets radioactifs (French National Radioactive Waste Management Agency)
ANSICHT	Methodik und Anwendungsbezug eines Sicherheits- und Nachweiskonzeptes für ein HAW-Endlager im Tonstein (Methodology and application of a safety and demonstration concept for a HLW-repository in claystone)
BGR	Bundesanstalt für Geowissenschaften und Rohstoffe (Federal Institute for Geosciences and Natural Resources)
BMUB	Bundesministerium für Umwelt, Naturschutz, Bau und Reaktorsicherheit (Federal Ministry for the Environment, Nature Conservation, Building and Nuclear Safety)
DBE	Deutsche Gesellschaft zum Bau und Betrieb von Endlagern für Abfallstoffe
DOMPLU	Dome Plug Experiment
DOPAS	Full-scale Demonstration of Plugs and Seals
EBS	Engineered Barrier System
EDZ	Excavation damaged zone
ELSA	Schachtverschlüsse für Endlager für hochradioaktive Abfälle (Shaft seals for repositories for high level radioactive waste)
ESDRED	Engineering Studies and Demonstration of Repository Designs
ESP	Enhanced Sealing Project
FEP	Features, Events and Processes
HLW	High level waste
IAEA	International Atomic Energy Agency
ISIBEL	Überprüfung und Bewertung des Instrumentariums für eine sicherheitliche Bewertung von Endlagern für hoch radioaktive Abfälle (Review and Appraisal of the Tools available for a Safety Assessment of Final Repositories for HLW)
IVO PE LTD	Imatran Voima Oy Power Engineering Limited
JRC	Joint Roughness Coefficient
LILW	Low and Intermediate level Waste
LNPP	Leningrad Nuclear Power Plant
LSK	Leningrad Special Plant
NDA	Nuclear Decommissioning Authority
POPLU	Deposition Tunnel End Plug Experiment
RBMK	Реактор Большой Мощности Канальный (High Power Channel-Type Reactor)
RESEAL	A large-scale in-situ demonstration test for repository sealing in an argillaceous host rock
R&D	Research and Development
RDTI	Research and Development Technological Institute
SANTOS	Sicherheitsanalytische Untersuchungen für ein Endlager für radioaktive Abfälle in einer diagenetisch überprägten Tonformation in der Nachbetriebsphase (Investigation on long-term safety aspects of a radioactive waste repository in a diagenetic clay formation)
SGN	Société Générale pour les Techniques Nouvelles (engineering subsidiary of the COGEMA Group, France)
SKB	Swedish Nuclear Fuel and Waste Management Company
SL	Short-lived
TACIS	Technical Assistance to the Commonwealth of Independent States
TSX	Tunnel Sealing Experiment
TUBAF	Technische Universität Bergakademie Freiberg
URL	Underground Research Laboratory
VNIPIET	All-Russian Research and Design Institute for Energy Technology
VSG	Vorläufige Sicherheitsanalyse für den Standort Gorleben (Preliminary Safety Analysis of the Gorleben site)

1 Introduction

In the past, German research and development (R&D) activities regarding the disposal of radioactive waste, including spent nuclear fuel, focused mainly on domal rock salt because since the 1950ths rock salt was the preferred host rock formation. In addition, generic R&D work regarding alternative host rocks (crystalline rocks and claystones) had been performed as well for a long time but with lower intensity.

Around the year 2000, in context with the first exploration moratorium on the Gorleben site, the Federal Government decided to have argillaceous rocks and crystalline rocks investigated in more detail. As Germany does not have neither any underground research and host rock characterization facilities nor sufficiently detailed investigated crystalline or claystone formations, international cooperation received a high priority in the German R&D programme for high-level waste (HLW) disposal in order to increase the knowledge regarding alternative host rocks. Major cornerstones of the cooperation are joint projects and experiments conducted especially in underground research laboratories (URL) in crystalline rocks at the Grimsel Test Site (Switzerland) and the Hard Rock Laboratory (HRL) Äspö (Sweden) and in argillaceous rocks at the URL Mont Terri (Switzerland) and Bure (France).

In 2001, the topic of radioactive waste disposal was integrated into the agreement between the former Russian Ministry of Atomic Energy (Minatom, now Rosatom) and the German Ministry of Labour (BMWA), now Ministry of Economic Affairs and Energy (BMWi), on cooperation regarding R&D on the peaceful utilization of nuclear power (agreement on “Wissenschaftlich-Technische Zusammenarbeit” WTZ). The intention was to have a new and interesting opportunity for international R&D cooperation regarding HLW disposal in alternative host rocks and the unique possibility to perform site-specific work, to test the safety demonstration tools available, and to expand the knowledge to all aspects specific to these host rocks. Another motivation for joining this cooperation was the intent to assist Russian engineers and scientists in their integration into the international scientific community concerned with radioactive waste disposal and to share advanced safety approaches.

Based on the WTZ agreement, a comprehensive and versatile cooperation has been implemented in the past 13 years. Joint R&D activities regarding radioactive waste disposal in claystones based on site investigation activities in the Leningrad region were agreed as permanent part of this cooperation in 2011. The Russian side has been represented by the FGPU "National Operator for Radioactive Waste Disposal" (NO.RAO), All-Russian Research and Design Institute for Energy Technology (VNIPIET), the St. Petersburg Branch of the Institute for Geoecology of the Russian Academy of Science and the Khlopin Radium Institute, while three major R&D organizations, the Federal Institute for Geosciences and Natural Resources (BGR) in Hanover, Gesellschaft für Anlagen- und Reaktorsicherheit (GRS) gGmbH in Brunswick, and DBE TECHNOLOGY GmbH (DBETEC) in Peine have been the permanent participants from the German side.

The corresponding joint R&D activities were pooled in the BMWi-funded R&D project "Investigation on long-term safety aspects of a radioactive waste repository in a diagenetic clay formation" (Sicherheitsanalytische Untersuchungen für ein Endlager für radioaktive Abfälle in einer diagenetisch überprägten Tonformation in der Nachbetriebsphase – SANTOS)

The disposal of low and intermediate level waste (LILW) in near surface repositories is an internationally accepted best practice that provides long-term safe containment and isolation of radioactive waste. Accordingly, and taking into consideration that the Leningrad region hosts a large number of facilities and research institutes that generate radioactive waste as well as radioactive waste storage facilities such as for example the Leningrad Nuclear Power Plant (LNPP) and the Leningrad Special Plant (LSK) Radon, during the last years site investigations have been carried out to assess the suitability of two potential near surface

repository sites (see chapter 2), where the LILW generated in the Leningrad region (see chapter 5.1) can be safely disposed of. Furthermore a conceptual design for the potential near surface repository (see chapter 5.2) has also been developed.

In general, the long-term containment of the radioactive waste inside repositories located in clay formations is primarily ensured by the host rocks. In addition to the suitability of the selected repository site a sealing concept consisting of a multi-barrier system that protects the biosphere from the potential harmful effects caused by the radioactive waste shall be properly designed (see chapter 6.2). To minimize the potential risks associated with the presence of the radioactive waste, the design of these barriers shall take into consideration the principles of redundancy and diversity as well as the immediate and long-term performance of the barriers over the time, which may significantly vary depending on the materials and concepts proposed.

The acceptable level of safety of the barriers and therefore of the repository as a whole, is demonstrated by the results of the safety assessment, in which the reliability and performance of the individual barriers is comprehensively assessed. In order to demonstrate the integrity of barriers, the potential impacts that may affect the performance of each sealing element shall be considered (see chapter 6.3). The starting point to identify the potential impacts on the sealing elements is the development of a specific Features, Events and Processes (FEP)-Catalogue for the repository, which provides an overview of all relevant processes that shall be considered, and allows quantifying their associated impacts.

The present report, which has been prepared in the framework of the above mentioned project SANTOS, describes the conceptual approach of a complete sealing system for a near surface repository concept located at the “Radon Site”. The developed sealing concept consists of disposal drift seals, access drift seals, shaft seals and a ramp seal. Furthermore, it presents the methodology that is used in Germany in order to demonstrate the integrity of sealing elements in repositories and it provides an exemplary demonstration of the integrity of the proposed ramp sealing element (see chapters 6.3.5 and 6.3.6). Finally, it presents and applies the modelling framework existing in Germany to simulate the radionuclide release from the repository to the biosphere using deterministic and probabilistic methods.

2 Geological situation

The area of investigation lies around 70 km NE of Saint Petersburg. As part of the Leningrad region, the area is located in terms of its regional geology in the zone where the Russian Plate (as part of the East European Platform) collided with the Baltic Shield (Figure 2-1). The collision of these geotectonic units had a considerable influence on the geological development of the region. The tectonic movements associated with the collision caused the crystalline basement of the Russian Plate to be broken up into blocks which have been subject to vertical movements since Precambrian times. Troughs or synclines developed as a result of the tectonic dislocations of the individual blocks.

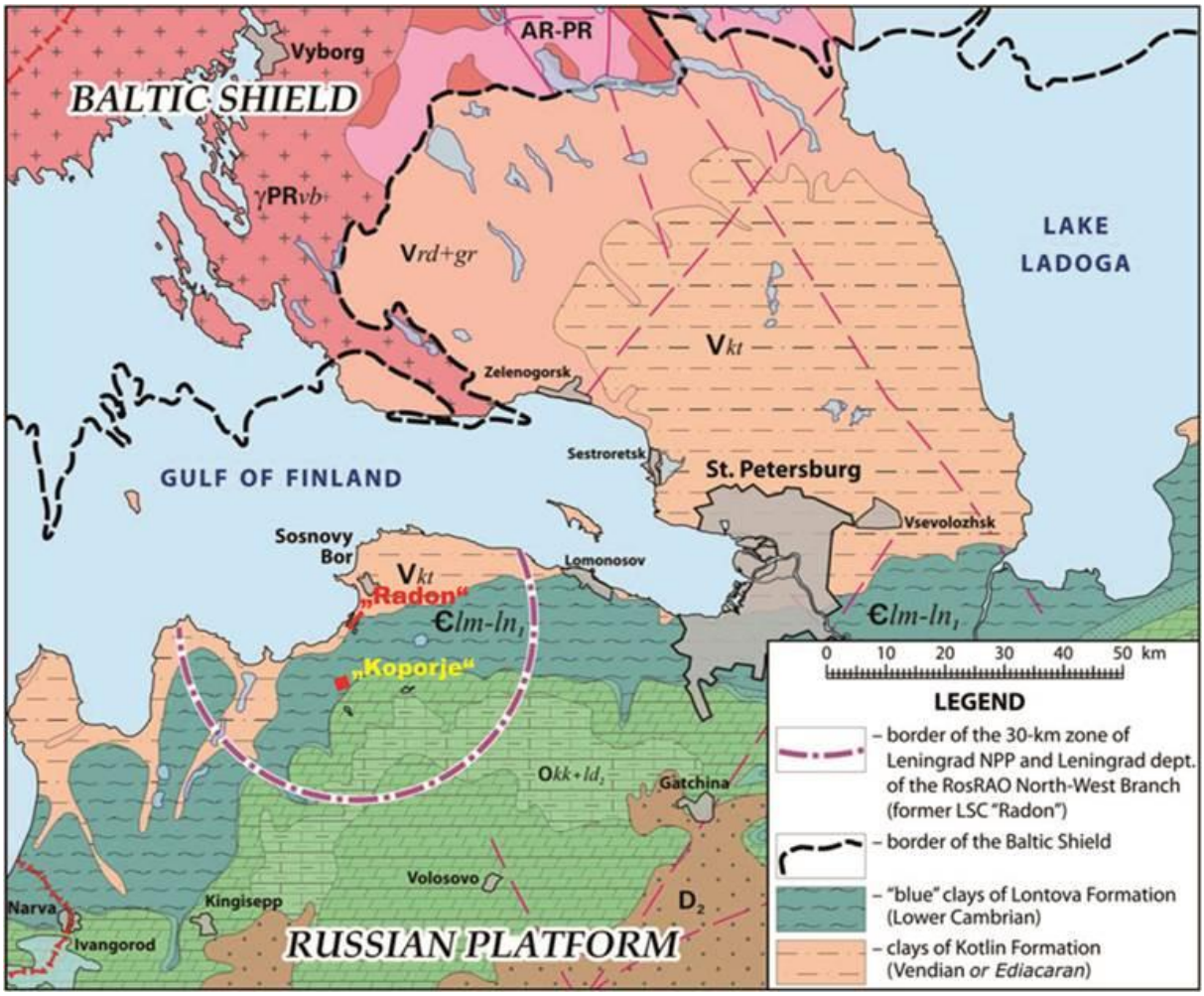

Figure 2-1: Geological map of the Leningrad region showing the distribution of the Vendian and Cambrian clay formations worthy of investigation on the southern coast of the Gulf of Finland (from: Anderson et al. 2011).

Comprehensive geological exploration has been undertaken in this region in the last approximately 25 years by various organisations on behalf of different clients or ministries (e.g. the "Atomenergoproject", or the "Energoizyskaniy" institute, or by "Neftegazgeodesiya"). The most important phases of the investigation of this site are as follows:

- 1988 - 1990: Project of the Radium Institute and Nevskgeologiya
- 1993/1994: VNIPIET and other organisations (inter alia Nevskgeologiya)
- 1997: TACIS project with VNIPIET, IVO PE LTD (Finland), SGN (France), AEA Technology (UK), and Lenmetrogiprotrans
- 2007/2008: Rumynin project team (for Radon).

On the basis of the investigations carried out in the past, and preliminary safety assessments, two clay formations have been identified in the Leningrad region as potential candidates for the final disposal of radioactive waste: the Vendian (approx. 560 million years old) Upper Kotlin Clays, and the Lower Cambrian (approx. 530 million years old) Blue Clays. The work to select a location for the repository concentrated on the area to the south of Sosnovyi Bor (Figure 2-2).

Figure 2-2: Areas in which geological exploration has been carried out since the 1980s (Consortium DBE/ANDRA/NDA/SKB 2008; from: Rumynin 2011).

The northern part of the area of investigation which has been looked at since the 1980s is characterised by surface outcrops of Lower Cambrian clays, whilst the southern part is in the area of surface outcrops of Ordovician limestone of the Ischorsk Plateau (Anderson et al. 2006). The Blue Clays were evaluated on the basis of exploration data obtained for an area in the vicinity of Koporje (Figure 2-2) (Daschko 2006, Anderson et al. 2006). This area is around 10 km south of the Gulf of Finland and located 12 - 19 km from the city Sosnovyi Bor. The Blue Clays in the Koporje area have a maximum thickness of 116 m (Daschko 2006). The area of investigation of the Vendian clays is also located on the southern coast of the Gulf of Finland and consists of a strip outcropping at the surface between the Gulf of Finland and the Cambrian formation (Figure 2-3).

The lower part of the sedimentary succession above the crystalline basement in the area of investigation is formed by the Vendian Kotlin Horizon (Figure 2-4), whose argillaceous sequence is considered to be a favourable target horizon for the construction of a repository for

low and intermediate level radioactive waste (Anderson et al. 2006, Rumynin 2011). The sediments of the Kotlin Horizon are the oldest rocks above the crystalline fundament of the Russian Platform and consist of the sandy sediments of the Gdovsk Horizon, and the Upper Vendian Kotlin Clays. The Kotlin Clays outcrop at the surface on the southern coast of the Gulf of Finland. They dip to the south-east below the Lower Cambrian Blue Clays. Further to the south-east, these rocks are covered by Upper Devonian rocks. The depth of the Kotlin Horizon increases from north to south: from 40 m - 70 m (Baltic Shield) down to 1200 m - 1400 m (Moscow Syncline). The thickness of the Vendian clays varies from 80 m to 170 m in the south-east (Pereverzeva et al. 2008).

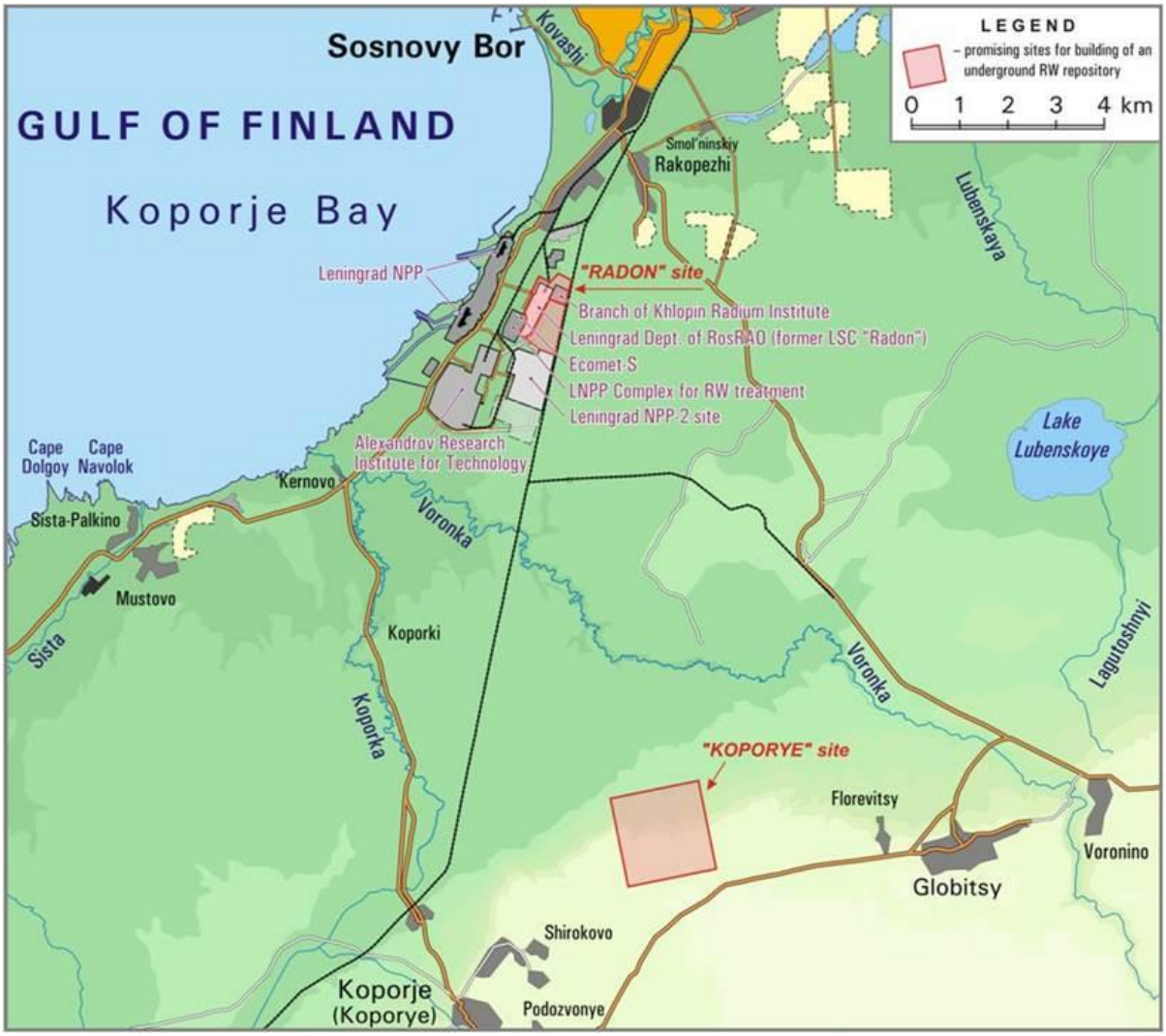

Figure 2-3: Location of the "Koporje" and LSK "Radon" sites of investigation (Anderson et al. 2011).

The Lower Kotlin Horizon is widespread, consists of sandstones and forms an aquifer. The Upper Kotlin Horizon consists of clays/argillites and lies at depths between 5 m and 120 m in the Leningrad region. The thickness varies between 12 m and 120 m. The marine transgression in the Cambrian covered the Vendian Kotlin Horizon south-east of the Gulf of Finland with Cambrian sediments (Anderson et al. 2006). The lower part of the Cambrian system is called the Lomonosov Horizon, and consists of coarse grained terrigenous rocks comprising sands and poorly-cemented sandstones. The Lomonosov Horizon is an aquifer. Its thickness is around 1.5 m to 40 m.

The Cambrian sequence of the Lontov Clays outcrops south-east of the Lomonosov Horizon. The thickness of this horizon varies between 2 m to 200 m and is 100 m - 200 m thick in the

south-western part of the Leningrad region. Because of the high concentration of glauconite, these clays have a green to blue-grey colour. This formation is called the "Blue Clay" because of its colour, and is also being looked at as potential host rocks for the construction of a repository.

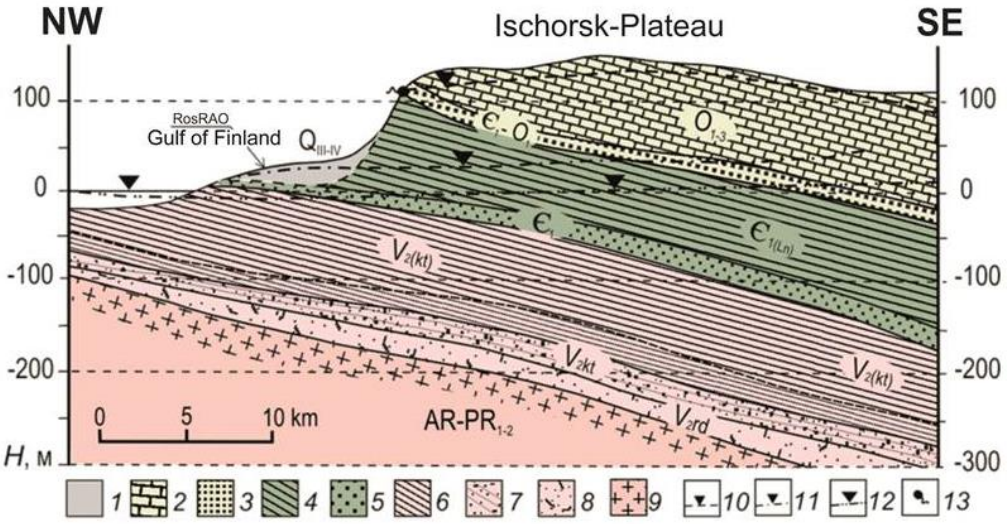

Figure 2-4: Schematic hydrogeological profile along the Sosnovyi Bor - Volosovo line (see Fig. 2-2) in the Leningrad region (from: Anderson et al. 2006).

1 - aquifer in Quaternary sediments, 2 - aquifer in Ordovician sediments, 3 - aquifer in Cambrian sediments, 4 - Lontovsk Series of Lower Cambrian rocks (impermeable layer), 5 - Lontovsk aquifer (*Lomonosov aquifer. Cambrian sand*), 6 - Upper Vendian Kotlin Horizon (impermeable layer), 7 - 9 Upper Vendian sediments Vkt_1: 7 - impermeable layer in the Kotlin aquifer complex, 8 - Lower Kotlin aquifer (Gdovsk Horizon), 9 - Strelna aquifer, 10 - groundwater level of Archaic-Proterozoic aquifer, 11 - groundwater level of the Ordovician aquifer, 12 - groundwater level of the Lomonosov aquifer, 13 - springs

The Cambrian rocks end with the slightly consolidated argillaceous sandstones of the Lukatisk and Tiskretsk Horizons with a thickness between 5 m and 15 m. Together with the sands of the Tosno Series, they form the Cambrian-Ordovician aquifer which is present over the whole of the Ischorsk Plateau (Figure 2-4). In the higher stratigraphic sequence are the shales of the Nagorsk Horizon and the predominantly clay dominated sequence of the Laetsk Horizon. These form an impermeable layer with a thickness of approximately 5 m which separates the Cambrian-Ordovician aquifer from the overlying Ordovician aquifer. The average thickness of the Ordovician is approximately 50 m.

The Ordovician aquifer is located immediately below the Quaternary sediments. The minor thickness of the Quaternary sediments leads to the development of karst relief features in the Ordovician carbonates. The area was covered by ice four times during the Quaternary, and this largely sculpted the relief in the area (Anderson et al. 2006). The Quaternary sediments consist of the Ostashkovsk and Holocene rocks, and have a thickness of 1.5 m - 2 m to 50 m. They consist of sand, argillaceous sand, loam and peat.

In hydrogeological terms, the area of investigation belongs to the north-western part of the Leningrad deep basin. Several hydrogeological stockworks and horizons are identified in the Leningrad region. Groundwater in both the Lomonosov Horizon as well as the Quaternary sediments flows in the direction of the southern coast of the Gulf of Finland.

The top of the Cambrian clays has a highly differentiated relief in the Ischorsk Plateau. This is attributed to the plastic "squeezing out" of the clays during the formation of the plateau (Pereverzeva et al. 2008).

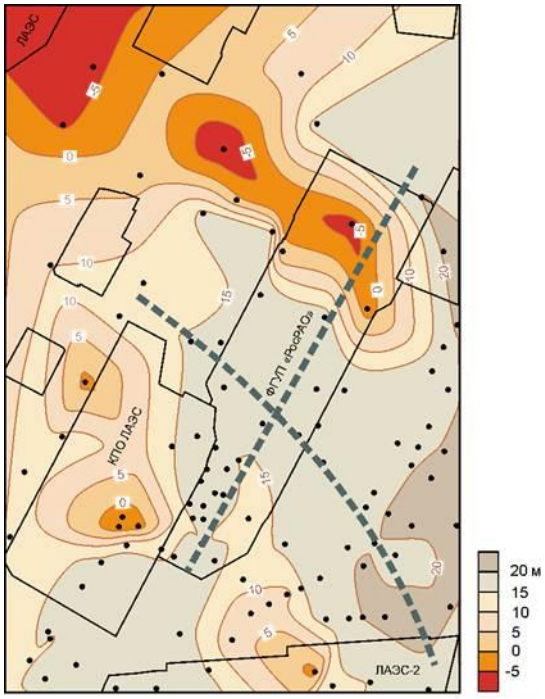

Another special feature of the Cambrian clays in the Leningrad region is the presence of numerous erosion channels associated with tectonic faults or glacial processes ("Quaternary channels", Figure 2-5). These erosion channels cut down up to 19 m below sea level (Pereverzeva et al. 2008).

Figure 2-5:
Depth map for the basis of the Quaternary sediments in the LSK "Radon" site showing the existence of “Quaternary channels” in this region (Rumynin 2011, pers. Comm.).

The hydrogeological stockworks existing within the sedimentary layers of the area of investigation are separated from one another by the impermeable Vendian and Lower Cambrian sequences (Figure 2-4). The Gdovsk aquifer is located in the lower part of the sedimentary succession and is one of the most highly exploited aquifers in the Leningrad region.

The Vendian Kotlin Clays then follow, and are overlained by the Lomonosov Horizon consisting of sands and slightly-consolidated sands of the Lower Cambrian. It has a filtration coefficient of between 0.2 m/day and 5.3 m/day. This Lower Cambrian aquifer is covered by layers of the impermeable Blue Clays. The overlying slightly consolidated clay-bearing Cambrian sands with a thickness of 5 m to 15 m, and the iron sands of the Lower Ordovician with a thickness of 10 m to 15 m, form a Cambrian-Ordovician groundwater stockwork which is widespread over the Ischorsk Plateau. There is no hydraulic connection between the Cambrian-Ordovician aquifer and the Lomonosov stockwork.

Another Ordovician aquifer is located in the fractured and karstified limestones and dolomites of the Ordovician immediately below the Quaternary rocks. This upper hydrological stockwork consists of numerous local aquifers. The groundwater here is located at depths of around 1.5 m (Anderson et al. 2006).

Because the Leningrad region is located in the contact zone of the Baltic shield and the Russian Platform, the crystalline basement in the region has been broken up into individual blocks under the influence of orogenic processes (Schöneberg & Neugebauer 1987). Most of the movement took place along the block boundaries and the major fault systems. These movements in the basement gave rise to faults and fractures extending up into the overlying sedimentary succession. The movements along the fault zones were reactivated during the glacial periods. This subjected the clay layers to strong compressive stresses. The fluctuating stress and stress release during the ice ages was responsible for the formation of the fractures within the claystones (Daschko 2006).

In general, the Leningrad region is considered favourable from a seismic point of view because it is part of the Russian Platform. However, the distribution, development and tectonic activity of the fault zones in the region are described very differently in various reports. The

largest, proven and assumed faults in the region are shown in the geological map in the “Geological and Ecogeological atlas of the Russian Baltic Region” (Petrov et al. 2010) (Figure 2-6).This map shows that the nearest large proven faults lie approximately 10 km from Sosnovyi Bor.

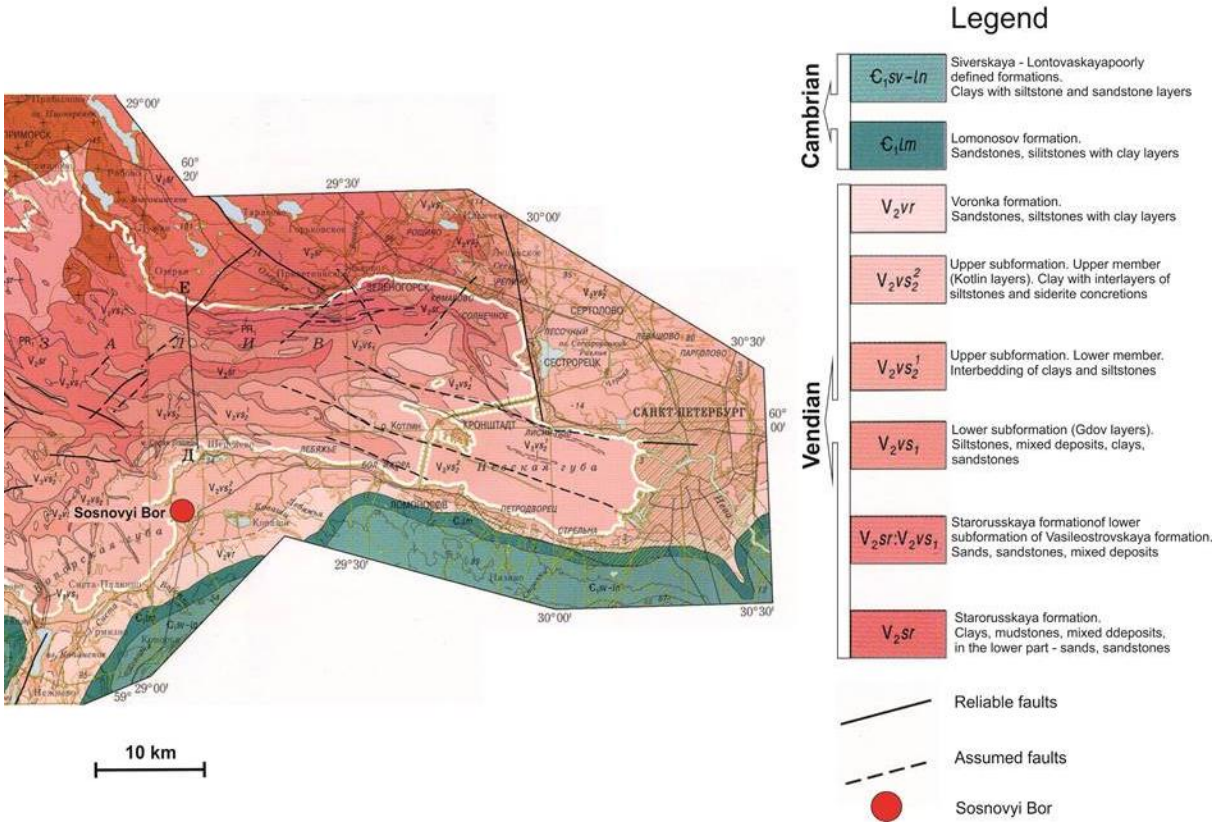

Figure 2-6: Geological map of the pre-Quaternary sediments showing the proven and assumed faults (Petrov et al. 2010).

Because of its position in the contact zone of the Baltic Shield and the Russian Platform, the Leningrad region is characterised by minor recent geodynamic activity as verified by raised Radon values in the soil air (Daschko 2006). Weak movements of individual structural blocks in the lithosphere give rise to relatively frequent but weak earthquakes. In the case of the geodynamic movements, the cores of the blocks remain stable and the movement and/or the associated changes in the rocks occur along the block boundaries and/or along the regional fault zones. The rate of movement of the basement blocks along the active fault zones in the Leningrad region in the recent period is maximum 2 mm/year (Anderson et al. 2006).

The movements of individual tectonic blocks give rise to the development of faults and/or fractures in the Vendian and Cambrian rocks. The fractures in the claystones are usually closed, however, and only open up when the in-situ pressure is decreased or when excavated. The fracturing is more intense in the Vendian clays than in the Lower Cambrian clays. The high plasticity of the Blue Clays minimises the consequences of deformation processes within the rocks (Daschko et al. 2011).

The results of Daschko (2006) reveal that the Blue Clays can be divided up into zones according to their degree of fracturing, whereby the fractures are characterised by differences in their genesis (tectonic, glacio-tectonic, lithogenetic, weathering, etc.). At the end of the Cretaceous, the Cambrian clay layers were exposed at the surface. This has led to decompaction and weathering of the clays. Moreover, neotectonic fracturing of the upper clay horizons took place. The clay layers were subjected to strong compressive stresses during

the ice ages, and to de-stressing when the ice withdrew from the area, which all led to additional fracturing of the clay horizons.

The data currently accessible to the German side makes it impossible to forecast the future development of seismic events in the area of investigation. There are still no reliable investigation results available on how the underground workings in the claystones would react to tectonic movements of the structural blocks (Anderson et al. 2006).

Radiomagnetotelluric and seismic surveying, as well as geoelectric surveying, were carried out in the area of investigation to explore the geologic underground. These surveys were used to map the numerous paleochannels (Figure 2-5) in the area of investigation attributable to Quaternary glaciation (Rumynin 2011). These investigations allowed the reconstruction of the influence of the glaciation processes on the underground geology in the region.

Moreover, data on the oxygen isotope composition of the groundwater in the area of investigation is also available (Kühnlenz & Hammer 2014). Since the isotope composition of the precipitation correlates with the air temperature, the isotope analysis enables reconstruction of the climate which existed when the groundwater was formed. The relationship between the oxygen isotope composition of the water and the average annual temperature is described as follows (Dansgaard 1964 in Pereverzeva et al. 2008):

$$\delta^{18}O = 0.69t - 13.6‰.$$

According to their isotopic composition, the groundwater with $\delta^{2}H<-110‰$ and $\delta^{18}O<-13‰$ ("light" groundwater) indicate precipitation which fell under cold climatic conditions, i.e. at an average annual temperature of approx. 0 °C and lower. The isotope analysis was undertaken on cores taken from the LSK Radon and Leningrad AKW-2 sites. In addition, water samples from the Lomonosov aquifer were also analysed. The results show that there are clear fluctuations in the $\delta^{18}O$ isotope values in the Kotlin Clays along a vertical profile. A peak in the isotopically "light" water occurs at a depth of approximately 40 m ($\delta^{2}H<-110$ ‰; $\delta^{18}O<-13$ ‰). This indicates cold climatic conditions during infiltration of this water (13,000 - 15,000 years ago). However, a zone of isotopically heavy water was identified at a depth of 120 m which indicates the existence of a warm climatic period. The water in this zone must therefore have infiltrated into the clay layer during the interglacial (70,000 - 120,000 years ago) (Pereverzeva et al. 2008).

3 Site specific models

3.1 Geological model

Within the project a geological 3D model for the *Radon* site in the Leningrad region has been created. The model area is situated at the southern coast of the Gulf of Finland. The region is located in the area of surficial distribution of Kotlin clay of Vendian age (approx. 635 to 541 Mill. years old) (Figure 3-1a). The entire area of the model region covers approx. 25 km^2 (4.4 km x 5.7 km). In the NW about 40% of the model area lies in the Gulf of Finland. The part of the model area (approx. 9.6 km^2) marked with a green quadrate (Figure 3-1b) was modeled using collected data from project-relevant boreholes.

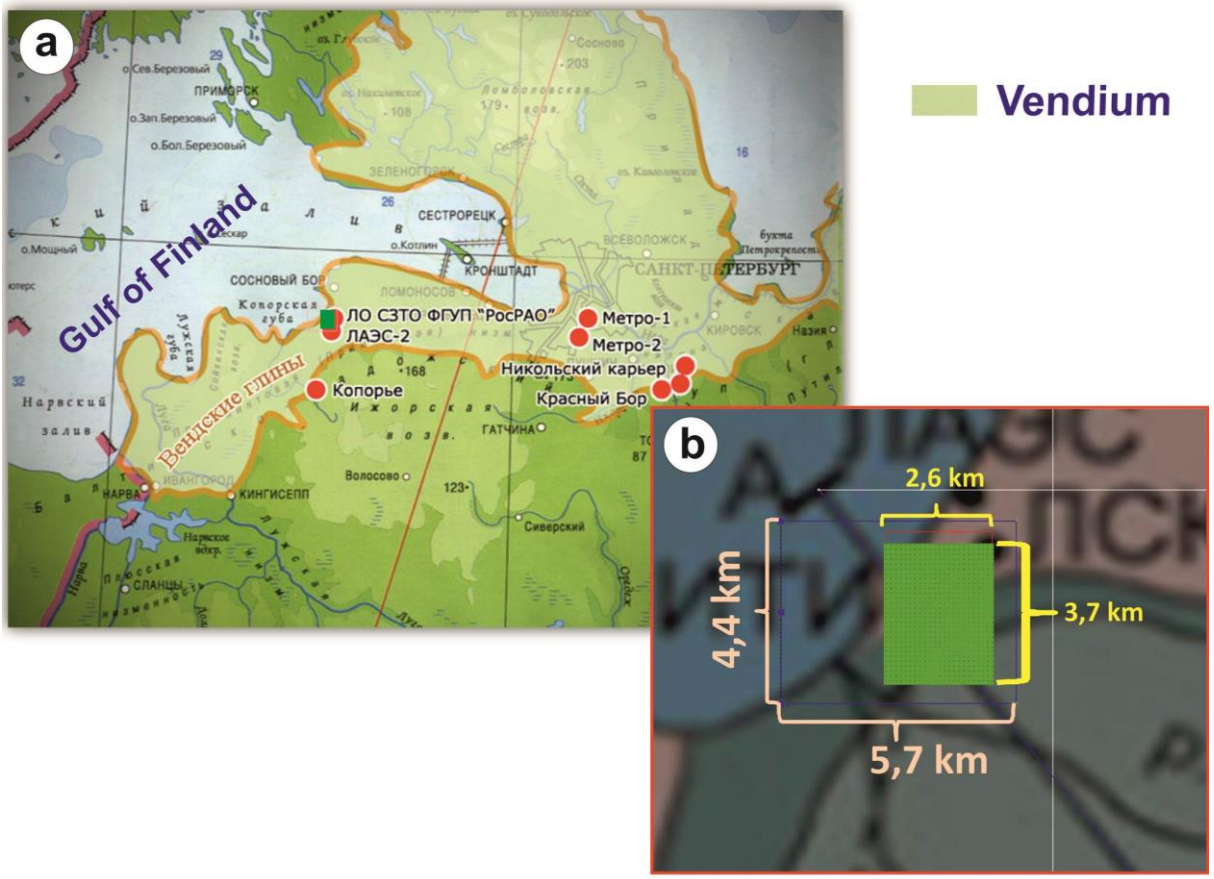

Figure 3-1: Geographic position (a) and dimensions of the model area (b). The boreholes representing the basis for modeling are positioned within the green area.

3.1.1 Data base for the geological model

Topographic and geological maps of the region, as well as a reference profile trending from the Gulf of Finland to the SE, have been considered for 3D model construction (Figure 3-2). The reference profile is greatly exaggerated and presents a very strong generalized geological situation in the region. It cannot be integrated into the 3D model true to scale, but it plays a crucial role for the development of the 3D model.

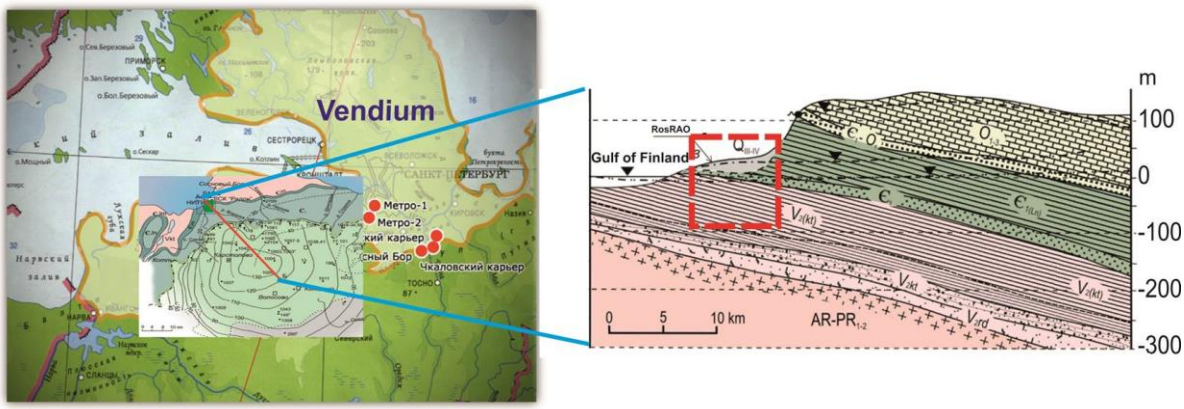

Figure 3-2: Geographical maps (left) and reference profile (right). The red frame shows the approximate model area.

Detailed information about the underground in the model area (green area in Figure 3-1b) were obtained from borehole loggings and core descriptions provided by Russian co-workers. A large number (426) of short boreholes with a length of less than 50 m was investigated (Figure 3-3a). The main purpose of these boreholes was the monitoring of hydraulic properties and the mapping of Quaternary channels. These boreholes reach the target horizon (Kotlin clay) but do not pierce it. Only 20 boreholes could be used to investigate deeper lying clay layers. They reach a depth of up to 178 m below surface and partly intersect the basis of the Kotlin Clay horizon.

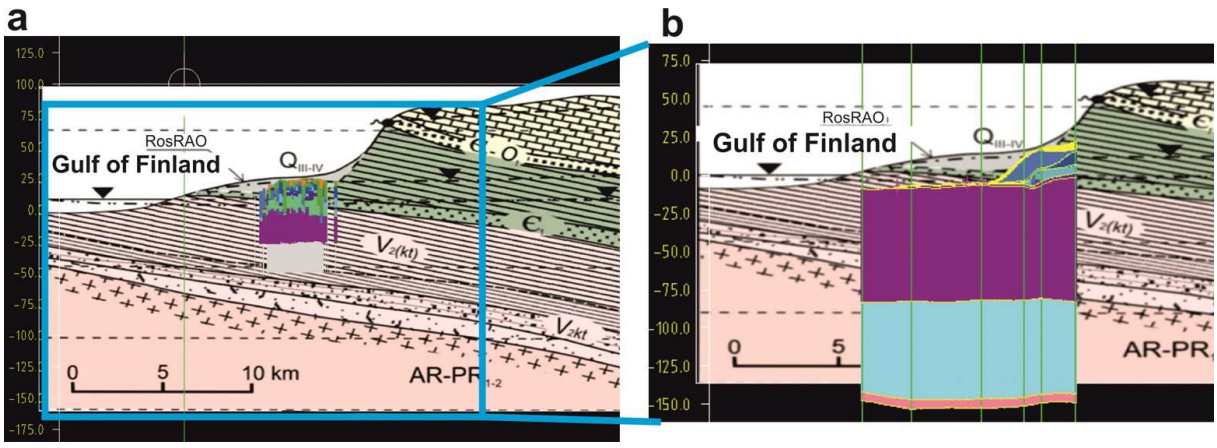

Figure 3-3: Position of the boreholes within the reference profile (a). Construction of the guiding profile for the 3D model on the basis of reference profile and boreholes (b).

3.1.2 Development of the geological model

The 3D model was created with the commercial program *openGEO* (Hammer et al. 2012). In a first step all accessible data were incorporated into the 3D space with their coordinates. In a second step the layer sequences for the 3D model were defined. Detailed lithological layer sequences of the model area were slightly simplified in a way that some layers with very small thickness or similar properties with neighboring layers, were brought together resulting in a final number of eight layers (Figure 3-4).

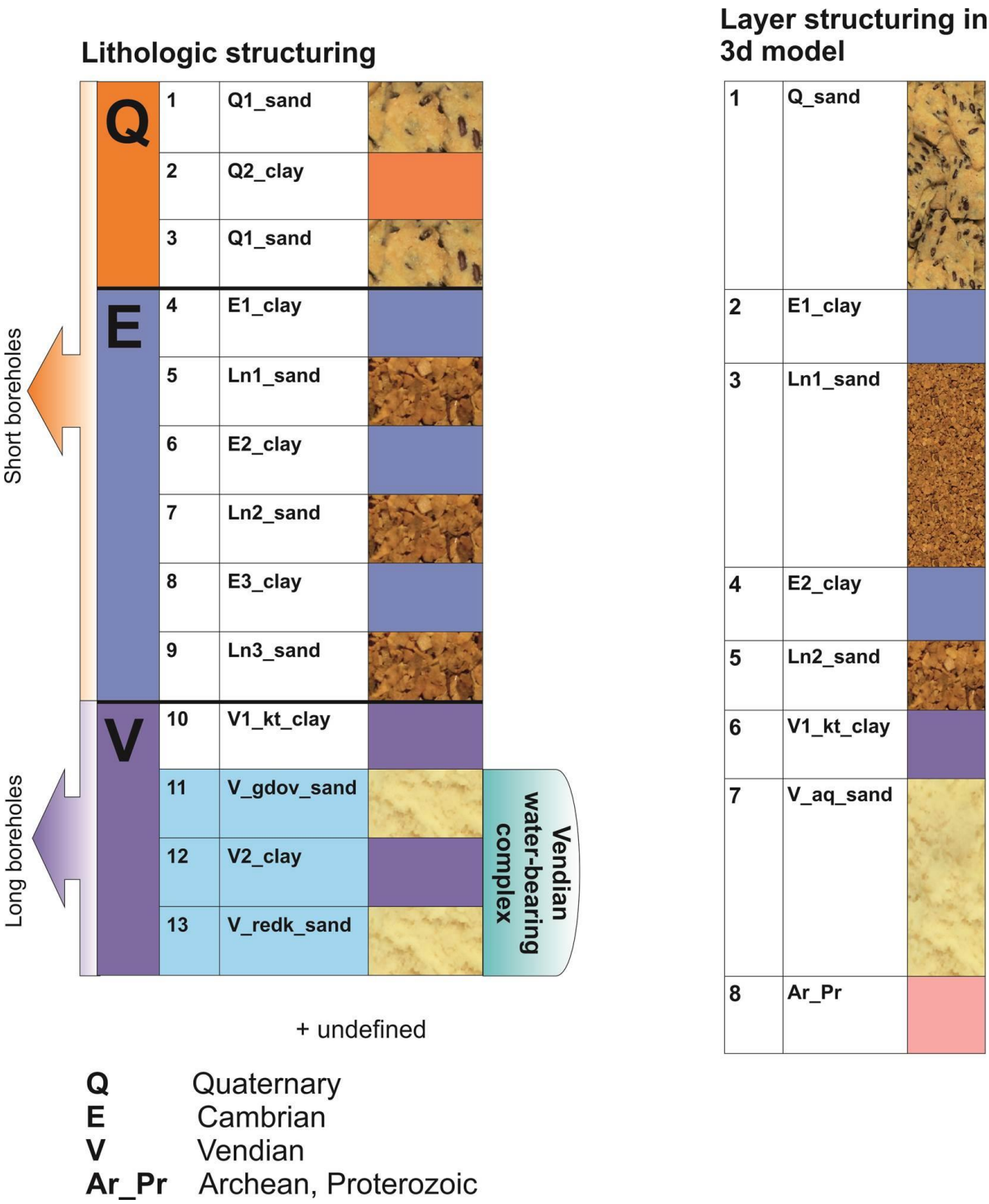

Figure 3-4: Layer sequences in the model area (left) and in the 3D model (right). Legend: Q1_sand = aquifer of permeable Quaternary sands, Q2_clay = low permeable Quartenary clay, E123_clay = Cambrian low permeable clay, Ln123_sand = Cambrian permeable sediments, Lomonosov aquifer, V1_kt_clay = Vendian Kotlin Clay, V_gdov_sand = Vendian aquifer, V2_clay = Vendian clay, V_redk_sand = Vendian Redkensker aquifer.

The guiding profile for the 3D model was derived by a combination of the reference profile and the boreholes (Figure 3-3b). The reference profile provides information about the layer sequences and their distribution in depth while the boreholes give the exact information about the layer thickness. The new guiding profile (Figure 3-3b, profile 1-1' in Figure 3-5a) presents only a small part of reference profile in the NW.

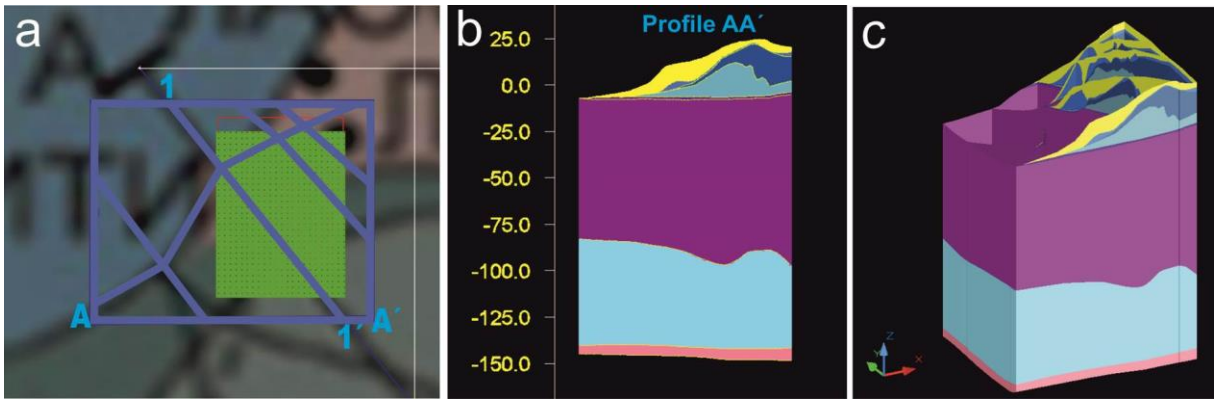

Figure 3-5: Profiles in the model area (a), profile A-A` with an exaggeration factor of 50 (b), all profiles incorporated in the 3D model (c).

In order to improve the knowledge about the distribution of geological layers in the model area apart from the guiding profile 1-1' (Figure 3-5b), in the model four additional cross-cutting profiles were added by BGR and four additional profiles were depicted as outer boundaries. This was done for modeling the basis- and top-surfaces of different stratigraphic layers (Figure 3-5c). The maximum thickness of the entire layer sequences in the model area is 175 m. Some of the upper thin layers are partly represented by sand-lenses. Hence, the modeling has been carried out with an exaggeration factor of 50 (Figure 3-5b, Figure 3-5c).

For simplification, sand-lenses of the same stratigraphic sequence were not modeled separately but connected to each other forming a very thin, continuous layer, so that each stratigraphic horizon within the model is represented by only one 3D body. The upper stratigraphic layers in the model (up to the top Kotlin Clay layer) are characterized in great detail due to a large number of boreholes and therefore characterized by a heavily structured surface. (Figure 3-6, Figure 3-7).

Only a few boreholes have a depth of more than 100 m and only some of them pierce the Kotlin horizon. They provide an overview of the thickness of the Kotlin Clay layer, but do not give an imagination about the relief of this layer. The relief of the basis surface of the Kotlin horizon and underlying layers are represented by relatively flat surfaces (Figure 3-7b, Figure 3-8b).

For constructing the stratigraphic layers in the form of 3D bodies, first of all the sub-horizontal surfaces have to be constructed. One surface represents a joint face between two stratigraphic sequences (stratigraphic boundary) and is the basis of one layer and at the same time the top side of the subjacent layer. The surfaces of the 3D model are exclusively created by the borehole data available. As an example, to create the top surface of the Kotlin horizon the stratigraphic boundary points of the Kotlin layer in the digital boreholes are connected by construction lines (Figure 3-6). These lines (line framework) are formed into polygons, which are used to model the layer surface by triangulation (Figure 3-7a). In order to get a solid body, the top and basis surface of one stratigraphic layer and the vertical boundaries of the model area have to be merged (Figure 3-7b). This process is stepwise performed for the other stratigraphic units (Figure 3-7c).

In general, the crucial element of the 3D model is the line framework (Figure 3-8a). On the basis of a solid line framework a correct triangulation and creation of 3D bodies is possible (Figure 3-8b).

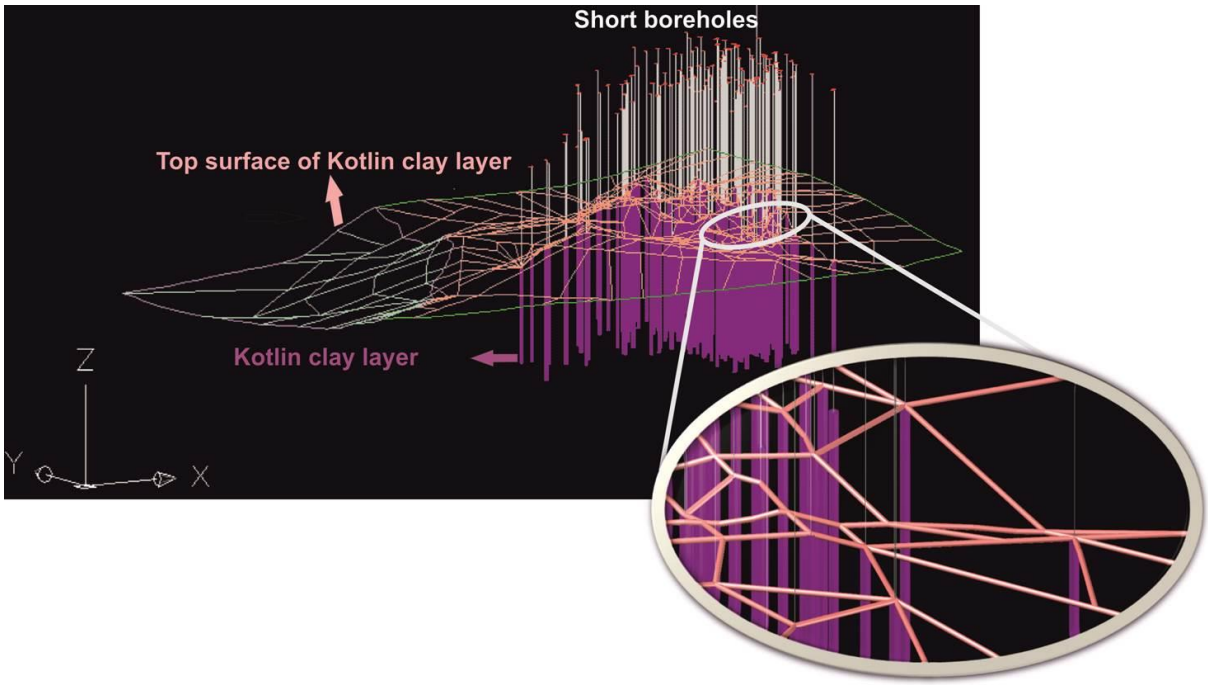

Figure 3-6: Modeling the top surface of the Kotlin clay layer.

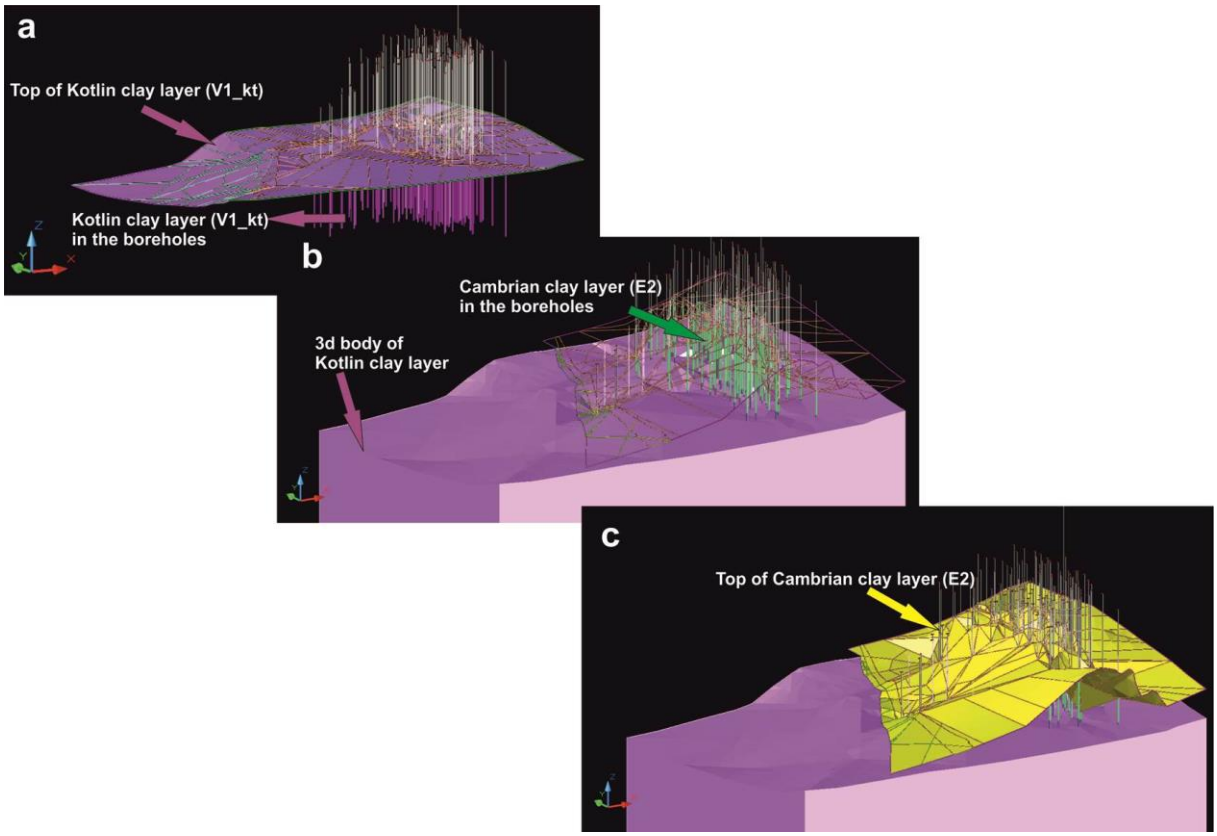

Figure 3-7: Construction of the surface by using borehole information (a), construction of a 3D body (b), combination of different stratigraphic layers in the 3D model.

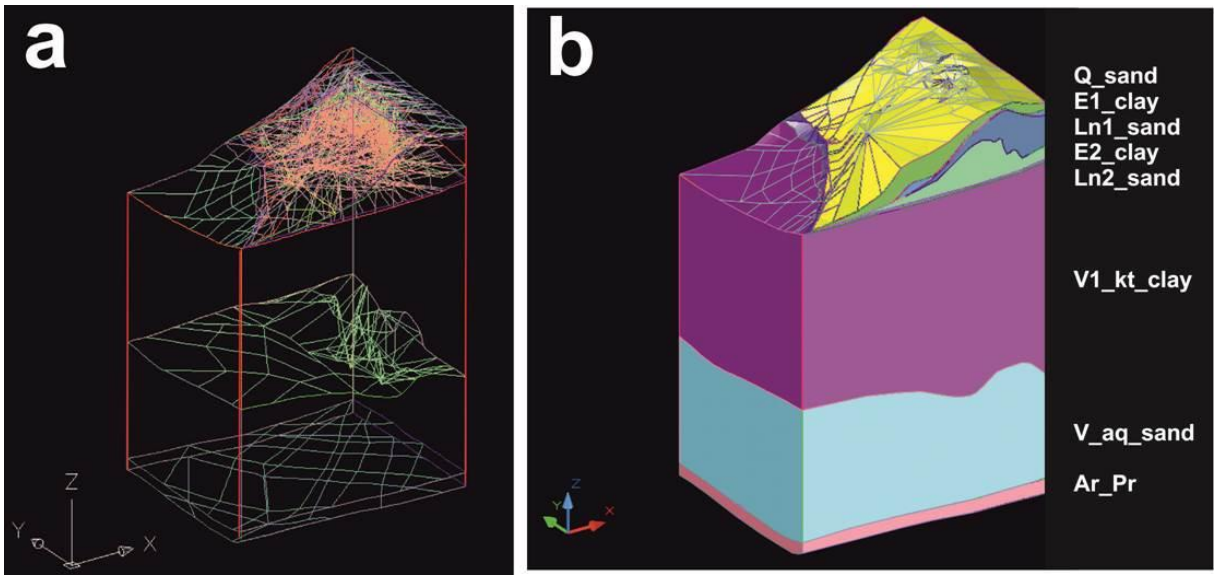

Figure 3-8: Framework of lines necessary for the creation of the 3D model (a), 3D model constructed on the bases of line framework (b).

Due to a very strong vertical exaggeration (50) the final 3D model (Figure 3-8b) shows a very differentiated relief and a thick Kotlin horizon, whereas the model in real scale is represented by very thin, partly not recognizable layers (Figure 3-9).

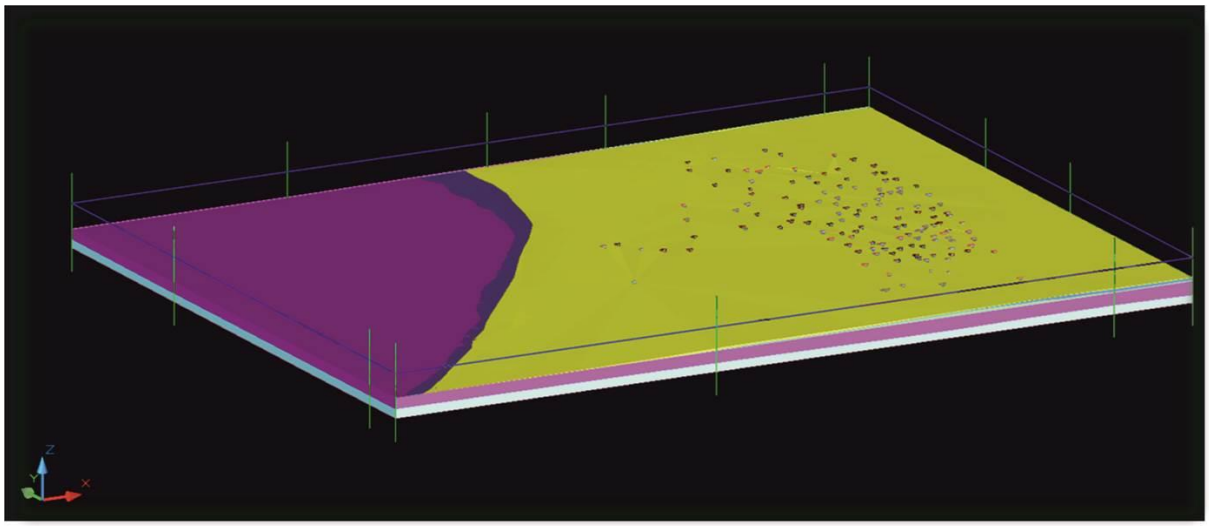

Figure 3-9: Finished 3D model in the true scale.

To determine a suitable position of the repository within the Kotlin horizon, the repository layout, the thickness, the depth and the position of the Kotlin horizon with regard to the coastline were taken into account (Figure 3-10). The final 3D model is a basis for numerical modeling.

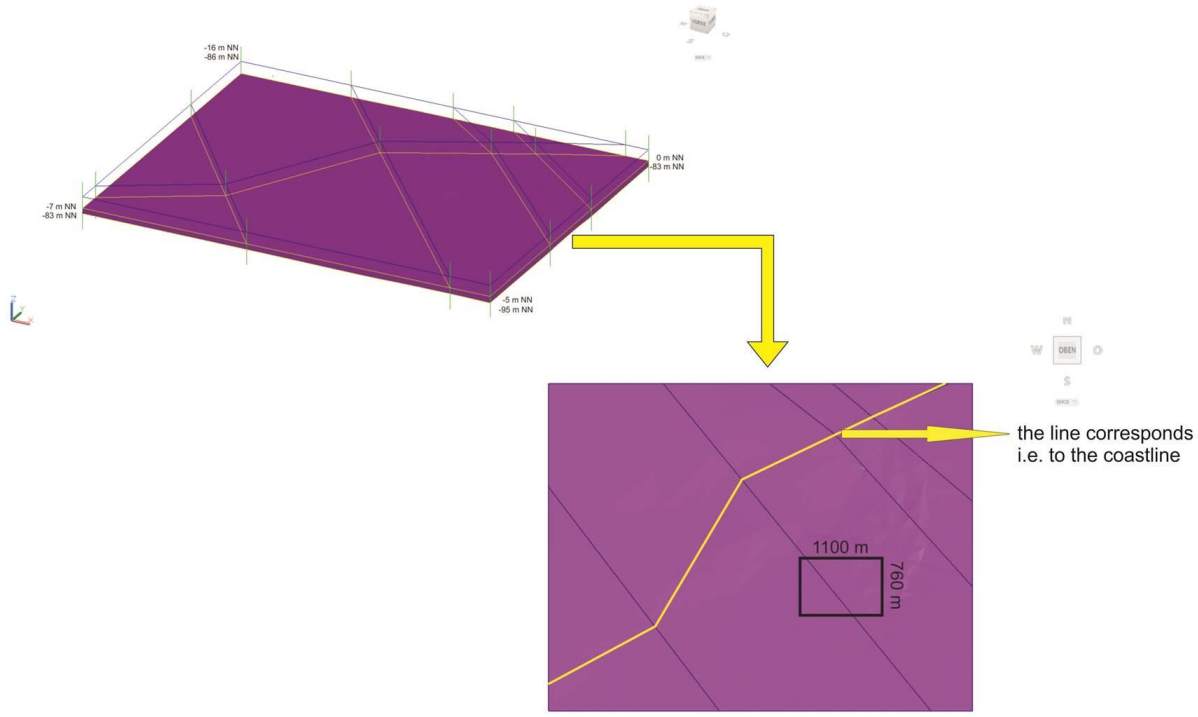

Figure 3-10: Determination of area and position of the repository within the Kotlin Clay layer.

3.2 Repository model

3.2.1 Mine layout construction in context with the geology

The objective of this chapter is the generation of the actual mine layout directly in context with the geology using the VIRTUS software platform (Wieczorek et al. 2014). VIRTUS is a tool for analyzing and conspicuously visualizing the complex safety-relevant processes occurring in a repository. The strengths of the software VIRTUS are the visualization and geometrical optimization of geological structures for numerical calculations as well as the planning of subsurface facilities using built-in methods and user interfaces for generating such structures. A model generated this way can then be read directly into the numerical simulation code for calculations.

A typical VIRTUS workflow starts with the import of a geological model. With the attention focused on the generation of the subsurface facilities, a simplified geological model was used that does not cover the entire stratigraphy. The geological model compromises one solid body representing the geological unit Kotlin Clay (V1_kt_clay, see Chapter 3.1.2) (Figure 3-11).

However, geological models generated this way are usually made up of triangulated surface meshes that do not comply with the quality requirements to facilitate the subsequent finite element mesh generation. Therefore, VIRTUS was designed to provide automated pipeline tools to geometrical correct and improve the geological models imported.

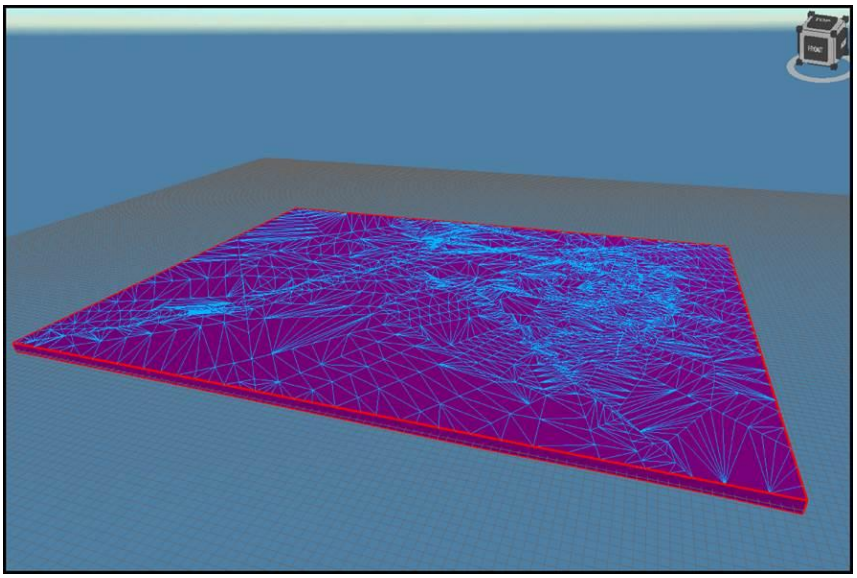

Figure 3-11:
Geological model used and imported into the VIRTUS software package.

In order to realize an improvement of triangulated surface meshes, the algorithms for simplification (MeshSimplification) and regularization (Remeshing) were applied (Wieczorek et al. 2014). The algorithms for simplification and regularization of triangle meshes are geared to concepts of recent publications in computer graphics research and were developed further according to the requirements of VIRTUS. Figure 3-12 shows a model selection after using the simplification and regularization algorithms. The internal validation for characterization of the triangular shape shows that the number of well-shaped triangles could be increased from 37% to 90%.

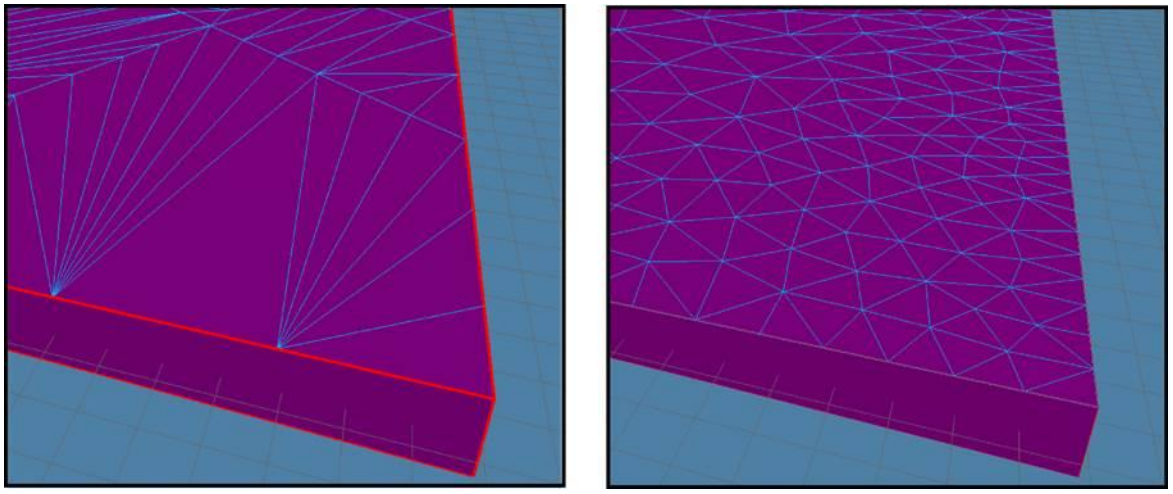

Figure 3-12: Geological model before (left) and after (right) simplification and regularization.

After generating the required geological model, the subsurface facilities were constructed based on the mine layout presented in Chapter 5.2. The mine layout is represented by an undirected graph and can be complied by adequate combinations of drifts, intersections and shafts. Based on the so-defined mine structure a three-dimensional surface model is generated automatically. Details of corner arcs at bends, intersections or drift ends are parameterized and are considered during generation of the 3D geometry. The mine structure generated as defined in Chapter 5.2 is shown as a surface model in Figure 3-13.

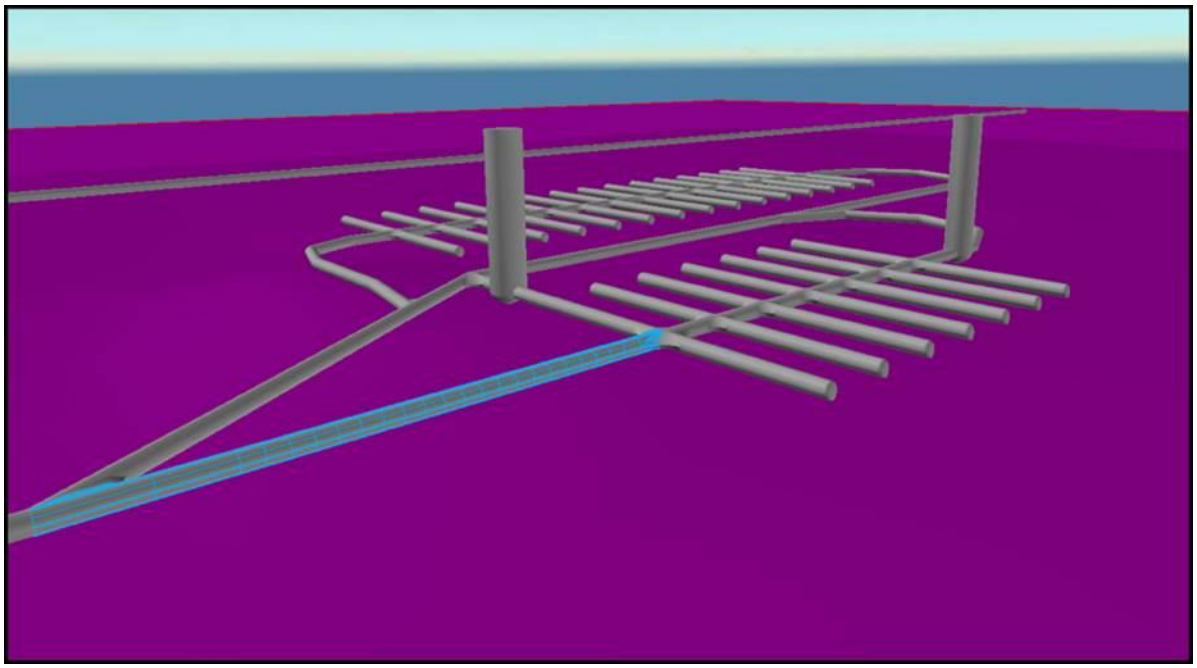

Figure 3-13: Mine structure constructed in VIRTUS using the build-in methods.

VIRTUS is just a functional prototype characterized by some limitations. The construction of drifts is currently limited to line segments and drift curves can only be constructed indirectly by manual sequencing individual drift segments (Figure 3-14). Also, the construction tool for shaft generation has up to now only been implemented rudimentarily. Moreover, geometrical flaws were observed at drift crossings (Figure 3-14). The surface model of the mine could therefore not be bonded with the geological model and exported to a FEM solver as a result of the observed degenerated surface mesh.

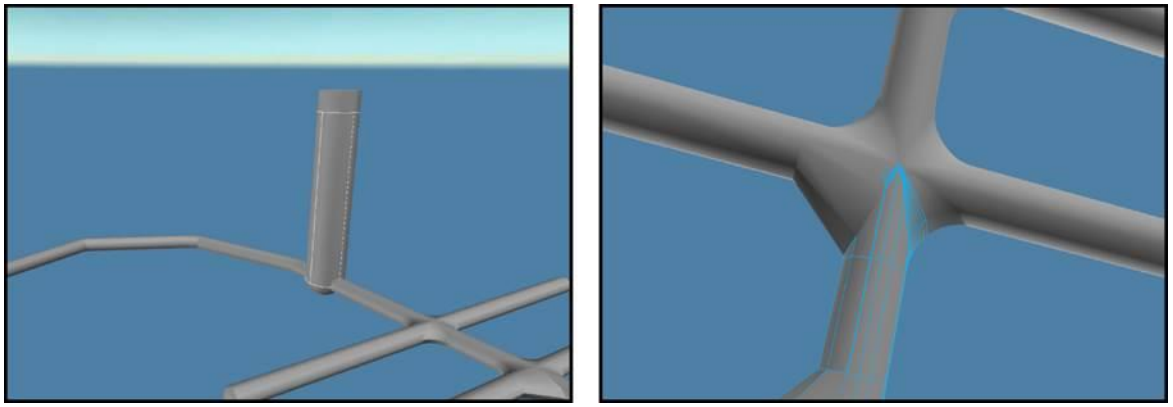

Figure 3-14: Construction of drift curves by sequencing line segments (left) and observed geometric flaws at drift crossings (right).

The software package VIRTUS allows institutions participating in repository projects to automatically improve geological models as well as to quickly plan and generate virtual mine designs in complex geological structures. These models can be exported and used in numerical simulations which mean a considerable simplification for modelling.

4 Site specific data base

4.1 Data on the rock composition and properties

The composition and the geomechanical properties of rocks (including stability, tensile strength) as well as hydraulic properties and retention capacities (dispersion and transport properties, sorption capacities) of the claystones in the area of investigation have been comprehensively analysed since the 1980s. This information is required for the elaboration of a final repository concept, for verifying the long-term safety of the planned repository, and for planning the operation of the repository.

Investigations were carried out on both clay formations (Vendian Kotlin Clays and Cambrian Blue Clays). Studies on the Vendian Kotlin Clays were mainly undertaken on samples from the territories of the Leningrad NPP-2 and LSK (Leningrad Special Kombinat) "Radon". The investigations of the Lower Cambrian Blue Clays were mainly done on samples from the area north-west of Koporje.

4.2 Mineralogy and lithology of the potential host rocks

The mineralogical investigations comprise analysis of the granulometric composition of the rocks, and X-ray diffraction analysis of the whole rocks, and the clay fraction (Pereverzeva et al. 2008, Anderson et al. 2006).

The mineralogical analysis revealed that the Blue Clays are composed of illite, kaolinite, biotite, muscovite and quartz. The mineralogical composition is summarised as follows:

- Quartz - 30 - 36 %
- Clay minerals - 23 - 29 %; of which approximately 80 - 89 % illite and 11 - 20 % kaolinite
- Biotite - 13 - 16 %
- Muscovite - up to 11 %
- Feldspar - 8 - 10 %.

The Blue Clays are classified as aleurite clays according to their granulometric composition (dominant grain size: 0.05 - 0.005 mm). The finest fraction consists of illite (hydromuscovite), hydrobiotite, glauconite and chlorite, and rarely also montomorillonite. There are also rare large aggregates of iron sulphides (pyrite, marcasite). The light mineral fractions primarily consist of quartz (74 %), as well as feldspar, micas, chlorite and glauconite. The heavy mineral fraction is dominated by zircon, tourmaline, rutile and epidote (Anderson et al. 2006, Daschko et al. 2011). Because of their higher plasticity and higher clay content when compared to the Vendian Kotlin Clays, some specialists consider the Blue Clays to be more favourable as a host rock for the construction of a final repository (Daschko 2005).

The analysis results of the X-ray phase analysis of samples from the LSK Radon site reveal that the Vendian Clays consist primarily of clay minerals but also of quartz, siderite, chlorite and orthoclase. The inventory of clay minerals consists of a mixture of illite (67 - 76 %), and kaolinite (16 - 27 %), with a small amount of chlorite. In the same way as the Blue Clays, the Kotlin Clays can also be classified as polymineralic illite-kaolinite dominated clays. The fine fraction (< 0.002 mm) of the Upper Kotlin Clays consists of hydromica, kaolinite, and other clay minerals. This means that the Kotlin Clays have a relatively good swelling capacity (Pereverzeva et al. 2008, Daschko et al. 2011).

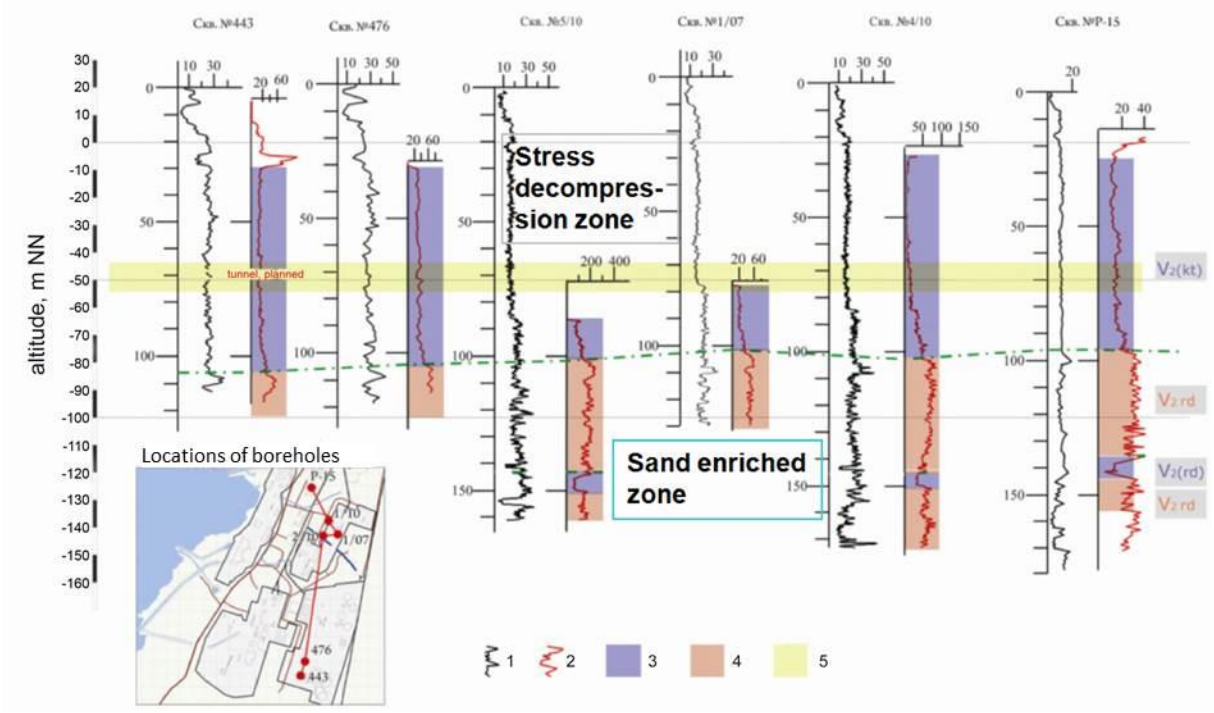

Figure 4-1: Results of borehole logging in the Radon site. 1 – mR/h, 2 – Ωm, 3 – mainly clayey horizon, 4 - strongly argillaceous intermediate horizon, 5 - zone scheduled for tunnel drifting (Rumynin 2011).

The lithological variability of the Vendian Clays was investigated by geophysical borehole logging in the LSK Radon site, which allowed the sequence to be subdivided into various units based on the lithological parameters. Several methods were used for this classification: logs of the natural radioactivity and gamma-gamma density logs, geoelectric logs, and logging of the natural electric field. Figure 4-1 shows some of the results of the borehole logging. The black plot shows the gamma ray logs from several boreholes. The low values of 5 - 10 mR/h are typical of sand layers. The values between 15 and 30 mR/h indicate the presence of clay layers. The high gamma values in the clays are attributable to the high K_2O concentrations, as well as raised concentrations of accessory U/Th-bearing minerals in the clays. The red plot shows the electrical resistance of the rocks. Values of 80-100 Ωm indicate the presence of sands. Clays with interbedded sand, argillite and aleurolite have values of 20 - 30 Ωm. The lowest values of up to 10 Ωm are characteristic of pure plastic clays.

4.3 Hydraulic conductivity

In-situ tests and laboratory experiments were carried out to determine the hydraulic conductivity (k_f) to describe the filtration properties of the Vendian Kotlin Clays (Figure 4-2). Pressure sensors were positioned in boreholes to measure the pore pressure (Pereverzeva et al. 2008, Rumynin 2011). The hydraulic conductivity determined with the help of laboratory experiments reveals an average $4.8 \cdot 10^{-7}$ m/day ($5.56 \cdot 10^{-12}$ m/s) for the Vendian Kotlin Clay (Pereverzeva et al. 2008, Rumynin 2011).

The hydraulic conductivity of the Blue Clays was determined on the basis of laboratory analysis. It is about $7.6 \cdot 10^{-6}$ m/day ($8.8 \cdot 10^{-11}$ m/s) in the vertical direction and is slightly higher in a horizontal direction with $1.8 \cdot 10^{-5}$ m/day ($2.08 \cdot 10^{-10}$ m/s).

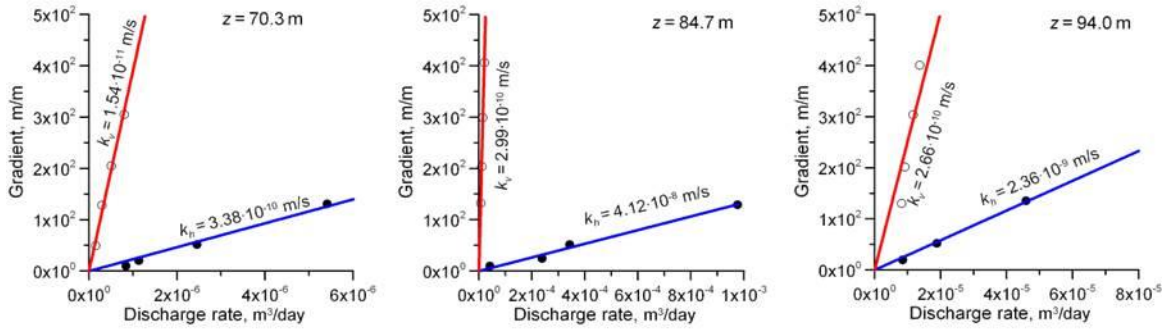

Borehole number	Depth, m	Along layering, m/s	Across layering, m/s	Anisotropy factor
5/10	48.6–49.0	$6.94 \cdot 10^{-11}$	$1.50 \cdot 10^{-11}$	4.6
4/10	51.8–52.1	$4.63 \cdot 10^{-11}$	$6.94 \cdot 10^{-12}$	6.7
1/07	55.2–55.35	N.d.	$5.79 \cdot 10^{-12}$	N.d.
1/07	65.8–65.95	N.d.	$5.79 \cdot 10^{-12}$	N.d.
4/10	69.2–69.5	$2.20 \cdot 10^{-10}$	$1.62 \cdot 10^{-11}$	13.6
7/11	70.3–70.6	$3.38 \cdot 10^{-10}$	$1.54 \cdot 10^{-11}$	22
7/11	84.7–85.0	$4.12 \cdot 10^{-8}$	$2.99 \cdot 10^{-10}$	138
7/11	94.0–94.25	$2.36 \cdot 10^{-9}$	$2.66 \cdot 10^{-10}$	8.9

Figure 4-2: Results of laboratory determination of permeability of clays from the Radon site showing anisotropy of permeability and higher permeability along layering in comparison to permeability across layering (Rumynin 2011).

The structure of the Lower Cambrian clays was investigated by Daschko et al. (2005, 2006, and 2011) and divided up into various zones based on the fracturing of the rocks. The filtration and sorption capacities of the Blue Clays were determined for each zone based on this zonation (Daschko 2005 and 2006, Anderson et al. 2006).

Daschko (2006) carried out hydraulic conductivity calculations for the fractured zones, i.e. tectonic fault zones in the Blue Clays in the upper clay layer down to a depth of 20 m. This revealed that the hydraulic conductivity of the clay layers was dependent on the degree of fracturing, the fracture aperture, and the size of the block. A much lower density and higher natural water content was determined in the upper fractured horizons of the Blue Clays. The in-situ measurements reveal a hydraulic conductivity of the fractured zone of the Blue Clays of more than 10^{-3} m/day ($1.16 \cdot 10^{-7}$ m/s).

4.4 Sorption and diffusion

The experiments carried out to determine the sorption and diffusion capacities can be used to derive estimates of the radionuclide retention capacity of the Blue Clays and Kotlin Clays. The laboratory analysis of the retention capacity of the Lower Cambrian Blue Clays for the radionuclides ^{90}Sr, ^{137}Cs, $^{239/240}$Pu and ^{95}Am, was carried out in the laboratory of the Radium Institute in St. Petersburg. Moreover, the barrier properties of the clays under the influence of radioactive radiation as well as simultaneous activation of microbial activity, were also investigated (Anderson et al. 2006, Daschko 2005, Daschko et al. 2011).

Rumynin et al. (2003) analysed the sorption and diffusion capacities of the Lower Cambrian Blue Clays by using the tracers ^{36}Cl and ^{90}Sr. The experiments revealed that the diffusion coefficients of chloride and strontium are very similar under isotonic conditions and measured $(5.7\text{-}7.4) \cdot 10^{-5}$ and $(4.2\text{-}4.3) \cdot 10^{-5}$ m^{2}day^{-1} in solutions with lower (0.1) and higher (3.0) ion concentrations respectively. The rising ion concentrations the coefficient of the molecular diffusion drops by a factor of approximately 2 under isotonic conditions. This dependency is

weaker under non-isotonic conditions. The sorption capacity of radioactive strontium decreases with increasing ion concentrations. The calculated sorption coefficient K_d is 4.2 and 0.7 cm^3g^{-1} (1.57 cm^3g^{-1} for non-isotonic conditions) for 0.1 and 3 g-equiv l^{-1} $SrCl_2$ solutions respectively. The desorption of previously absorbed ions from the clay samples is 3 - 4 times higher than the associated values for diffusion out of the solution in the sample (Rumynin et al. 2003).

On the basis of these investigations, the adsorption capacity of the Blue Clays appears to be relatively low and varies to a minor degree along the sedimentary succession. According to the published data, this value varies along the profile from 10.2 to 13.4 mg-equiv/100 g. The samples reveal a relatively high retention capacity for the radionuclides strontium, caesium, plutonium and americium. The distribution coefficient of strontium was 10^2, americium 10^3 and plutonium 10^4. The experiments revealed that the "retention time" for the diffusion transport through the clay layer with a thickness of 1 m was 5,000 years for caesium, 300 years for strontium and 50,000 years for plutonium. However, the authors pointed out that these findings could not be directly extrapolated to the inhomogeneous clay formation (Anderson et al. 2006, Daschko 2006).

Daschko (2006) determined that a relatively low sorption capacity is characteristic for the Lower Cambrian Blue Clay despite its high clay concentration (35 - 60 %). This is explained by the shielding of the thin dispersed clay particles by a film of organic components. The coefficient of molecular diffusion is 10^{-4} m^2/day in the fractured blocks of the Blue Clay. The effective porosity is less than 1/3 of the total porosity. This gives rise to a low sorption capacity with respect to radionuclides.

Sorption and diffusion experiments carried out on the Kotlin Clays were undertaken as part of the investigation of the LSK Radon site (Pereverzeva et al. 2008, Nikulenkov 2011). The diffusion processes for the radionuclides ^{90}Sr, ^{60}Co, ^{137}Cs and $^{239/240}Pu$ were analysed from core samples taken from the upper (20.5 - 20.65 m), middle (76.4 - 76.55 m) and lower (133.25 - 133.40 m) sections of the Vendian bedded succession. Measurements revealed that there is no regular trend in the change in sorption coefficients in the depth interval from 0 to 100 m (Figure 4-3).

Samples taken from deeper boreholes (> 100 m) (red line in Figure 4-3) revealed a significant decrease in their sorption coefficients. This is associated with the special lithological characteristics of the clay at this depth. The aleurite content rises significantly and there is a transition into an aquifer (Nikulenkov 2011).

A comparison of the radionuclides with one another reveals significant differences in the sorption values (Figure 4-3). The findings revealed that $^{239/240}Pu$ has the maximum adsorption properties and ^{90}Sr the minimum adsorption properties. According to the coefficient of molecular diffusion, the radionuclides form a series (^{90}Sr > ^{60}Co > ^{137}Cs > $^{239/240}Pu$), which is the reverse order when compared to the diffusion values (Figure 4-4). The coefficient of molecular diffusion of the radionuclides decreases as the sorption coefficients increase. The penetration depth of the radionuclides in the samples was less than a few hundredths of a millimetre during the experimental time period (Pereverzeva et al. 2008).

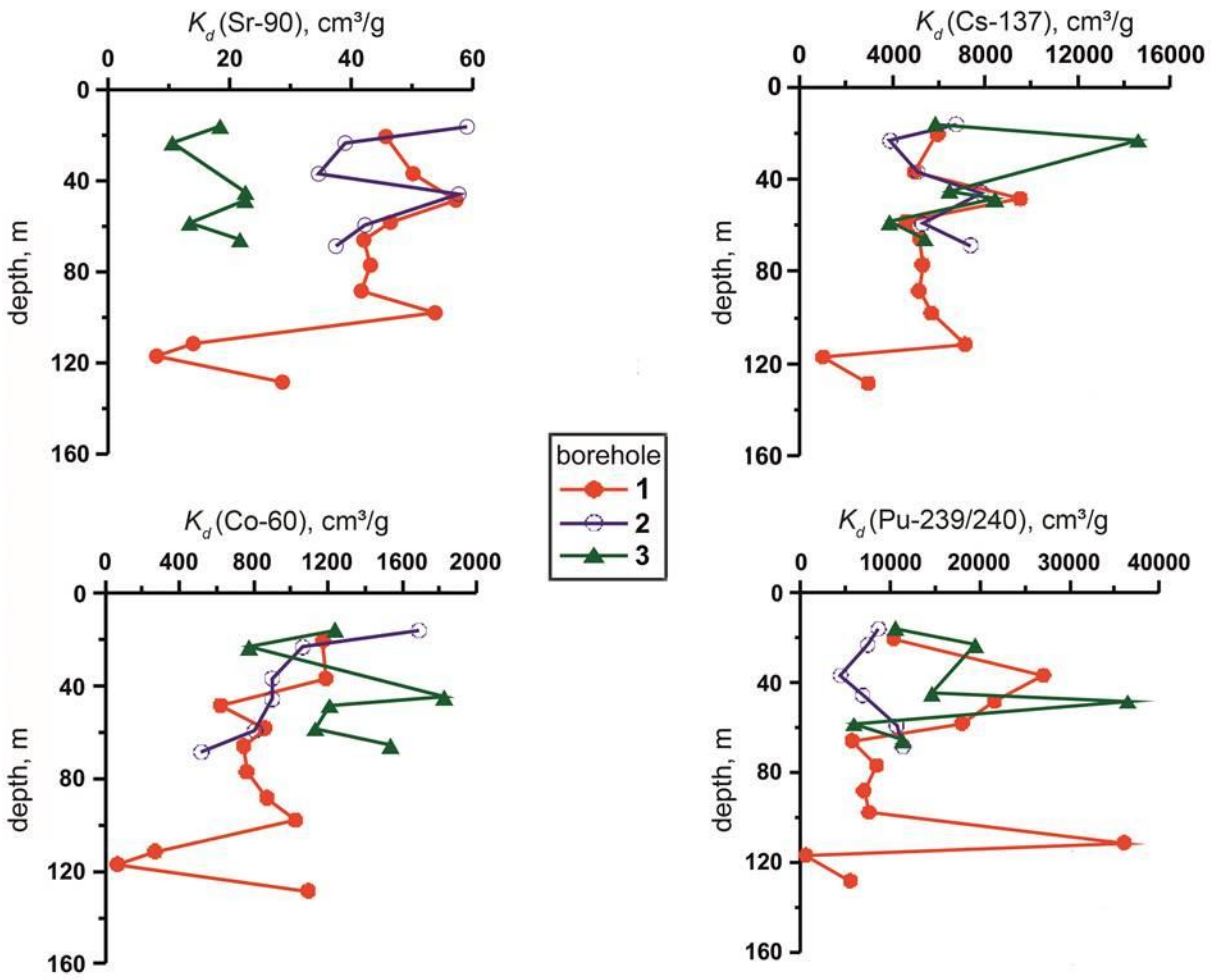

Figure 4-3: Variations in sorption coefficients (K_d, cm^3/g) within the Kotlin Clays (Nikulenkov 2011, Rumynin 2011).

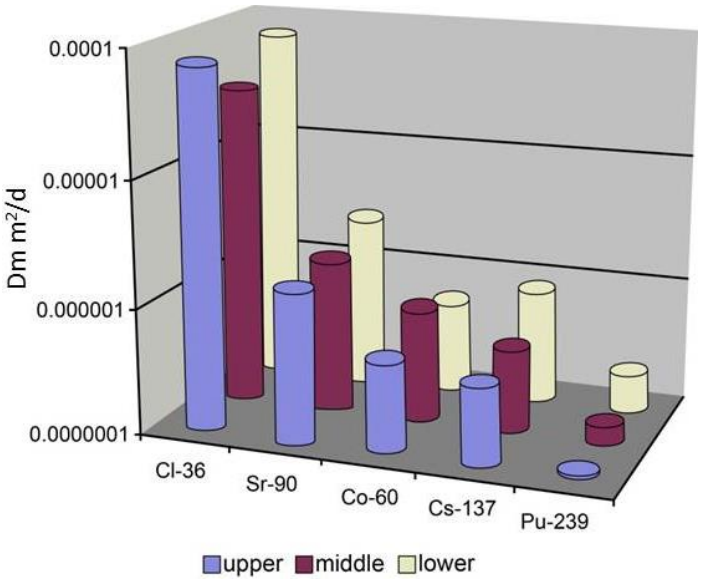

According to Anderson et al. (2011), the diffusion transport of the radionuclides ^{90}Sr and ^{137}Cs in the Upper Vendian and Lower Cambrian Clays would not exceed a distance of 1 m over the verification period (300 - 500 years) in the case of destruction of the containers.

Figure 4-4:
Diffusion coefficients of radionuclides for samples taken from the Kotlin Clays at various depths (upper=20,5-20,65m, middle=76,4-76,55m, lower=133,25-133,40m) (Nikulenkov 2011, Rumynin 2011).

4.5 Physical properties and deformation behaviour of the claystones

The following parameters were measured and evaluated dependent on depth as part of investigations of the physical and mechanical properties of the claystones: density (g/cm^3), moisture content (%), plasticity value (%), Young's modulus and strength parameters (Rumynin 2011, Daschko et al. 2011). Analysis of the physical properties of the Leningrad clays revealed an often abrupt, irregular change in properties with depth. This is attributable to the heterogeneous lithological composition of the clay formations and/or the presence of sand intercalations. The Cambrian Blue Clays are more inhomogeneous than the Vendian Clays.

4.5.1 Density

The saturated density in the upper part of the Blue Clays is 1960 - 2220 kg/m^3, and rises to 2120 - 2280 kg/m^3 at greater depths (Daschko & Volkova 2004). Densities in the range of 2120 - 2340 kg/m^3 were determined for the Vendian Clays (Figure 4-5, left). The diagram clearly shows that the density usually rises with increasing depth (Pereverzeva et al. 2008). According to Daschko et al. (2011), the density of the Upper Kotlin Clay is in the range of 2170 - 2240 kg/m^3. There is a general trend for the density to increase and the moisture to decrease with increasing depth (Pereverzeva et al. 2008).

4.5.2 Porosity and water content

The Blue Clays are wetter and more plastic than the Vendian clays (Daschko et al. 2011). The natural water content of the Blue Clays varies from 23 – 28 % in the upper part to up to 15 – 18 % at a depth of 40 m. The physical porosity is 30 % (Daschko & Volkova 2004). The natural water content of the Vendian Kotlin Clays varies between 10.2 % and 19.8 %, and reduces with increasing density and depth (Figure 4-5, right; Pereverzeva et al. 2008). Tang et al. (2010) determined a porosity of the Vendian Clays of 22 – 27 % based on lab experiments.

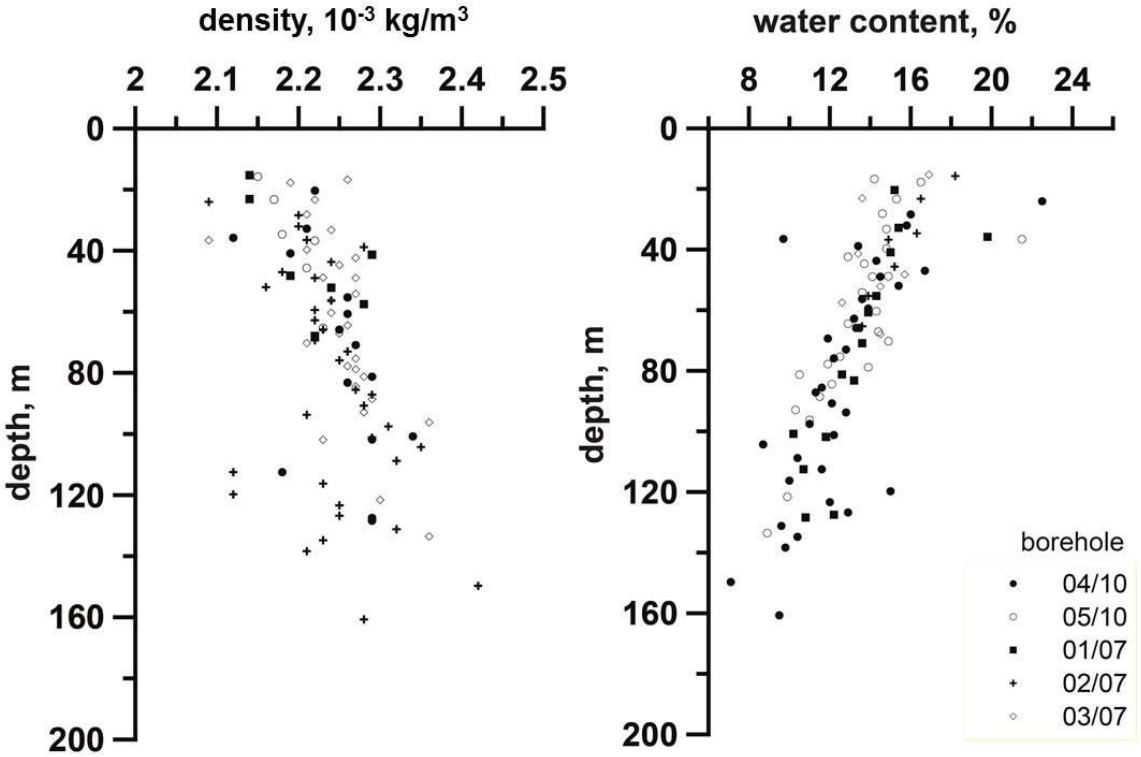

Figure 4-5: Change of density (left) and natural water content (right) of the Kotlin Clays with increasing depth (Pereverzeva et al. 2008).

4.5.3 Rock mechanical properties of the clays

Rock mechanical parameters describing the deformation behaviour of the clays in the Leningrad region were determined by laboratory investigations of core material from boreholes drilled at the LSK Radon site (Vendian Kotlin Clays), and at the area in the vicinity of Koporje (Blue Clays). Triaxial and uniaxial pressure (compression) tests were carried out on the Vendian Kotlin Clays (Tang et al. 2010, Pereverzeva et al. 2008). The following parameters were determined by pressure tests: Young's modulus, shear strength, dependence of the Young's modulus on vertical stress, and the dependence of permeability on void ratio.

On the basis of uniaxial and triaxial pressure tests, Pereverzeva et al. (2008) determined that there was a characteristic increase of the Young's modulus (E) with increasing depth for the Kotlin Clays at the LSK Radon site, as well as at the Leningrad Nuclear Power Plant (NPP) subarea (Figure 4-6). The Young's modulus is 20 MPa to 50 MPa in the upper, strongly fractured horizons. It increases with increasing depth (from approximately 50 m), and reaches 80 to 140 MPa. The change of E with increasing depth can be described as follows:

$$E = 0.9 \cdot H + 24.5 \quad \text{(with H = depth in m).}$$

In the fractured zones of the clays E varies between 20 MPa and 180 MPa, which is due to a locally high disintegration of the rocks (Daschko et al. 2011).

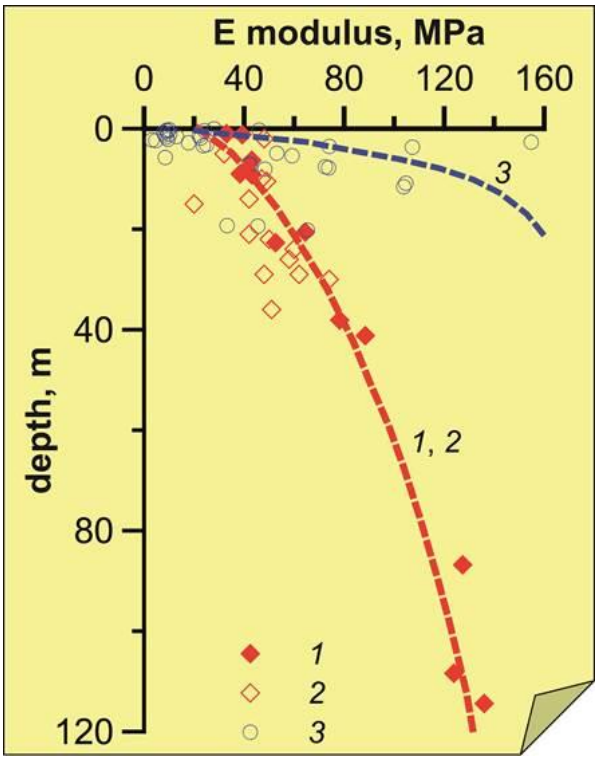

Triaxial pressure (compression) tests were carried out on seven samples from various depths in the Kotlin Clays (32.75 m to 83.25 m). There was a large scatter in the results because of the irregular distribution of clay and sand fractions within the samples. An average tensile strength (failure) of the Kotlin Clays was determined. The cohesion value was 4.61 MPa at an angle of friction of 23°. The experiments revealed that the tensile strength E rises with increasing depth (Figure 4-6, Pereverzeva et al. 2008).

Figure 4-6:
Variations of Young's modulus (E) of Kotlin Clays from Radon and Leningrad NPP sites with increasing depths (1,2,3 = different boreholes), (Pereverzeva et al. 2008).

Tang et al. (2010) carried out additional hydromechanical laboratory investigations on core samples from the Vendian Kotlin Clays (LSK Radon site). The triaxial and oedometer tests (compression tests) enabled the mechanical as well as the hydraulic properties of the Vendian clays to be investigated. Three core samples were taken from various depths for the experiments (23.1 m, 78.4 m and 126.6 m below ground level). The core from a depth of 23.1 m was located close to the Lomonosov aquifer. The core taken at a depth of 78.4 m was in the middle of the Kotlin Clay horizon, and the core from a depth of 126.6 m corresponds to the lower part of the Kotlin Horizon.

The peak in shear strength measured at various initial pressures (1000 kPa, 600 kPa and 300 kPa) ranged from 2.06 MPa to 3.82 MPa. The results of the uniaxial pressure tests, i.e. the dependence of the Young's modulus (E) on the vertical stress are shown in Figure 4-7 for three test samples taken from different depths (Od03-126.6 m, Od02-78.4 m, Od01-23.1m). Figure 4-7 shows the loading and unloading curves. It can clearly be seen that different values of E were observed in the three specimens at the same stress level (e.g. 20 MPa). The Young's modulus for sample Od03 from a greater depth is much higher than of sample Od02. The smallest E is seen for the sample taken from the upper part of the sedimentary layers (Od01). E increases with increasing depth.

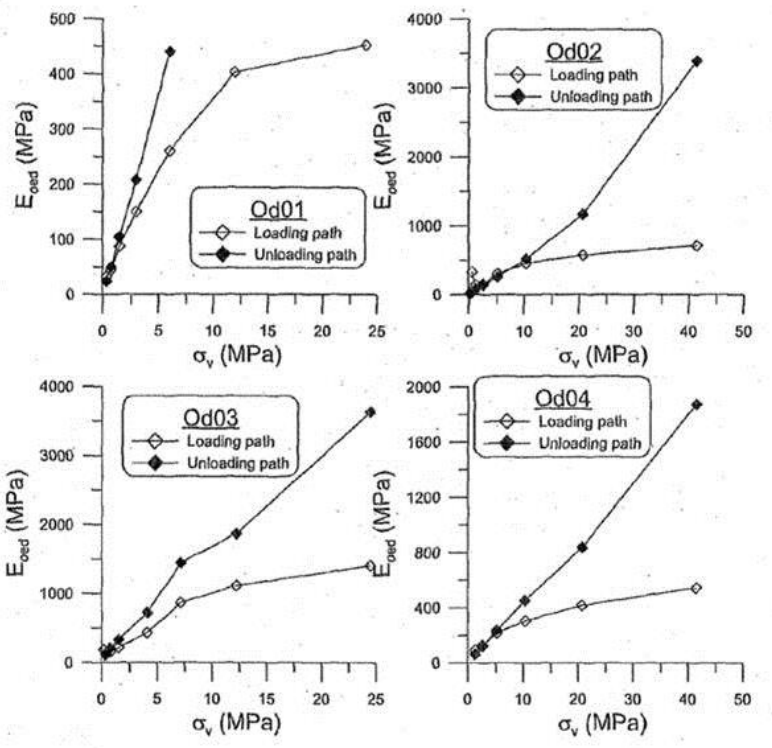

Figure 4-7:
Uniaxial pressure (compression) tests: dependency of Young's modulus on vertical stress (Tang et al. 2010).

In addition, uniaxial compression tests (oedometer tests) were carried out using NaCl solution which has a similar electrical conductivity as the in-situ pore water. The results allow determining the dependency between void ratio and permeability (Figure 4-8). In the core sample from a depth of 23.1 m, the hydraulic conductivity rises from 10^{-10} m/s to 10^{-9} m/s, whilst the void ratio rises from 0.2 to 0.25. In the sample taken from a depth of 78.4 m, the hydraulic conductivity increases from $2.1 \cdot 10^{-11}$ to $4.1 \cdot 10^{-10}$ m/s, alongside an increase in the void ratio from 0.26 to 0.32 (Tang et al. 2010).

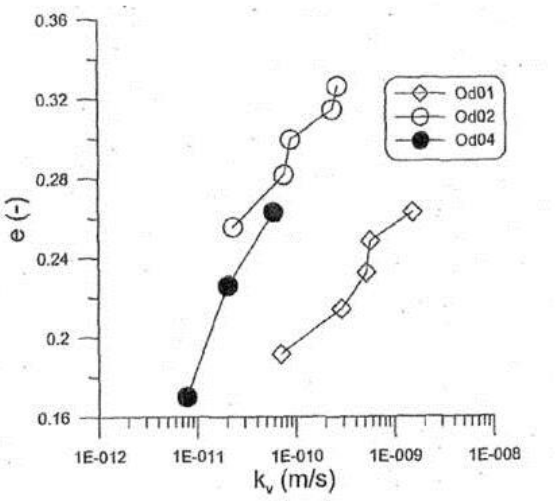

Figure 4-8:
Uniaxial high pressure (compression) tests: dependency of permeability on the void ratio (Tang et al. 2010).

The failure or tensile strength of the Blue Clays was evaluated on the basis of uniaxial experiments. A comparison was made between the failure of the Blue Clays within and outside of tectonically disturbed zones. The deformation properties of the clays largely depend on the depth and the fracturing of the rocks. The shear strength and Young's modulus of the Blue

Clays were measured on samples from various depths, and taking into consideration various degrees of fracturing (Daschko et al. 2011). The Young's modulus in the upper part of the sedimentary layers (down to 15 - 20 m depth) is 15 MPa to 25 MPa. Triaxial compression tests revealed that the failure, characterised by the cohesion value, is 0.3 MPa - 4 MPa at a friction angle of 8° - 10°. The coherence is much lower in the deeper zone than in the upper part (down to 25 m). This is due to the higher fracturing in the upper part of the horizon. The degree of fracturing of the rocks has a clear influence on the deformation behaviour of claystones. The degree of deformation is low when there is a higher tensile strength (failure) and when the stress is applied parallel to the bedding. The deformation behaviour is ductile when the failure is low and the stress is applied orthogonal to the bedding (Schulze 2009).

The relationship between the deformation properties of clays and the fracturing was investigated by Plechkova (1997) and Daschko et al. (2011). They determined that the deformation had a brittle-plastic character in the upper part of the layer (10 - 20 m interval). The relative deformation decreases down to 3.5 - 5.5% at a depth of 20 - 40 m, but the deformation character still remains brittle-plastic. The character of the deformation is brittle below a depth of 40 m where there is no longer any decompression (Pereverzeva et al. 2008).

4.6 Comparison of the Leningrad region clays with other clay formations

The physical properties of the argillaceous host rocks in the Leningrad region are similar to other claystones studied in Lithuania, Belgium and United Kingdom for the construction of repositories (see comparison in Table 4-1 and Table 4-2). The average values of the main parameters of the Leningrad Blue Clays vary only slightly from those of the clay formations in other countries used as a comparison (see Table 4-1 and Anderson et al. 2006).

Table 4-1: Comparison of some properties of Clays (Cyziene et al. 2005 in Kühnlenz & Hammer 2014).

Parameter	Blue Clays in the Leningrad region	Blue Clays (Lithuania)	Boom Clay (Belgium)	Oxfordian Clay (UK)
Density (kg/m^3)	1960 - 2310	2200 - 2250	1900 - 2100	2210
Porosity (%)	26 - 35	17 - 28	33	30
Strength (MPa)	0.3 - 4	0.7 - 1.2		
Water content (mass-%)	11 - 24		15 - 22	16
Hydraulic conductivity (m/day)	10^{-5}		10^{-7}	$5 \cdot 10^{-7}$

Table 4-2: Comparison of physical and geomechanical properties of clays from the Leningrad region and from Northern Germany (Daschko & Volkova 2004, Gerardi 2005, Hoth et al. 2007, Müller et al. 1987, Pereverzeva et al. 2008, Schnier 1986 a,b and 1987, Tang et al. 2010, Wittke 1991).

Formation	Density (saturated) (kg/m^3)	Hydraulic conductivity (m/d)	Failure strength (MPa)	Young's modulus (MPa)	Water content	Porosity (%)
Kotlin Clays (Vendian)	2120 (0 - 20m 2340 (bottom)	$4.8 \cdot 10^{-7}$ ($5.56 \cdot 10^{-12}$ m/s)	Cohesion 4.61; angle of friction 23°	72	19.8% (top) 10.2% (bottom)	23-28
Blue Clays (Cambrian)	1960-2220 (0 - 40 m) 2120-2280 (< 40 m)	Vertical: $7.6 \cdot 10^{-6}$ ($8.8 \cdot 10^{-11}$ m/s) Horizontal $1.8 \cdot 10^{-5}$ ($2.08 \cdot 10^{-10}$ m/s)	Cohesion 0.3-4; angle of friction 8°-10°;	15-25 (15-20 m)	23-28% (top); 15-18% (depth 40 m)	30
Lower Cretaceous (Northern Germany)	2350 (Middle and Lower Albian); 2450 (Hauterivian); 2420 (Barremian - Hauterivian)	$8.6 \cdot 10^{-8}$ m/day = $1 \cdot 10^{-12}$ m/s	Cohesion 3.2-4.14; angle of friction 29.3-30.6° (Barremian-Hauterivian)	5010-10750 (Barremian-Hauterivian)	Barremian 0.7-6.7 Wt%; average 5.6+/-1.1 Wt%	7 (effective) (Hauterivian) 15.5 (effective) (Barremian)

4.7 Special geological characteristics to be considered

The conditions for the planned repository at the Sosnovyi Bor site in the vicinity of St. Petersburg primarily deviate on the grounds of the shallow depth (< 100 m) from already existing repository concepts in deep clay formations, e.g. in the Swiss Opalinus Clay, or in the Jurassic claystones of the Paris Basin. The information already gained on final disposal in deep clay formations can only partially be extrapolated to shallow clay formations, which means that many parts of the concept need to be adjusted to suit the specific site conditions. Consideration here must be given to the site geology, as well as the specifications of the waste, to estimate the amount of gas which may be produced and to deduce the relevant transport paths. High gas production (Mönig 1998) and a low rock pressure must be taken into consideration in the description of the transport paths and the geomechanical calculations.

The Blue Clays of the Leningrad region are a relatively thin barrier (< 100 m). This means that a particularly important role is played in the planned repository by the technical and geotechnical barriers. The part of the rocks providing the containment lies between two aquifers which need to be given special consideration when designing the layout and the concept. A special barrier system needs to be designed under the given conditions of a position between two aquifers (Rumynin 2011).

The following geological aspects need to be taken into special consideration especially when elaborating a final repository concept for the Sosnovyi Bor region (Figure 4-9, Rumynin 2011):

- The aquifers below and above the host rocks (the Vendian Gdovsk aquifer and Lower Cambrian Lomonosov Horizon)
- Fracturing of the host rocks (Kotlin Clays, upper part of the Blue Clays)
- Increase in sand content in the Kotlin Clays towards the base
- Decompaction (deconsolidation) of the Kotlin Clays towards the top
- Paleochannels above the planned repository zone.

The Lower Cambrian Blue Clays have a less favourable mineralogical composition compared to the Vendian claystones because of their high concentration of illite (and in parts glauconite). Illite has a low swelling capacity compared to e.g. montmorillonite. The Blue Clays and the Kotlin Clays have high anisotropies with regard to their composition and their properties, which is primarily attributable to numerous sandy intercalations.

The fractured block structure primarily attributable to decompression and/or pressure release in the shallow horizons, found in the upper part of the Cambrian Blue Clays, can also be a restricting factor. Claystones with hydraulically permeable fractures must be excluded when selecting a repository site because they fail to meet the criterion for low permeability (Lux et al. 2005).

The Kotlin Clays lie between two aquifers: the Lomonosov Horizon (Cambrian) above, and the Gdovsk Horizon (Vendian) below. Raised chloride concentrations have been proven in the groundwater in the Lomonosov Horizon. This increases the aggressiveness of the water with respect to metallic repository components. The Gdovsk Horizon below the planned repository is used to supply water in the region. Moreover, this Vendian groundwater horizon contains artesian groundwater, and is characterised by an instable hydrodynamic regime. This is why the safe containment of the radioactive waste – particularly with respect to aquifers, plays a significant role in evaluating the safety and the development of the repository concept.

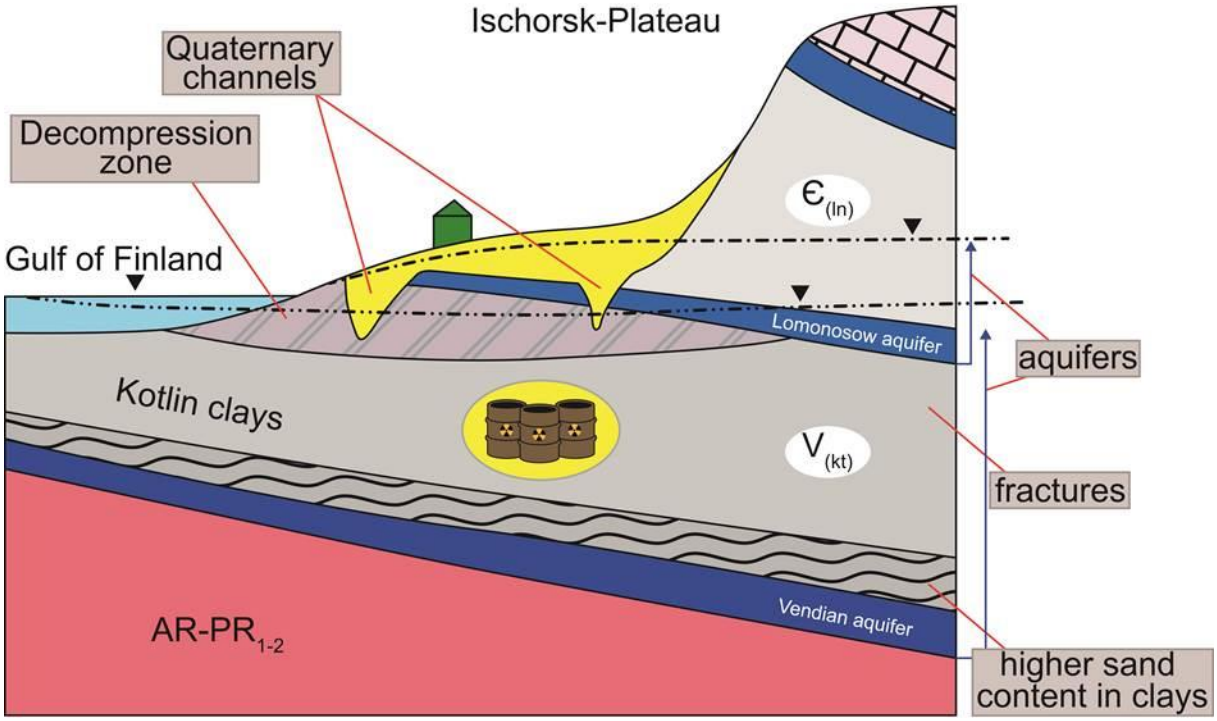

Figure 4-9: The topics which need to be taken into consideration especially in the long-term safety evaluation for the planned repository in the clays of the Leningrad region (Rumynin 2011).

The region is characterised by low tectonic and seismic activity. However, special regional features such as the block structure of the crystalline basement, the existence of regional fault zones, and neotectonic movements of individual geotectonic blocks needs to be taken into consideration when carrying out the subsequent long-term safety evaluation. Areas with fault zones in the underground and the boundary regions between structural blocks need to be excluded when selecting a site for the construction of a repository. The zones with deeply weathered or fractured clay horizons must also be excluded from the site selection process to avoid the risk of radionuclide migration along fractures or fault zones.

Based on the partly sub-optimal geological conditions, a special role will have to be played by engineered barriers. They have to be designed to compensate for any deficits in the clay rocks, and to ensure the safe isolation of the radioactive waste (Anderson et al. 2006).

5 Repository concept

5.1 Radioactive waste inventory

The Leningrad region hosts a large number of facilities and research institutes that generate radioactive waste. It also hosts radioactive waste storage facilities, such as for example the LNPP and LSK Radon. Due to the fact that a solution for disposing of the radioactive waste generated in the region is needed, efforts to implement a waste repository in the region have been made since some years ago. As a results of these efforts, the Technical Assistance to the Commonwealth of Independent States (TACIS) project “Concept and programme for the realization of a radioactive waste repository for short-lived low- and intermediate-level waste in the Leningrad Region” was implemented in the nineties with the general objective of preparing sound basis for decisions that the Russian authorities shall make in regard to the implementation of a future L/ILW disposal facility in the Leningrad region.

In the course of the above mentioned TACIS project (Consortium DBE/ANDRA/NDA/SKB 2008), information regarding the amount and characteristics of radioactive waste generated by the main waste producers was collected and a forecast regarding the future volumes of generated radioactive waste was provided. In total it was estimated that ca. 250,000 m³ of L/ILW, containing the main part of this waste radionuclides with a half-life of 30 years or less, will be generated in the Leningrad region. This estimation included the waste arising from the decommissioning of LNPP reactors. In addition, the types of containers qualified in the Russian Federation for the disposal of radioactive waste were also identified.

It shall be noted that in the course of the TACIS project major deficiencies in regard to the quality of the collected data were identified, in particular in regard to data related to the content of radionuclides and other safety relevant materials. These deficiencies derived in significant uncertainties in regard to the potential suitability of part of the waste streams for being disposed of in a near surface repository. For this reason, it was suggested to carry out further waste characterization investigations before disposing of the radioactive waste in the foreseen near surface repository.

5.1.1 Radioactive waste streams

The information provided by the results of the TACIS project (Consortium DBE/ANDRA/NDA/SKB 2008) was received from OSCJ VNIPIET in response to a detailed questionnaire, which was completed with data from former TACIS projects. Saint Petersburg and the Leningrad region is a major scientific and industrial centre, where hundreds of industrial, research and development (R&D), medical and other institutions that generate liquid and solid radioactive waste are located. According to Consortium DBE/ANDRA/NDA/SKB (2008), the main radioactive waste producers in the region are:

- The LNPP, which included four power units High Power Channel-Type Reactor (RMBK)-1000 that will be decommissioned in the near future and, therefore, will generate significant amount of decommissioning radioactive waste. It is also foreseen that four[1] new reactors (two of them are currently being constructed) will start their operation in the next years, which will therefore generate additional radioactive waste.
- The LSK Radon, which is a regional centre for radioactive waste collection, processing and storage. It has been in operation since 1962 and receives radioactive waste from enterprises and institutions in Kaliningrad, Novgorod, Pskov and other regions including Karelia and Komi.
- R&D Technological Institute, which is currently named A. P. Aleksandrov (RDTI).
- CJSC “Ekomet-C”, which is specialized in processing radioactive metallic wastes.

[1] http://www.world-nuclear.org/information-library/country-profiles/countries-o-s/russia-nuclear-power.aspx

Taking into account that the final conditioning and storage of the radioactive waste will only take place at the LNPP and LSK Radon sites, it is expected that these two enterprises will be the ones that will deliver the radioactive waste that shall be disposed of in the future repository. According to the results of the TACIS Project (Consortium DBE/ANDRA/NDA/SKB 2008), the total unconditioned radioactive waste generated in the Leningrad region until the year 2030 was estimated to be 209,000 m³ (including the waste resulting from the decommissioning of two RBMK reactors at the LNPP). Most of this waste (over 90%) will be L/ILW-SL containing mostly radionuclides with a maximum half-life of 30 years.

5.1.2 Conditioned radioactive waste

In addition to the information on unconditioned waste presented above (see chapter 5.1.1), the results of the TACIS project (Consortium DBE/ANDRA/NDA/SKB 2008) also provided data on the characteristics as well as on the number of the packages that will contain conditioned radioactive waste and will be generated until 2020 in the Leningrad region. These estimations concluded that 15,880 containers containing conditioned radioactive waste will be generated at LNPP and LSK Radon sites until 2020, which in total will have a total volume of 63,370 m³. Additional information in regard to the total number of containers containing conditioned radioactive waste that will be generated until 2020 is provided in Table 5-1.

Table 5-1: Projection of expected amount of conditioned wastes at LNPP and LSK Radon generated until 2020 based on Consortium DBE/ANDRA/NDA/SKB (2008).

Producer	Container	Type of conditioned waste	Specific activity [kBq/kg]	Radionuclide composition	Containers until 2020	Total volume until 2020 [m³]
LNPP	ZshZK-1	Solid (compacted) LLW	< 10^3	^{60}Co, ^{54}Mn, ^{55}Fe, ^{137}Cs, ^{134}Cs, ^{95}Nb	4400	49320
	ZshZK-2	Solidified (bituminised) waste	10^3 - 10^7	^{60}Co, ^{54}Mn, ^{55}Fe, ^{90}Sr, ^{137}Cs, ^{134}Cs, ^{95}Nb	7200	
		Solid (compacted) ILW	10^3 - 10^7	^{60}Co, ^{54}Mn, ^{55}Fe, ^{137}Cs, ^{134}Cs, ^{95}Nb	360	
		Solid (metallic) ILW	10^3 - 10^7	^{60}Co, ^{54}Mn, ^{55}Fe, ^{137}Cs, ^{134}Cs, ^{95}Nb	72	
LSK Radon	NZK-MR	Bituminised LLW	β, γ-emitters: <$1{\cdot}10^6$	β, γ- emitters: ^{137,134}Cs: 80% ^{90}Sr: 5% REM: 5% ^{60}Co: 10%	444	14050
		Bituminised ILW	β, γ-emitters: from $1{\cdot}10^6$ to $8.4{\cdot}10^7$		132	
		Solid LLW in metal drums	β, γ-emitters: <$1{\cdot}10^6$ α- emitters: < $7.4{\cdot}10^3$	β, γ- emitters: ^{54}Mn: 1-2% ^{59}Fe: 2-3% ^{60}Co: 5-7% ^{65}Zn: 1-2% ^{90}Sr: 10-15% ^{95}Zr: 10-15% ^{95}Nb: 10-15% ^{106}Ru: 1-2% ^{134}Cs: 1-2% ^{137}Cs: 10-15% ^{144}Ce: 5-7% ^{147}Pm: 10-15% α- emitters: ^{210}Po: 5%; ^{238}Pu: 10% ^{239}Pu: 80%; ^{226}Ra: 5% ^{241}Am: 1%	2928	
		Solid ILW in metal drums	β, γ-emitters: from $1{\cdot}10^6$ to $1.16{\cdot}10^8$ α- emitters: < $7.4{\cdot}10^3$		348	
TOTAL					**15880**	**63370**

According to Consortium DBE/ANDRA/NDA/SKB (2008), NZK-MR containers consist of reinforced concrete structures of parallelepiped shape containing solidified L/ILW (cemented and bituminized in drums or in initial packages or without them). ZshZK-1 and ZshZK-2 consist of reinforced concrete shielding containers containing 200 l metal drum-packaged low-level solid radioactive waste. Detailed information regarding the characteristics and the design of the containers can be found in Consortium DBE/ANDRA/NDA/SKB (2008).

5.2 Conceptual design for the repository

The conceptual design for the repository that has been considered for the development of the sealing concept was developed in 1997 by a Consortium formed by the companies IVO POWER ENGINEERING LTD., SGN and AEA TECHNOLOGY in the framework of a TACIS project financed by the European Union (Consortium SGN/IVO/AEA 1997-A).

According to the results of the above mentioned TACIS project (Consortium SGN/IVO/AEA 1997-A), the general purpose of the proposed repository concept is to isolate all L/ILW generated in the Leningrad region (including St. Petersburg) from the biosphere for as long as the results of the safety assessments show that they are hazardous to the environment and to the health of the members of the public (300 years are typically considered for this type of facilities).

Based on the results of the site investigations, it was decided to envisage the repository in the middle of the Kotlin Clay formation. However, the proposed concept for the repository was developed taking into consideration the geological conditions of the “Koporje site”. The conceptual design foresees that the radioactive waste will be transported to the repository through a transport tunnel (ramp) that will connect the underground disposal areas with the facilities located on the surface of the site. Moreover two ventilation shafts (fresh and exhausted air shafts) will also connect the underground openings with the surface.

The construction of the repository is planned to be carried out in different phases. In the initial construction phase, five disposal drifts in the first disposal area, one drift to store auxiliary and service systems and all galleries necessary for the normal operation of the repository (e.g. access, working and maintenance galleries, etc.) will be constructed (see Figure 5-1). In further construction phases, the construction of the disposal drifts in the first disposal area will be completed and the second disposal area will be constructed. In total 44 drifts will be constructed inside the repository. The first disposal area will consist of 13 disposal drifts and 1 drift to store auxiliary and service systems. The second disposal area will consist of 30 disposal drifts (see Figure 5-2).

According to the results of the TACIS project (Consortium SGN/IVO/AEA 1997-A), all disposal drifts will have the same dimensions. They will have a width of about 25 m, a height of about 13 m, and a total length of approximately 100 m (see Figure 5-2). Moreover, each access to the disposal drifts will have a length of 10 m and diameter of 8.5 m. The distance between two disposal drifts will be 44 m. The working galleries will have the same diameter as the access galleries (i.e. 8.5 m). The transport tunnel will have an internal diameter of about 5.6 m (including a lining with a thickness of about 15 cm), a length of approximately 310 m and will connect the mine openings with the surface (at approximately 30 m above the underground openings). Finally, the ventilation shafts will have a diameter of 6 m and a depth of approximately 100 m.

It shall be noted that due to the plastic nature of the Kotlin Clay, it is expected that liner systems will be built in all underground openings (including the shafts) to provide mechanical support. Detailed information in regard to the thickness of the liner in the different under-

ground openings is provided in the conceptual design developed in the course of TACIS project (Consortium SGN/IVO/AEA 1997-A).

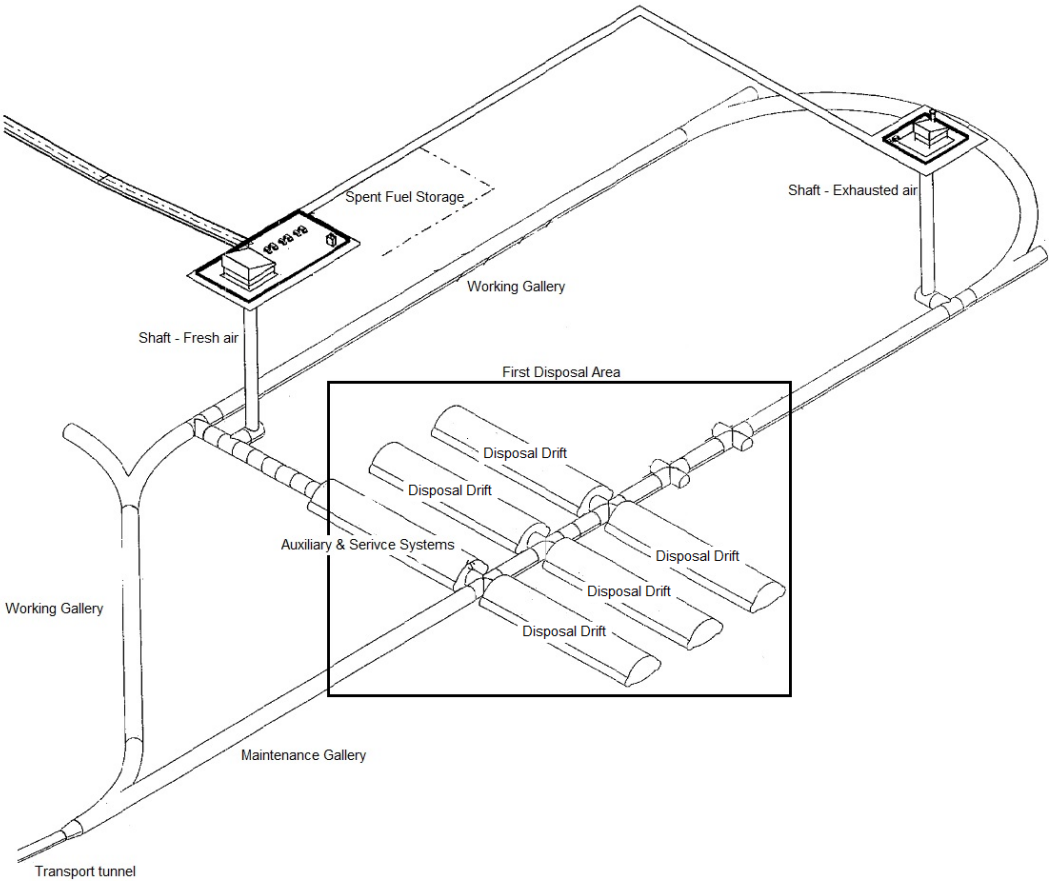

Figure 5-1: Representation of the repository after completion of the initial construction phase based on the results of the TACIS project (Consortium SGN/IVO/AEA 1997-B).

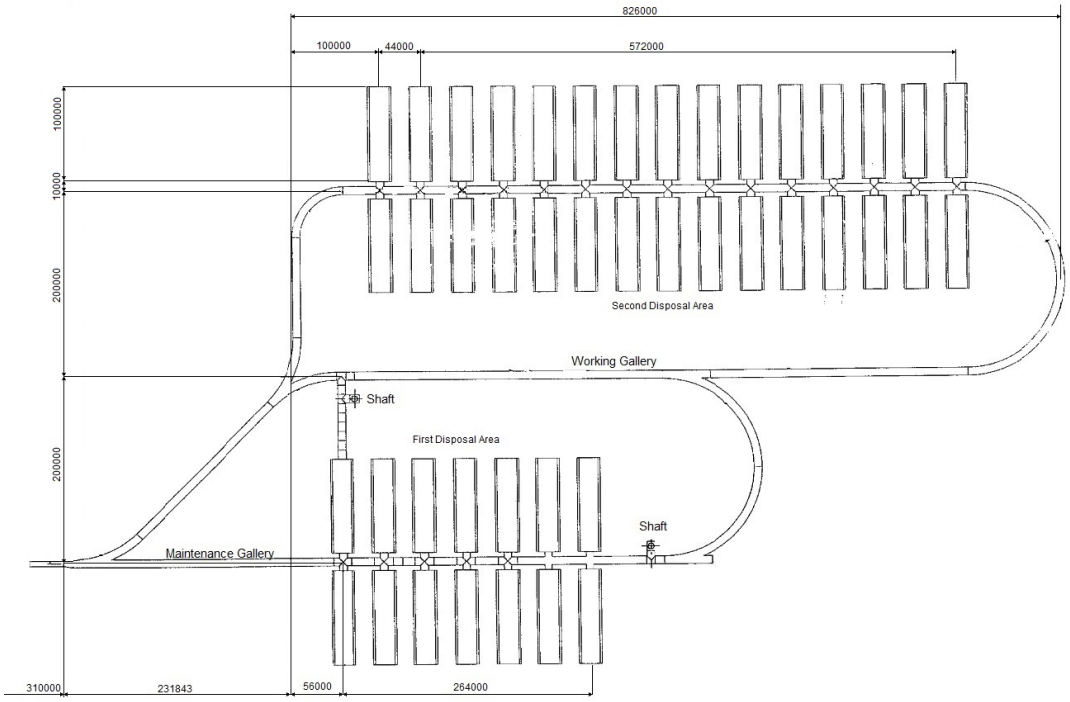

Figure 5-2: Overview of the repository after completion of all construction activities based on the results of the TACIS project (Consortium SGN/IVO/AEA 1997-B) (measures are provided in mm).

6 Sealing system

6.1 System elements

Based on the results of large-scale tests as well as on the existing experience, nowadays various sealing materials are considered to be suitable for sealing L/ILW radioactive waste repositories in clay formations. In order to ensure that performance of the sealing materials contributes to fulfil the safety functions of the engineered barrier system (EBS), the suitable sealing materials shall be long-term stable and compatible with the chemical properties of the host rock and of pore water.

In order to ensure the compliance of the repository multi-barrier system with the principles of redundancy and diversity, the sealing concept proposed for the L/ILW repository at the “Radon Site” (see chapter 6.2) includes different sealing elements at different repository locations. The sealing elements have been designed taking into consideration the hydraulic, mechanical, thermal and chemical requirements as well as the expected impacts at the specific sealing locations. The following subchapters of the present document provide a short overview of potential materials that can be used to seal radioactive waste repositories in clay formations.

6.1.1 Bentonite elements

Bentonite is a general term used for various swellable clay minerals with a content of montmorillonite higher than 50%. The swelling properties of bentonite result from the ability of this material to store water molecules between the layers of the clay minerals, leading this water storage to a volume expansion or a pressure increase. In addition, bentonite minerals have a high sorption capacity of radionuclides.

Bentonite is a long-term stable sealing material that has properties similar to those of the host rock (i.e. clay) and that will successfully perform during the required functional period. For these reasons bentonite is used in the mining industry and in radioactive waste repositories as sealing material in drifts and shafts. In the specific case of vertical openings such as shafts or boreholes, a high dry density and good connection to the host rock can be achieved if lose bentonite is compacted in situ. This stepwise installation and compaction allows the construction of long sealing elements, the technical feasibility of which has been already demonstrated in different large-scale in-situ experiments carried out in different countries such as the German R&D project “Shaft seal Salzdetfurth” (Breidung 2002) and the Belgium project “RESEAL 2” (Van Geet et al. 2009).

In horizontal openings such as drifts, pre-compacted bentonite blocks are used. They enable the filling of the free cross-section to a high degree and their high density minimizes potential settlements after installation of the sealing element, which reduces the risk of void spaces at the roof of the drift. Void spaces between the blocks or between the blocks and the host rock can be filled and compacted with lose bentonite. Moreover, the shape of the blocks can be adjusted to the requirements and conditions at the sealing locations. The general feasibility of pre-compacted bentonite blocks for sealing underground horizontal openings has been already demonstrated by the results of different experiments such as the Canister Retrieval Test carried out in Sweden (Dueck et al. 2011) and the large scale in situ tests carried out in the Salzdetfurth and Sondershausen salt mines in Germany (Gruner et al. 2008).

Finally, it shall be noted that the performance of bentonite sealing elements can be optimized by integrating equipotential elements that will allow a homogeneous wetting during the saturation of bentonite. Equipotential elements are made of a material with high capillary rise such as for example sand with a low component of clay or silt. According to Schumann et al. (2009) they are suited for shaft and drift sealing purposes in underground repositories.

6.1.2 Bitumen and asphalt elements

Bitumen is a low volatile residue that is composed of a colloid-disperse mixture of different hydro carbonates generated during the distillation of mineral oil.

At room temperature and atmospheric pressure bitumen has a density of 1000 to 1060 kg/m³ and is solid. However, the addition of mineral aggregates allows the modification of its density and viscosity. By increasing its temperature, its viscosity increases and liquid characteristics become more important.

Bitumen is insoluble in and impermeable to water. It is widely stable against most acids, aggressive solutions, salts and bases. However, organic solvents, such as benzene or toluene, can solve bitumen. Bitumen has low specific heat capacity (1.7 – 1.9 J $kg^{-1}K^{-1}$ at 0 - 200°C) and low thermal conductivity (0.16 $Wm^{-1}K^{-1}$), and its long-term behaviour is shown, for example, in asphalt lakes. Moreover, bitumen is also long-term stable against radiation (Burkhardt & Egloffstein 1995) and shows small microbiological degradation (Wolf 1989).

Bitumen can be classified into different categories according to its production process, its use and its properties. From the point of view of the production process, bitumen can be classified into bitumen produced as result of distillation, oxidation (hardened), high vacuum or polymer modified bitumen processes. Distillation bitumen is the residue from mineral oil distillation and is the simplest type of bitumen. Oxidation of the bitumen causes the bitumen to become less temperature-sensitive and increases its viscosity, having oxidized bitumen higher hardness than distillation bitumen.

Bitumen is used as redundant and diverse sealing material to bentonite. While bentonite needs some time for water intake to fully develop its sealing properties, bitumen achieves full sealing properties directly after its installation.

6.1.2.1 Pure bitumen elements

The installation of bitumen is possible under both cold and hot conditions. Hot bitumen (up to 190°C) is liquid and can be easily casted into prepared sections. During the cooling process, the viscosity increases and bitumen becomes solid. Under constant loads and during long periods, bitumen reacts like a fluid, which allows bitumen flowing into remaining gaps and potential cracks, for example into the excavation damaged zone (Jobmann 2016).

The impermeability of bitumen as well as its good adhesion allows achieving a low integral permeability at the sealing location using thin sealing elements. Bitumen is not mixable with water. For this reason and due to its lower density, during water intake from below, bitumen stays at the top of the water column. To avoid shifting between water and bitumen in case of water intake from the top, it is possible to weight the bitumen with filler (finest aggregates).

Finally, it shall be noted that the combination of different types of bitumen is generally possible.

6.1.2.2 Bitumen filled gravel elements

For sealing purposes over large lengths or depths, especially in shafts, it is possible to combine bitumen and gravel (crushed rock) into one sealing element (Glaubach et al. 2016). The main material used to fill and seal the cross-section of the mine opening is the gravel, which among other characteristics has a high porosity of approximately 30 to 40%.

After the successful installation of the layer of gravel, the remaining pores can be filled using hot bitumen with high fluidity and good wetting properties that will penetrate into the excavated EDZ and will allow the complete and immediate sealing of the cross-section of the underground opening.

6.1.2.3 Mastic asphalt elements

Mastic asphalt is mainly composed of 35 to 55% of aggregates, 20 to 30% of filler, and approximately 7 % of bitumen. However, the exact mixture depends on its application. Mastic asphalt is mainly used in road construction and civil engineering and their sealing properties are well known from the closure of mine shafts.

Under hot conditions (up to 230°C) mastic asphalt is still spreadable and pourable, which allow, despite its high content of solids, an easy installation. During its installation, compaction of the mastic asphalt is not necessary. Moreover, during temperature change, slow load rates or constant loads, the viscoelastic properties of mastic asphalt allow preventing cracks.

Mastic asphalt is usually used as an immediate effective seal material that is complementary to clay or bentonite sealing elements.

6.1.3 Concrete sealing elements

Concrete is a composite material mainly composed of fluid cement, additives and water, which hardens over time.

Various international investigation programs assessing the suitability of cement-based sealing elements for repositories in clay and crystalline formations are currently ongoing. Examples of these investigations include the project “Full-scale Demonstration of Plugs and Seals” (DOPAS) (Hansen 2015), with the “Dome Plug Experiment” (DOMPLU) and “Deposition Tunnel End Plug Experiment” (POPLU), the "Tunnel Sealing Experiment" (TSX) (Guo et al. 2005) and the experiment “Enhanced Sealing Project” (ESP) in Canada (Martino et al. 2011).

6.1.4 Abutments

Abutments have the main functions of limiting the potential deformation of sealing elements and of holding the sealing elements in their place. To fulfil these functions, abutments are usually made of concrete, which have high resistance against mechanical loads. The presence of tensile stresses in the concrete structure can be avoided by selecting an adequate abutment form. For example, in addition to the typical cylindrical shape of the shafts and drifts, other designs for the abutments such as multiple-geared abutments or truncated cone abutments are possible. However, it shall be noted in order to avoid unnecessary sources of complications, it is recommended to keep the design of the abutments as simple as possible.

According to the current state-of-the-art, concrete abutments are made of non-reinforced concrete. In this way the gas generated inside the repository due to the corrosion of the steel is minimized. To replace reinforced concrete, other options such as fiberglass reinforcement is currently being considered; however this option still requires substantial additional research and development effort.

The selection of the cement and the aggregate is determined by the required strength of the abutments as well as by other requirements (e.g. chemical, etc.) and constraints. Moreover, the abutments are usually located directly next to bentonite sealing elements in order to provide sufficient stability to them,

Interactions between cement, clay minerals and pore water are primarily expected in the presence of water with a pH value higher than 11. A prerequisite for the formation of such water is the access of pore water and the onset of cement corrosion in the existing geochemical environment. In order to minimize these interactions, it is recommended to use non-alkaline non-reinforced concrete containing portlandite (low pH concrete) (NEA 2012). Low pH concrete has higher density, and because of the characteristics of pozzolanic additives that contains, it also has lower permeability than conventional concrete. The lower permea-

bility is relevant because is usually associated with lower susceptibility to cracking. The combination of these properties leads to a reduction of the amount of fluid that will flow through the concrete and therefore may prevent the corrosion of the concrete.

The technical feasibility and functionality of abutments made of low pH concrete has been demonstrated in the framework of the European ESDRED project “Engineering Studies and Demonstration of Repository Designs” (Andra 2005, Alonso et al. 2008). Moreover, in the framework of other international repository projects, abutments made of low pH concrete are also foreseen.

The potential interactions between cementitious materials, the host rock and the backfill material in an underground repository in a clay formation still need to be quantitatively assessed. For example, it shall be assessed how potential chemical interactions may affect the long-term stability and functionality of the cementitious materials, the behaviour of the materials and their corrosion, and the development of the backfill material.

6.1.5 Backfill

In order to limit the deformations of the host rock, one basic requirement for the closure of the repository is the complete backfilling of all mine openings. All parts of the drifts and shafts, that are not equipped with sealing elements, shall be backfilled. Backfill materials have three main functions. First of all, they shall isolate the radioactive waste by acting as an extra barrier to the waste. Moreover, they shall provide stability to the mine openings, avoiding in this way their potential collapse. It shall be noted that such a collapse may lead for example to an enlargement of the EDZ around the disposal drift and may also damage the waste disposal packages. Finally, it shall reduce the hydraulic conductivity of the underground openings and, therefore, it shall have similar hydraulic properties to those of the clay formation. It shall be noted that backfill materials may in some cases also fulfil sealing functions.

One potential solution is to use excavated material, which is available in huge amounts and has comparable chemistry to those of the host rock, as backfill material. This option can reduce the costs related to the transport of material and will reduce the stock of material stored on the surface of the repository. Other typical backfill materials used are gravel or crushed rock, which can also provide mechanical stability to the underground openings.

The backfill material is usually dropped into the drift and, if necessary, it is compacted. Materials of small grain size can be backfilled, for example, using slinger trucks. If the backfill material has a fine grain structure, pneumatic installation is also possible. Hydraulic installation (pumping) is typically used for the installation of concrete-based or slurry backfill material.

Special admixtures like high performance concrete, self-compacting concrete, or the addition of pozzolanic content can be used to low the permeability of the backfill material. The substitution of cement by pozzolanic admixtures, such as silica fume, influences the permeability as well as the hydration heat of the backfill material. Silica fume has particle sizes smaller than one micrometre and a high content of reactive silica. The small grain size reduces the size of the pore and the higher reactivity of pozzolanic admixtures reduces the free water content and capillary pores. Silica fume does not reduce the porosity, but it changes the ratio of capillary to gel pores and, hence, the permeability of the concrete. The substitution of 5 to 10% of cement type I or II by silica fume can significantly decrease the hydraulic conductivity of the concrete. Finally, by adding silica fume, bleeding can be reduced and pumpability improved (Chan et al. 1999).

6.2 Conceptual design

In general, the long-term containment of the radioactive waste inside repositories located in clay formations is primarily ensured by the host rock. However, in order to ensure a successful containment of the radioactive waste, additional geotechnical barriers shall be properly designed and installed. The design of these barriers shall be developed taking into consideration the principles of redundancy and diversity. Moreover, the potential risks associated with the presence of the radioactive waste and the performance of the barriers over the time shall be considered. Thus, the long-term safety of the repository shall be ensured by a robust, reliable, passive, redundant, diversified and maintenance-free multi-barrier system that fulfils its overall function even though individual barriers fail to perform as expected.

The definition of the functional period of the sealing elements depends on the long-term development of the repository. For the L/ILW near surface repository at the “Radon Site”, taking into consideration the general purpose of the proposed repository concept (see chapter 5.2), the containment of the radioactive waste inside the repository shall be fulfilled for at least 300 years (Consortium SGN/IVO/AEA 1997-A).

Taking into consideration the above mentioned requirements as well as the characteristics of the repository site and the conceptual design for the repository (see chapter 5.2), the proposed sealing system will consist of the following elements:

- 44 disposal drift seals;
- 5 access drift seals; and
- 2 shafts seals
- 1 ramp seal

A schematic overview of the proposed locations for the sealing elements inside the repository is provided in Figure 6-1:

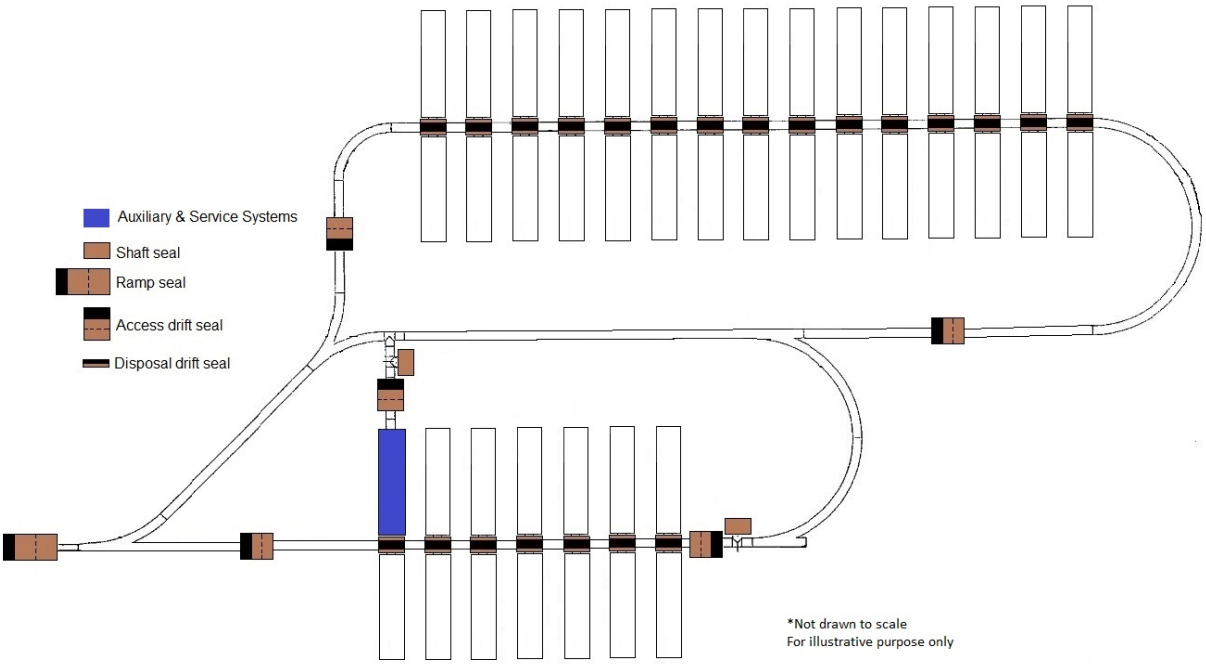

Figure 6-1: Overview of the proposed locations for the sealing elements inside the repository.

The sealing concept is based on the principle that any fluid coming from the surface shall always has to go at least through three seals (shaft or ramp seal, access drift seal and dis-

posal drift seal) before being in contact with the radioactive waste disposed of in the disposal drifts. A schematic view of the sequence of the sealing elements is provided in Figure 6-2. The same principle is applied to contaminated fluids that may potentially migrate from the disposal drifts to the biosphere.

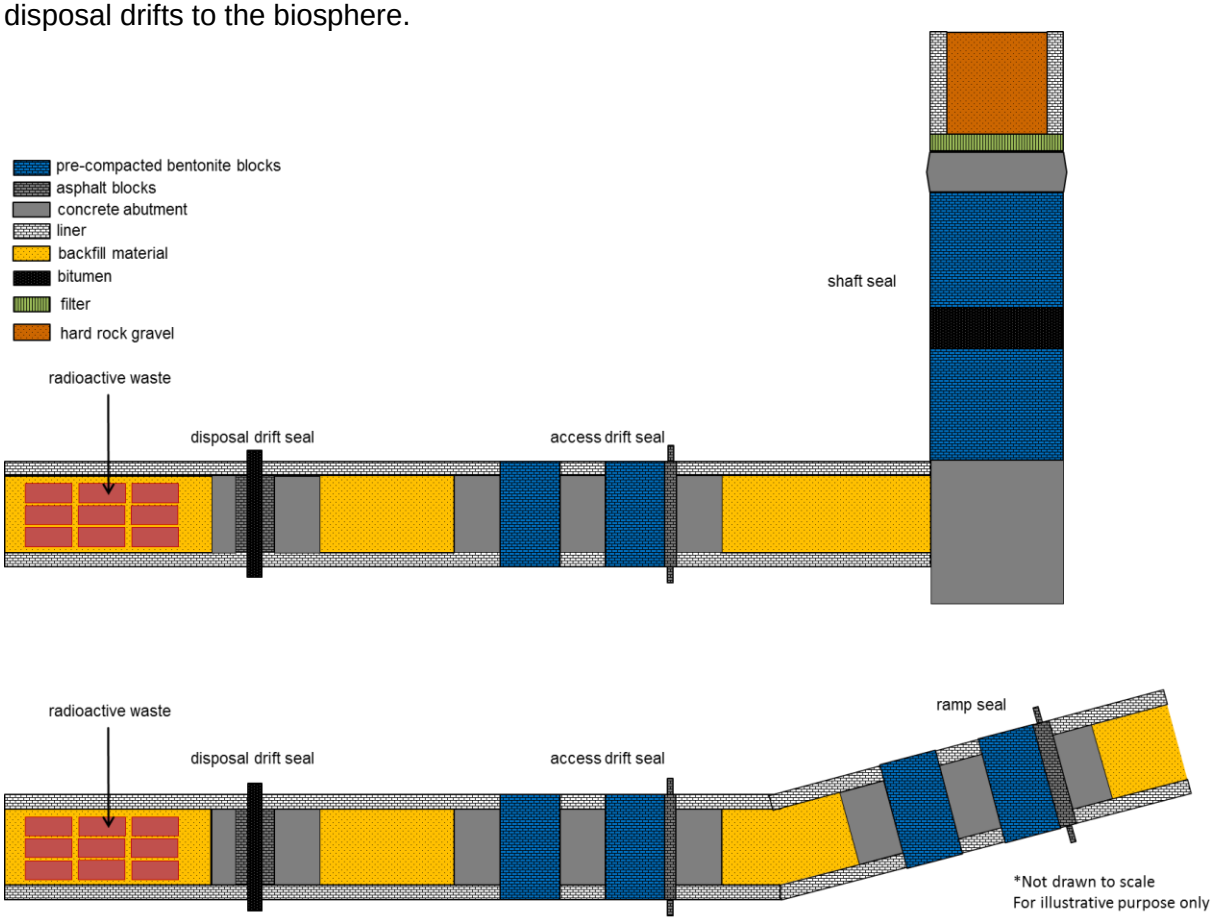

Figure 6-2: Schematic overview of the proposed sequence of sealing elements.

As already mentioned in previous chapters, the Kotlin Clay shows a good swelling capacity. For this reason and due to the fact that the excavated material will retain its properties and sufficient quantity of it will be available, it seems reasonable to use it to backfill the access drifts. However, if the amount of swellable minerals in the host rock does not provide an adequate swelling capacity to properly seal the underground openings, a mixture of other swellable clays and the excavated clay can be also used. Moreover, if required, sand can be added to the excavated material or to the mixture of swellable materials to modify the mechanical and the hydraulic properties of the backfill material.

Experiments with appropriate mixtures of recycled excavated material (Callovo-Oxfordian Clay) and bentonite (MX80) have been already carried out in the Underground Research Laboratory (URL) Bure (France) and have shown positive results (Zhang 2012). It shall be noted that before using a mixture containing previously excavated bentonite, the mixing proportions shall be adjusted taking into consideration the specific characteristics of the host rock.

For the specific case of the disposal drifts, the possibility of using a buffer material consisting of a mixture of clays with an increased swelling capacity shall be also considered. It shall be noted that the backfill material used in the disposal drifts shall fulfil a retention function against potential released radionuclides. This function shall be fulfilled already in early post-closure periods to effectively and instantaneously prevent the potential migration of radionu-

clides from a defective or damaged container and shall be ensured during the whole functional period of the sealing system.

6.2.1 Disposal drift seals

After backfilling, the disposal drifts shall be sealed. The main function of these seals is to minimize the potential migration of fluids from and to the disposal drifts. This function shall be fulfilled at least until the corresponding access drift seal completely fulfils its sealing functions. The functional period of the disposal drift seals shall be estimated in future phases of the present project by means of comprehensive process analyses.

To ensure the fulfilment of their function, the disposal drift seals shall be designed being compliant with the following requirements:

- *Hydraulic requirements*: The sealing elements shall effectively seal the disposal drifts against any fluid (gases and liquids), delaying in this way the potential migration of the fluids from and to the disposal drifts.
- *Mechanical requirements*: The sealing elements shall be stable under the expected pressure caused by the rock mass and by potential fluids.
- *Chemical requirements*: The sealing elements shall be chemically stable during their whole functional period.
- *Biological requirements*: The sealing elements shall have a sufficient resistance to microbial degradation at least during the functional lifetime of the barrier.

The disposal drift seals will be formed by two sealing elements made of asphalt that will surround an element made of bitumen (see Option 1 in Figure 6-3 and Figure 6-4). Moreover, these sealing elements will be surrounded by two abutments made of high strength non-reinforced concrete, which have the main function of keeping the asphalt and bitumen elements in place.

For further safety assessments it is recommended to estimate the potential gas production within each of the disposal galleries. If high gas pressure build ups are to be expected which may lead to an integrity failure of either the disposal drift seal or the surrounding host rock, the asphalt-bitumen module could be exchanged by a similar plug consisting of a bentonite-sand mixture which is tight against water but permeable to gas (see Option 2 in Figure 6-3 and Figure 6-4).

For safety reasons, during the operation of the repository, it shall be ensured that at least two accesses to the disposal area are always available. For this reason, and in order to allow disposal and closure activities to be carried out in parallel, it is assumed that after completing the disposal of radioactive waste in one disposal drift, this shall be closed in such a way that the access to the other disposal drifts is not limited (see Figure 6-3).

After completing the disposal activities in one disposal area, the abutments located in the access drifts will be further developed, forming a double abutment that will fill the cross section of the access drifts (see Figure 6-4). Assuming that the development of the pressure inside all disposal drifts will be similar, it is assumed that the presence of the double abutments will help to counterbalance the impact resulting from pressures in opposite disposal drifts.

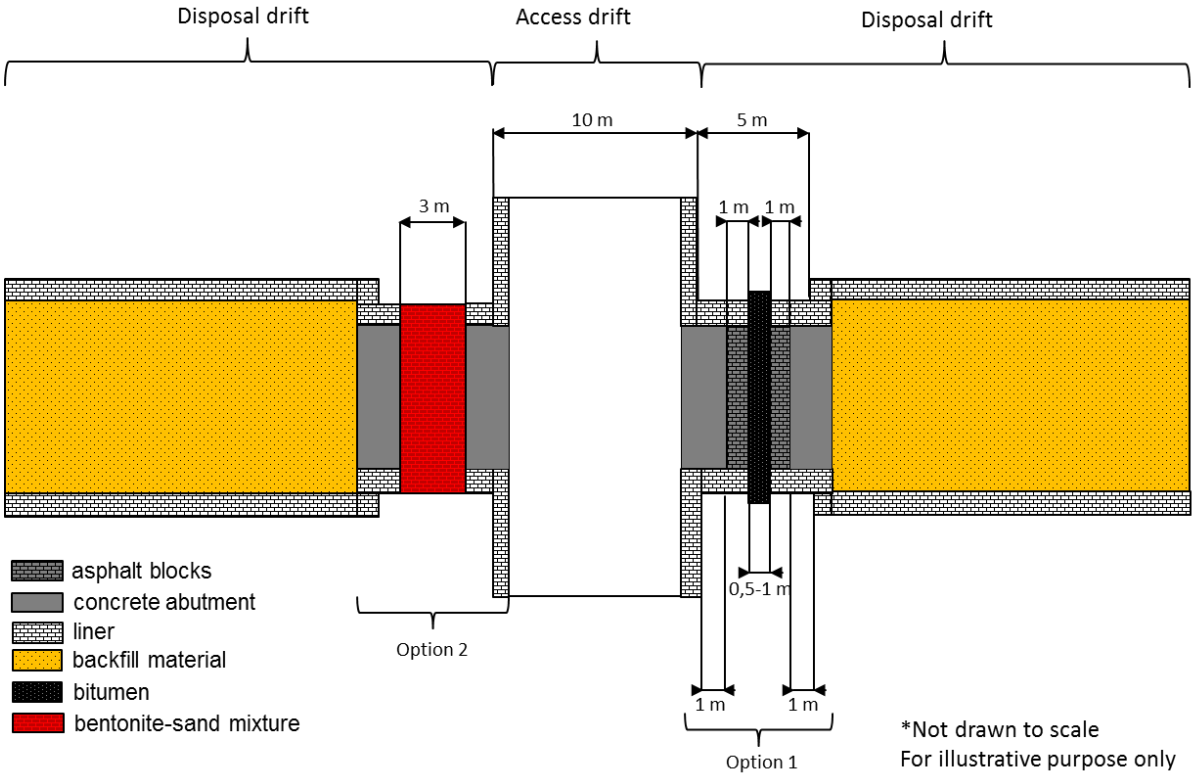

Figure 6-3: Overview of proposed disposal drift seal options during the operational phase (option 1: asphat/bitumen seal, right; option 2: bentonite seal, left).

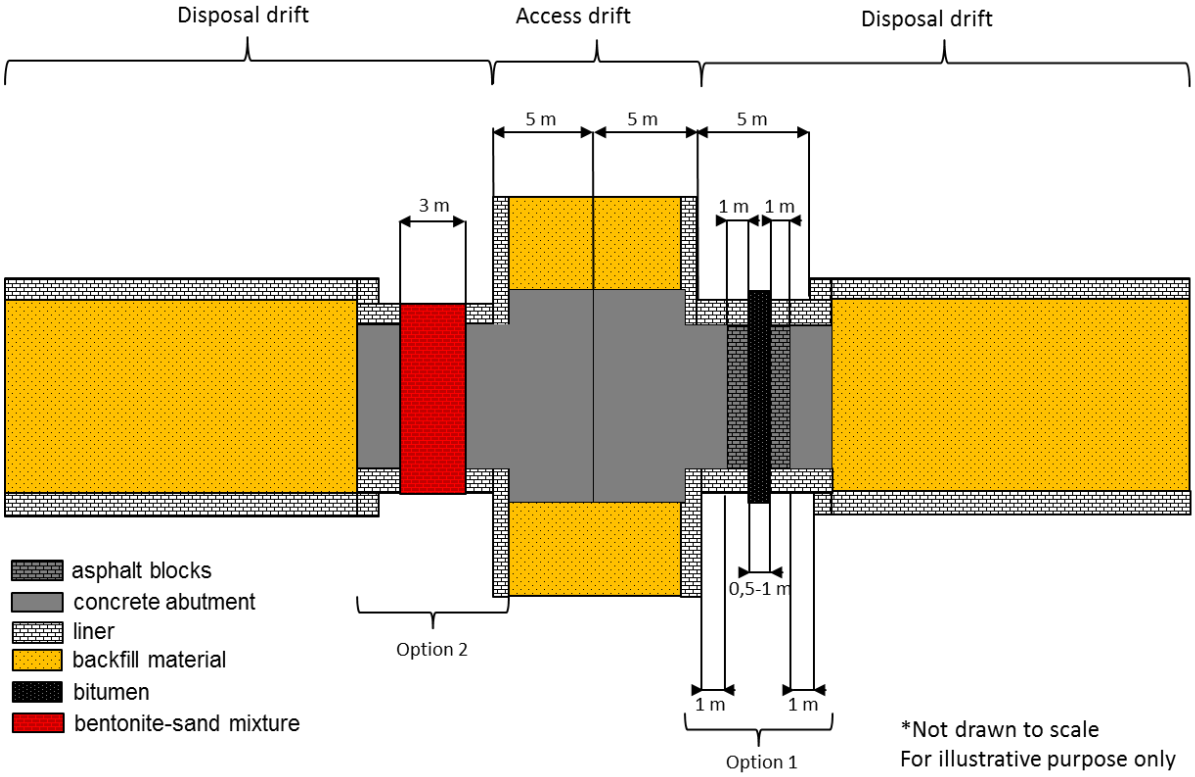

Figure 6-4: Overview of proposed disposal drift seal options at the end of the operational phase (option 1: asphalt/bitumen seal, right; option 2: bentonite seal, left).

In addition, the bitumen elements will have a slot along the drift contour with a depth of about 1 m, which will be filled with the corresponding bitumen. The slots will interrupt the liner, will divide potential pathways, will create hydraulic cut-offs and, therefore, will allow minimizing the migration of the fluids in the axial direction along the EDZ. The depth of the slots depends on the predicted EDZ and on the sealing and healing properties of the host rock. The EDZ is characterized by cracks and fractures that increase the hydraulic conductivity. However, in clay these cracks and fractures close over time. This process is known as sealing and healing.

Investigations carried out by the TU Bergakademie Freiberg (Kudla et al. 2009) showed that the hot installation of asphalt blocks in underground openings is due to operational safety reasons not recommendable. For this reason, the asphalt sealing elements will consist of cold asphalt blocks, which will melt by applying external pressure and heat on them.

The seal will have a total length of approximately 10 or 11 m. The abutments located in the disposal drifts will have a length of approximately 1 to 2 m; 1 m is foreseen for each asphalt element and between 0.5 and 1 m for the element made of bitumen. If Option 2 is implemented, the length of the plugs consisting of a bentonite-sand mixture is estimated to be approximately of 3 m. These dimensions have been estimated in an initial design step taking into consideration the geometry of the repository concept and the characteristics of the site. Detailed engineering calculations shall be carried out to prove the integrity of the proposed disposal drift sealing elements and, therefore, to prove that the function of the seals will be fulfilled.

6.2.2 Access drifts seals

The disposal drifts are connected to the shafts and to the transport tunnel by underground maintenance and working galleries, also called access drifts. The access drifts shall also be sealed, providing in this way an additional barrier between the shaft or the ramp seals and the disposal drifts. The access drifts seals have been designed in such a way that the potential migrated radionuclides shall in all cases at least pass through two seals (i.e. a disposal drift seal and an access drift seal) before they can reach the deepest parts of the shafts or of the ramp.

These seals shall fulfil two main functions. On the one hand they shall avoid the potential migration of fluids that may flow through the shafts and the ramp, especially before their closure, to the disposal areas. On the other hand they shall delay the potential migration of contaminated fluids from the disposal drifts to the shafts and to the ramp. To ensure the fulfilment of their function, the access drift seals shall be designed being compliant with the following requirements:

- Hydraulic requirements: The sealing elements shall delay the potential migration of fluids from and to the disposal areas. They shall provide an immediate effective seal against potential fluids that may flow through the shafts and through the ramp.
- Mechanical requirements: The sealing elements shall be stable under the expected pressure caused by the rock mass and by potential fluids.
- Chemical requirements: The sealing elements shall be chemically stable during their whole functional period
- Biological requirements: The sealing elements shall have a sufficient resistance to microbial degradation at least during the functional lifetime of the barrier.

The access drift seals (see Figure 6-5) will be formed by two bentonite elements that will provide redundancy, and one asphalt element that will provide diversity. Moreover, three abutments will be built. The liner at the location of the sealing elements will be removed.

If the bentonite is saturated, the increasing swelling pressure will have impact on the abutments and on the asphalt element. However, displacements on both outer sides of the seals are limited by the abutments. If the pressure increases, the asphalt will be squeezed and will improve its contact with the host rock, decreasing in this way the hydraulic conductivity in that area. The detailed properties of the seal are defined by the used type of bentonite. Different chemical compositions from different deposits, such as Na-rich bentonite like MX-80 or Ca-rich bentonite influence the chemical behaviour, sorption capacity, swelling pressure and permeability. The finally selected bentonite must be comparable to the host rock and the pore water.

The asphalt element of the access drift seals will be located at the side of the access drift seals closer to the shaft to ensure that the sealing function, especially of blocking incoming water, is fulfilled immediately after the installation of the seal. This principle has also been applied in a sealing concept for a repository in clay formations in Germany (Jobmann & Lommerzheim 2015). The installation of the asphalt element will be carried out in the same way as described for the disposal drift seals.

The long-term function of the seal is fulfilled by the bentonite elements, while the immediate function is fulfilled by the asphalt element. The asphalt element shall fulfil its function until complete saturation of the bentonite elements, and the full swelling pressure and thus the full sealing capacity is achieved. According to the results of the R&D project “Shaft Seals for Repositories for High Level Waste” (Schachtverschlüsse für Endlager für hochradioaktive Abfälle – ELSA) Phase II (Herold et al. 2016), the performance of the asphalt in similar conditions can be ensured for several thousands of years. However, the concrete functional period of the access drift seals shall be determined in future phases of this project by means of comprehensive process analyses.

The asphalt elements will have a slot with a depth of approximately 1 m along the drift contour that will be filled with the corresponding material asphalt in order to minimize the migration of fluids in the axial direction along the EDZ. The appropriate depth of the slots shall be determined taking into consideration the results of the analysis of the EDZ.

As already mentioned, in this case three abutments made of concrete are foreseen. Two of them will surround the sealing elements, while one abutment will be located between the bentonite elements. The main function of the abutments is to keep the bentonite in place and to avoid a potential increase of the volume of the bentonite element. By keeping the volume of the bentonite element constant, it will be ensured that the swelling pressure increases. For this reason the abutments shall be designed to mechanically resist the pressure caused by the rock mass as well as the swelling pressure. Moreover, liquids such as water may flow through the abutments. It is necessary to select a type of concrete material with adequate chemical interactions between the concrete, the pore water and the bentonite. Negative chemical interactions are, for example, the exchange of cations between pore water and bentonite. These interactions reduce the swelling capacity of the bentonite and may increase the hydraulic conductivity in the area where the seal is installed. These chemical effects can be avoided by using low pH-concrete.

The proposed abutments will be made of high-strength non-reinforced concrete. The selection of a non-reinforced concrete is made to avoid potential cracking caused by corrosive elements. The concrete and the asphalt elements will protect the bentonite from hydro-mechanical erosion. However, since the function of the abutments can be affected by chemical agents, the mechanical stability of the two outer abutments shall be increased by adding a supportive backfill material in front of and behind these elements. ANDRA carried out some tests, which show that the appropriate mechanical properties (i.e. pressure of 20 MPa at an inclination angle of 40°) of such supportive backfill material can be achieved by mixing clay and sand with a mixing ratio of 50/50 (ANDRA 2005).

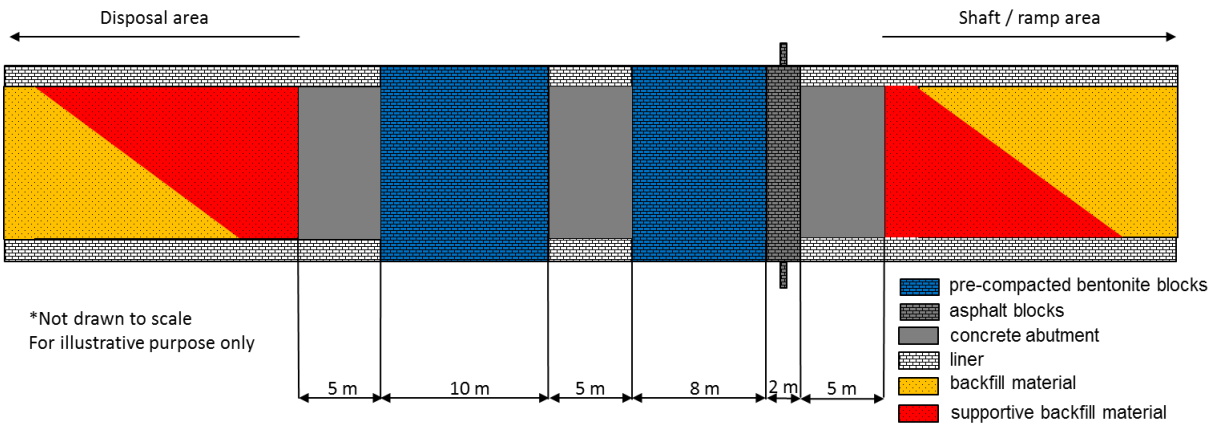

Figure 6-5: Overview of the proposed access drift seal.

The proposed access drift seals will have a total length of approximately 35 m. The abutments will have a length of 5 m. 10 m and 8 m are foreseen for the first and the second bentonite element. The asphalt element has a length of 2 m. These dimensions have been preliminary estimated taking into consideration the geometry and dimensions of the repository concept and the characteristics of the site. Detailed engineering calculations shall be carried out to determine suitable dimensions and to prove the integrity of the proposed sealing elements and, therefore, to prove that the function of the seal will be fulfilled.

6.2.3 Shaft seals

Shafts create a direct connection between the biosphere and the underground openings of the repository. For this reason, shafts are a critical pathway that shall be properly closed in order to ensure the containment of the radioactive waste inside the repository.

The two shafts foreseen in the near surface repository at the “Radon Site” will have a depth of approximately 100 m and after the operation of the repository they shall be properly sealed. It is expected that the geological structure between the two shafts of the repository will no vary significantly. For this reason, the structure of the sealing system of both shafts is assumed that will be the same. The main function of the shaft seals is to limit the inflow of fluids to the underground openings as well as to delay the potential release of contaminated fluids from the underground openings to the biosphere. To ensure the fulfilment of their functions, the shaft seals shall be designed being compliant with the following requirements:

- *Hydraulic requirements*: The sealing elements shall delay the potential migration of fluids through the shafts. They shall provide an immediate effective seal against potential fluids that may inflow to the shaft (e.g. from the surface or from the aquifers).
- *Mechanical requirements*: The sealing elements shall be stable under the expected lithostatic and hydrostatic pressures as well as under the expected swelling pressure of the host rock.
- *Chemical requirements*: The sealing elements shall be chemically stable during their whole functional period.
- *Biological requirements*: The sealing elements shall have a sufficient resistance to microbial degradation at least during the functional lifetime of the barrier.

The proposed design for the shaft seals has been developed taking into consideration the above mentioned requirements as well as the lithological profile (see Figure 6-6) at the “Radon Site”. Due to the limited thickness of the clay barrier (ca. 100 m) of the shafts, the shaft seals mainly consist of one sealing module that will be located in the Kotlin Clay formation, just below the Lomonosov formation.

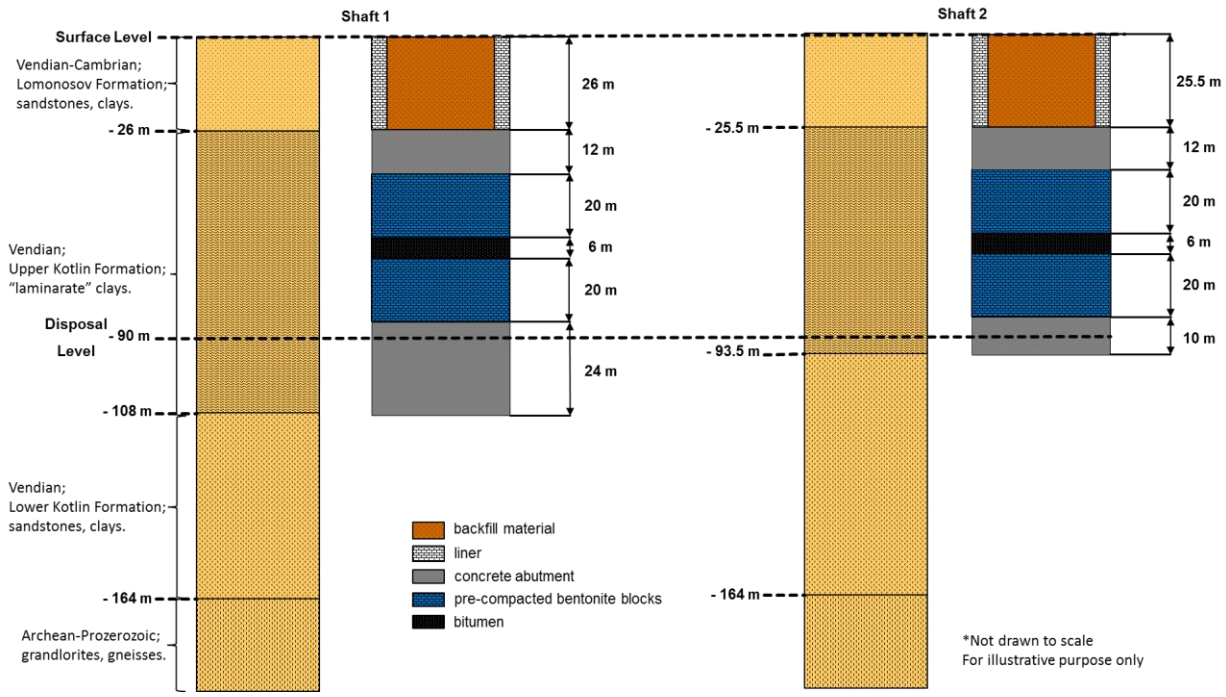

Figure 6-6: Lithological profile and location of the shaft seals.

The sealing module will mainly consist of a bitumen element enclosed by two bentonite elements. Moreover, two abutments are also foreseen. Finally, it has been assumed that the disposal level will be located about 90 m below the surface level.

Due to the swelling pressure of the bentonite, it is expected that the bitumen core will be squeezed leading to an enhanced sealing of the contact zone to the rock. The bitumen element will be formed by a layer of soft bitumen (e.g. distilled bitumen 70 - 100) surrounded by two layers of hard bitumen (e.g. oxidized bitumen 85/25) known as the "Hard Shell – Soft Core" system (Kudla et al. 2009), combining in this way the advantageous properties of soft and hard bitumen. On the one hand, hard bitumen is more stable against changes in pressure, which makes it more long-term stable than soft bitumen. On the other hand soft bitumen has a better wetting capacity and reacts faster to short-term changes in pressure, which enhance the sealing effect of the sealing element. Finally, it shall be noted that the combination of distilled and oxidized bitumen is in general unproblematic.

The long-term function of the seal will be fulfilled by the bentonite elements, while the immediate function will be fulfilled by the bitumen element. The bitumen element shall fulfil its function until the complete saturation of the bentonite elements, and therefore, until the full swelling pressure and thus the full sealing capacity is achieved. The functional period of the shaft seals shall be determined in future phases of the present project by means of comprehensive process analyses.

The bentonite sealing element is duplicated and will consist of bentonite pre-compacted blocks. In this way the concept is compliant with the principle of redundancy. Due to the fact that extensive data in regard to Ca-bentonite is available (Breidung 2002, Jobmann 2002, Engelhardt et al. 2011, Müller-Hoeppe et al. 2012), the Ca-bentonite is proposed as reference material. Some favourable properties of this material are its low permeability, its plasticity, its swelling capacity and its capacity for retaining radionuclides. Optionally, by admixing for example 20% of sand, the compaction of the material could be increased and the mechanical properties improved, without increasing the permeability of the seal to water. If necessary, by admixing sand the permeability of the seal to gases can be also increased.

The two abutments shall be designed to mechanically resist the pressure caused by the rock mass as well as the swelling pressure. The proposed abutments will be made of high-strength non-reinforced concrete. This type of concrete has a higher density and a lower permeability than the conventional concrete, so that the amount of penetrating water and hence the degradation of the concrete will be reduced. In addition, due to the lack of reinforcement, cracking caused by corrosion products will be avoided. The technically feasibility and functionality of concrete abutments has been demonstrated by the results of large-scale tests carried out by ANDRA in the framework of the ESDRED project (ANDRA 2005).

The remaining space (on the upper part of the shaft) can be filled with hard rock gravel. As an alternative, the material resulting from the excavation of the shaft or a mixture of this excavated material with other materials with high swelling capacity could be used. However, it shall be noted that the suitability of clay or a mixture of clay with other materials as shaft backfill material has not been yet proved. The construction of the shaft seals will be one of the last actions that will be carried out in the course of the repository closure. It shall be noted that before sealing the shafts, all shafts internals shall be completely removed.

The proposed shaft seals will have a total length of approximately 100 m. The upper abutments will have a length of approximately 12 m and the lower abutments of 24 m in Shaft 1 and of 12 m in Shaft 2 respectively, 20 m are foreseen for the bentonite elements and 6 m for the bitumen element. These dimensions have been preliminary estimated taking into consideration the geometry and dimensions of the repository concept and the characteristics of the site. Detailed engineering calculations shall be carried out to prove the integrity of the proposed shaft sealing elements and, therefore, to prove that the function of the seal will be fulfilled.

6.2.4 Ramp seal

The ramp creates a direct connection between the biosphere and the underground openings of the repository. For this reason, it is a critical pathway that shall be properly closed in order to ensure the containment of the radioactive waste inside the repository.

The ramp seal has the same function as the shaft seal, which is limiting the inflow of fluids to the underground openings as well as delaying the potential release of contaminated fluids from the underground openings to the biosphere. To ensure the fulfilment of these functions, the ramp seal shall be designed being compliant with the following requirements:

- *Hydraulic requirements*: The ramp seal shall delay the potential migration of fluids through the ramp. It shall provide an immediate effective seal against potential fluids that may inflow to the ramp (e.g. from the surface of the repository). In this case it shall be noted that the ramp will be fully located in the host rock (i.e. Kotlin Clay), so that potential water directly inflowing from aquifers is not expected.
- *Mechanical requirements*: The ramp seal shall be stable under the expected pressure caused by the rock mass and by the potential fluids.
- *Chemical requirements*: The sealing elements shall be chemically stable during their whole functional period.
- *Biological requirements*: The sealing elements shall have a sufficient resistance to microbial degradation at least during the functional lifetime of the barrier.

The conceptual design for the ramp seal (see Figure 6-7) is very similar to the design of the access drift seals. However, in this case the length of the ramp (ca. 300 m) allows increasing the dimensions of the sealing elements. Two bentonite elements consisting of bentonite pre-compacted blocks will provide redundancy. For the same reason as for the access drift seals, Ca-Bentonite is proposed as reference material. The asphalt element of the ramp seal will also be significantly longer and will be located at the side closer to the surface to ensure that

fresh water inflow along the ramp into the mine can be instantly avoided. Thus, the long-term function of the ramp seal is fulfilled by the bentonite elements, while the short-term function is fulfilled by the asphalt element. The asphalt element shall fulfil its function until the complete saturation of the bentonite elements, and therefore, until the full swelling pressure and thus the full sealing capacity is achieved. According to the results of the R&D project ELSA Phase II (Herold et al. 2016), the performance of the asphalt in similar conditions is ensured for several thousands of years. The functional period of the ramp seal shall be determined by means of comprehensive process analyses. The installation of the asphalt element will be carried out in the same way as described for the disposal and access drift seals.

In a similar way as for the disposal and access drift seals, the asphalt elements will also have a slot with a depth of approximately 1 m along the drift contour, which will be filled with asphalt with the aim of minimizing the migration of fluids in the axial direction along the EDZ. The appropriate depth of the slots shall be determined taking into consideration the results of the analysis of the EDZ in terms of depth and permeability.

Finally, three abutments made of concrete are foreseen. Two of them will surround the sealing elements, while one abutment will be located in the centre between the bentonite elements. The abutments shall be designed to mechanically resist the pressure caused by the host rock, the hydrostatic pressure at the location of the ramp seal and the swelling pressure caused by the bentonite elements. The bentonite element next to the asphalt element will squeeze the asphalt during the development of the swelling pressure improving the tightness of the contact zone between the asphalt and the rock.

The proposed abutments will be made of high-strength non-reinforced concrete. The selection of a non-reinforced concrete has been made to avoid potential cracking caused by corrosion products. The concrete and the asphalt elements will protect the bentonite from hydro-mechanical erosion.

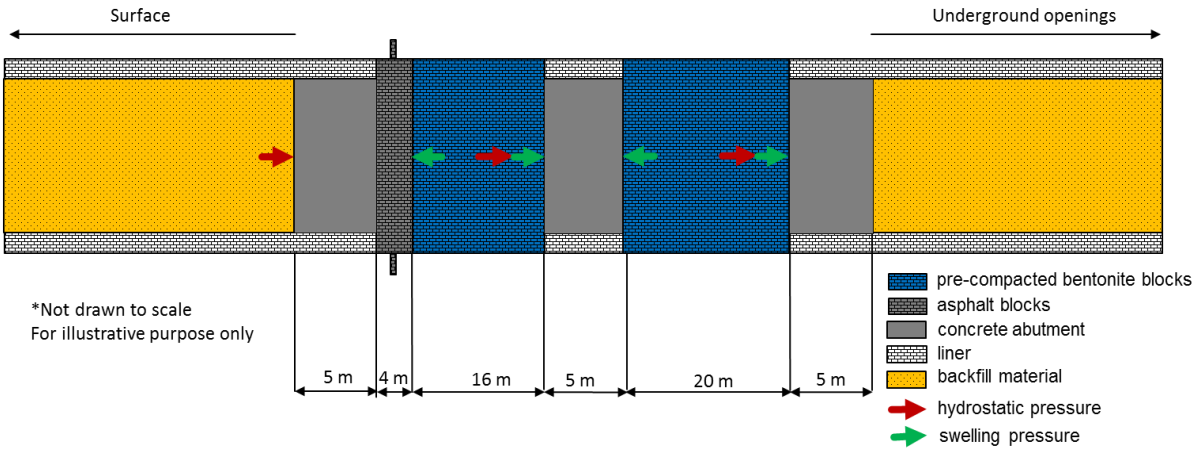

Figure 6-7: Overview of the proposed ramp seal.

The proposed ramp seal will have a total length of 55 m. The abutments will have a length of 5 m, 16 m and 20 m are foreseen for the first and the second bentonite elements respectively and 4 m for the element made of asphalt. These dimensions have been preliminary estimated taking into consideration the geometry and dimensions of the repository concept and the characteristics of the site. Detailed engineering calculations shall be carried out in future phases of the present project to prove the integrity of the proposed ramp sealing elements and, therefore, to prove that the function of the seal will be fulfilled.

6.3 Demonstration of the integrity of the geotechnical barriers

As defined in the International Atomic Energy Agency (IAEA) Fundamental Safety Principles (IAEA 2006), the fundamental safety objective that shall be considered in all radioactive waste management facilities and activities, including the disposal of radioactive waste, is “to protect people and environment from harmful effects of ionizing radiation”.

To achieve this general objective and taking into consideration the risks associated with the presence of a radioactive waste repository (i.e. the potential negative radiological impact on the health of the members of the public and on the environment), the radioactive waste shall be properly isolated and confined. These safety functions are fulfilled by a multi-barrier system that comprises the natural geological barrier provided by the repository host rock, its surroundings and the biosphere, and by the EBS.

The seals have the main safety function of preventing the potential contact of fluids (liquids or gas) with the radioactive waste disposed of in the repository and, therefore, to prevent the migration of radionuclides from the repository to biosphere. Thus, they are an important part of the EBS.

From this general safety function, a set of general recommendations and requirements that shall be considered when designing the sealing system for a radioactive waste repository can be derived:

- All disposal drifts shall be separated from each other
- All underground openings shall be completely backfilled
- The sealing components shall be stable during their functional period
- The sealing system shall minimize all fluid movements
- The design of the sealing system shall consider redundancy and diversity
- The sealing system shall be maintenance free without any re-adjustments and
- The sealing system shall be built as a simple and robust construction

This general requirements lead to specific requirements that shall be taken into consideration to develop the design of the technical barriers of the repository. For the specific case of the design of the sealing system as whole as well as of the individual sealing elements, in addition to the expected loads, the expected boundary conditions and the future evolution of the repository shall be considered. An overview of the strategy for demonstrating the compliance of the design of the sealing system with the requirements is provided in the following chapter (see Chapter 6.3.1).

6.3.1 Compliance of the sealing system design with the requirements

The strategy for demonstrating compliance of the design of a sealing system with the requirements has been developed and applied in the course of German R&D projects (i.e. “Review and Appraisal of the Tools available for a Safety Assessment of Final Repositories for HLW” (*ISIBEL*) (Krone et al. 2013) and "Safety Assessment Methodology for a German High-level Waste Repository in Clay Formations" (Jobmann et al. 2017).

This strategy consists of a semi-probabilistic, reliability-oriented concept that uses partial factors and is based on the internationally accepted Eurocodes (JRC & DG-ENTR 2008). The Eurocodes are a series of ten European standards that in engineering can be considered as state-of-the-art for demonstrating the load-bearing capacity of a structure, i.e. the ability of a structure to perform according to the required standards under induced loads.

The acceptable level of safety of the barriers, and therefore of the repository as whole, is demonstrated by the results of the safety case, in which the reliability and performance of the individual barriers is comprehensively assessed. To demonstrate the compliance of the seal-

ing system with the defined requirements, first of all, the requirements on the multi-barrier system as a whole as well as on the individual subsystems (e.g. sealing system) shall be derived from the safety goals. The compliance with the requirements is then demonstrated by means of individual assessments that are selected taking into consideration the specific characteristics of the EBS as well as the potential impacts that may affect the system.

According to the current state-of-the-art in technology, the following individual assessments are necessary for demonstrating compliance of the EBS with the design requirements:

- Demonstration of sufficient hydraulic resistance (demonstration of tightness) and
- Demonstration of sufficient load bearing capacity (structural integrity):
  - Demonstration of structural stability
  - Demonstration of crack limitation
  - Demonstration of deformation limitation
  - Demonstration of filter stability
  - Demonstration of long-term stability

The individual assessments are essential for demonstrating the effectiveness of a sealing construction and thus, compliance with the design requirements. In addition, the feasibility of the sealing system shall be also assessed and demonstrated. An overview of how the long-term calculations carried out in the framework of a long-term safety assessment are connected to the above mentioned individual assessments is provided in Figure 6-8.

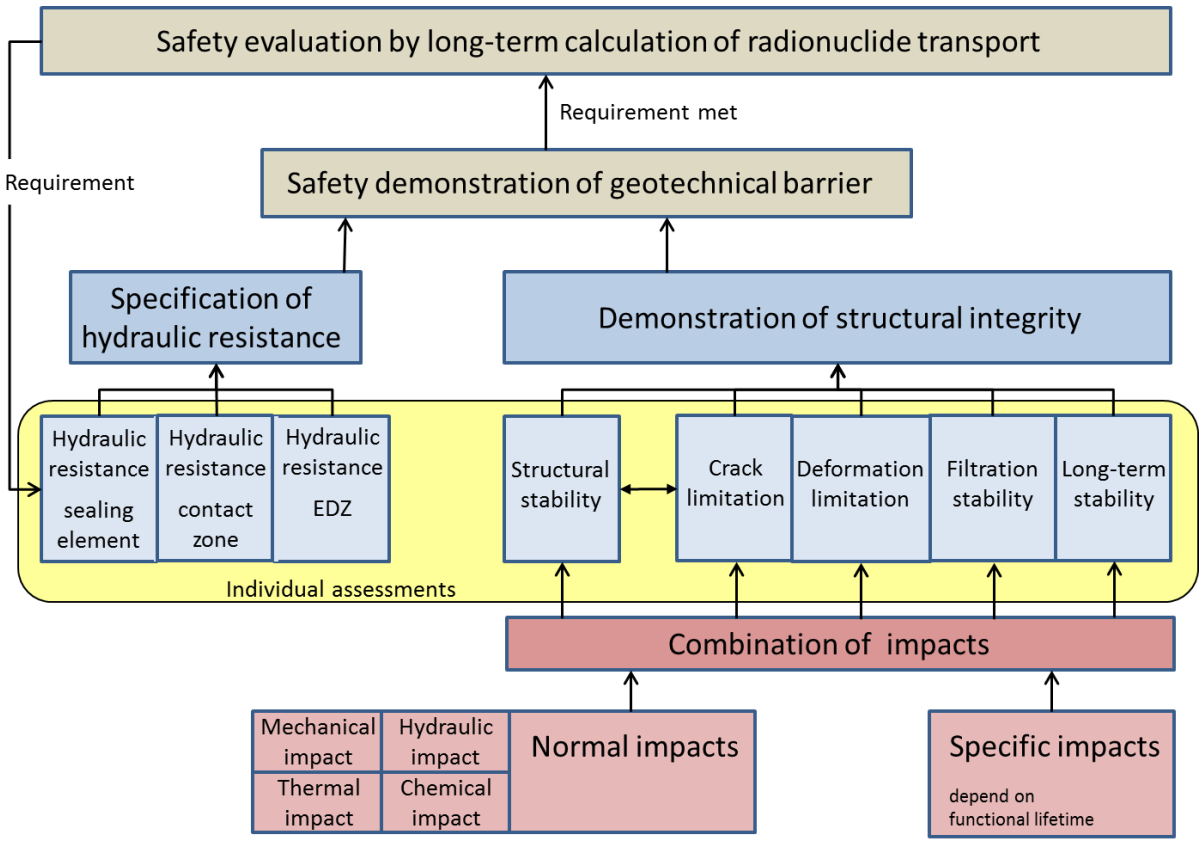

Figure 6-8: Structure of demonstration of compliance of the EBS with the design requirements, modified after (Müller-Hoeppe et al. 2012).

6.3.2 Individual assessments

In the following subchapters, the individual assessments that shall be carried out to demonstrate the compliance of a sealing concept with the design requirements are described in more detail.

6.3.3 Hydraulic resistance

The assessment of the hydraulic resistance of individual sealing elements and of the sealing system as a whole shall take into account not only the sealing elements, but also the hydraulically effective contact zones at the interface to the rock and to the EDZ next to the sealing elements. For this reason, the hydraulic resistance shall be assessed separately for all three parts (the sealing element, the hydraulically effective contact zone at the interface to the rock and the EDZ).

The hydraulic resistance of a sealing element can be determined by the results of in-situ tests or of tests carried out in a laboratory. The hydraulic resistance of the EDZ can be determined by the results of in-situ measurements in the vicinity of the seal locations, which will provide information about how the hydraulic conductivity varies as a function of the distance to the drift contour. It shall be noted that, in principle, the determination of the hydraulic conductivity of the contact zone is associated with highest uncertainties. However, using a combination of sealing elements made of different materials such as bentonite and bitumen, these uncertainties can be reduced. For example, due to the swelling pressure of the bentonite, the seals will be pressed to the contour of the rock mass and the bitumen or asphalt will be squeezed and will then fill out the rough surface of the contact zone, reducing in this way the hydraulic conductivity of the contact zone.

Finally, the hydraulic resistance of the sealing construction as a whole shall also be demonstrated. An example of an assessment of the hydraulic resistance of a sealing construction can be found in the assessment carried out by DBE TECHNOLOGY GmbH in 2013 (Herold & Müller-Hoeppe 2013).

6.3.4 Structural integrity

To demonstrate the structural integrity of a sealing element, five different individual assessments shall be carried out.

6.3.4.1 Structural stability

Sealing performance and load bearing are the two main functions of seals in underground repositories. These functions shall be achieved by means of a series of sealing elements that will be installed in underground openings. However, the performance of each sealing element will be associated with one of the two mentioned functions. For example, load bearing and, therefore, structure stability are functions that are associated with the performance of the abutments, which can be constructed using cohesive (e.g. concrete) or non-cohesive (e.g. gravel) materials.

On the one hand, in abutments made of cohesive material, the demonstration of the structural stability of the mechanical load-bearing capacity is covered by the assessment of the crack formation because a mechanical damage of cohesive materials is always preceded by the formation of cracks. If the formation of cracks is avoided, the mechanical damage of the material can be excluded and, therefore, the mechanical load-bearing capacity can be demonstrated. Otherwise, if the formation of cracks cannot be avoided, the mechanical load-bearing capacity of the sealing element shall be proved separately.

On the other hand, in abutments made of non-cohesive material, the load-bearing capacity of the sealing elements is defined by the stability of the settlement.

6.3.4.2 Crack limitation

The demonstration of limited crack formation is relevant for both, sealing elements and abutments made of cohesive material. Crack formation is induced by excessive mechanical stress on the individual components or by thermo-mechanical/chemical processes during installation of the sealing elements. An example of crack formation due to changes in volume and/or temperature can occur in the process of cooling hot installed bitumen or asphalt sealing elements. As their temperatures decrease, their volumes shrink, leading this volume shrinkage to a decrease of the effective sealing length (i.e. decrease of length of the sealing element) and, therefore, to a potential detachment of the sealing element from the drift or shaft contour.

Cracks may be also formed when the fluid pressure criterion in the sealing element and in the contact zone is exceeded. An example of this specific case occurred in the large-scale shaft seal construction experiment carried out in Salzdetfurth (Germany), where the pressure of the sealing element made of bentonite increased too fast and, thus damaged the sealing element (Teichmann et al. 2002).

6.3.4.3 Deformation limitation

Sealing elements used in underground repositories are usually designed in such a way that their positional stability is ensured by the construction of abutments. This measure is especially necessary for sealing elements made of swellable materials.

The swelling process of a sealing material leads only to a complete sealing of the underground opening when the planned swelling pressure of swelling element is reached. However, if in the course of the swelling process the volume of the sealing element expands without limits, the required swelling pressure will not be reached. For this reason and in order to ensure the positional stability of the sealing elements, the abutments shall be resistant to the deformation of the sealing elements and shall be firmly fixed to the rock mass.

6.3.4.4 Filtration stability

The filtration stability of the sealing elements can be described as the avoidance of erosion and suffosion processes (see Figure 6-9). The filtration stability shall be assessed in the surroundings of the rock mass, where the risks of erosion and suffosion may be higher due to the high hydraulic gradients caused by fluid inflow from aquifer and special attention shall be paid to the saturation phase of bentonite elements. A lack of filtration stability may cause for example loss of tightness of a sealing element.

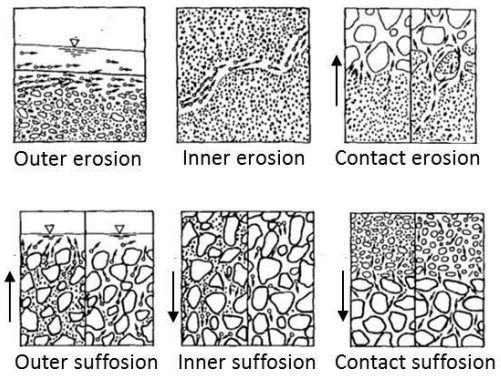

Figure 6-9:
Basic erosion and suffosion processes (DGGT 1997).

6.3.4.5 Long-term stability

Sealing elements in radioactive waste repositories usually shall fulfil the defined safety functions during long-term periods. For this reason the long-term performance of the materials used in the seals, such as swelling materials (e.g. clay, bentonite, etc.) or long-term stable materials (e.g. asphalt, bitumen, etc.) shall be verified by natural analogues or by advanced studies. It shall be noted that for materials, the properties of which are expected to be altered over time such as for example cement-based concrete materials, an appropriate functional period shall be defined.

6.3.5 Partial safety factor method

To demonstrate the compliance of the design of a sealing element with the applicable requirements, the limiting value evaluation of the impacts on the structure of the sealing element and of the resistance of the structure to these loads shall be carried out (i.e. the existing stresses shall be compared with the nominal design stresses, which can be derived from the strengths of the materials, by means of limiting criteria). In order to meet the applicable design requirements, the basic principle that shall be met is that the resistance of the structure shall withstand the loads applied on it.

The design values, also called “rated values”, for the individual assessments are derived from characteristic values of the impacts on the engineered barriers and from the properties of the barriers combined with partial safety factors (this approach is represented in Figure 6-10).

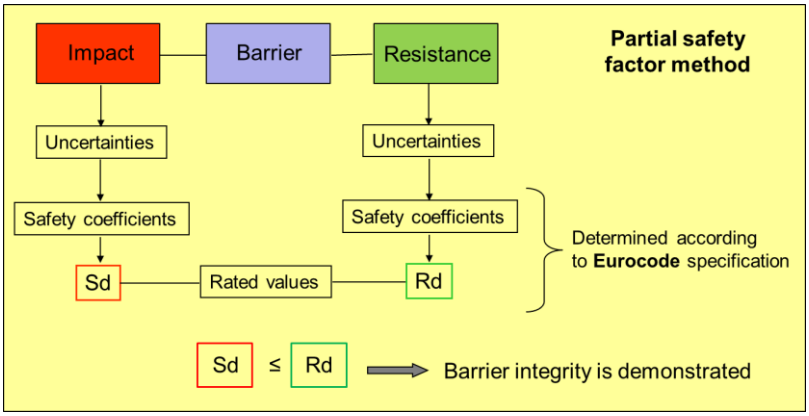

Figure 6-10:
Partial safety factor method (Jobmann et al. 2017).

On the one hand the effects of the impacts (S_d) are increased by applying partial safety factors. On the other hand the resistance of the sealing elements (R_d) is conservatively decreased also by applying partial safety factors. In some cases, uncertainties in regard to the potential impacts and/or to the properties of the structures shall be also considered. The basic principle

$$S_d \leq R_d \tag{6.1}$$

is divided into specific calculations that allow determining the impacts as well as the resistance of the structures. On the one hand, the effects of the impacts on the structures (S_d) are calculated as follows:

$$S_d = \gamma_{Ed} * I\,(F_{di};\, a_{di};\, X_{di}) \tag{6.2}$$

With:

γ_{Ed} partial factor for model uncertainty in the impacts model
F_{di} design values for impacts
a_{di} design values for the geometric parameters
X_{di} design values for the construction material properties

The design values for the impact action F_d are calculated by multiplying the characteristic individual value (F_k) by the partial factor of the (γ_f) action:

$$F_d = \gamma_f * F_k \tag{6.3}$$

The design values of the construction material properties X_d are calculated as follows:

$$X_d = \frac{\eta * X_c}{\gamma_m} \tag{6.4}$$

With:

η conversion factor for duration of loading, moisture, etc.
X_c characteristic value for the building material properties
γ_m partial factor of the construction material property

On the other hand, the resistance of the structure is calculated as follows:

$$R_d = \frac{1}{\gamma_{Rd}} * R\ (a_{di};\ X_{di}) \tag{6.5}$$

With:

γ_{Rd} partial factor for model uncertainty in the resistance model
a_{di} design values the geometric parameters
X_{di} design values for the construction material properties

The design value for the geometric parameter (a_d) is calculated by adding the nominal value (a_{nom}) and the deviation from the nominal value (Δa) that has been considered (Eq. 6.6).

$$a_d = a_{nom} + \Delta a \tag{6.6}$$

The deviation from the nominal value is derived from the expected changes in the respective parameter and shall be especially taken into consideration for parameters that react sensitively. An example is the effective length (buckling length) of a steeply inclined rocked layer, where changes in the length will directly affect the buckling behaviour and, therefore, the deviation from the nominal value shall be considered.

The factors that influence the structures can be determined by both, deterministic and probabilistic methods. For example, the geometry of the structure will be derived from the results of the design and the stress model. The impacts on the structure can be determined based on statistics and on limit value assessments. The properties of the construction materials can be determined based on statistics (Müller-Hoeppe & Krone 1999).

If the applicable standards and regulations do not contain suitable partial safety factors, these can be determined by means of probabilistic methods and calibration (Kreienmeyer et al. 2008). Figure 6-11 schematically illustrates the methods used for determining partial safety factors.

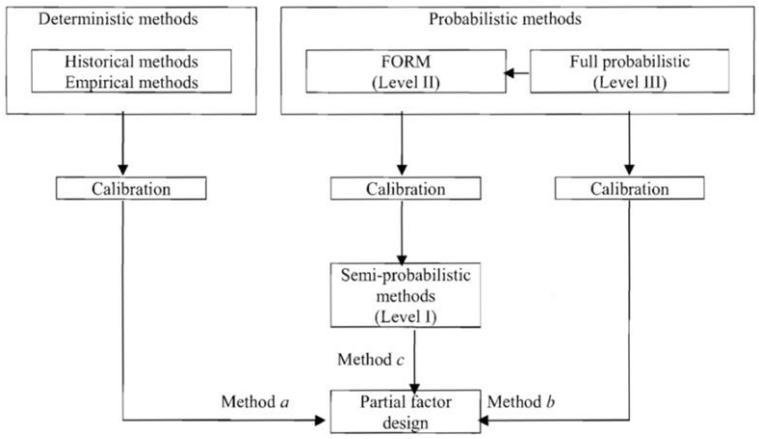

Figure 6-11:
Reliability methods for determining partial safety factors (Eurocode 0 2010).

The safety concept is necessary to ensure that the design is compliant with the applicable requirements. It shall be noted that the loss of tightness of the sealing structures would result in “danger to life and limb” and, therefore, the demonstration of their tightness shall be carried out considering the same reliability level as in the demonstration of the ultimate limit states (Kiefer 1997). Unlike in the Eurocodes, the term “resistance” does not only refer to mechanical stability. This term is used synonymously to the prevention of a “danger to life and limb” and, therefore can be also used, for example, for the hydraulic resistance and others. Compliance with the defined reliability level in the corresponding individual assessment ensures then the functional integrity of the structure.

In order to carry out the individual assessments according to DIN 1054:2010-12 (DIN 1054 2010), four general design situations shall be considered:

- Constant / steady / permanent design situation
- Temporary design situation
- Exceptional design situation and
- Earthquake

The individual assessments provide information regarding the reliability of a structure. To demonstrate the reliability of a structure, a specific confidence level or failure probability shall be met. In the framework of the demonstration of an ultimate limit state, a failure probability (p_f) of 10^{-4} for the intended lifetime of the structure is sufficient (Müller-Hoeppe & Krone 1999). Thus, the demonstration of the effectiveness of the safety functions indicates that the probability that a barriers fails during its expected lifetime is $p_f = 10^{-4}$. The survival probability (p_s) of the barrier is then $p_s = 1 - p_f$ (Müller-Hoeppe & Krone 1999).

Finally, to perform the individual assessments, the expected impacts on the sealing elements shall be determined. To obtain a comprehensive overview of all processes related to the presence and operation of a repository, a site specific FEP-catalogue shall be developed. The FEP-catalogue is a sound basis for developing the probable evolution of the repository over time (reference scenario) as well as less probable evolutions (alternative scenarios). In all cases, the FEP that may have significant impact on the sealing elements of the EBS shall be identified. Based on these identified FEP, the expected loads on the sealing elements shall be derived to carry out the respective individual assessments. More details on this method can be found in Herold & Müller-Hoeppe 2013. An exemplary application of this method is provided in the following chapter.

6.3.6 Exemplary demonstration of the integrity of the ramp seal

To ensure that the proposed sealing concept for the L/ILW repository at the “Radon Site” fulfils the long-term containment of the radioactive waste in the repository, the integrity of the following barriers shall be demonstrated for:

- *Disposal drift seals* consisting of one sealing element made of pre-compacted blocks of bentonite and a thinner element made of asphalt. These elements are surrounded by two abutments made of concreted.
- *Access drift seals* consisting of the same elements than the disposal drift seals. However, the bentonite sealing elements are significantly longer and are duplicated.
- *Shaft seals* consisting of one sealing element made of bitumen that is enclosed by two bentonite elements. These elements are surrounded by two abutments made of concrete.
- *Ramp seal* consisting of the same elements and structure than the access drift seals. The only difference lies in the dimensions of the sealing elements.

To exemplify the methodology used to demonstrate the integrity of the sealing elements, the permeability of the ramp seal and the stability of the related abutments have been assessed in the following subchapters.

The ramp seal has been selected taking into consideration that the ramp is one of the main radionuclide migration pathways (in addition to the shafts) that connect the underground openings with the surface. Moreover, it shall be noted that due to the fact that the current concepts for the German repositories do not foresee the construction of ramps inside the repositories, the demonstration of the integrity of the ramp seal in the course of the present project may demonstrate that the methodology developed in Germany for demonstrating the integrity of shaft and drift seals can be also used to demonstrate the integrity of ramp seals, and therefore may provide added value to this methodology.

6.3.6.1 Hydraulic resistance of the asphalt sealing element

According to the structure of compliance demonstration of an engineered barrier (Figure 6-8) an important part of the analysis is the specification of the hydraulic resistance (cf. Chapter 6.3.3) of the structure. It is important to note that the hydraulic resistance does not only comprise the hydraulic resistance of the barrier itself but also the contact zone to the surrounding rock and the EDZ at the location of the barrier. In this sense it is called the “integral permeability” of the structure.

6.3.6.1.1 Permeability of the asphalt sealing element

According to Arand et al. (1992), for asphalt sealing elements with certain characteristics (i.e. the remaining void spaces in the asphalt element represent less than 3 % of the total volume of the sealing element) an extremely low hydraulic conductivity of $k_f < 10^{-16}$ m/s can be assumed. Moreover, it has been assumed that the remaining void spaces are not connected and, therefore, a continuous connection within the sealing element does not exist. This assumption is also valid for high pressure gradients within the sealing element.

6.3.6.1.2 Permeability of the contact zone

The permeability of the contact zone is mainly determined by the roughness at the rock contour and by the characteristics of the sealing material. It is assumed that before installing the asphalt sealing element the lining of the ramp will be removed by means of adequate mining techniques. For this reason, the adherence of the asphalt at the rock surface shall ensure the proper seal of the contact zone between the asphalt sealing element and the rock contour. By applying appropriate primer coatings this adhesive effect can be considerably increased (Glaubach et al. 2008).

However, despite the favourable adhesion properties of the asphalt, a potential “weak area” may be formed at the contact zone between the asphalt sealing element and the rock contour. This “weak area” may have a higher permeability and therefore the risk associated with the potential formation of cracks in this area may also increase. Crack limitation is then an aspect that shall be further assessed in the course of the assessment of the integrity of the seal.

Finally, it shall be noted that according to Wagner (2005), generally the integrity of the joints is ensured when the minimum main tension is larger than the in-situ fluid pressure. For the specific case of cohesive materials such as for example asphalt, the adhesive strength of such materials shall also be considered.

6.3.6.1.3 Permeability of the EDZ

At this stage of the project, the depth, at which the sealing element will be installed, cannot be precisely determined. For this reason a conservative depth of 90 m (disposal depth) below the surface level has been considered for calculation purposes. The internal diameter of the ramp, after removal of the lining, will be approximately 5.63 m (Consortium SGN/IVO/AEA 1997-B). As already mentioned in previous chapters, the repository and therefore the ramp seal will be located in the Kotlin Clay formation, which has cohesion of 4.61 MPa and an angle of internal friction of 23° (Pereverzeva et al. 2008). Knowing the cohesion and the angle of internal friction and applying equation 6.7, an unconfined compressive strength of the rock of 13.93 MPa has been estimated.

$$\sigma_D = \frac{2c*\cos\varphi}{1-\sin\varphi} \qquad (6.7)$$

with

σ_D unconfined compressive strength of the rock [MPa]
c cohesion [MPa]
φ angle of the internal friction [°]

It shall be noted that at this stage of the project, on-site investigations to determine the characteristics of the EDZ have not yet been carried out. However, the Kotlin Clay at the “Radon Site” has some similarities to the characteristics of other clay formations that are planned to host radioactive waste repositories in Europe, where some on-site investigations to determine the characteristics of the EDZ have already been carried out (Figure 6-12).

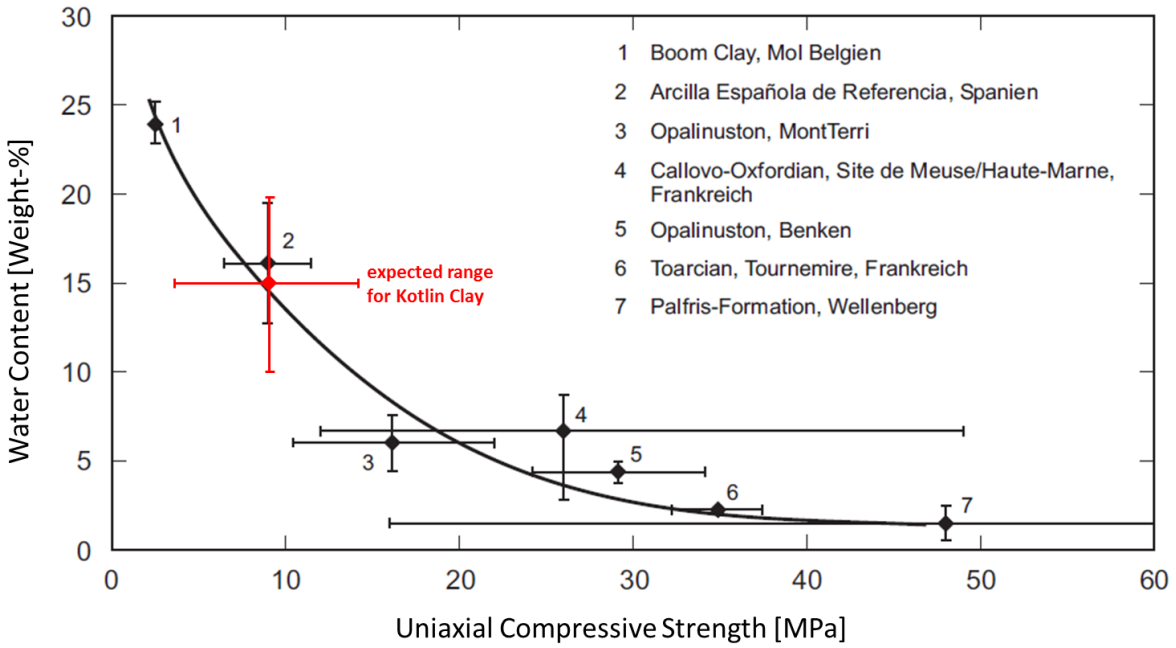

Figure 6-12: Overview to typically properties at different European clay formations in comparison to expected properties at Kotlin Clay, based on Kudla et al. (2009) and Nagra (2002).

Due to the fact that detailed data in regard to on-site measurements carried out to study the permeability distribution around an underground opening at Mont Terri URL (Bossart et al. 2004) are available, the results of these measurements have been used as a basis for estimating the extension of the EDZ. Based on these results, it has been assumed that the excavation activities will lead to an extension of the EDZ (r_{EDZ}) of approximately 3.4 m. It shall be remarked again that these values are based on results of on-site measurements carried out at Mont Terri URL and therefore shall be confirmed in future phases of the project by the results of on-site investigations at the “Radon Site”.

As already mentioned, at this stage of the project there is still no information in regard to the potential development and distribution of the permeability in the EDZ. However, Jobmann (2014) compiled measurement results from different literature sources that can be used as reference values. For example, in the course of the on-site investigations carried out at Mont Terri URL (Bossart et al. 2004), six boreholes were used to measure the permeability distribution in the EDZ (Table 6-1). The permeability at the deepest parts of the boreholes lies in the range of 2 to $4 \cdot 10^{-16}$ m². This permeability is assumed to be the permeability of the undisturbed host rock.

As an illustrating example these values were used to estimate the average permeability of the EDZ as $m_x = 2.7 \cdot 10^{-15}$ m² with a standard deviation $s_x = 2.76 \cdot 10^{-13}$ m² and a variation coefficient $V_x = 1.02 \cdot 10^{2}$.

Table 6-1: Permeability distribution of the EDZ of an underground gallery at the Mont Terri URL (Bossart et al. 2004).

Distance [m]	Borehole-5 K [m²]	Borehole-6 K [m²]	Borehole-7 K [m²]	Borehole-8 K [m²]	Borehole-9 K [m²]	Borehole-10 K [m²]
0.2	2.00E-12	3.00E-14	1.50E-14	1.50E-13	2.00E-14	1.30E-13
0.3	3.50E-14	1.00E-14	2.00E-14	2.00E-14	5.00E-15	2.00E-15
0.4	3.50E-15	2.50E-16	2.00E-15	3.00E-14	2.00E-15	7.00E-16
0.5	8.00E-16	2.50E-16	3.00E-15	2.00E-15	1.50E-15	2.50E-16
0.6	4.00E-16	2.50E-16	4.00E-15	8.00E-16	2.50E-15	2.50E-16
0.7	4.00E-16	2.00E-16	1.50E-15	8.00E-16	2.50E-15	2.50E-16
0.8	4.00E-16	2.00E-16	1.00E-15	8.00E-16	2.50E-15	2.50E-16
0.9	4.00E-16	2.00E-16	1.00E-15	8.00E-16	2.50E-15	2.50E-16
1.0	4.00E-16	2.00E-16	1.00E-15	8.00E-16	2.50E-15	2.50E-16

The preferred approach to determine the design value of the permeability is presented in Appendix D.7 of the Eurocode 0 (2010). The design value is determined from a log-normal distribution, assuming that all measured values are normally distributed. The design value can be obtained by applying equation 6.8, which is based on the procedure presented in Appendix 7.8 of the Eurocode 0 (2010).

$$X_d = \frac{\eta_d}{\gamma_m} * e^{[m_y + k_n * s_y]} \quad (6.8)$$

with
X_d = Design value, η_d = Uncertainty factor, γ_m = Partial safety factor, m_y = Normalized average, s_y = Normalized standard deviation, k_n = Specific coefficient

The partial safety factor (γ_m) and the uncertainty factor (η_d) can be determined from relevant standards, in this case the Eurocode 7 (2009) and DIN 1054 (2010) respectively. On the one hand, based on the Eurocode 7 (2009), the applicable uncertainty factor is 1.0. On the other hand, according to DIN 1054 (2010), it has been determined that the partial safety factor applicable to the series of permeability measurements is 1.3. Based on the results of the above presented measurements, the normalized average value (m_y = -33.55) and the standard deviation (s_y = 2.0434) of the log-normal distribution have been also calculated. The coefficient (k_n) for the characteristics values has been determined on the basis of the data provided in Table D.1 of the Eurocode 0 (2010). In this case, for n = 54 and the above mentioned variation coefficient (V_x), it has been determined the coefficient k_n = 1.64 (see Figure 6-13).

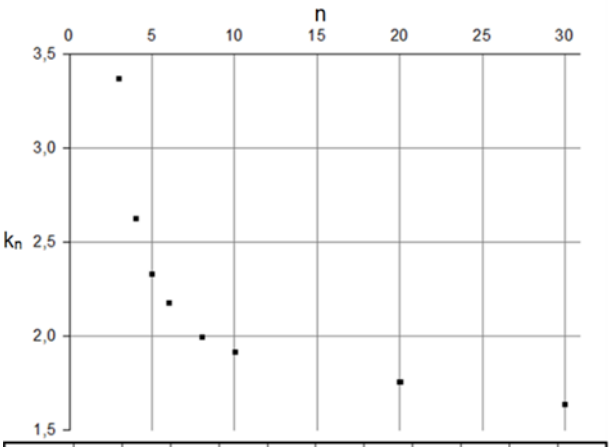

n	1	2	3	4	5	6	8	10	20	30	∞
V_x known	2,31	2,01	1,89	1,83	1,80	1,77	1,74	1,72	1,68	1,67	1,64
V_x unknown	–	–	3,37	2,63	2,33	2,18	2,00	1,92	1,76	1,73	1,64

Figure 6-13:
Values of kn for the 5% characteristic value based on Table D1 (Eurocode 0 2010).

The design value for the permeability of the EDZ at the test site has been estimated to be $K_{EDZ} = 5.9 \cdot 10^{-14}$ m². To allow a comparison with the Kotlin Clay, the design value is normalized to the permeability of the undisturbed host rock. The ratio between K_{EDZ} and K_0 is 295. Transferred to Kotlin Clay, a permeability $K_{EDZ} = 1.68 \cdot 10^{-16}$ m² is estimated. It shall be noted

that this assumption is based on the results of the measurements carried out at the Mont Terri URL. For this reason, in future phases of the present project and as additional data from site investigations become available, this value shall be refined.

6.3.6.1.4 Integral permeability of the asphalt sealing element

Assuming that a quality-assured installation of the asphalt sealing element will be carried out, the integral permeability of the asphalt sealing element only depends on the permeability of the ALZ. Applying equation 6.9, the estimated integral permeability for the asphalt sealing element is $K_{int,Asp} = 2{,}47 \cdot 10^{-16}$ m².

$$K_{int} = \frac{K_D * A_D + K_K * A_K + K_{EDZ} * A_{EDZ}}{A_D} \quad (6.9)$$

with

$K_{int,Asp}$	Integral permeability of the asphalt sealing element	$2.1 \cdot 10^{-18}$ m²
K_D	Permeability of the sealing element	$10^{-\infty}$ m²
K_K	Permeability of the contact zone	$10^{-\infty}$ m²
K_{EDZ}	Permeability of the EDZ	$1.68 \cdot 10^{-16}$ m²
A_D	Area of the sealing element	24.89 m²
A_K	Area of the contact zone	0 m²
A_{EDZ}	Area of the EDZ	36.63 m²

6.3.6.2 Hydraulic resistance of the bentonite sealing element

Similar to the asphalt sealing element the “integral permeability” of the bentonite sealing element is estimated.

6.3.6.2.1 Permeability of the bentonite sealing element

The ramp sealing concept (see chapter 6.2.4) foresees that the bentonite sealing element will consist of Ca-bentonite similar to the one used in the large-scale experiment “Shaft seal Salzdetfurth” (Breidung 2002). This material is the result of a binary mixture of bentonite granulates and pellets. Each pellet has a volume of approximately 0.10 m³, being in total about 70 to 80% of the mixture. The granulate bentonite material has a grain size that ranges from 0 to 3 mm (Gruner et al. 2008).

Since no values resulting from in-situ tests in regard to the potential permeability of similar bentonite sealing elements are known, the design values have been determined on the basis of the data presented in the existing literature. Karnland et al. (2006) determined the permeability of bentonite by applying Darcy’s law. The calculated permeability refers to bentonites in saturated state and the test medium used was pure water. In a similar way, the permeability of bentonite in a Spanish reservoir was determined (Galicia 2002). Finally, Kröhn (2004) compiled permeability values for sodium bentonite (MX-80) from various literature sources. However, no information regarding the conditions of the experiments has been provided. In order to determine the design values for the bentonite element currently foreseen in the ramp seal, only permeability values of bentonites with a dry density ranging from 1600 to 1800 kg/m³ have been considered (Figure 6-14).

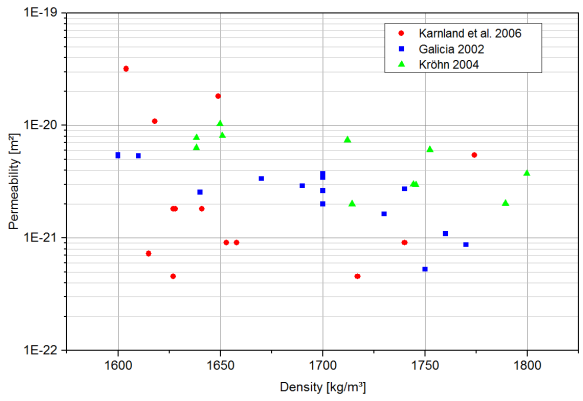

Figure 6-14:
Permeability of saturated samples as a function of the dry density of the bentonite.

Moreover, in order to facilitate the comparison of the values from the different sources, the hydraulic permeability values obtained from Karnland et al. (2006) and from Galicia (2002) have been converted into the concept of permeability according to equation 6.10 provided below.

$$K = \frac{k_f * \eta}{\rho_{Fl} * g} \qquad (6.10)$$

with
K = Permeability [m²], k_f = Hydraulic conductivity [m/s], η = Dynamic viscosity [10^{-3} Pa·s], ρ_{Fl} = Fluid density [kg/m³], g = Gravitational acceleration [m/s²]

As a fluid, it has been considered pure water in an ambient temperature of 25°C (density: 1000 kg/m³, dynamic viscosity: $0.891 \cdot 10^{-3}$ Pa·s). The calculated values are presented in Table 6-2.

Source	Dry density [kg/m³]	k_f [m/s]	K [m²]	ln(K)
(Karnland et al., 2006)	1,604	3.5E-13	3.2E-20	-44.90
	1,615	8.0E-15	7.3E-22	-48.67
	1,618	1.2E-13	1.1E-20	-45.97
	1,627	2.0E-14	1.8E-21	-47.76
	1,627	5.0E-15	4.5E-22	-49.14
	1,628	2.0E-14	1.8E-21	-47.76
	1,641	2.0E-14	1.8E-21	-47.76
	1,649	2.0E-13	1.8E-20	-45.45
	1,653	1.0E-14	9.1E-22	-48.45
	1,658	1.0E-14	9.1E-22	-48.45
	1,717	5.0E-15	4.5E-22	-49.14
	1,740	1.0E-14	9.1E-22	-48.45
	1,774	6.0E-14	5.4E-21	-46.66
(Galicia, 2002)	1,600	5.9E-14	5.4E-21	-46.68
	1,600	6.0E-14	5.4E-21	-46.66
	1,610	5.9E-14	5.4E-21	-46.68
	1,640	2.8E-14	2.5E-21	-47.42
	1,670	3.7E-14	3.4E-21	-47.14
	1,690	3.2E-14	2.9E-21	-47.29
	1,700	2.2E-14	2.0E-21	-47.66
	1,700	3.8E-14	3.5E-21	-47.12
	1,700	2.9E-14	2.6E-21	-47.39
	1,700	3.8E-14	3.5E-21	-47.12
	1,700	4.1E-14	3.7E-21	-47.04
	1,730	1.8E-14	1.6E-21	-47.86
	1,740	3.0E-14	2.7E-21	-47.35
	1,750	5.8E-15	5.3E-22	-49.00
	1,760	1.2E-14	1.1E-21	-48.27
	1,770	9.6E-15	8.7E-22	-48.49
(Kröhn, 2004)	1,650	-	1.0E-20	-46.02
	1,651	-	8.1E-21	-46.26
	1,638	-	7.8E-21	-46.31
	1,638	-	6.3E-21	-46.51
	1,712	-	7.4E-21	-46.35
	1,752	-	6.1E-21	-46.55
	1,745	-	3.0E-21	-47.27
	1,744	-	3.0E-21	-47.26
	1,714	-	2.0E-21	-47.66
	1,789	-	2.0E-21	-47.65
	1,800	-	3.7E-21	-47.03
			Mean m_y:	**-47.31**
			Standard deviation s_y:	**0.9850**
			Variation coefficient V_y:	**0.0208**

Table 6-2: Permeability and dry density of bentonite based on the values provided by Karnland et al. (2006), Galicia (2002) and Kröhn (2004).

The average permeability m_x of the considered data is $2.8 \cdot 10^{-21}$ m² with a standard deviation $s_x = 5.9 \cdot 10^{-21}$ m² and a coefficient of variation $V_x = s_x/m_x = 0.476 = 47.6$ %). The calculated design value of the permeability of the bentonite sealing element is $K_{int\ Ben} = 1.2 \cdot 10^{-20}$ m², which has been calculated by applying equation 6.9.

The analysis of the data available in the existing literature leads to the conclusion that Na-bentonites (e.g. MX-80) have a lower permeability in comparison to Ca-bentonites (e.g. bentonite used in the large-scale experiment “Shaft seal Salzdetfurth” (Breidung 2002)) with the same density. However it shall be noted that a final decision in regard to the final selection of the most appropriate material to be used as sealing element in the ramp seal can only be made after knowing the exact geochemical properties of the host rock and of the pore water as well as the impacts on the sealing system.

6.3.6.2.2 Permeability of the contact zone

The exact form and characteristics (e.g. permeability) of the contact zone are not known at this stage of the project. However, it is assumed that before installing the bentonite sealing element the lining of the ramp will be removed by means of adequate mining techniques. Irregularities at the contour will mainly depend on the behaviour of the rock and on the characteristics of the tools used to remove the lining. However, it shall be noted that certain surface roughness will always appear. It is assumed, that by means of quality assurance activities in the course of the installation of the bentonite sealing element and due to the swelling properties of clay minerals, the potential irregularities and remaining void spaces at the contact zone will be properly sealed.

By gradually paving and by compacting the loose bentonite mixture, a good contact between the sealing material and the contour will be achieved. The contact surface of the bentonite sealing element may form a potential “weak area”, which may have a higher permeability and therefore the risk associated with the potential formation of cracks in this area may also considerably increase. Crack limitation is an aspect that shall be then considered in the course of the assessment of the integrity of the seal.

The preliminary rough estimation of the permeability of the contact zone is based on the fact that the permeability of the contact zone will mainly depend on the roughness of the contour and on the width of the remaining void space. The width of the void space should be determined taking into consideration the granular size of the bentonite. The bentonite that forms the sealing element is characterized by a particle structure formed by grains with a size in the range of a few µm. According to Madsen (1998), the grains of bentonite that can be found in mixtures such as for example binary mixtures have a maximum grain size of 63 µm. As a preliminary approximation, it is conservatively assumed that the width of the remaining void spaces will be twice the maximum grain size.

The characteristics of the surface of the contact zone shall be determined taking into consideration the characteristics of the contour. At this stage of the project, a high roughness of the contour is assumed. According to Barton (1982), the maximal Joint Roughness Coefficient (JRC), i.e. 20, can be assigned to the contour, which corresponds to approximately 5 cm per meter of amplitude of the surface roughness of the contact zone (see Figure 6-15).

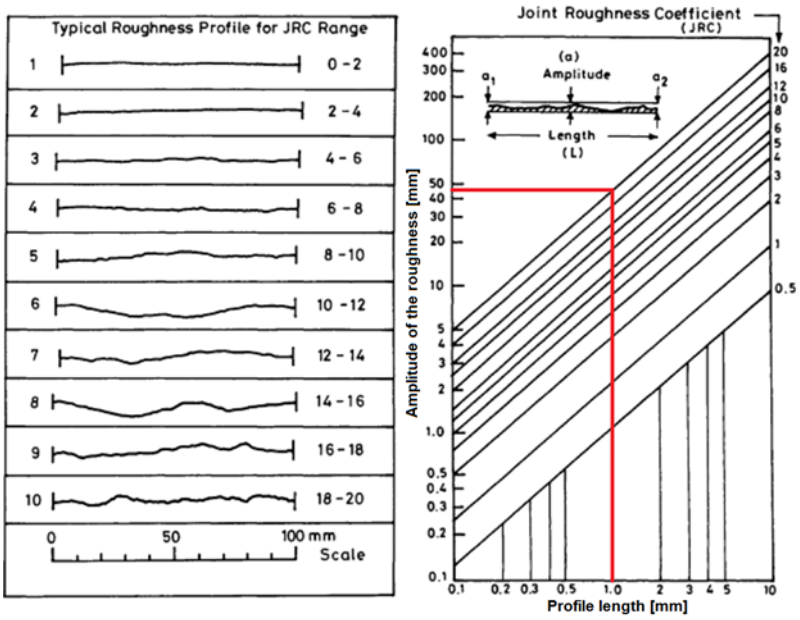

Figure 6-15:
Determination of the JRC (marked in red) (Singh & Goel 1999).

According to Barton (1982), the hydraulic effective width can be determined from the width of the void spaces and from the JRC (equation 6.11)

$$b_{hyd} = \frac{b^2}{JRC^{2,5}} \qquad (6.11)$$

with
b_{hyd} = Hydraulic effective width [µm], b = Width of the void spaces [µm], JRC = Joint Roughness Coefficient.

Assuming a width (b=2·d_{max}) of 126 µm, a roughness (JRC) of 20 and applying equation 6.11, we obtain a hydraulic effective width of 8.9 µm. The contour (r = 2.815 m) will have a theoretical surface of $2.5 \cdot 10^{-4}$ m². According to Witherspoon et al. (1980), from the hydraulic effective width it is possible to calculate the permeability of the void spaces using equation 6.12). In this case, the permeability of the contact zone is estimated to be $6.6 \cdot 10^{-12}$ m².

$$K = \frac{{b_{hyd}}^2}{12} \quad (6.12)$$

with
b_{hyd} = Hydraulic effective width [µm], K = Permeability [m²].

The described approach allows assessing the properties of the contact zone. However, it shall be noted that at the current stage of the project, this evaluation is based on several assumptions that have been made to cover the existing uncertainties. For this reason, all values and characteristics of the contact zone that have been assumed shall be determined by means of appropriate investigations in future phases.

6.3.6.2.3 Permeability of the excavation damaged zone

The form and characteristics of the EDZ at the location of the bentonite sealing element can be considered to be analogue to the EDZ at the location of the asphalt sealing element (see chapter 6.3.6.1.3). Applying the reasoning presented in chapter 6.3.6.1.3, it has been estimated that the EDZ will have a depth of approximately 3.4 m and that the permeability of the EDZ K_{EDZ} will be $1.68 \cdot 10^{-16}$ m².

Due to the fact that at this stage of the project on-site investigations at the “Radon Site” to determine the characteristics of the EDZ have not been yet carried out, it shall be noted that this value is based on the results of the measurements carried out at the Mont Terri URL. For this reason, in future phases of the present project and as additional data from site investigations become available, this value shall be refined.

6.3.6.2.4 Integral permeability of the bentonite sealing element

The integral permeability of the bentonite sealing element is mainly determined by the permeability of the EDZ. The characteristic values used to calculate the integral permeability are:

K_D = $1.2 \cdot 10^{-20}$ m²
K_K = $6.6 \cdot 10^{-12}$ m²
K_{EDZ} = $1.68 \cdot 10^{-16}$ m²
A_D = 24.89 m²
A_K = $2.5 \cdot 10^{-4}$ m²
A_{EDZ} = 36.63 m²

Applying equation 6.9, an integral permeability $K_{int,Ben}$ of $3.14 \cdot 10^{-16}$ m² for the bentonite sealing element can be estimated. This permeability is mainly attributable to the assumed characteristics of the EDZ and contact zone. The permeability of the contact zone, due to its limited dimensions, has limited impact on the integral permeability of the bentonite sealing element. It shall be noted that at this stage of the project various assumptions in regard to the characteristics of the site have been made. These assumptions are mainly based on existing literature data, which lead to a very low integral permeability of the bentonite sealing element. However, these assumptions also lead to uncertainties that shall be reduced in next

phases of the project, as detailed data resulting from additional site investigations become available.

6.3.6.2.5 Assessment of the integral permeability of the bentonite sealing element

It is assumed that after installation of the bentonite sealing element, pore water will flow into the bentonite sealing element and after some time this will become saturated. The time necessary to saturate the bentonite sealing element depends on the sealing design, different properties of the sealing element and is basically pressure driven. The time for saturation can be typically estimated assuming that the pore water flow will behave as an advective flow dependent of the time and of the evolution of the pressure on the sealing element and the complete ramp sealing (see Figure 6-16). This assumption implies applying Darcy's law. However, it shall be noted that at this stage of the project a model to calculate the pressure on the sealing elements over time has not been developed yet.

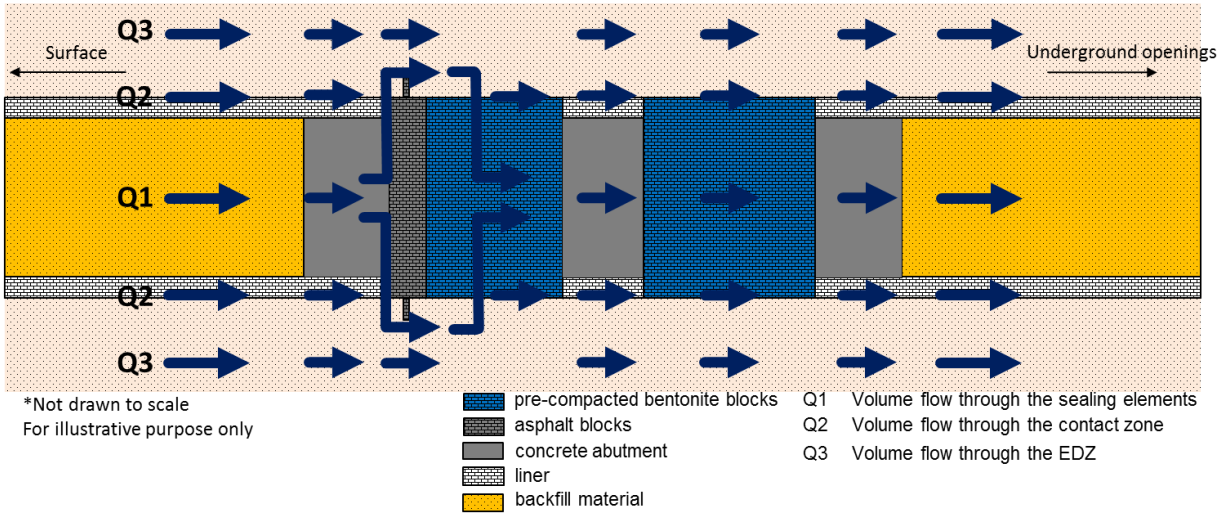

Figure 6-16: Expected volume flow through the ramp sealing elements.

The saturation of the bentonite starts after the sub flow Q3 (see Figure 6-16) passes the asphalt element. In order to estimate the time that will be necessary to saturate the bentonite sealing element, a constant pressure over time has been assumed. The pressure can increase up to the hydrostatic pressure in maximum. Equation 6.13 gives a simple approach to estimate saturation time of one bentonite element based on Darcy's law:

$$t = \frac{L_D^2 \cdot \eta \cdot n \cdot (1 - S_0)}{2 \cdot K_{int} \cdot p_F} \quad (6.13)$$

with

L_D = Length of the sealing element [m], K_{int} = Integral permeability of the sealing element [m²], t = Time [s], p_F = Hydrostatic pressure [Pa], η = Dynamic viscosity of the fluid [Pa·s], n = Porosity [-], S_0 = Initial saturation [-].

The hydrostatic pressure on the sealing element has been estimated applying equation 6.14 and assuming that the sealing element will be located at the deepest end of the ramp, i.e. at a depth of approximately 90 m.

$$\rho_F = g * h * \rho_G \quad (6.14)$$

with

p_F = Hydrostatic pressure [Pa], h = Height [m], g = Gravitational acceleration [m/s²], ρ_G = Density [kg/m³].

Assuming an initial saturation of 75%, a porosity of 25%, a dynamic viscosity of $1 \cdot 10^{-3}$ Pa·s, a length of each bentonite sealing element of 16 m, an integral permeability of the sealing ele-

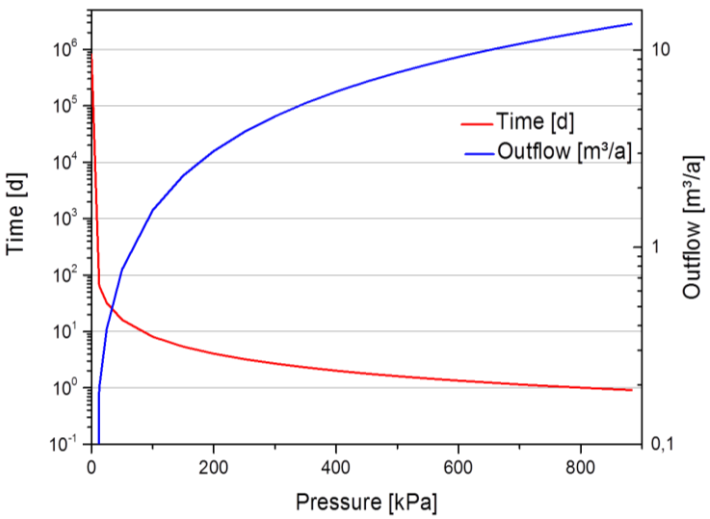

ment of $3.14 \cdot 10^{-16}$ m², the complete saturation of the bentonite sealing elements is expected to occur in about 1 year in case of an instant hydraulic pressure of 882,000 Pa (Figure 6-17).

Figure 6-17:
Expected time for saturation and resultion outflow based on Darcy's law, for pressures within the range of zero to hydrostatic pressure.

The saturation of the bentonite sealing elements will result in a constant increasing volume flow that can be estimated by applying equation 6.15:

$$\dot{V} = \frac{K_{int} \cdot p_F \cdot A_D}{\eta \cdot L_D} \quad (6.15)$$

with
$\dot{V}$ = Volume flow [m³/s], A_D = Area of the sealing element [m²], K_{int} = Integral permeability of the sealing element [m²], p_F = Hydrostatic pressure [Pa], η = Dynamic viscosity of the fluid [Pa·s], L_D = Length of the sealing element [m].

After saturation of the bentonite sealing element, the volume flow through the bentonite sealing elements is estimated to be up to 13.58 m³/a in case of hydraulic pressure (see Figure 6-17). In the available literature, different approaches to determine whether a sealing element can be considered to be tight or not, can be found. For example, according to Wagner (2005), to assess the tightness of a sealing element the average evaporation rate can be considered. According to this approach, a sealing element can be considered to be tight when the volume flow is lower than 40 m³/a. However, Gruner et al. (2008) defined a considerably lower volume flow (5 m³/a) for tight sealing elements.

6.3.6.3 Abutments

The concrete abutments placed at the upper part and at the centre of the ramp sealing element shall ensure the stability of the sealing element. In this first draft version of the sealing concept, simple cylindrical abutments are proposed. The length of the abutments can be determined taking into consideration the tensile stress in the sealing element and the shear stress at the contact zone by applying equations 6.16 and 6.17 (Sitz 1981).

$$\mathrm{erf}\, L_{W,bz} = r \cdot \sqrt{\frac{0{,}375 \cdot (1+\nu) \cdot p}{\sigma_{Z,zul}}} \quad (6.16)$$

with
$\mathrm{erf}\, L_{w,bz}$ = Required length to withstand the tensile stress [MPa], r = Radius [m], p = Pressure on the surface of the abutment [MPa], ν = Poisson ration of the abutment [-], $\sigma_{Z,zul}$ = Tensile stress at the abutment [MPa].

$$\mathrm{erf}\, L_{W,T} = \frac{A \cdot p}{U \cdot \tau_{zul}} \quad (6.17)$$

with
$\mathrm{erf}\, L_{w,T}$ = Required length to dissipate the static load [m], A = Cross sectional area [m²], p = Pressure on the surface [MPa], U = Perimeter [m], τ_{zul} = Shear stress at the contact zone [MPa].

According to the current conceptual design of the sealing elements the abutments in the ramp will have a radius of 2.815 m and, therefore, a surface of 24.89 m² and a perimeter of 17.68 m. The Poisson ration of the concrete is 0.2 and the mean tensile strength of the concrete type C35/45 ($f_{ctk,0,05}$) is 2.2 MPa. By applying equation 6.18 (Eurocode 2 2010) the design value of the concrete tensile strength can be calculated.

$$f_{ct} = \alpha_{ct} \cdot \frac{f_{ctk,0,05}}{\gamma_C} = 0{,}7 \cdot \frac{2{,}2 {}^{N}/_{mm^2}}{1{,}5} = 1{,}03\ MPa \qquad (6.18)$$

f_{ct} Design value of the concrete tensile strength [MPa]
α_{ct} Coefficient to consider the long-term effects [-]
$f_{ctk,0,05}$ 5%-Quantile of the characteristic value of the concrete tensile strength [MPa]
γ_c Partial safety factor for concrete [-]

The calculated designed value of the concrete tensile strength can then be used as the tensile strength at the abutment ($\sigma_{Z,zul}$) to calculate the required length of the abutment to withstand the tensile stress (erf $L_{w,bz}$) (see equation 6.16).

The shear strength between the host rock and the abutment will be determined by the characteristics of the contact zone. However, at this stage of the project the mechanical properties of the contact zone are still not known. For this reason, in order to assess the suitability of the foreseen abutments, the cohesion of the host rock and the splitting tensile strength of the concrete ($f_{ctk,sp}$) shall be considered. The cohesion of the Kotlin Clay at the "Radon Site" is assumed to be 4.61 MPa (Pereverzeva et al. 2008) and the concrete splitting tensile strength can be calculated by applying equation 6.19 (HeidebergCement 2014).

$$f_{ctk,sp} = \frac{f_{ctk,0,05}}{0{,}9} \qquad (6.19)$$

$f_{ctk,sp}$ Concrete splitting tensile strength [MPa]
$f_{ctk,0,05}$ 5%-Quantile of the characteristic value of the concrete tensile strength [MPa]

Assuming that concrete of the strength class C35/40 will be used to build the abutments, the calculated concrete splitting tensile strength ($f_{ctk,sp}$) is 2.44 MPa. By using the calculated splitting tensile strength and applying equation 6.18 we obtain a design value ($f_{ct,sp}$) of 1.12 MPa. This calculated design value can be used as shear stress at the contact zone (τ_{zul}) in equation 6.17 to calculate the required length of the abutment to dissipate the static load (erf $L_{w,\tau}$).

At this stage of the project a model to calculate the pressure on the sealing elements over time has not been developed yet. For this reason the minimal required length of the abutments has been determined assuming that the pressure on surface of the abutments will be the result of two main circumstances. On the one hand the swelling pressure caused as a result of the saturation of the bentonite sealing elements. On the other hand the hydrostatic pressure at the depth at which the ramp seal will be placed (Figure 6-18).

As shown in Figure 6-18, the abutment located at the side of the ramp seal closer to the surface and the abutment located in the centre of the ramp seal will withstand pressures applied on both sides of the abutments. However, the abutment located at the deepest part of the ramp may withstand pressures applied only on one side of the abutment and therefore seems to be the most critical one. For this reason the required length of the abutments have been calculated taking into consideration the specific circumstances of the abutment located at the deepest part of the ramp.

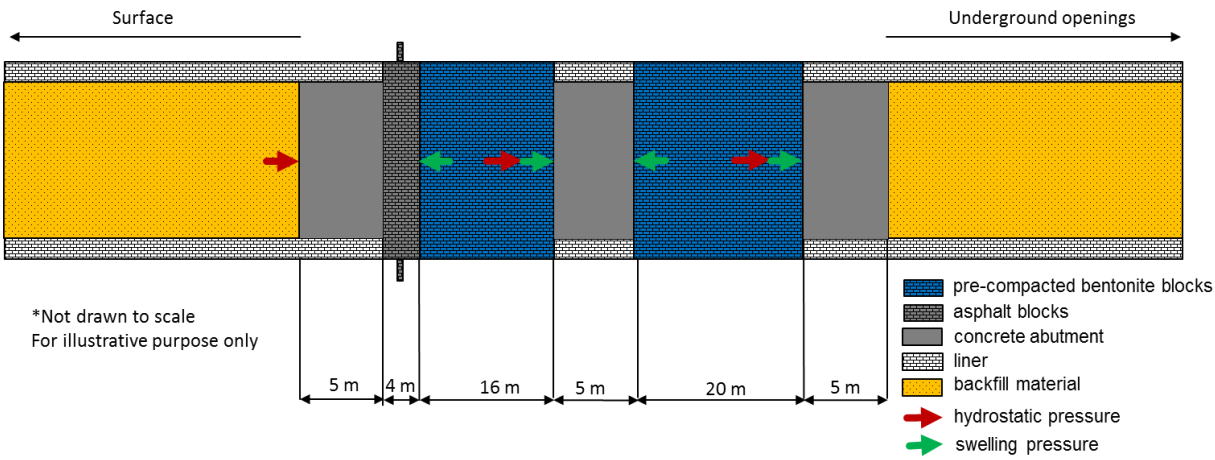

Figure 6-18: Pressure on the surface of the abutments in the ramp.

Assuming a depth of 90 m and by applying equation 6.13 the hydrostatic pressure has been estimated to be 826,200 Pa. At this stage of the project is not possible to determine the swelling pressure caused by the saturation of the bentonite sealing elements. For this reason, for calculation purposes, based on the results of the large-scale experiment “Shaft seal Salzdetfurth” (Breidung 2002) it has been assumed that a swelling pressure of approximately 1 MPa is required to properly seal the contact zone and therefore the ramp.

Based on these assumptions and applying equations 6.16 and 6.17, the required length of the abutment to withstand the tensile stress (erf $L_{w,bz}$) and the required length of the abutment to dissipate the static load (erf $L_{w,T}$) have been estimated to be 2.5 m and 2.3 m respectively. Due to the high level of uncertainty at this stage of the project, following a conservative approach results in a proposed ramp seal concept with a length of the abutments of 5 m, which is to ensure that the abutments will withstand the expected impacts and therefore will fulfil their function.

7 Specific process analyses regarding the sealing system

To increase the system understanding some process analyses regarding the sealing system have been performed. These analyses comprise the problem of plug implementation with regard to the long-term safety, the gas pressure build up in an emplacement chamber and the gas migration through the underground openings.

7.1 Numerical investigation on plug implementation

The first process analysis was performed to investigate the influence of the plug implementation on the host rock. It has been done by using numerical simulations with a special focus on the dismantling of the drift liner at the sealing location.

7.1.1 Model description

3D numerical simulations were performed using FLAC3D (Itasca 2012a, b). The model which extends from the ground level down to a depth of z=150 m, is 90.0 m long in the x-direction and 75.0 m long in the y-direction. The tunnel is located at the center of the model at a depth of 75.0 m. The tunnel crosses the model along the x-axis and has a radius of 5.6 m. For symmetry reasons, only half of the host rock and the tunnel need to be modeled. The mesh model consists of 464,640 hexahedral zones (Figure 7-1).

Roller boundary conditions are applied at both boundaries in x-direction. A roller boundary condition suppose that only the degree of freedom perpendicular to the boundary face is fixed while gridpoints are free to move along the two other degrees of freedom parallel to the boundary face. The boundary in y-direction located 75 m from the model center and the bottom boundary in z-direction are also held by the roller supports. The top of the model is free to deform.

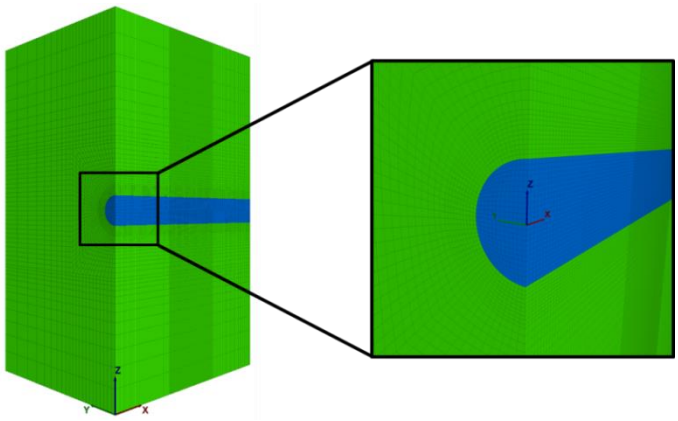

Figure 7-1:
Illustration of model discretisation.

The model is divided into five different sections along the x-axis (Figure 7-2, left).

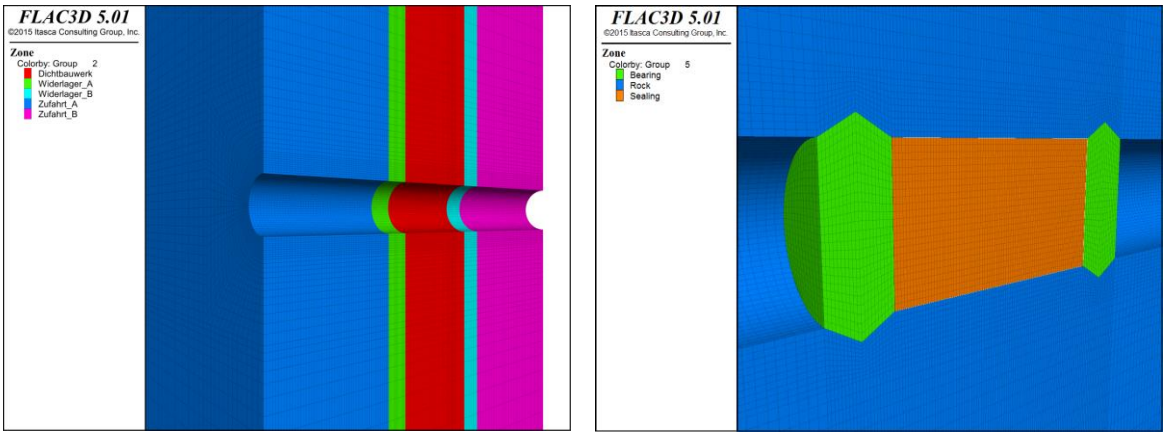

Figure 7-2: (Left) The sections along the x-axis will contain the sealing material (red) and two abutments (green and cyan). (Right) The sealing system, consisting of two abutments and the sealing material in between.

After the excavation of the tunnel, the central model section (red) contains the sealing material. The two adjacent sections contain abutments while the sections at the model boundary remain as an open tunnel (Figure 7-2, right). The final seal is assumed to have a length of 20.0 m. Each abutment has a length of 5.0 m and reaches 1.5 m into the surrounding rock.

Since the simulated tunnel will be located in a claystone the strain-hardening/softening ubiquitous joint model (SUBI) is used (Itasca 2012b). It is based on a Mohr-Coulomb material with the possibility to define a plane of weakness. For the matrix as well as the bedding a Mohr-Coulomb failure criterion with a tension cutoff is considered. In addition the cohesion, the tensile strength, the friction and dilation angle are able to harden or soften after the onset of plastic yield (Figure 7-3).

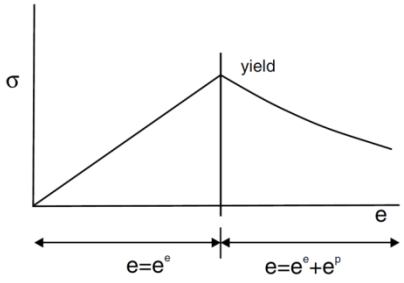

Figure 7-3:
Softening behaviour after plastic yield (Itasca 2012b).

The softening/hardening parameters are functions of the plastic strain provided by user defined FLAC3D tables. The softening/hardening tables are defined via four values: The initial friction angle, the residual friction angle and two plastic deformations eps1 and eps2 (Figure 7-4). From the onset of plastic yield to a deformation of eps1, the friction angle stays at the initial value. The complete softening occurs between deformations of eps1 and eps2. For plastic deformations higher than eps2, the friction angle remains at the residual value. The eps1 and eps2 values are user defined. It is possible to assume either a continuous softening, or a rather instantaneous softening.

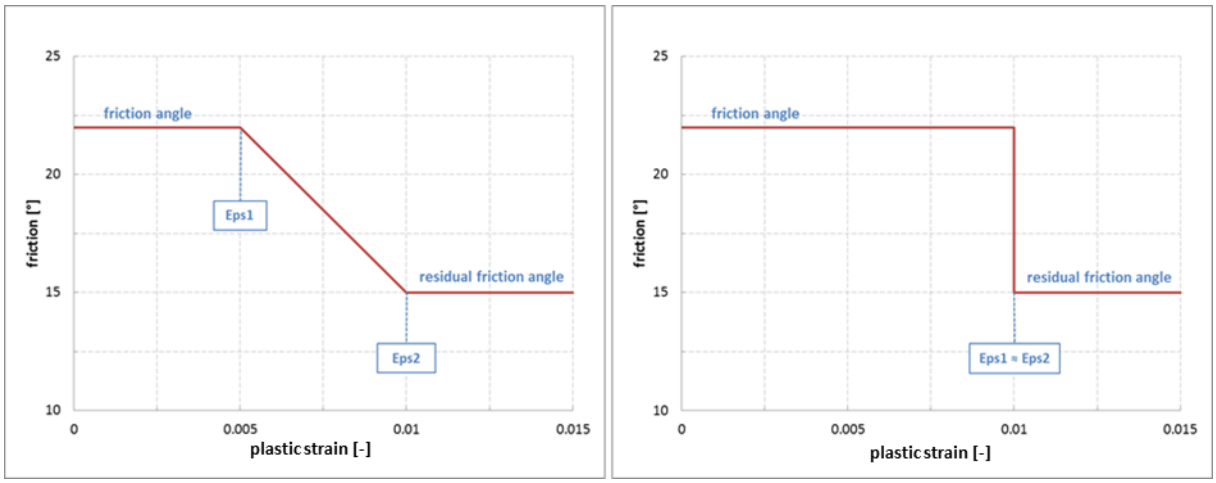

Figure 7-4: Examples of softening tables with a contious softening (left) and an instantaneous softening (right).

Table 7-1 gives the values of the SUBI parameters used during the simulations. For conservative reasons, an instantaneous softening as illustrated in Figure 7-4 (right) is considered.

Parallel to the tunnel excavation, an elastic support (lining) is installed. The properties correspond to a B50 concrete lining with a density of 2200 kg/m^3, a Young's modulus of 40.0 GPa and a Poisson Ratio of 0.2, similar to the support material used in the former R&D project GENESIS (Jobmann et al. 2007). A B50 concrete is also used as a material for the abutments. The sealing material is corresponding to a bentonite (Jobmann et al. 2007) with a

density of 2000 kg/m^3, a Young's modulus of 200.0 MPa and a Poisson Ratio of 0.45. The parameters are summarized in Table 7-2.

Table 7-1: List of material parameters used (Kühnlenz & Hammer, 2014).

Parameter	Unit	Value	
Density	[kg/m^3]	2250.0	
Young's Modulus	[MPa]	100.0	
Poisson Ratio	[-]	0.3	
Bedding Dip Angle	[°]	0.0	
Bedding Dip Direction	[°]	90.0	
		Matrix	**Bedding**
Tensile Strength	[MPa]	0.1	0.05
Residual Tensile Strength	[MPa]	0.04	0.02
Cohesion	[MPa]	0.5	0.20
Residual Cohesion	[MPa]	0.2	0.07
Friction Angle	[°]	22.0	18.0
Residual Friction Angle	[°]	15.0	12.0
Dilatancy	[°]	10.0	10.0
Residual Dilatancy	[°]	0.0	0.0

Table 7-2: Mechanical properties of the tunnel support and the sealing system

Parameter	Unit	B50 (Support & abutment)	Bentonite
Density	[kg/m^3]	2200.0	2000.0
Young's Modulus	[GPa]	40.0	200.0
Poisson Ratio	[-]	0.20	0.45

7.1.2 System evolution

The tunneling process is simulated by a sequential excavation of the corresponding elements. The simulation of the concrete lining is realized by using the FLAC3D shell structural elements. After completing, a removal of the tunnel lining at the plug location is performed. Afterwards the sealing system can be installed, including the two abutments.

In order to understand the behavior and to determine the structural integrity of the host rock during the excavation, specific variables are recorded. The magnitude of displacement is the resultant deformation which occur in the x-,y- and z-direction in the model. It gives an overview of the convergences which occur in the host rock when the tunnel is being excavated. With the displacement in the z-direction, deformations at the top of the drift can be estimated. The EDZ is calculated from the occurred strain in each zone. If the strain in the zone reaches the maximum elastic strain level, then plasticity takes place according to Figure 7-3 and the zone is considered as damaged. The stress ratio is calculated as the quotient of the occurred deviatoric stress over the shear resistance of the claystone in the zone. The stress ratio is calculated independently for the matrix part and the bedding part of the zone according to the SUBI material model. Therefore, the stress ratio of a zone is the maximum of both ratios. The stress ratios are defined as follows:

Shear failure criterion of the matrix:

$$f_s = \sigma_1 - \sigma_3 \cdot N_\varphi + 2 \cdot c \cdot \sqrt{N_\varphi} = 0$$

Resulted stress ratio for the matrix:

$$\eta_{Matrix} = \frac{\sigma_1 - \sigma_3 \cdot N_\varphi}{2 \cdot c \cdot \sqrt{N_\varphi}}$$

with:

σ_1: minimum principal stress, σ_3: maximum principal stress, c: cohesion, φ: friction angle

$$N_\varphi = \frac{1 + \sin\varphi}{1 - \sin\varphi}$$

Shear failure criterion of the bedding:
$f_s = \tau + \sigma_{xx} \cdot \tan\varphi - c = 0$

Resulted stress ratio for the bedding
$\eta_{Matrix} = \frac{\tau}{\sigma_{xx} \cdot \tan\varphi - c}$

with:
σ_{xx}: normal traction component on the bedding
$\tau = \sqrt{{\sigma_{xz}}^2 + {\sigma_{xy}}^2}$: tangential traction component on the bedding

The minimum and maximum principal stresses give the stress state in the model. Particularly, positive stresses lead to tensile failure and maximum stress concentrations show implicitly the regions where softening is occurring in the model.

7.1.3 Simulation of tunnel excavation

The primary stress conditions correspond to the stress state in the rock mass before any excavations. These stresses are equal to the weight of the rock and therefore increase linearly over the depth. With regard to Table 7-1 the vertical stress is zero at the ground surface and increases to -3.31 MPa at 150 m. Compression stresses are negative per convention. Since a stress anisotropy factor of 0.5 is imposed in the model, the horizontal stresses are equal to half of the value of the vertical stress. The horizontal stresses at 150 m should then be equal to -1.65 MPa.

7.1.3.1 Excavation of the tunnel without lining

The tunnel is first excavated without a lining. The excavation length is set to 2 m. This leads to 45 excavation steps. Figure 7-5 shows an illustration of how the tunnel is numerically excavated. The tunnel zones are grouped in a new group slot to generate 45 excavation groups. The excavations take place by removing the excavation group. After which the deformations occur and stress redistribution takes place.

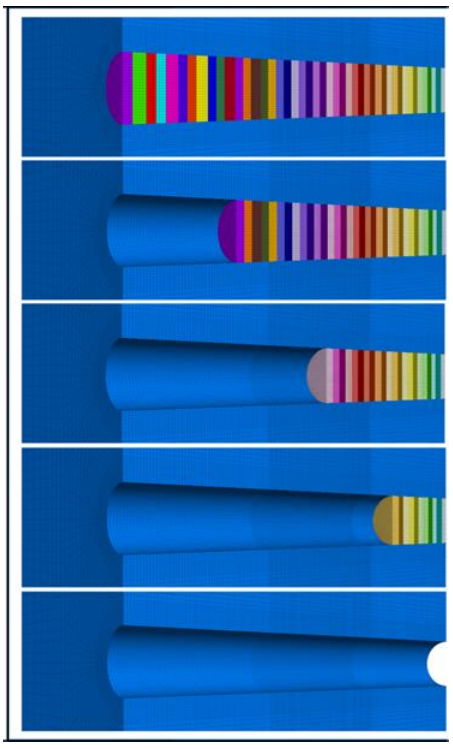

Figure 7-5: Excavation sequence of the tunnel without lining.

Evaluation of displacements

Figure 7-6 shows the occurred deformations during the excavation process. The displacements (or deformations) are ranged between 0 cm (blue color) and 30 cm (red color). The illustrated displacements are the magnitude of displacements in x-, y- and z-direction. It can be observed that the displacements increase with the excavation progression. An important part of the rock mass surrounding the tunnel is subjected to high deformations. At the end of the excavation, the contour line of the regions of the rock mass where the displacements reached 30 cm (red region) is located at about 20 m deep in the rock over the top of the tunnel. The displacements at the ground surface reach more than 15 cm. The maximum displacement at the top of the tunnel is about 1.2 m. The elevation of the tunnel floor reaches 60 cm. This represents a vertical convergence of 1.8 m. This means that the tunnel will have a radius reduced by about 0.9 m. In horizontal y-direction, displacements at the side wall of the tunnel have their maximum at 60 cm.

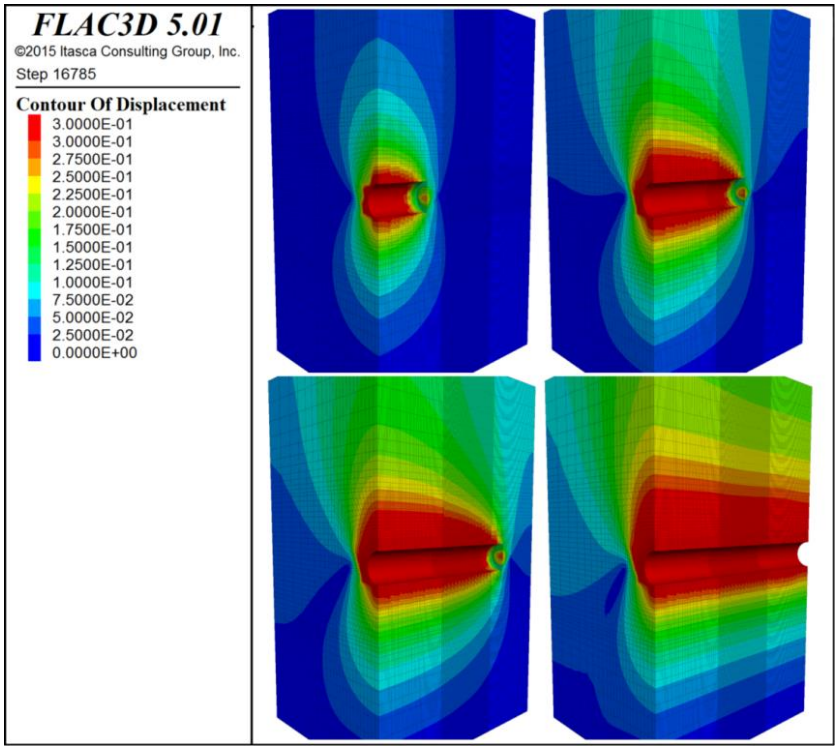

Figure 7-6:
Displacement magnitude at four different excavation steps.

Evaluation of the EDZ

Figure 7-7 shows the resulting excavation damaged zone in several excavation steps. A zone is damaged when the plastic strain in each zone reaches the plastic strain limit which is set to 1%. The damaged zone is then shown in red. The influence of the excavation process can be observed: A peak of damaged zone occurs after every excavation step. This takes place every two meters. Every peak has a length of up to 15 m. Between the peaks, the strain reaches up to 80% of the plastic strain level.

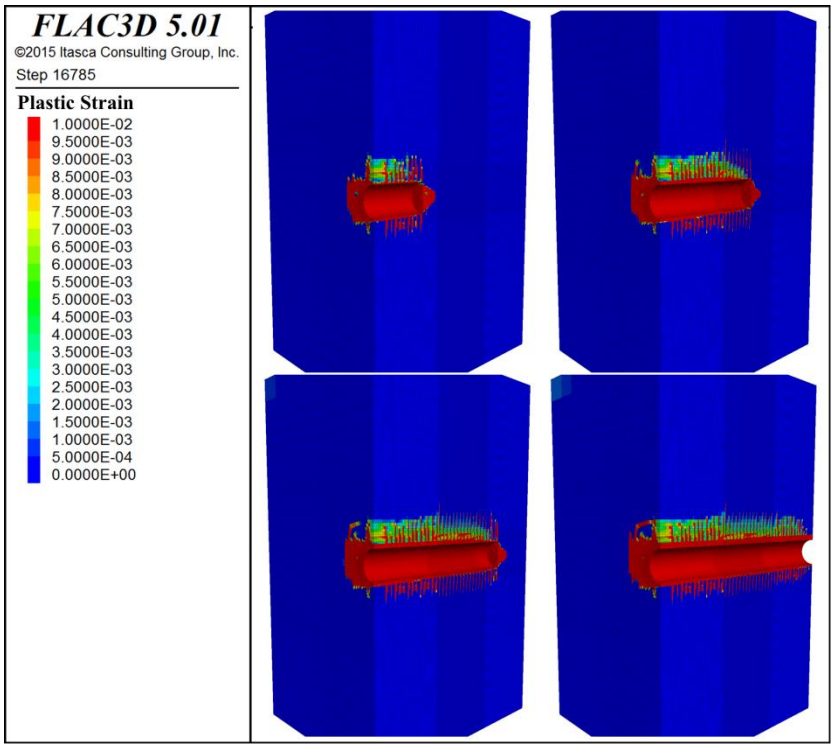

Figure 7-7:
Zones with plastic strain at four different excavation steps.

The integrity of the claystone in the regions between the damaged peaks cannot be warranted. From a conservative perspective, it can be considered that the excavation damaged zone surrounds the complete length of the tunnel over a depth of up to 15 m.

Evaluation of stress ratios

In order to have an overview of the strength reserve of the rock after being stressed due to the excavation, the stress ratios for the matrix and bedding parts of the claystone are calculated for each finite difference zone. The stress ratios are shown in Figure 7-8 for the matrix and for the bedding. A stress ratio of 1 represents the damaged zones.

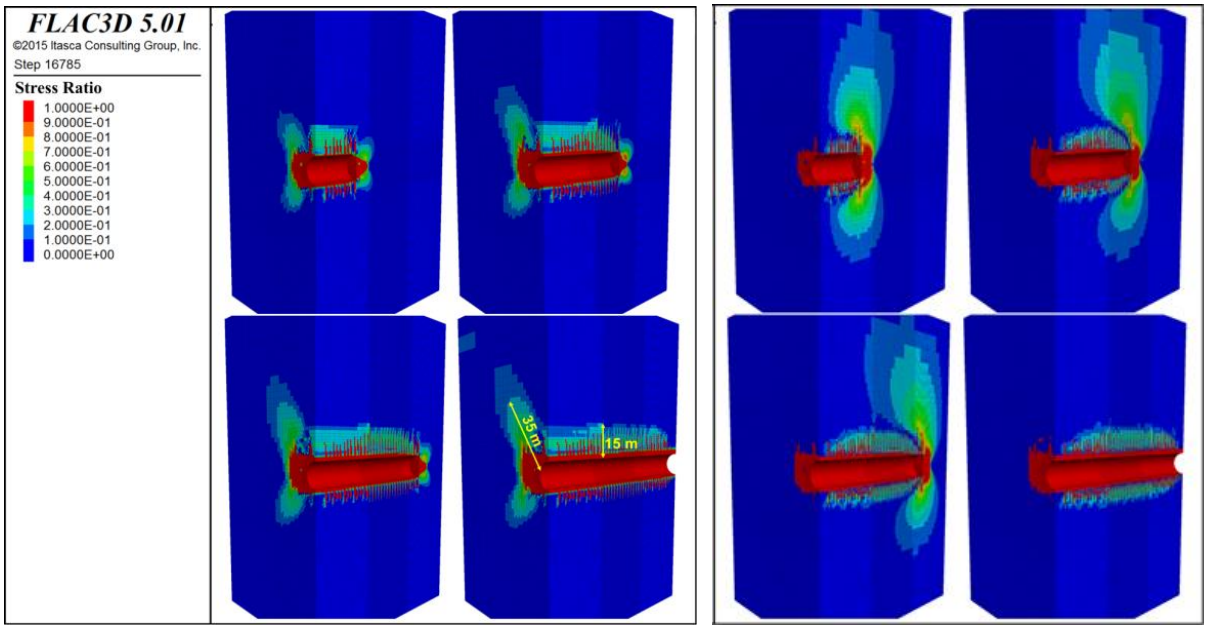

Figure 7-8: Stress ratio of the matrix part (left grapfs) and the bedding part of claystone (right graphs) at four different excavation steps.

The evaluation of the stress ratio of the matrix shows that the matrix is stressed in the surrounding region of the tunnel. Particularly, the more stressed regions of the rock mass matrix reach 15 m from the top, and 35 m from the wall in the 45° and 135° directions clockwise from the z-axis. The maximum stress ratio at the limit of the stressed regions is about 0.5 (Figure 7-8). The examination of the stress ratio of the bedding in Figure 7-8 shows an important stressed region at the front of the excavated tunnel progressing with the excavation. Even at the ground surface, 70 m above the excavation, the rock mass is still stressed to 10% of the mechanical strength of the rock. In addition, the surrounding region of the tunnel is also stressed up to 50% in the bedding part of the claystone. Although the structural integrity of the rock is not endangered, the rock is still stressed and phenomena like microcracking and dilatancy which may lead to an increase of permeability cannot be excluded.

7.1.3.2 Excavation of the tunnel with lining

In this case, the excavation of the tunnel is accompanied by the installation of a shell lining. Figure 7-9 shows the excavation process with lining. The lining is here illustrated in yellow and consists of a 20 cm concrete shell structure. The model parameters for the concrete are given in Table 7-2. From a structural engineering perspective, the shell lining is a combination of a plate and a membrane structure. A plate structure can carry loads in its normal direction. This leads to bending moments and shear forces in the structure. A membrane can carry load only in its longitudinal direction. Thus, only normal forces occur as reactions in the structure. A shell structure, which combines the structural behavior of both precedent structures, can then support bending moments, shear and normal forces.

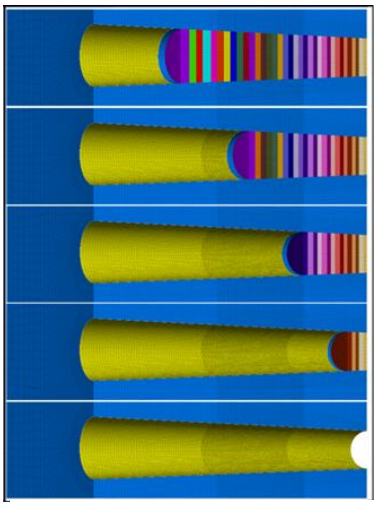

Figure 7-9: Excavation process with successive lining.

These moments and forces are necessary for the structural design of the lining shell structure. Frictions between the lining and the surrounding rock are not considered. Constructible measures are assumed to be performed during the installation of the lining to avoid these frictions.

Evaluation of displacements

The displacements in the model during several excavation steps are shown in Figure 7-10. One can see that only a very small area surrounding the tunnel is subjected to deformation. The displacement magnitude is limited to less than 15 cm directly at the tunnel wall but de-decreases rapidly to less than 5 cm in a distance of a very few meters from the tunnel wall. Thus, the structural integrity is improved in comparison to the case without lining (see Figure 7-6). The maximum displacement in the vertical direction is 14 cm at the top and 16 cm at the bottom of the tunnel. Only about 7 cm occur in the horizontal direction at the tunnel wall.

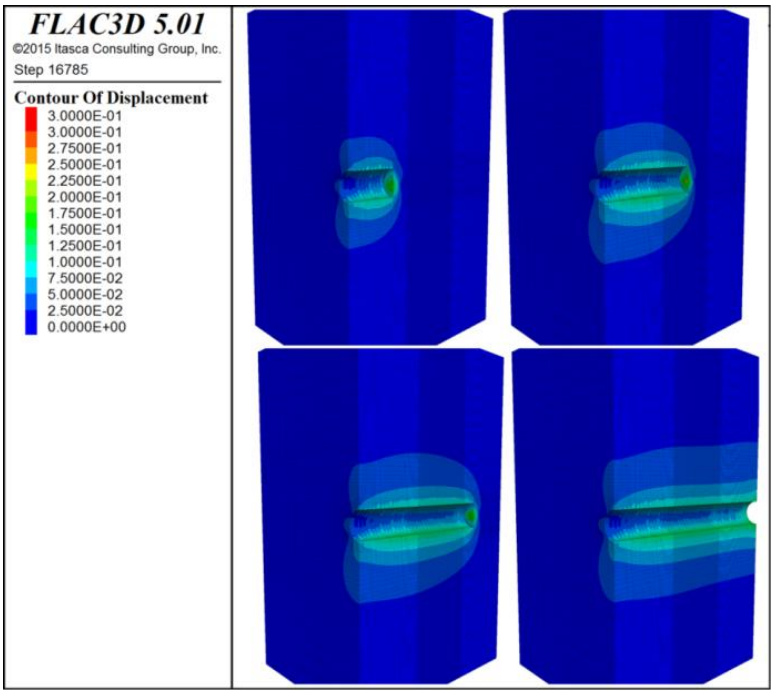

Figure 7-10:
Displacement magnitude at four different excavation steps..

Evaluation of the EDZ

Figure 7-11 illustrates the strain rate resulting from the excavation of the tunnel with the installation of the lining for several excavation steps. In comparison to the excavation without a concrete lining on can notice a net reduction of the damage. The maximum extension of damage is found in only three meters distance from the tunnel wall. The damage reached more than 15 meters in the case without lining.

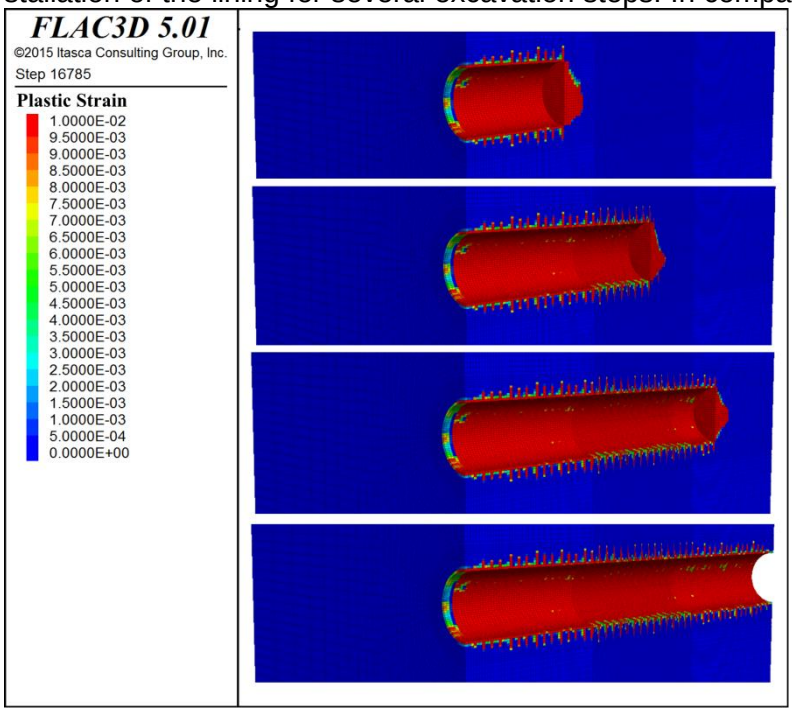

Figure 7-11:
Plastic strains at four different excavation steps.

Evaluation of stress ratios

The evaluation of the stress ratio of the matrix presented in Figure 7-12 (left) shows that the matrix is stressed only in the area next to the tunnel wall, especially at 45° and 135° clockwise from the z-direction over a depth of 7 m from the wall. There, the stress ratio is always smaller than 0.4 to 0.5. The stressed region at the front of the excavation is due to the loosening of claystone which occur during excavation.

The contour plot of the stress ratio in the bedding part of claystone illustrated in Figure 7-12 on the right side shows that the bedding is stressed in radial direction of the tunnel. The loosening at the front of the tunnel leads also here to high stress ratios. Nevertheless, the stressed region at the front goes up to 1 m deep in the rock whereas the rock mass was stressed up to the ground surface in the case of excavation without lining.

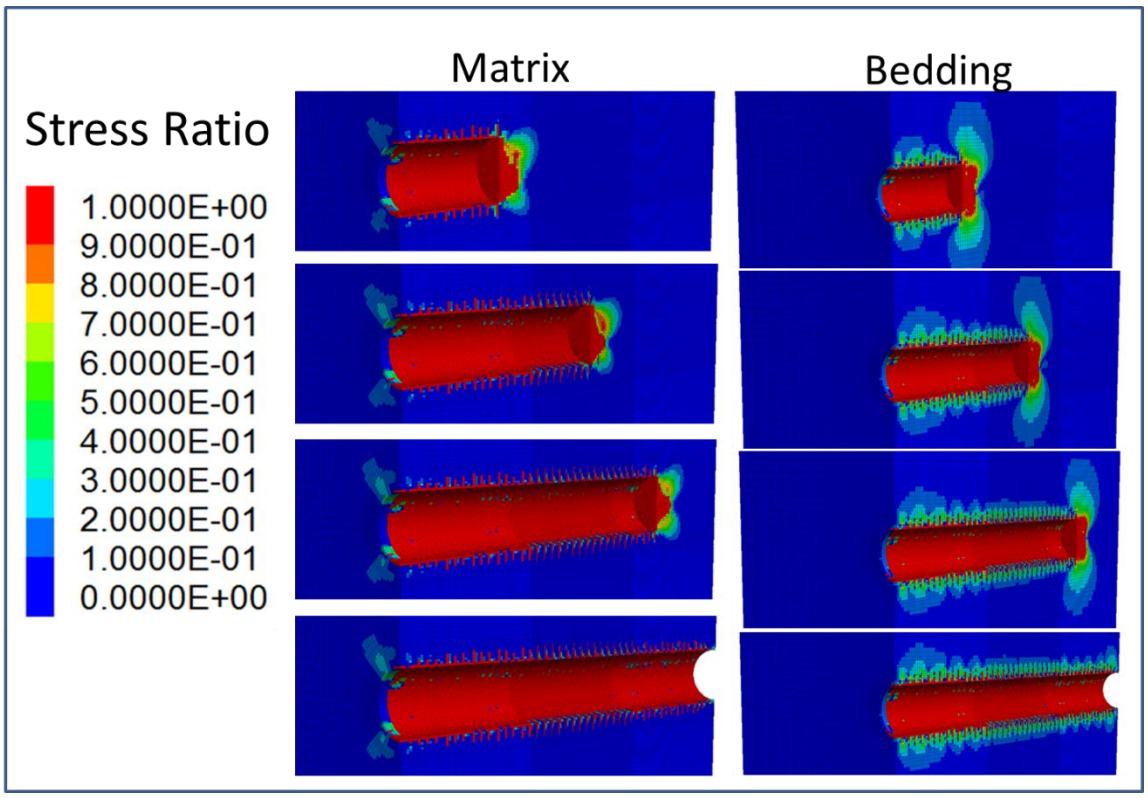

Figure 7-12: Stress ratio of the matrix (left) and of the bedding (right).

7.1.4 Simulation of lining removal and plug implementation

For the bentonite plug a linear elastic behavior is applied. In order to keep the swelling bentonite plug in place, two abutments made of concrete are foreseen according to Figure 7-2. The abutments require an additional excavation in radial direction of the tunnel to assure an anchoring in the rock mass. In order to estimate the structural stability of the rock during the plug implementation, several approaches have been investigated.

7.1.4.1 Sequential removal of the tunnel lining over the complete plug length

The first approach consists of removing the lining over a length of five meters where the first abutment is installed. This step is followed by a further excavation in radial direction of the tunnel considering the geometric shape of the abutment and its anchoring in the host rock. Thereafter, the lining is successively removed in steps of 2 m over the complete length of the bentonite plug. Finally, the excavation for the second abutment is done.

Figure 7-13: shows the contour of the displacement magnitude at the end of the excavation. One can observe that the displacements increase over the complete plug length. A region surrounding the plug starting from the tunnel wall up to 13.5 m deep into the rock at the top, and up to a depth of 10.5 m from the floor is subjected to high deformations. This area is marked with a line in Figure 7-13.

The minimum of displacement in this region is 20 cm at the boundary line and the deformations reach more than 50 cm at the top of the tunnel.

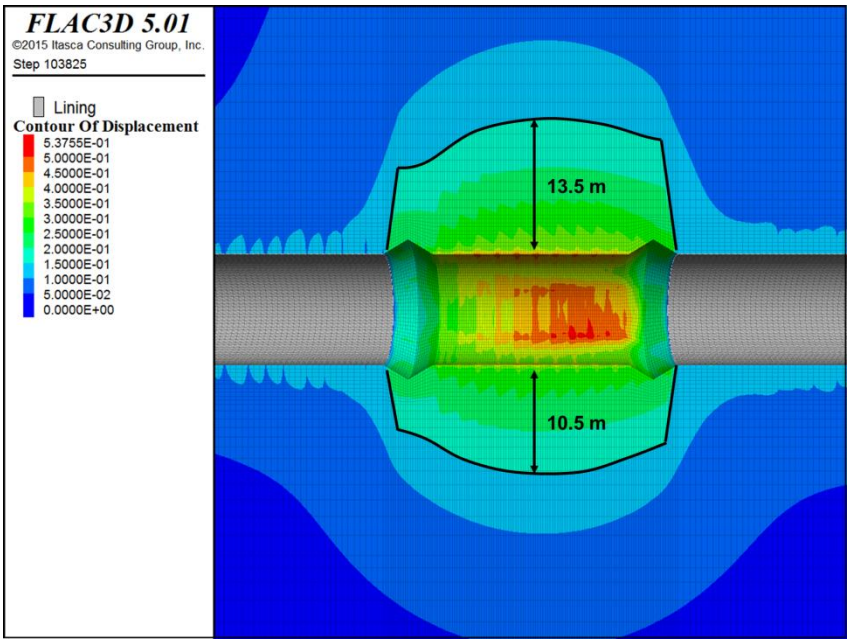

Figure 7-13:
Displacement magnitude in the plug area.

The contour plot of the plastic strain which results after the removal of the lining is shown in Figure 7-14. The enlargement of the tunnel in the places where the abutments will be installed causes some distinctive damage peaks at the boundary to the remaining concrete lining. These peaks have a depth of 15 m into the rock. They mark the boundaries of the area enclosed by a line in Figure 7-13 where large displacements occur and where stress relaxation takes place.

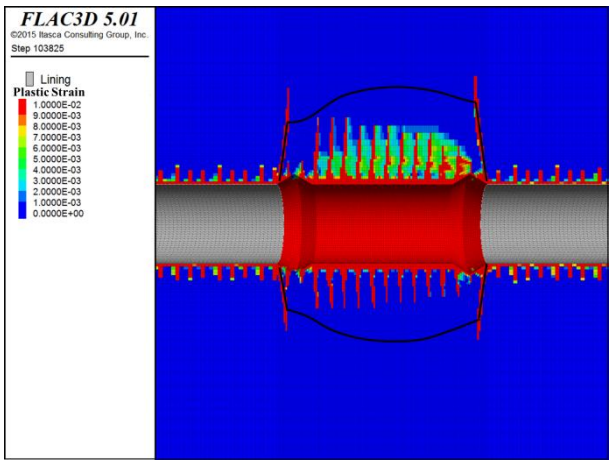

The damage structure along the plug length is similar to those observed during the installation of the lining (cf. Figure 7-11) but instead of three meters plastification depth, the plastification penetrates up to ten meters into the rock.

Figure 7-14: Plastic strain in plug area.

Since the tunnel is unsupported after the removal of the lining, deformations occur along the plug length. These deformations lead to a propagation of the plastification which has been initiated during the excavation of the tunnel. It is therefore obvious that the plastification which occurs along the plug length and the damage at the level of the abutments are caused by different phenomena. In order to explain the plastification at the level of the abutments, it is important to analyze the shear stresses in the model.

Figure 7-15 (left) shows the shear stresses which occur in the rock at the end of the removal and excavation works. One can observe high shear stress concentrations at the level of the abutments directly at the boundary to the remaining lining. One can therefore assume that the remaining lining influences the observed shear stresses. To verify this assumption, the static model illustrated in Figure 7-15 (right) is considered. This model is a structural idealization of the 3D model simulated with Flac3D. The rock over the complete length of the sealing construction is represented by a structural beam. The lining is represented by structural supports at both ends of the beam. The deformations of the rock mass are the load acting on the beam. The influence line of shear forces resulting from this static model is shown in the figure as well.

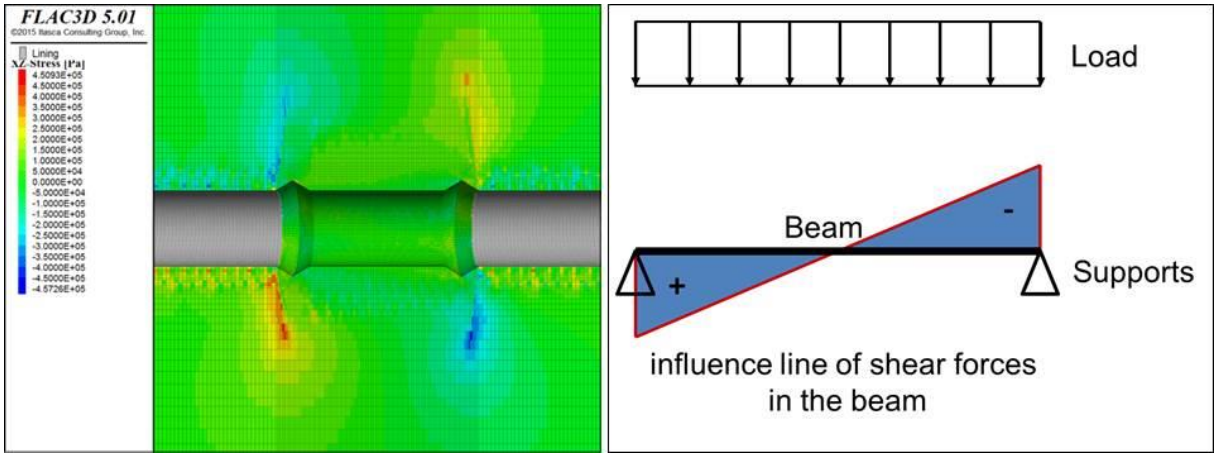

Figure 7-15: Shear stresses in the model (left), Analogy to a structural beam (right).

One can observe that the shear forces in the beam due to the load are maximal directly at the supports. In addition, the shear forces at the supports are antimetric. This antimetry can also be observed in the shear distribution of the 3D model in Figure 7-15 (left). One can conclude that the analogy of a structural beam reproduces and thus illustrates the behaviour of the tunnel after the removal of the lining over the complete length of the plug. The plastification peak at the location where the abutments will be installed can be explained by the fact that the tunnel is supported by the lining in the area of the abutments. At this location, the shear stresses are maximal in analogy to the structural beam. This shear stresses lead therefore to high plastification peaks next to the remaining lining.

The stress ratio distribution for the matrix of claystone is plotted in Figure 7-16. The Figure shows that the matrix is stressed principally at the top of the tunnel over the excavated length. The stress area surrounds the plastified damaged zones. The maximum stress ratio reaches up to 50% of the matrix shear resistance. The plastified zones are characterized with a stress ratio of 100%. The matrix is not stressed in the part of the tunnel where the lining is still present.

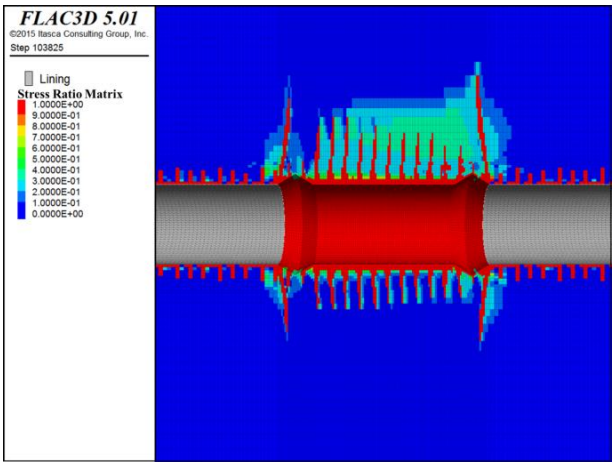

Figure 7-16:
Stress ratio for the matrix part of the rock.

The stress ratio distribution of the bedding part of the claystone presented in Figure 7-17 shows that an important part of the rock is stressed in the bedding part of claystone. The rock is stressed up to 30 m above the top and up to 20 m under the drift floor. The stressed area is concentrated at both ends of the excavated part of the tunnel and surrounds the plastification peak due to the shear stresses.

The stress ratio in the area surrounding the peaks next to the lining ends decrease progressively from 100% in the plastified zones to 0% several meters from the peak. Therefore, one can deduce that the stress ratio distribution observed is due to stress redistribution which takes place when the shear stresses induced damage peaks occur. In addition, it becomes evident that the shear stresses which occur due to the support effect of the lining at both ends of the newly excavated drift part lead principally to a plastification in the bedding. This stresses don't seem to influence the matrix. The stress ratio distribution in the surrounding area of the plug is limited to 20% of the bedding shear strength.

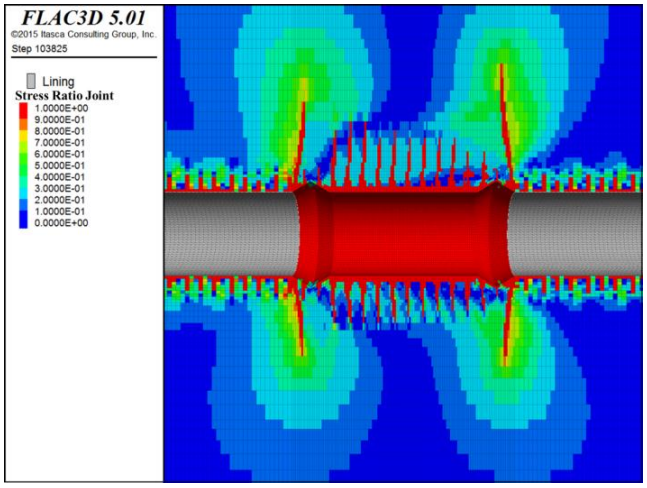

Figure 7-17:
Stress ratio for the bedding part of the claystone.

7.1.4.2 Sequential removal of the tunnel lining and installation of the plug

The second approach consists of installing the abutments and the bentonite sealing element after the sequential removal of the lining. The lining is first removed over a length of five meters which is the thickness of the first abutment. Then the excavation of the cone shape part of the abutment takes place. Finally, the first abutment is installed. The process continues with the sequential removal of the lining segment over two meters followed by the sequential installation of the sealing element. At the end of the installation of the last sealing segment, the lining at the second abutment is removed and the cone shape is excavated and the abutment is installed. Figure 7-18 shows a sequence of how the process is implemented in Flac3D. The sequential excavation of the both abutments and the first and last sealing segment is illustrated. An equilibrium iteration is performed after each removal and installation step. Due to conservative reasons and due to the fact that the transient (rheological) behavior of claystone is not considered, the full convergence of the rock after the removal of each lining segment takes place. The resulting plastification is therefore maximal and thus conservative. By synchronizing the removal of the lining with the installation of the abutments and the sealing element, the resulting damage can significantly be reduced.

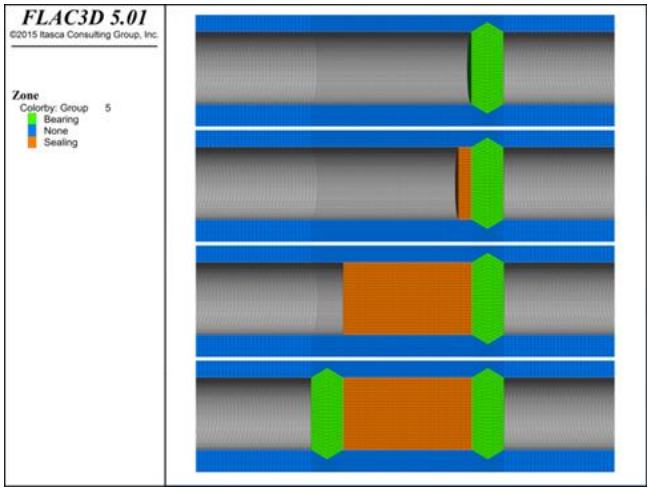

Figure 7-18:
Sequential removal of the lining and installation of the sealing element and abutments.

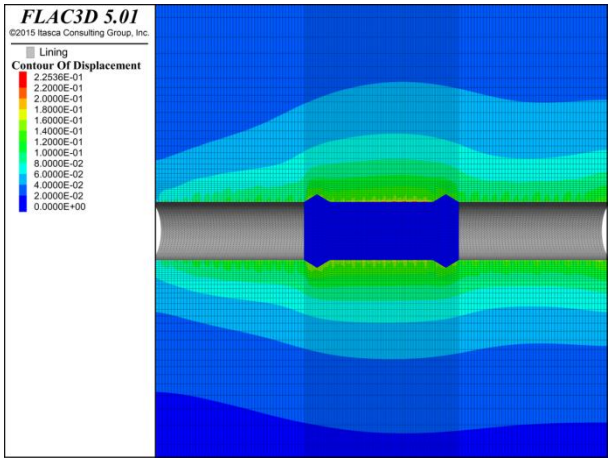

Figure 7-19: Displacement magnitude in the plug area.

Figure 7-19 shows the magnitude of the displacements at the end of the installation of the second abutment. The comparison of the occurred displacements in comparison to the case directly after the installation of the lining in Figure 7-10 shows that no significant change occurs after the removal and installation of the sealing element and abutments. The displacements two meters deep in the rock along the sealing length are less than 12 cm which is acceptable.

Figure 7-20 shows the contour plot of the plastic strain in the model. No significant increase of damage in the rock area surrounding the plug occurs. The maximal plastification is located at the second abutment. The maximum plastification depth is 5 m. The evaluation of the stress ratio of the matrix in Figure 7-21 (left) shows only a negligible increase which is concentrated at the abutments. Looking at the stress ratio of the bedding (Figure 7-21, right), one notes a decrease of the ratio in the seal area compared to the part of the tunnel which is still supported by the lining. Only at the location of the abutments where the plastification is maximal, some peaks of 9 m depth (in comparison to 5 m at the end of the installation of the lining) are noticed where the rock is stress to up to 50 % of its strength.

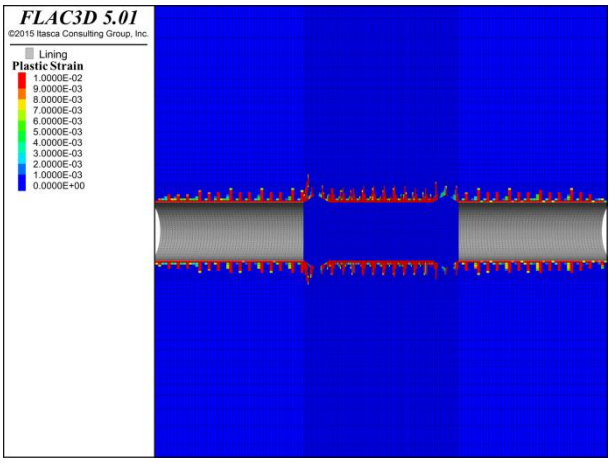

Figure 7-20:
Plastic strain in the plug area.

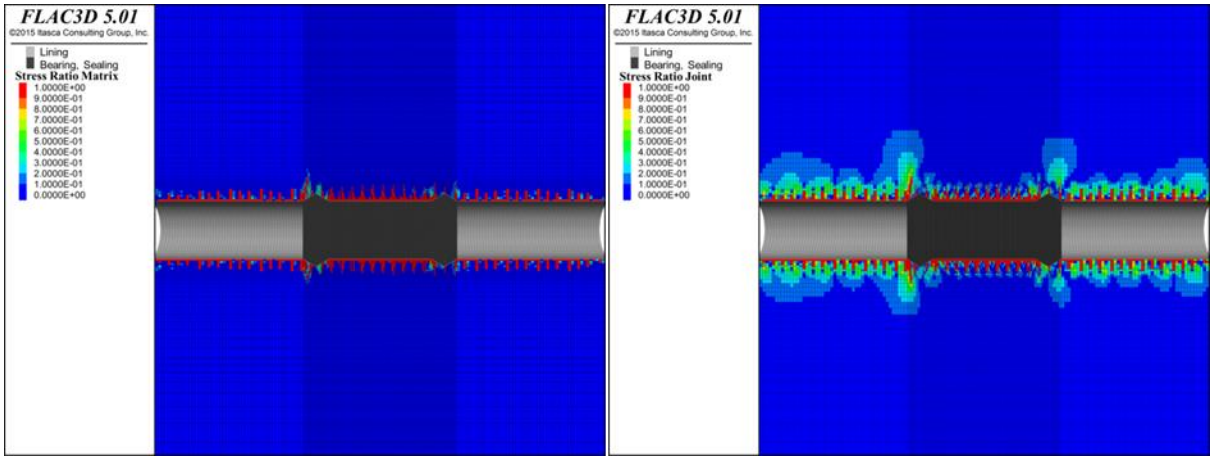

Figure 7-21: Stress ratio of the matrix (left) and the bedding (right) of claystone.

7.1.5 General conclusions

In conclusion, the simulation of the excavation without lining shows that the entire model is subjected to high deformations. Even at the ground surface, 70 m above the tunnel, displacements up to 20 cm have been calculated. The convergence of the tunnel reaches 1.8 m in vertical direction and 1.2 m in horizontal direction. Due to the excavation, stress redistribution takes place and leads to the formation of an arched structure above the tunnel which redirects the stresses acting on the excavation in other rock areas. The damaged zone due to the excavation reaches up to 15 m into the rock mass surrounding the tunnel. At last, due to the excavation, an important part of the model is stressed to up to 50% of the mechanical strength of the matrix and the bedding part of claystone. According to this fact, it can be concluded that the structural integrity of the rock is jeopardized. The tunnel has to be excavated with a supporting lining.

The excavation of the tunnel with the installation of a concrete lining leads to a significant improvement of the geomechanical integrity of the rock. At the end of the excavation, displacements of only 15 cm at the top and 7 cm at the tunnel wall are expected. The analysis of the stresses in the rock model showed that the stress redistribution remains minimal and no arched structure was built. It was also possible to estimate the loads acting on the lining which is necessary for the structural design of the lining. Finally, the resulting EDZ due to the excavation were significantly smaller in comparison to the excavation without lining. The plastified zones are concentrated in the areas of stress relieving which occur during the convergence of the rock after every excavation step before the installation of the lining segment. The evaluation of the stress ratios of the matrix and the bedding part showed that the rock is only stressed in the direct vicinity of the tunnel wall.

The remove of the lining over the complete sealing and abutment length leads to significant damage in the rock. This damage is characterized by high plastification peaks which occur due to two different phenomena: Along the seal length, the plastification which occurred after the excavation of the tunnel is intensified by the deformation of the rock when the lining is removed. At both ends of the lining, high shear stresses occur due to the support effect of the remaining lining. This could be explained with the analogy of a structural beam. This shear stresses lead to damage in the bedding part of the rock. According to these results, one can conclude that a removing the lining over the complete sealing and abutment length and then installing the bentonite plug is not possible.

The sequential removal of the lining followed by a sequential installation of the abutments and the sealing element do not lead to a significant plastification. The maximum of plastification is concentrated at the location of the abutments and is limited to a depth in the rock of only 5 m. The increase of displacements is also minimal. One can conclude that the sequential removal of the lining and the parallel installation of the abutments and the sealing element is a suitable way of sealing a drift without jeopardizing the host rock in the plug area.

7.2 Gas pressure evolution in the drift system

Gas production occurs in the repository from anaerobic corrosion of iron and other metals, but also from microbial degradation of organic matter deposited along with the radioactive waste. The gas production leads to a gas pressure increase in the repository that potentially can affect the geotechnical as well as the geological barriers if the gas pressure is exceeding design limits.

The gases can flow due to gas pressure gradient along the repository drifts (see Figure 7-22). Gas flow into the saturated clay host rock may be due to two-phase flow if the pressure in the repository exceeds the gas-entry pressure or if new pathways are created in case the gas pressure in the repository exceeds the minimal stress of the formation. Since the

gas-entry pressure for clays is usually very high, two-phase flow is expected to be less likely (Shaw 2013). In this chapter, simulations performed by GRS using the TOUGH2 EOS5 code (Pruess et al. 2012) are presented to examine the gas pressure evolution and the gas flow in the repository to estimate potential pressure stresses of the geotechnical and geological barriers and to evaluate whether a fracturing of the clay formation and a creation of new pathways could potentially occur.

Figure 7-23 shows a representative section of the repository from the repository layout given in (Consortium SGN/IVO/AEA Technology 1997-A), which was chosen to be used as basis of the 3D TOUGH2 model. This section represents one emplacement field which consists of a central drift with two times 15 emplacement vaults which are aligned on both sides of the drift. The repository may consist of multiple of those repository sections. The dimension of the TOUGH2 model is 1050x220x100 m (length, width, height) with a discretisation of 10 m, resulting in the model to have 23,100 elements. A horizontal top view cross section of the model at the repository level depth is shown in Figure 7-24. The model introduces four different domains; the host rock, the drift, the emplacement vault and a drift sealing that isolates the emplacement field from the rest of the repository. All of those four domains are represented by different material properties in the model.

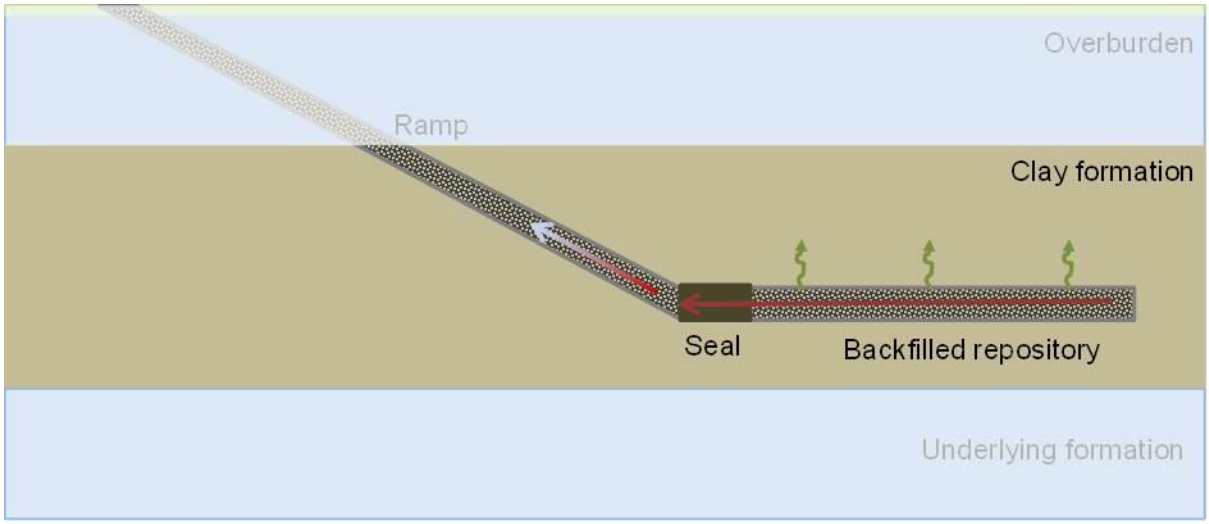

Figure 7-22: Schematic sketch of the repository layout (not to scale).

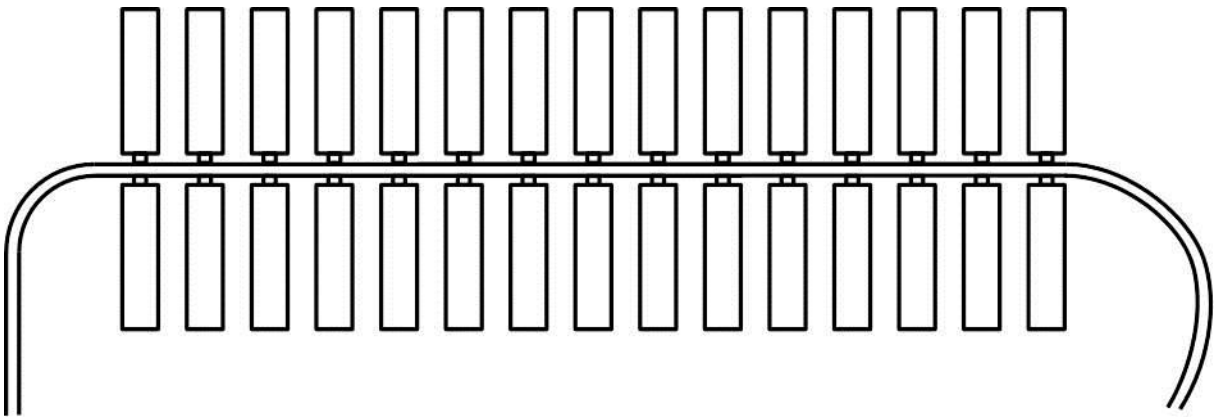

Figure 7-23: Schematic sketch of the representative repository section regarded in the TOUGH2 model, modified after (Consortium SGN/IVO/AEA Technology 1997-A).

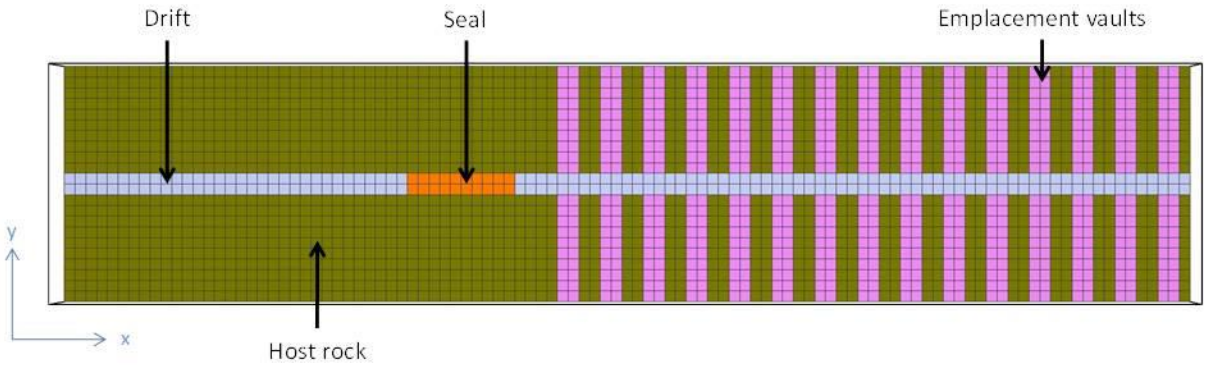

Figure 7-24: TOUGH2 model, top view of repository level.

The initial conditions for the hydrostatic pressure in the model are chosen according to the depth of the clay formation and a water density of 1000 kg/m^3. This results in a hydrostatic pressure of 1 MPa at the top of the model, 2 MPa at the bottom of the model and 1.5 MPa at the repository level. The drifts and the emplacement vaults are assumed to be initially saturated by 10 % and at atmospheric pressure (see Figure 7-25). The boundary conditions of the model are chosen to be fixed pressure at full saturation. For the drift exit an open boundary is simulated by using very large volumes for the two boundary model elements. Gas production was estimated in Consortium SGN/IVO/AEA Technology (1997-C) by modelling to be 0.93 moles of gas per cubic metre of repository volume for about 500 years after repository closure and quickly going down to 0 for later times. In the following, the gas production rate was chosen accordingly which equals to a production of $5.9 \cdot 10^{-8}$ kg_{H2} per second for each of the model elements of the emplacement vaults which are 10x10x10 m in size. It has to be noted that this gas production rate is small compared to the assumptions made for example for the German ERAM repository (Becker et al. 2009). There, the gas production is about one order of magnitude higher in rate, but also a factor of 2 shorter in time, if the gas production from anaerobic iron corrosion is regarded.

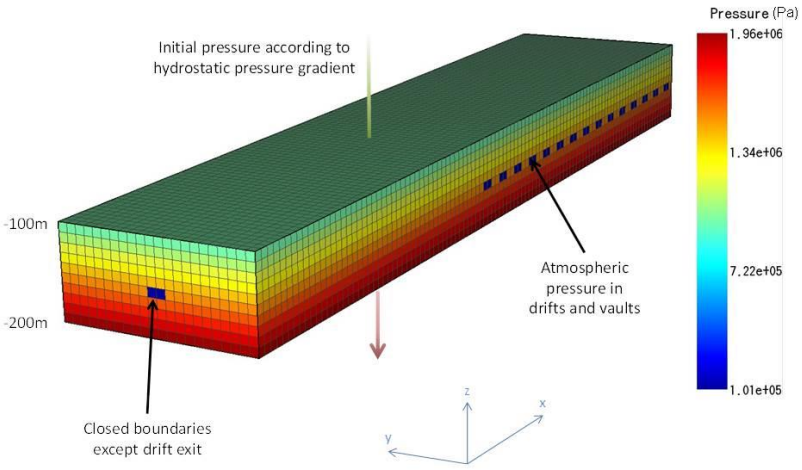

Figure 7-25: TOUGH2 model: 3D view with color coded pressure regime.

The parameters used for the material properties are given in Table 7-3, where λ, S_{lr}, S_{ls}, S_{gr} and P_0 are the shape parameter, residual water saturation, maximum water saturation, residual gas saturation and gas entry pressure in the equations for relative permeability and capillary pressure of the van Genuchten-Mualem model for two-phase flow in the notation as used in the TOUGH2 code and as defined in the appendices G and H of (Pruess et al. 2012). The results of the TOUGH2 simulations are shown in the Figure 7-26 to Figure 7-28.

Table 7-3: Material properties for the modelling with TOUGH2.

Parameter	Host rock		Drift		Seal		Vault	
Density [kg/m³]	2200	(1)	2650	(2)	2650	(2)	2650	
Porosity	0.25		0.2	(3)	0.05	(3)	0.25	(5)
Permeability [m²]	$5.6 \cdot 10^{-19}$		$1.0 \cdot 10^{-15}$		$1.0 \cdot 10^{-17}$		$1.0 \cdot 10^{-15}$	
Relative permeability								
λ	0.365	(2)	0.43	(2)	0.72	(4)	0.6	(5)
S_{lr}	0.2		0.25		0.095		0.25	
S_{ls}	1		1		1		1	
S_{gr}	0.174		0.2		0		0.2	
Capillary pressure								
λ	0.365	(2)	0.43	(2)	0.363	(4)	0.6	(5)
S_{lr}	0.012		0.2		0.04		0.2	
$1/P_0$ [1/Pa]	$3.53 \cdot 10^{-7}$		$2.0 \cdot 10^{-6}$		$1.0 \cdot 10^{-5}$		$2.0 \cdot 10^{-6}$	(2)
S_{ls}	1		1		0.9999		1	(5)

References: (1) Kühnlenz & Hammer 2014; (2) Weetjens et al. 2009; (3) Jobmann et al. 2016; (4) Yildizag 2008; (5) Nagra 2008

Figure 7-26 shows the temporal evolution of the gas pressure in the main drift of the emplacement field for three locations, in the middle of the emplacement field and at both faces of the drift seal. The temporal evolution is almost identical for the location in the centre of the emplacement field (blue line) and at the inner face of the seal (green line). This shows that the gas transport in the main drift equals out pressure gradients. Due to the low permeability of the seal there is however a pressure drop from the inner to the outer face of the seal (red line). The pressure significantly starts to increase after about 10 years and exceeds the hydrostatic pressure at the repository level after about 100 years. The pressure reaches its maximum after 500 years when the gas production ends and slowly decreases afterwards. The maximum pressures at the two locations in the emplacement field also exceed the lithostatic pressure at the repository level, which is only about 3.3 MPa due to the low repository depth. The maximum pressures might be lowered significantly by the construction of seals with higher gas permeability e.g. by adding sand to the bentonite of the seal material. Due to the low repository depth, the gas pressure has the potential to exceed the lithostatic pressure at the repository depth. The pressure evolution however has to be regarded as qualitative estimation only for the moment, due to the high uncertainty of the input data. More detailed simulations are necessary if more detailed data is available in the future.

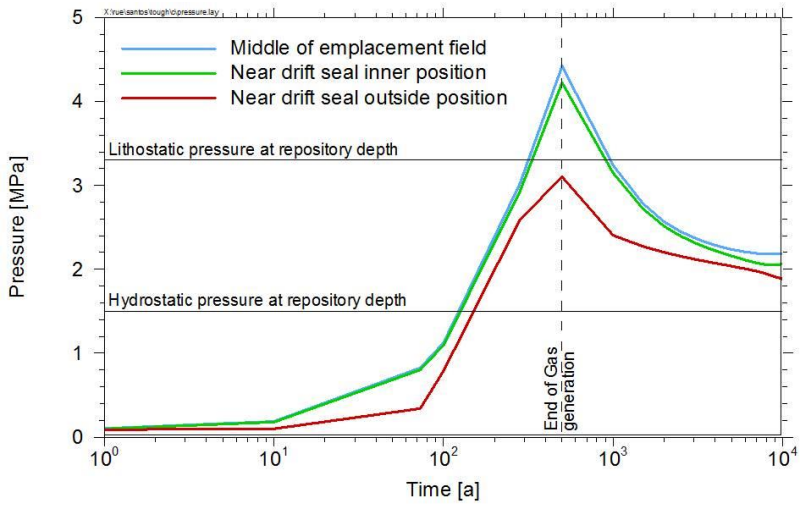

Figure 7-26:
Temporal gas pressure evolution for three different observation points in the drift.

Figure 7-27 shows a horizontal 2D cross section of the pressure distribution at the repository level for four different points in time. The initial condition at t = 0 shows atmospheric pressure in the repository drift system and hydrostatic pressure in the host rocks between the emplacement vaults.

Immediately after simulation start, the pressure in the host rock drops down to values near atmospheric pressure and later on increases again in a similar way than in the repository drift system. The maximum pressure reached is however lower than in the drift system and reaches around 3 MPa. While there is still a significantly higher gas pressure in the drift system after 10,000 years, the pressure in the host rock almost has gone down to hydrostatic pressure, again.

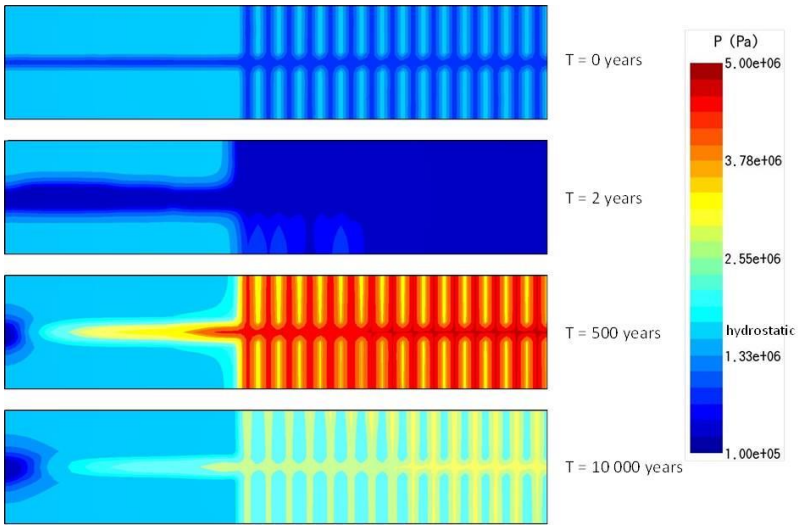

Figure 7-27:
Pressure distribution for a horizontal cross-section at the emplacement level.

Figure 7-28 shows a vertical 2D cross section of the gas saturation in the host rock for the time of maximum gas pressure after 500 years. There it can be clearly seen that the host rock remains fully saturated in the large part. Only a small boundary around the repository system might be slightly desaturated. Consequently, no gas transport in gaseous form occurs through the clay host rock. This result of course is only true if the assumption of a two-phase flow gas transport is valid for the host rock and no additional pathways are created in the host rock due to the high gas pressure. Figure 7-29 shows the temporal evolution of the liquid saturation in the drift. This figure shows that the drift remains only partly saturated until the end of the simulation time of 10,000 years. This is due to the high gas pressure in the drift which hinders the resaturation of the drift backfill. A partial saturation of the drift backfill lowers a potential transport of dissolved radionuclides in the liquid phase along the drift system.

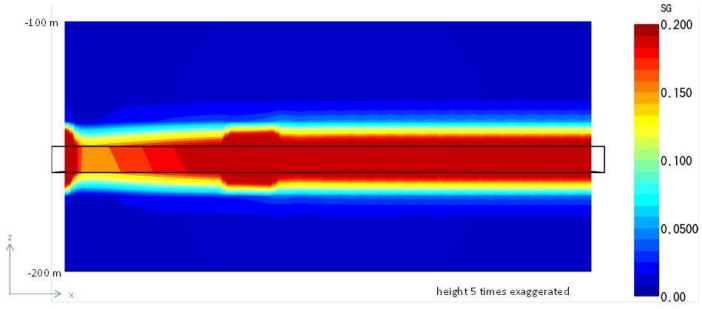

Figure 7-28: Saturation distribution for a vertical cross-section through the repository plane after 500 years.

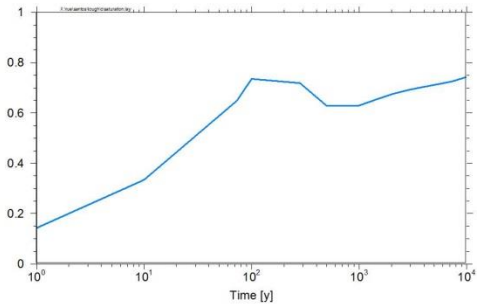

Figure 7-29: Temporal evolution of the liquid saturation in the drift.

8 Flow and transport simulations

8.1 Groundwater flow

On the basis of the geological model of the area as described in chapter 3.1.2 a three-dimensional groundwater flow model was set up. In the following, the model set-up is described, and results of groundwater flow simulations are discussed, including implications for future investigations.

The boundary surfaces of the different layers were exported from openGEO as raster data, transformed to asc data and then imported to ProMesh 4 (Reiter, 2017). ProMesh is a meshing software for unstructured grids of one, two or three dimensions. It supports different element types for meshing, and features tools to refine, re-mesh, partition, and transform meshes. Groundwater flow simulations were performed using the code d3f++ (distributed, density-driven flow), which was developed under the auspices of GRS (Schneider 2016). It is based on UG4, a powerful software framework for the simulation of complex partial differential equation based systems on massively parallel computer architectures (Vogel et al. 2013). One of the main characteristics of the code d3f++ is the possibility to simulate the groundwater flow and tracer transport in large, porous and/or fractured model areas over long periods in time. It is able to take the density-driven flow into account, which is of particular importance when regarding the groundwater flow in the vicinity of salt formations or regarding salt water influence in coastal areas. Pollutant transport is calculated taking the relevant transport mechanisms, such as advection, dispersion, diffusion and reaction, into account. In addition to radioactive decay, relevant interaction processes, such as sorption, precipitation, and diffusion into immobile pore waters can be regarded. Newest developments allow the consideration of heat transport and free groundwater tables.

The visualization of the results was done with Paraview (Ayachit 2015), an open-source, multi-platform data analysis and visualization application using qualitative and quantitative data analysis techniques.

8.1.1 Model geometry

The model grid was generated using quasi-prisms (characterized by two triangles, each located on one boundary surface, refined in z-direction). The resulting coarse grid consists of 6188 vertices, 23,436 edges and 10,768 volumes. Groundwater flow simulations were run using a refined grid with 48,072 volumes. The model of eight layers with a maximum overall thickness of ca. 177.14 m. has the dimensions of 5600 m in the x- and 4400 m in the y-direction. The three dimensional model domain is shown in Figure 8-1.

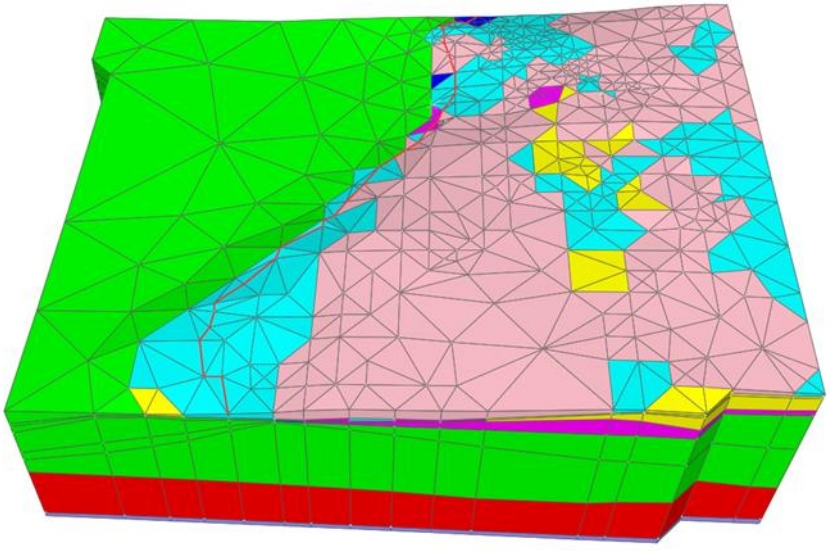

Figure 8-1:
Three-dimensional model domain.

The eight layers of the model are those described in chapter 3.1.2. The resulting hydrogeological model, including the coarse grid and the eight different layers, is depicted in Figure 8-2. The basis of the model is the Archean-Proterozoic base of the model (Ar_Pr), superimposed by the Vendian lower aquifer, the Gdovsk Horizon (V_aq_sand), which is the main aquifer and used for the water supply in the region. Likewise the Gdovsk Horizon, the Upper Vendian Kotlin Clay (V1_kt_clay) shows a wide distribution in the model area, and is the thickest layer in the model. The Cambrian system starts with a spatially restricted occurrence of the Lomonosov Horizon (Ln2_sand). The Lontov Clays ("Blue Clays") of the Cambrian sequence are represented in the model by the layer E2_clay, which cover approximately half of the model area. Another layer of sands (Ln1_sand) with a similar spatial extension as the Blue Clays is the Cambrian Ln1_sand, which can be summarized with Ln2_sand to a Cambrian-Ordovician aquifer. Another set of Cambrian Blue Clays (Ln1_Clay) is completing the Cambrian sequence. The top of the model is formed by sporadic occurrences of Quaternary sandy sediments (Q_sand).

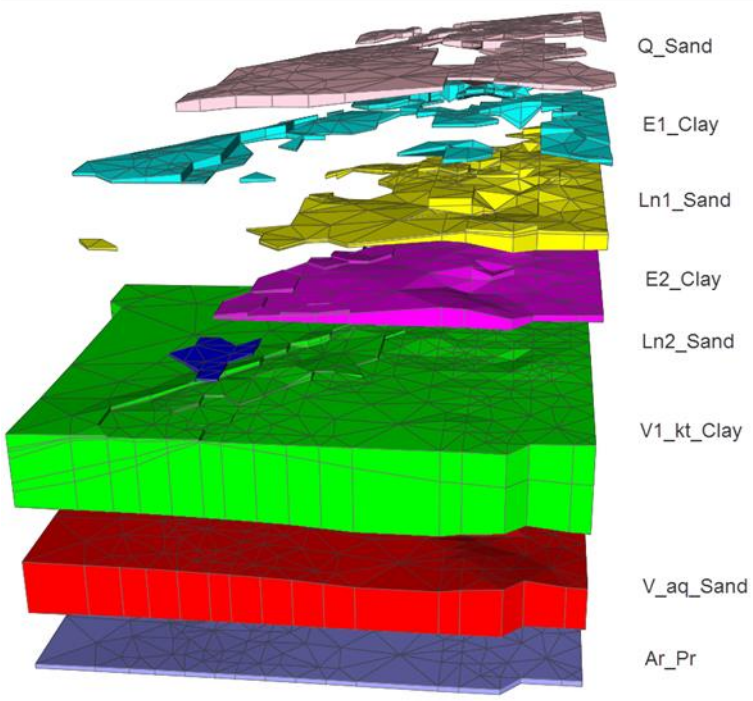

Figure 8-2:
Model domain with 8 layers, exploded view.

8.1.2 Hydrogeological parameters

The needed hydrogeological parameters for flow simulations are the porosity and the permeability of the layers. Unfortunately, only values for the permeability of the Blue Clays and the Kotlin Clays were available (chapter 4.3 and 4.6). Therefore, standard values for the porosity and permeability for clay and sand sediments were taken from literature (Hölting & Coldewey 2005) for the other layers. The lowest layer represents the crystalline, Precambrian base. Due to lack of information it is assumed to have a similar porosity and permeability values like the Blue Clays. Applying values of the higher permeable clays (Blue Clays instead of Kotlin Clays) also takes account of possible weathered sections in its upper part. Applied hydrogeological parameters are given in Table 8-1.

The north-western part of the model represents an area covered by the Gulf of Finland (Baltic Sea), thus salt concentrations have to be regarded in model simulations. According to Feistel et al. (2010), the salinity of the Baltic Sea in the region of the investigation area is ca. 4 PSU (practical salinity units). Accordingly, the maximum salt concentration was set to 4 kg/kg_{water}. The resulting density ranges from 998.2 kg m^{-3} to 1003.8 kg m^{-3}. The dependence of the density is assumed to be linear. The viscosity is set to $1.025 \cdot 10^{-3}$ Pa·s and kept constant. For salt transport, the molecular diffusion was set to $6.0 \cdot 10^{-10}$ m^2 s^{-1}. Applied transport parameters are summarised in Table 8-2.

Table 8-1: Material properties of different layers.

Parameter	Porosity [-]	Permeability [m²]
Q_sand*	0.3	$1.00 \cdot 10^{-12}$
E1_clay	0.05	$2.13 \cdot 10^{-17}$
Ln1_sand*	0.3	$1.00 \cdot 10^{-13}$
E2_clay	0.05	$2.13 \cdot 10^{-17}$
Ln2_sand*	0.3	$1.00 \cdot 10^{-13}$
V1_kt_clay	0.05	$5.69 \cdot 10^{-19}$
V_aq_sand*	0.3	$1.00 \cdot 10^{-13}$
Ar_Pr*	0.05	$2.13 \cdot 10^{-17}$

* Standard data taken from Hölting & Coldewey (2005)

Table 8-2: Transport parameters for the numerical model.

Parameter		Value
Molecular diffusion of salt	[m^2/s]	$6.0 \cdot 10^{-10}$
Fresh water density	[kg/m^3]	998.2
Density of salt water	[kg/m^3]	1003.8
Viscosity of water	[Pa·s]	$1.025 \cdot 10^{-3}$
Maximum Salinity	[g/kg]	4

8.1.3 Initial and boundary conditions

Initial conditions have to be set for the temperature and the salt concentration. Since the geothermal temperature gradient is assumed to have no effect on the groundwater flow for a model thickness of ca. 170 m, the temperature was set to 10°C for the entire model domain. The salt concentration needs to be stated in form of a relative concentration:

$$c_{rel} = \frac{c_{abs}}{c_{abs,\max}} \tag{8-1}$$

with

$$c_{abs} = \frac{m_{salt}}{m_{salt} + m_{H_2O}} \tag{8-2}$$

and

c_{rel} = relative salt concentration = relative salt mass fraction [-]
c_{abs} = absolute salt mass fraction [-]
$c_{abs,max}$ = maximum absolute salt mass fraction [-]
m_{tracer} = mass of salt [kg]
m_{H2o} = mass of water [kg]

The salt concentration at the model surface was set to $c_{rel} = 1$ where the model surface is below the coastline (surface covered by salt water, z = 0) and to $c_{rel} = 0$ where the model surface is above the coastline. Those salt concentrations are projected down to all other layers of the model as initial conditions.

To define the coastline, different sources of information were available. The geological model of the area already featured a coastline. Also, a water table contour map of the Quaternary aquifer is available and shown in Figure 8-3 (Rumynin, pers. information).

Matching the model coastline and the coastline of the water table contour map and at the same time matching the given landmarks, such as boreholes or infrastructure, to each other was not easy to realise. The coastline of the geological model, defined by a height of z = 0 m, and that given by the water table contour map, are differing spatially. Figure 8-4 depicts the coastline and the isolines of the ground surface for 10 m and 22 m from the geological model ("raster data"), as well as the coastline and the isohypses for 10 m and 22 m resulting from Figure 8-3 ("groundwater").

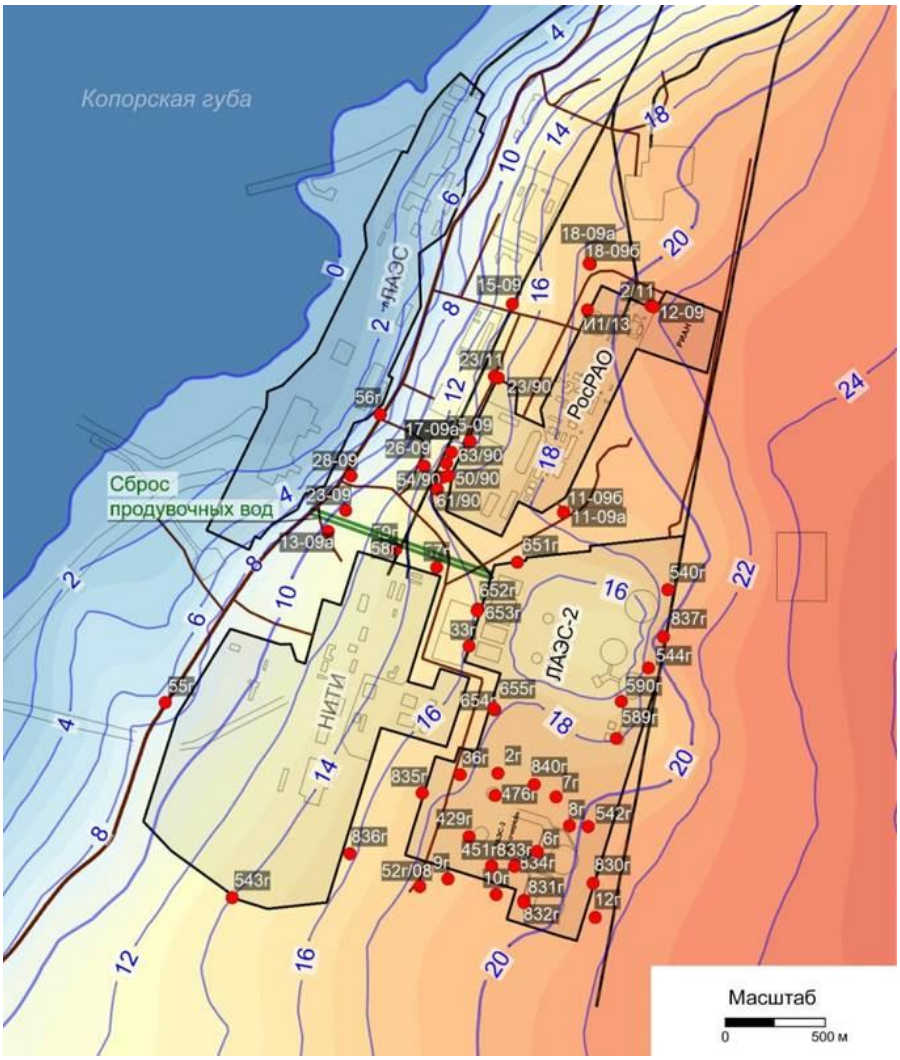

Figure 8-3: Water table contour map of the Quarternary aquifer of the investigated area, record date August 26, 2015 (Rumynin, pers. information).

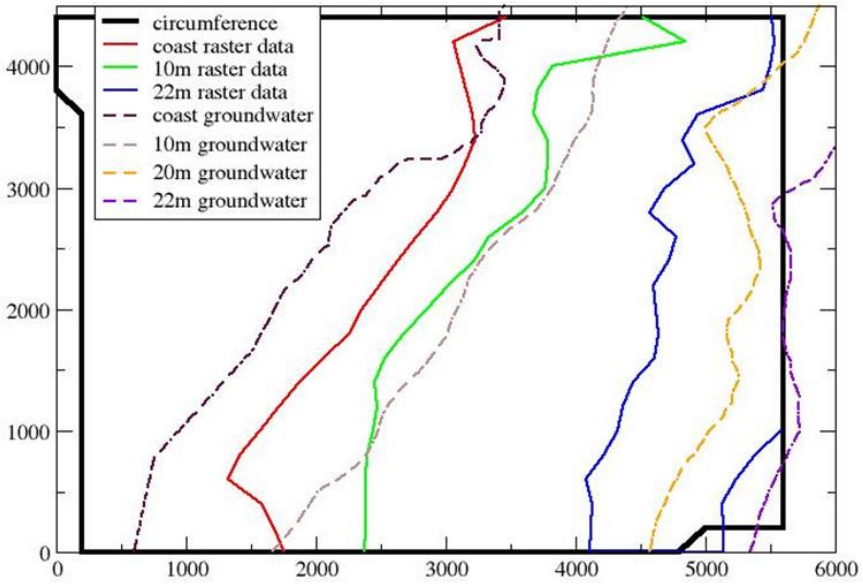

Figure 8-4: The coast line and some isolines of the ground surface from the geological model (“raster data”), compared to the coast line and the isohypses of the groundwater table (“ground water”).

The coast line of the model is located further to the east than the coastline in the water table contour map. Also, the isohypses are showing higher levels than the ground surface. For this reason, it was decided to apply the coastline from the water table contour map to the hydro-geological model. The ground surface of the model had to be modulated in order to fit the isohypses. This results in a Quaternary Q_sand layer, which has a larger lateral extent and a higher thickness in some parts than originally given by the geological model. Figure 8-5 shows the model domain with the modified Q_sand layer. It becomes visible, that also as a result of the modification, E2_clay is not cropping out at the surface anymore. This slight difference is not expected to have effects of the groundwater flow in the model because of the small spatial extent of the original outcrops.

Figure 8-6 is a comparison between the original and the modified Q_sand layers and the coastlines from the geological model and the water table contour map. All other layers are not affected by this procedure.

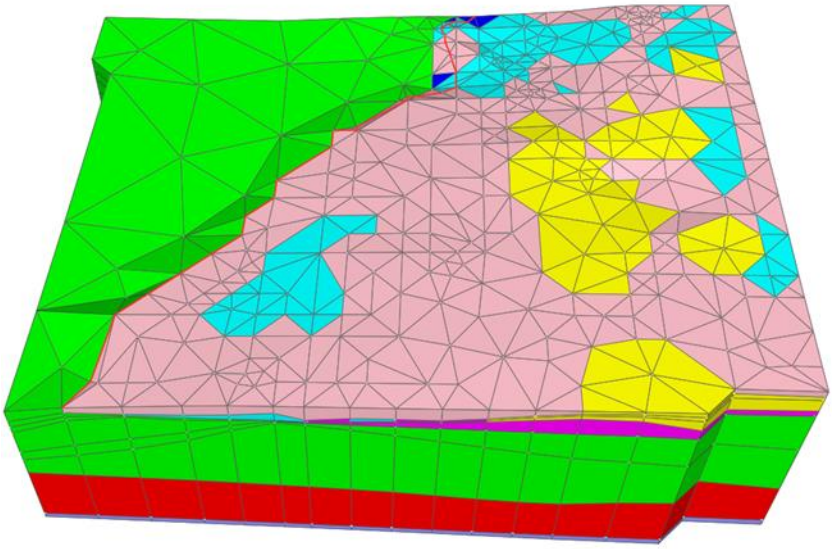

Figure 8-5:
Model domain with modified Q_sand layer (rose).

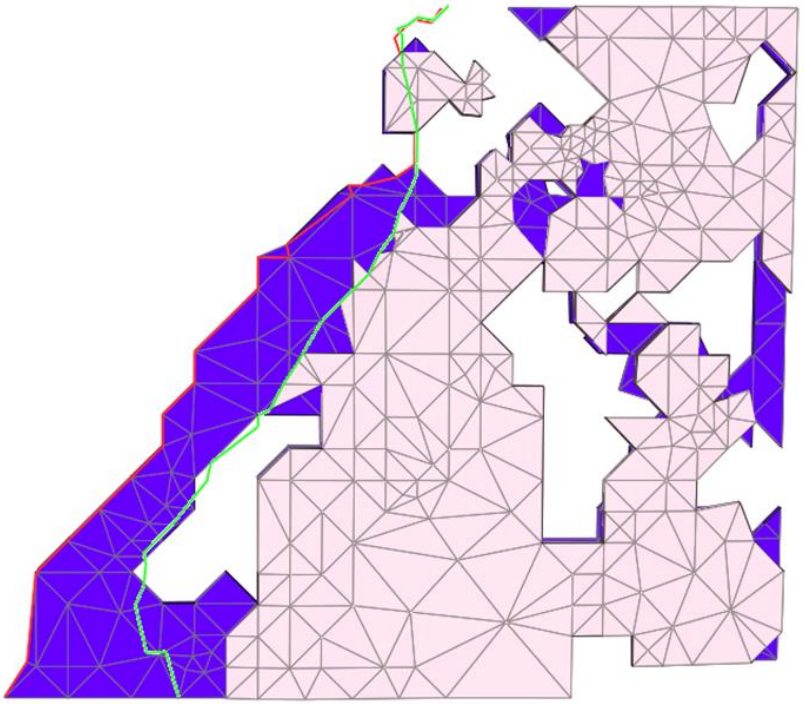

Figure 8-6:
Comparison of the coastline resulting from the geological model (green line) and from the groundwater contour lines (red line), and original (rose) and modified (purple) Q_sand layer.

The boundary conditions for the groundwater flow simulations (Figure 8-7) were set according to the information of the water table contour map. The northern and the southern boundary and the bottom of the model are impermeable boundaries. For the western and the eastern boundary, hydrostatic pressure was defined according to the water table. The salt

concentration at the eastern boundary is set to 0, while for the western boundary, the salt concentration is set to that of the Baltic Sea (c_{rel} = 1), the latter for a faster convergence of the model. That area of the model surface, which is covered by sea water, is characterized by a sea water salt concentration (c_{rel} = 1) and a hydrostatic pressure, taking the water column of the sea water into account. The land surface area of the model is allocated with an inflow of fresh water (c_{rel} = 0), representing a groundwater recharge. The mean annual precipitation in the region is 678 mm (Merkel 2017). Due to a lack of information about runoff and evaporation, land-use and vegetation, the annual groundwater recharge could only roughly be estimated. Thus, an annual recharge of 200 mm was assumed, resulting in $6.34 \cdot 10^{-9}$ m s^{-1} inflow at the surface. The groundwater table was regarded as static, thus no free water table was assumed in these simulations.

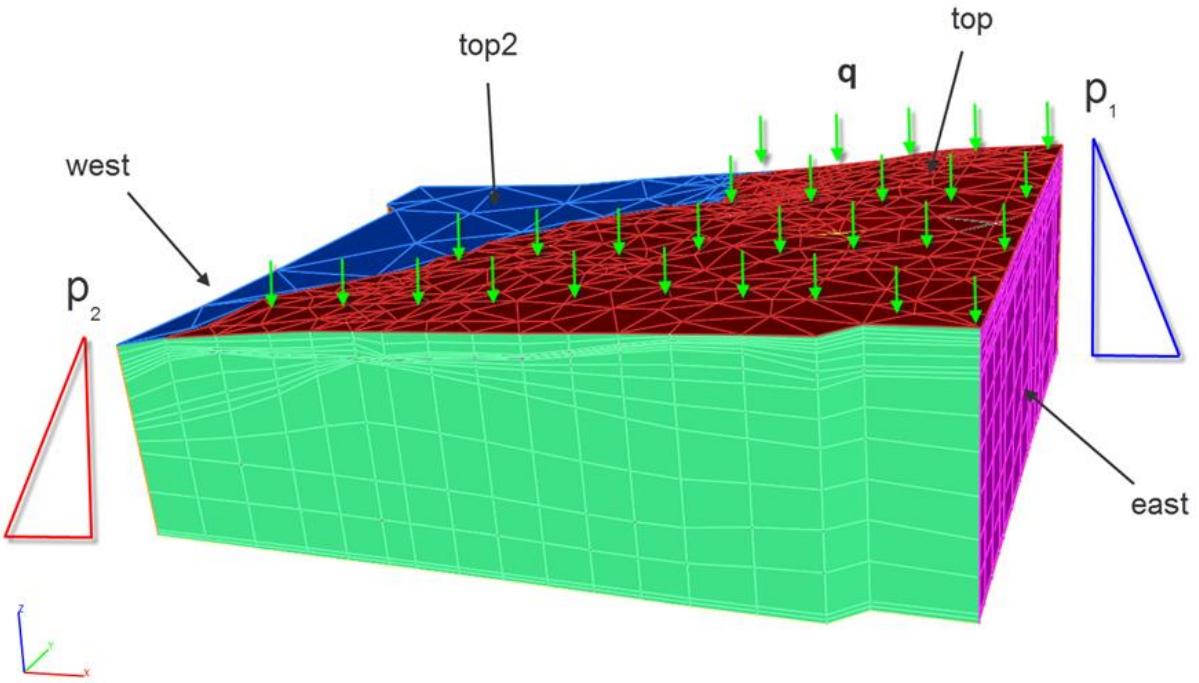

Figure 8-7: Boundary conditions for the groundwater flow model. The triangles are representing a hydrostatic pressure at the western and eastern boundary with c_{rel} = 0 at the eastern boundary and c_{rel} = 1 at the western boundary. Green arrows indicate a groundwater recharge with c_{rel} = 0 (top). At top2, covered by the Baltic Sea, a hydrostatic pressure with c_{rel} = 1 is assumed.

8.1.4 Results of the flow simulations

The model was run until reaching a model time of 2000 years. The groundwater flow is already in a steady-state by that time, whereas the salt concentration distribution in the model domain is still subject to changes. Figure 8-8 shows the relative salt concentration (“c”, colours) from fresh water (blue) to Baltic Sea water (red).

Highest velocities in the range of 10^{-7} m·s^{-1} can be observed near to the surface where the Quaternary sands (Q_sand) are spread. A large part of the groundwater recharge is drained as subsurface runoff to the coast with a locally restricted discharge area in the northern part of the model domain. Due to the inflow of fresh water from the top and the fresh water conditions at the eastern boundary of the model, the eastern part of the model domain is characterized by fresh water conditions. The isosurface of c_{rel} = 0.5 is shown in green in Figure 8-8. During the 2000 years model time, the isosurface is shifting westwards in the higher permeable aquifer, the Gdovsk Horizon (V_aq_sand). In contrast to that, the isosurface in the Kotlin Clay layer is only slightly changing its position. It is expected, that at a steady-state, the lower aquifer will feature fresh water conditions in the entire model domain (except at the western boundary with a fixed salt concentration).

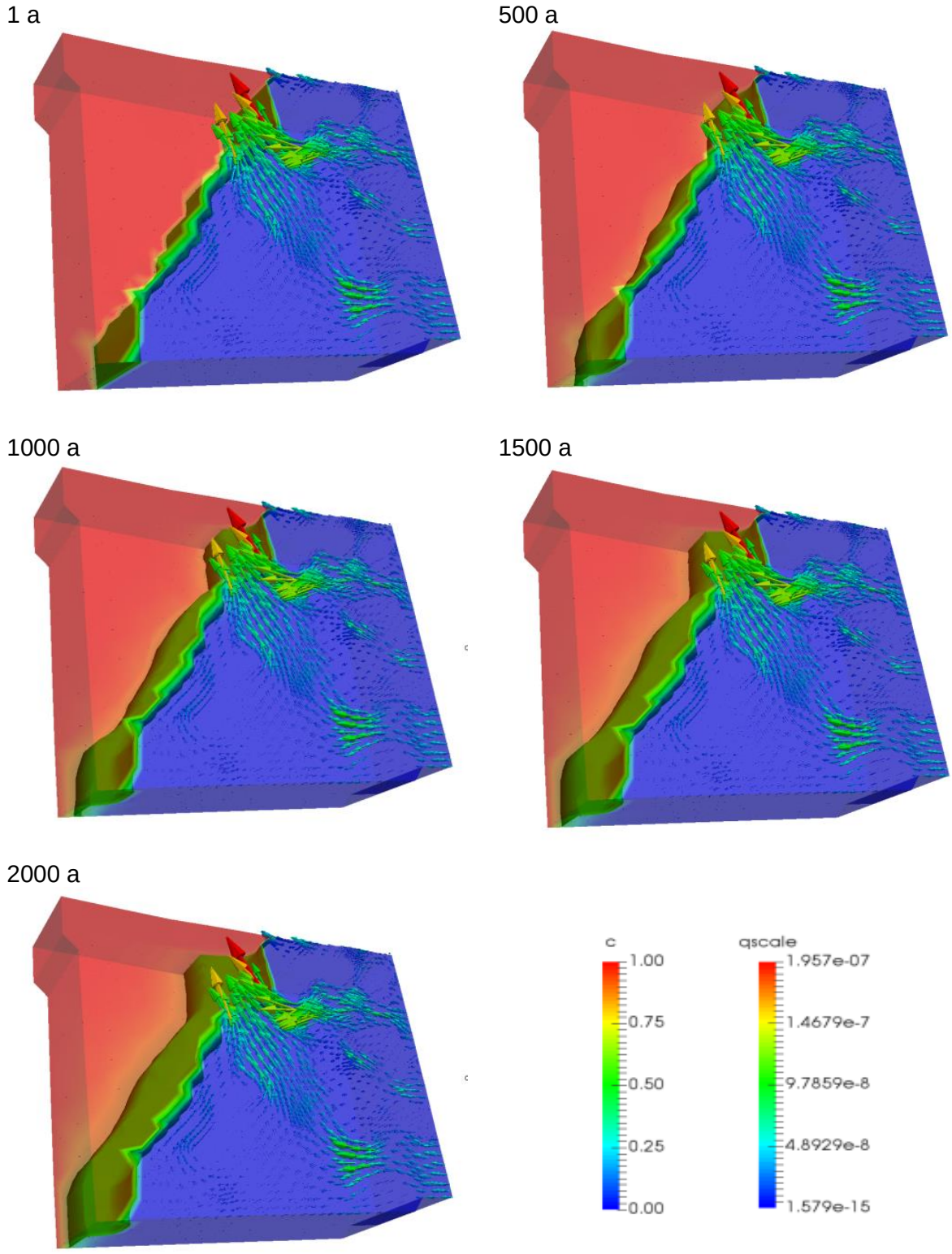

Figure 8-8: Block diagrams of the salt concentration (“c” [-]) at model times of 1 year, 500 years, 1000 years, 1500 years and 2000 years. The green surface shows the c_{rel}=0.5 isosurface. The colour and size of the flow arrows represent the velocity magnitude (“qscale” [m s^{-1}]).

A matter of particular interest is the flow velocity and the salt concentration in the vicinity of a potential repository site. Therefore, different cross sections are presented and discussed in the following, which display a detailed view on the flow conditions and salt concentrations in different depths. Their locations are depicted in Figure 8-9.

Figure 8-10 shows five cross-sections through the model domain from the west to the east at 400 m from the north boundary (a), 1100 m from the north boundary (b), 2200 m from the south and the north boundary (c), 1100 m from the south boundary (d) and 400 m from the south boundary (e) for a model time of 2000 years. Additional cross sections depicting the temporal evolution of the groundwater flow and salt distribution at those locations are given in annex A (Fig. A-01 to Fig. A-05).

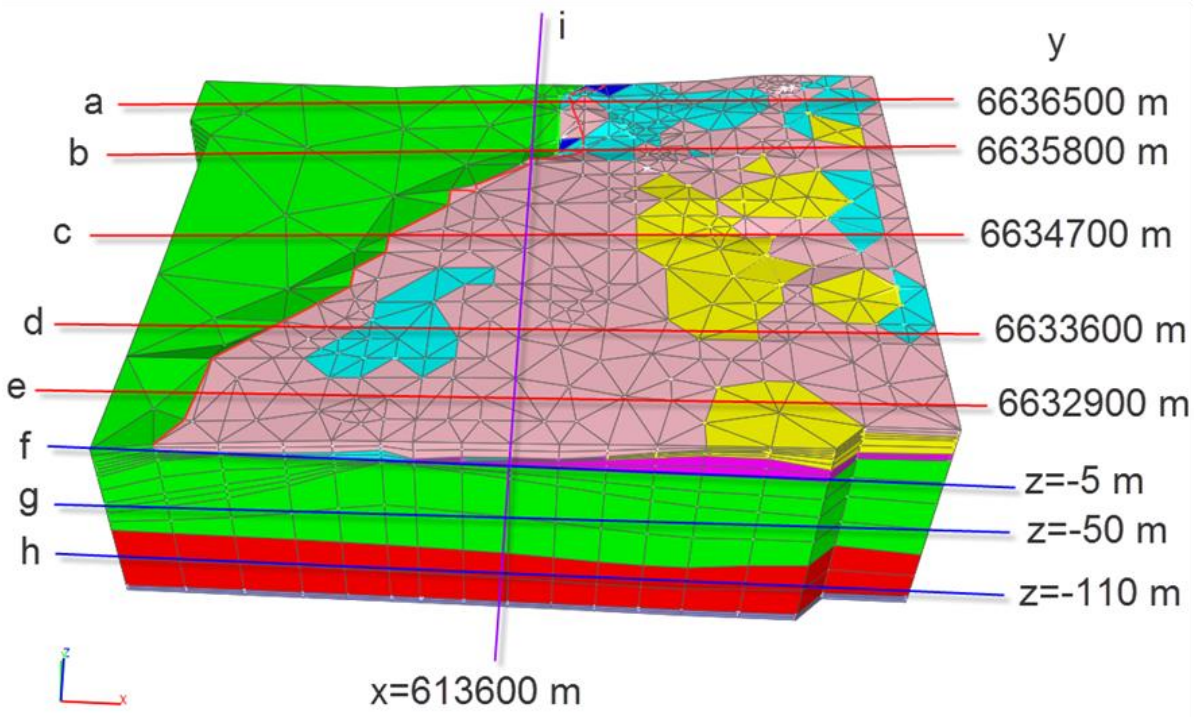

Figure 8-9: Block diagram with location of the cross sections and block diagrams.

It is clearly visible that highest flow velocities can be observed within the Quaternary aquifer at the surface. According to the distribution of the Quaternary sands, the high flow velocities are restricted to the southern and central part of the model, whereas in the northern part, where the sands are only locally distributed, the wide area of high velocities decreases (Fig. A-01). Also, elevated flow velocities occur in the lower Gdovsk aquifer, here in the range of up to $5 \cdot 10^{-9}$ m s^{-1} with peak velocities in the eastern part of the domain. Also in the lower aquifer, the flow velocity decreases from the south to the north. The lower aquifer shows a continuous distribution in the entire model domain, so the decrease has to be due to the boundary conditions. The difference in elevation as well as in groundwater level at the eastern boundary of the model is about 2 m between the north (lower) and the south (higher), resulting in the reduced flow velocity in the north. Within the Kotlin Clay layer, the flow velocity is reduced (see below).

Generally, the groundwater flow is directed to the west. At the margins of the Quaternary sands, the groundwater discharges. The groundwater flow direction also holds for the underlying sediments. Different flow patterns develop within the Kotlin Clay. In the south, the groundwater flows more or less horizontally to the west until reaching the centre of the model (east-west direction). There, a downwards component of the flow gains influence, as depicted in Fig. A-05 and Fig. A-04. Going further north, approximately in the centre of the model, the vertical component of the flow reverses. In the northern half of the model, an upward component is dominant in the western part. At the same time, the flow velocities are decreasing (see above). At the northern boundary, flow patterns show strong variations in the flow direction (Fig. A-01).

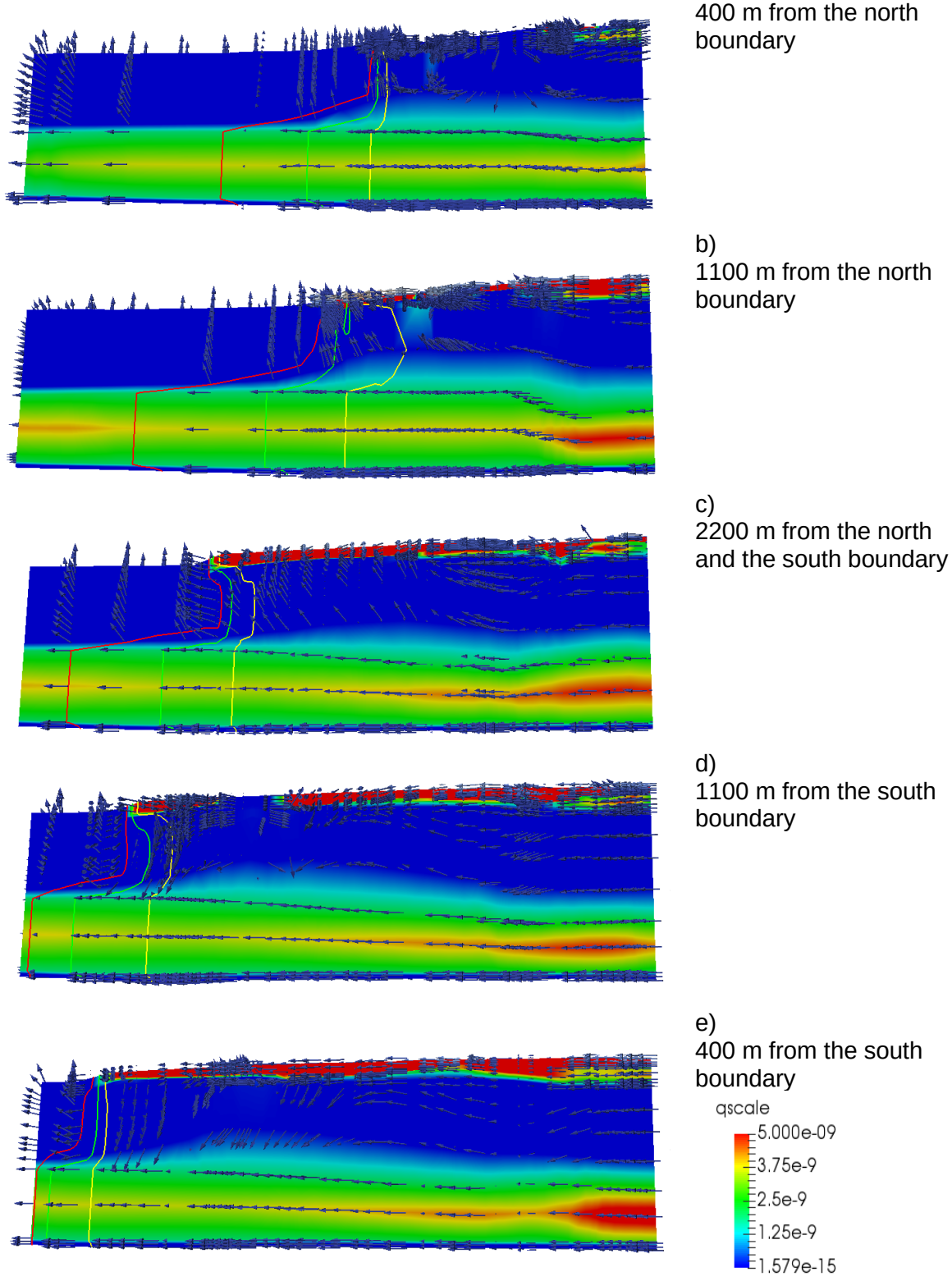

Figure 8-10: Cross-section at different locations for a model time t = 1 year, 500 years, 1000 years, 1500 years and 2000 years. The colour shows the magnitude of the velocity ("qscale", [m s^{-1}]), the arrows show the flow direction. The red, green, yellow lines show the isolines for c_{rel} = 0.9, 0.5 and 0.1, respectively. For locations of the cross sections a - e see Figure 8-9.

Isolines of c_{rel} = 0.9, 0.5 and 0.1 are given for all cross-sections. In the south, the coastline is close to the western model boundary. There, a boundary condition of c_{rel} = 1 is set. The fresh water inflow from the east into the lower aquifer causes a shift of the salt concentration front to the west. In the lower permeable aquitard this front is locally restricted to a smaller zone than in the higher permeable aquitard. Further north, the coastline moves to the east. With the greater distance to the western model boundary (and thus the fixed salt concentration of c_{rel} =1), the transition zone between fresh water and salt water broadens, especially in the higher permeable lower aquifer, as can be observed in Fig. A-03, Fig. A-02 and Fig. A-01. In the aquitard, this zone is generally not developed as broad as in the aquifer. In some parts, a reverse trend can even be observed with the isolines shifting eastwards (Fig. A-03 and Fig. A-02). These parts are approximately congruent with those, where the upwards component of the groundwater flow is observed.

The time series depicted in Fig. A-05 to Fig. A-01 show once again that the groundwater flow is in a steady-state already in the early stages of the model time, while the salt concentration distribution is still changing. It is expected that at a steady-state, the transition zone between salt water and fresh water will be located further to the west in the aquifer than in the aquitard, where the transition zone will be located in the area of the upwards groundwater flow.

The truncated block diagrams in Figure 8-11 are oriented perpendicular to those discussed above. These north-south striking cross-sections confirm the findings described so far. Especially in the upper layers with an non-continuous spatial distribution, the flow field is locally quite inhomogeneous and shows variances from the general flow directions. The northbound flow component is clearly visible in these figures. The flow patterns in the upper layers can be traced in the Kotlin Clay aquitard, although with a lower velocity. In contrast to that, the flow directions in the Gdovsk aquifer is homogeneously directed to the west.

Figure 8-12 shows the flow fields at the model surface and at 5 m, 50 m and 120 m below sea level (z = 0) at 2000 years model time. The temporal evolution of the flow field at the mentioned depths is depicted in Fig. A-06 to A-09. At the model surface, the highest flow velocities occur with also the highest variability of the flow directions. Here, the preferred flow paths are clearly visible by the higher flow velocities.

A certain part of the groundwater recharge is discharged at the surface after passing only the Quaternary sand and/or the Cambrian sands. At 5 m below sea level, the discharge area in the central to northern part of the model as well as along the coast line can well be identified. At 50 m below sea level, in the Kotlin Clay layer, the lowest flow velocities are observed with maximum values of $4 \cdot 10^{-10}$ m s^{-1}.

Flow patterns of the superimposed layers can be traced in this depth. Elevated flow velocities with a dominant flow direction to the west are observed in the Gdovsk aquifer at 120 m below sea level. While in the upper part of the model, the transition zone between fresh water und sea water is narrowly developed, this zone is broadened in the lower aquifer. The salt concentration is not yet in a steady-state.

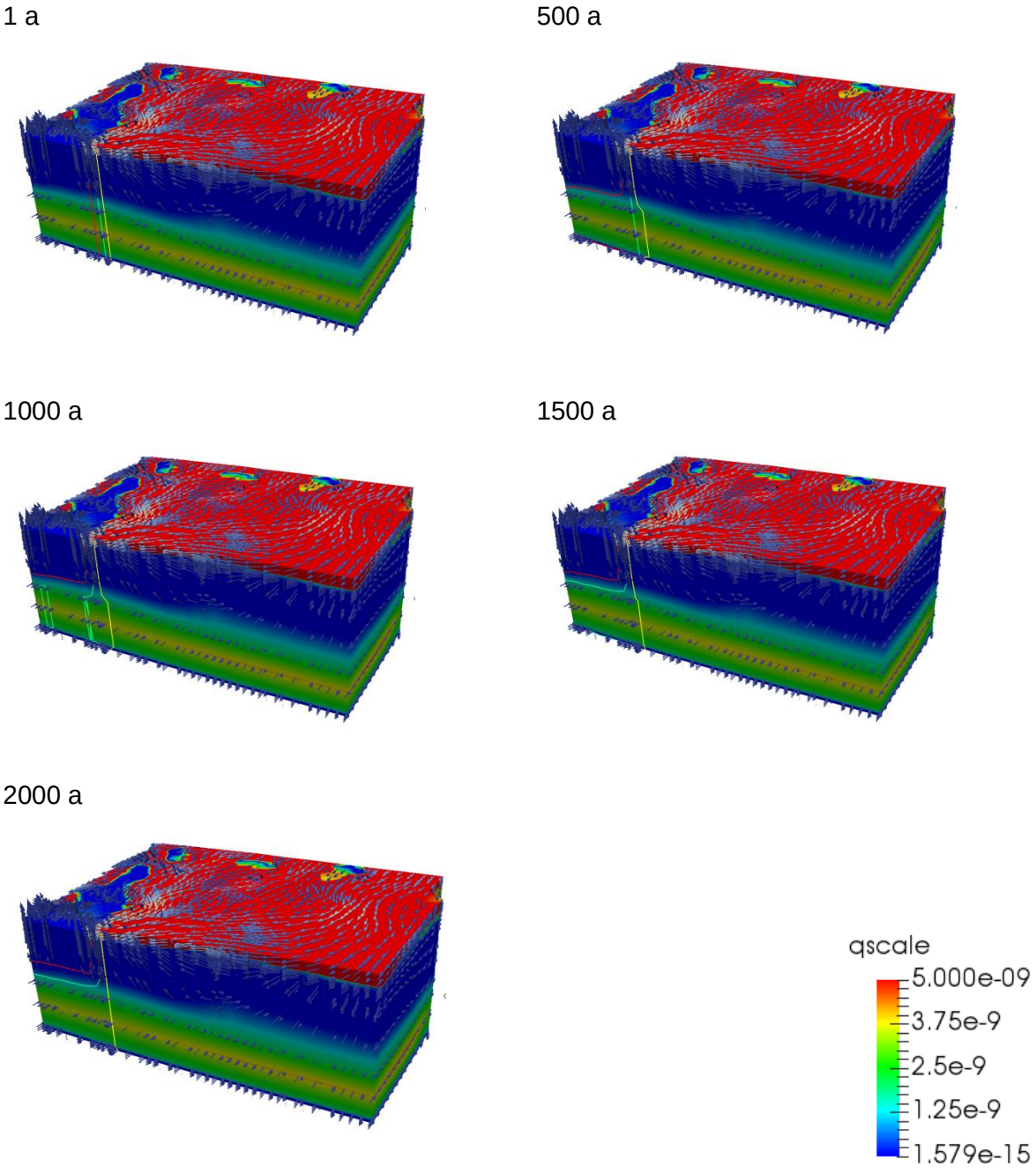

Figure 8-11: Truncated block diagrams at 2800 m to the east and west boundary (x = 613,600 m, location i in Figure 8-9) for a model time t = 1 year, 500 years, 1000 years, 1500 years, 2000 years. The colour shows the magnitude of the velocity ("qscale", [m s^{-1}]), the arrows show the flow direction. The red, green and yellow lines show the isolines for c_{rel} = 0.9, 0.5 and 0.1, respectively.

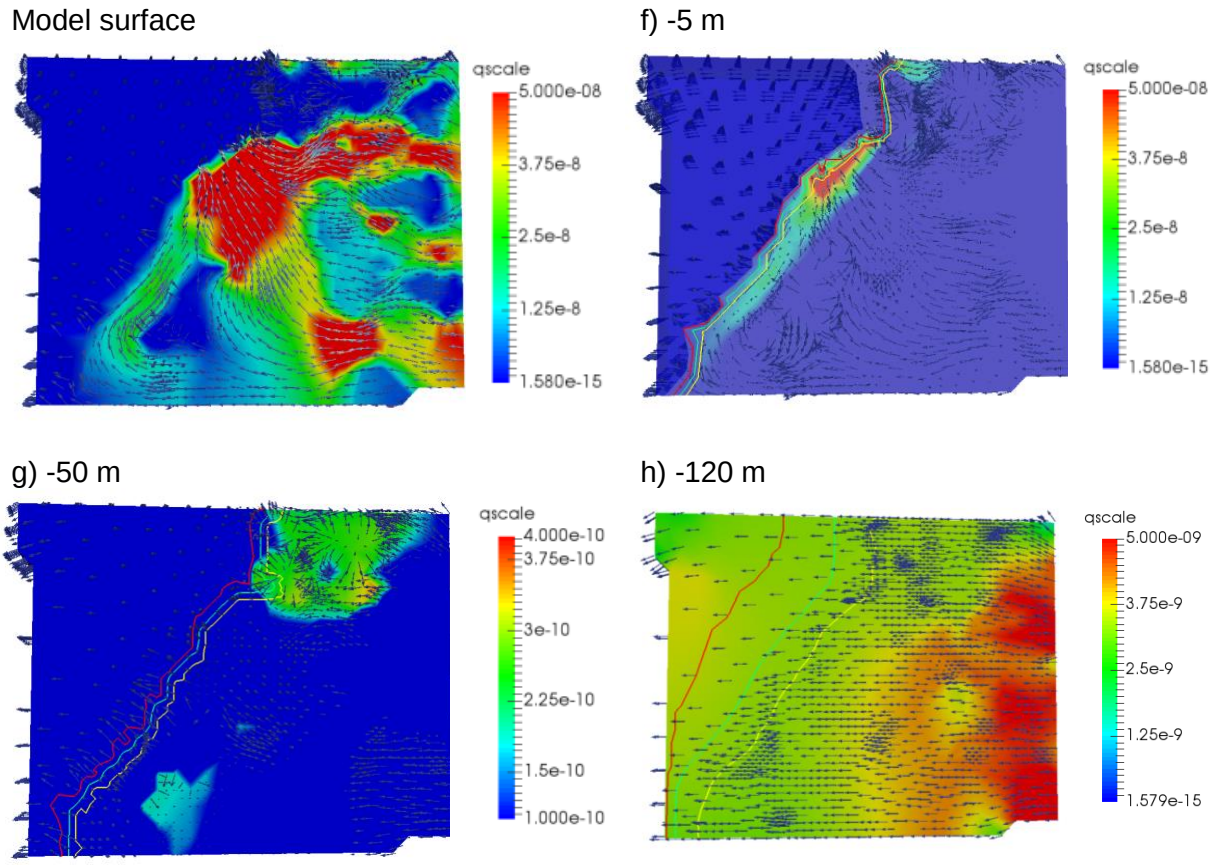

Figure 8-12: Model surface and cross-sections at z = -5 m, z = -50 m and z = -120 m. The colour shows the magnitude of the velocity ("qscale", [m s^{-1}], note the different scales), the arrows show the flow direction. The red, green and yellow lines show the isolines for c_{rel} = 0.9, 0.5 and 0.1, respectively. The transparent white plane in the figure for z = -5 m shows the area, where the model was cut off. The blue region is lower than z = -5 m. For locations of the cross sections f – h see Figure 8-9.

Fundamental key characteristics of the flow regime in the investigated area could be simulated with the presented groundwater flow model. The flow is generally directed to the west and shows highest flow velocities in the aquifers, i.e. the Quaternary sands and the Gdovsk aquifer. Lowest flow velocities are observed in the Kotlin Clay layer. Some of the findings of the simulations should be investigated in more detail, e. g. the vertical components of the flow. Concerning the construction of a potential repository site, it is crucial to know the possible transport paths of contaminants, including a transport to the surface and biosphere. Also, flow velocities, especially in the Kotlin Clay layer, and thus transport times from the depth of the potential repository to the surface cannot be reliably simulated based on the available data. It would also be favourable to assume a free groundwater table in flow simulations, which is also only reasonable based on more detailed data. With regard to subsequent transport simulations for contaminants released from a potential repository site, the salt concentration in the groundwater is important to know and could be simulated with more consolidated findings resulting from flow simulations.

Up to now, results of this model can only indicate tendencies. For a better representation of the groundwater flow, additional and more detailed data is needed. This includes:

- Hydraulic parameters for each of the geological layers (porosity, permeability)
- Initial conditions (salt concentration distribution in the model domain), and
- Boundary conditions (groundwater table, groundwater recharge, inflow and outflow over the lateral boundaries).

In summary, the presented work is a basis for further model simulations with more detailed data. Based on this, statements on the groundwater flow and potential contaminant transport will be possible.

8.2 Radionuclide transport

The radionuclide transport from the emplacement area to the biosphere is assumed to occur along two distinct pathways, which is the transport through the undisturbed host rock and the one along the drifts and shafts of the repository mine. In principle, the radiological assessment requires a coupled modelling of dissolved and volatile radionuclide transport along both pathways. However, there is currently no computer code available in Germany that allows such coupled modelling for the full system in clay host rock. The main reason is that there are still open questions about the mechanism of gas transport in the clay host rock and in highly compacted bentonite. According to the latest research, two-phase flow seems unlikely in clay, since the gas entry pressure is very high. A potential gas transport may occur through the so-called pathway dilation, which creates new pore space in the rock. The gas pressure needed to start this process depends on the mechanical properties of the rock and its stress state. However, the process of pathway dilation is not fully understood yet and no consecutive material laws exist that would allow predictive modelling of such a process in clay rock (Shaw 2013). For this reason, a repository concept may be preferable that considers gas storage areas or allows for a sufficient gas transport in drifts and shafts to evacuate all gases generated. In this case, there is no gas transport in the host rock and the transport in the host rock and the drift system could be modelled independently.

For transport in the liquid phase, the radionuclide transport modelling presented in the following has been performed with integrated performance assessment codes from the RepoTREND package (Reiche 2016) which was developed by GRS. For the transport in the gas phase, the code TOUGH2 (Pruess et al. 2012) has been used.

8.2.1 Radionuclide transport in the liquid phase

For the transport in the liquid phase, the flux from a representative section of the repository according to Consortium SGN/IVO/AEA Technology (1997-A) was modelled. For this case, one emplacement vault is considered for the modelling as representative section (marked red in Figure 8-13). For the calculated fluxes, the result of the simulation than has to be multiplied by the number of representative sections in the repository.

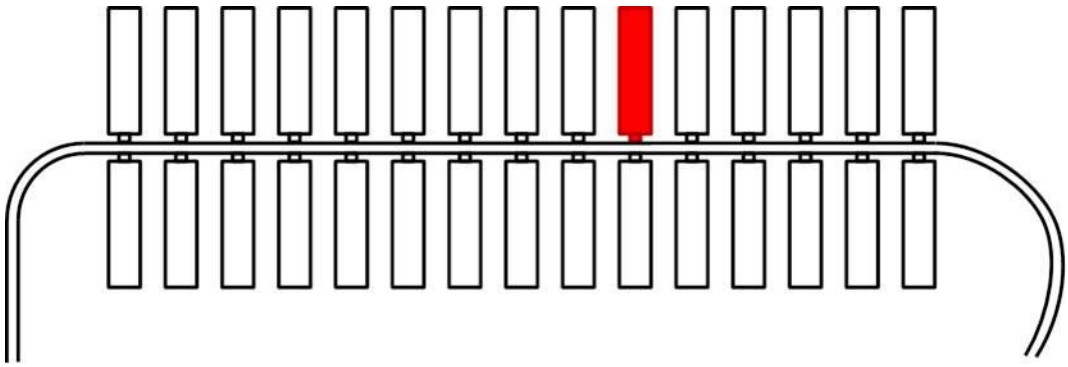

Figure 8-13: Repository layout with the representative section modelled for the radionuclide transport in the liquid phase marked in red.

A sketch of the model geometry is shown in Figure 8-14. The void spaces around the containers are considered to be backfilled and completely saturated at the beginning of the

modelling time. At the beginning all radionuclides are in the waste. The radionuclides are assumed to become completely dissolved in the pore water around the waste within 100 years. Some radionuclides may be precipitated if they reach their solubility limits. Neither temporal change nor lateral differences in chemical conditions are taken into account. Therefore, radionuclides will only reach their solubility limits at the source and nowhere else. The model considers the radionuclide transport through the 1 m thick cement lining of the emplacement vault and through the 43 m thick clay host rock towards the next aquifer. The 43 m clay layer itself consists of a 5 m thick EDZ (excavation disturbed zone) and 38 m of the undisturbed host rock layer. Depending on the codes used for modelling from the RepoTREND package, the transport in the cement as well as in the clay is either by diffusion only (code CLAYPOS) or by diffusion and advection (code POSA).

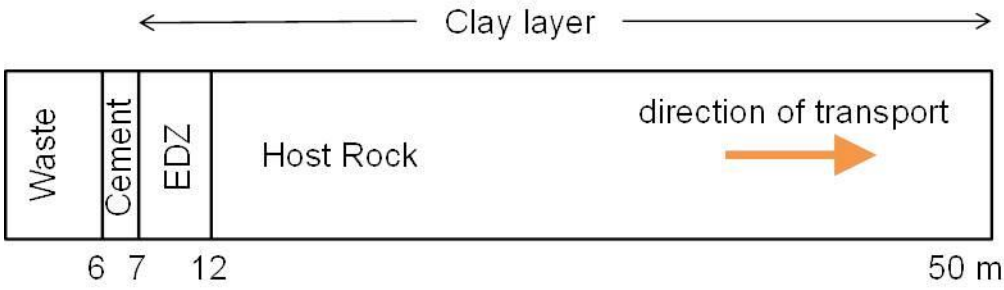

Figure 8-14: Sketch of the model geometry.

Site specific data has been used for the modelling if possible. If no site specific data was available, the missing data was supplemented from the following sources:

- **Repository geometry**: data about the geometry are deduced from the information about the geology of the site and from the concept for the repository layout as considered in earlier studies (Consortium SGN/IVO/AEA Technology 1997-A).
- **Radionuclide Inventory**: For the radionuclide inventory only very general information exists from earlier studies (Consortium SGN/IVO/AEA Technology 1997-C). This data is not sufficient to perform long-term safety assessments since information on some safety relevant nuclides like C-14 is missing. The nuclide spectrum given in Consortium SGN/IVO/AEA Technology (1997-C) was compared to radionuclide inventories presented in different national and international projects (Rübel et al. 2007). It was decided to use data from the Nirex Generic Disposal Inventory (Nirex 2001), which compared best relative to the leading nuclides given in Consortium SGN/IVO/AEA Technology (1997-C).
- **Solubility limits and radionuclide sorption data**: For the cementitious material environment in the near-field, no site specific data is available and therefore, data for the ILW emplacement area from (Nagra 2002b) has been used which was derived for a similar environment. For the host rock, site specific sorption data is available for four elements in (Pereverzeva et al. 2008). Since this data is in the same order of magnitude as data for the Opalinus Clay given in (Nagra 2002b), the existing data was supplemented by the data for the Opalinus Clay.
- **Diffusion coefficients**: For cementitious material in the near-field, no site specific data is available and data from (Nagra 2002b) has been used like for the sorption data. For the host rocks, site specific data for five elements is available in (Rumynin et al. 2003). This data deviates from data presented for other clay formations in the literature. Due to this reason, no element specific diffusion coefficients have been considered, but the existing site-specific values have been used for all elements.

Table 8-3 shows the transport parameter values considers together with their bandwidths assumed, while Table 8-4 shows the radionuclide inventory of about 10,000 m^3 of waste disposed of in one emplacement vault.

Table 8-3: Transport parameter values and bandwidths.

Parameter		Reference value	Lower bandwidth	Upper bandwidth
Host rock subdomain length [m]		50	45	55
Inventory		see table 7.2	ref. value/10	ref. value*10
Porosity cement [-]		0.25	0.23	0.28
Porosity clay anions [-]		0.13	0.05	0.28
Porosity clay other elements [-]		0.25	0.23	0.28
Diffusion coefficient cement [m^2/s]		5.37E-9	8.33E-10	6.85E-9
Diffusion coefficient clay [m^2/s]		5.37E-9	5.0E-11	6.85E-9
Solubility limit [mol/m^3]	Sr	3	2	6
	Zr	6E-3	6.0E-4	6.0E-2
	Mo	3E-2	3.0E-3	2
	Sn	1E-4	1.0E-4	8.0E-3
	Sm	2E-3	2.0E-4	2.0E-2
	Eu	2E-3	2.0E-4	2.0E-2
	Cm	2E-6	3.0E-7	1.0E-5
	Pu	6E-8	2.0E-8	6.0E-7
	U	1E-5	1.0E-5	5.0E-4
	Th	3E-6	8.0E-7	1.0E-5
	Am	2E-6	3.0E-7	1.0E-5
	Ra	1E-2	1.0E-3	2.0E-2
	Pb	3	3	not limited
	Pa	1E-5	1.0E-5	not limited
	Other	not limited	not limited	not limited

		cement	clay	cement	clay	cement	clay
Distribution coefficient K_d [m^3/kg]	C	0	0	0	0	0	0
	Cl	5E-3	0	3E-3	0	7E-3	0
	Ni	0	0.9	0	3E-2	0	20
	Co	0	0.4	0	1E-2	0	20
	Se	1E-3	0	7E-4	0	1E-3	0
	Sr	1E-3	1E-3	7E-4	1E-4	1E-3	5E-2
	Zr	10	10	2	0.3	30	300
	Mo	0	1E-2	0	1E-3	0	0.2
	Nb	0	4	0.7	0.1	1	100
	Tc	1E-3	50	7E-4	0.5	1E-3	500
	Pd	0	5	0	0.2	0	100
	Sn	10	100	2	0.2	30	1000
	I	1E-3	3E-5	7E-4	0	1E-3	4E-4
	Cs	5E-4	0.5	3E-4	9E-2	7E-4	6
	Sm	80	50	20	5	300	600
	Eu	80	50	20	5	300	600
	Cm	80	10	20	1	30	200
	Pu	0.1	20	7E-3	1	0.1	300
	U	2	20	1	0.5	2	200
	Th	80	50	20	10	300	200
	Am	80	10	20	1	300	200
	Np	0.1	50	7E-2	5	0.1	500
	Ra	5E-2	7E-4	3E-2	1E-4	7E-2	5E-3
	Pb	0.5	2	0.3	2E-2	0.7	300
	Pa	0.1	5	7E-2	0.2	0.1	100

Table 8-4: Radionuclide half-live and inventories.

Radionuclide	Half-life [y]	Inventory [Bq]	Radionuclide	Half-life [y]	Inventory [Bq]
C-14	5.732E03	1.75E14	Th-232	1.405E10	7.98E09
Cl-36	3.002E05	4.56E11	Th-228	1.913E00	4.18E05
Ni-59	7.502E04	3.04E14	Cm-245	8.500E03	5.32E09
Co-60	5.272E00	9.13E14	Pu-241	1.435E01	1.22E15
Ni-63	1.002E02	2.24E16	Am-241	4.322E02	1.63E15
Se-79	1.102E06	9.51E10	Np-237	2.144E06	3.27E12
Sr-90	2.864E01	3.27E15	U-233	1.592E05	3.69E10
Zr-93	1.500E06	1.37E13	Th-229	7.880E03	6.08E08
Mo-93	3.500E03	7.98E13	Cm-246	4.730E03	1.25E09
Nb-94	2.000E04	6.84E12	Pu-242	3.750E05	6.46E11
Tc-99	2.100E05	1.52E13	Am-242	1.410E02	2.24E12
Pd-107	6.500E06	1.56E10	U-238	4.468E09	1.41E12
Sn-126	2.345E05	1.98E11	Pu-238	8.774E01	2.47E14
I-129	1.570E07	6.08E10	U-234	2.455E05	3.04E10
Cs-135	2.000E06	2.43E11	Th-230	7.540E04	4.94E09
Cs-137	3.017E01	1.44E16	Ra-226	1.600E03	3.42E11
Sm-151	9.300E01	6.46E13	Pb-210	2.23oE01	3.19E11
Eu-154	8.606E00	3.54E12	Am-243	7.370E03	7.60E11
Cm-244	1.810E01	8.75E12	Pu-239	2.411E04	5.32E14
Pu-240	6.563E03	5.32E14	U-235	7.038E08	6.46E10
U-236	2.342E07	4.18E11	Pa-231	3.276E04	2.70E10

8.2.1.1 Deterministic simulations

Deterministic simulations have been performed using the code CLAYPOS taking into account diffusive transport only and the code POSA taking into account diffusion and advection. Since POSA is a transport code only, the mobilisation of the waste and the transport in the cementitious near field was also simulated with CLAYPOS in this case. In the following, plots of the annual exposure rates versus time are presented as result of the simulations. These annual exposure rates are calculated from the simulated annual radionuclide fluxes at the outer boundary of the host rock. To calculate a radionuclide concentration, the radionuclide flux is diluted in an amount of water of 500 m^3/a, which is representative for the minimal amount of water consumed by a reference group of 10 persons. If transport and dilution in the aquifer would be taken into account, accordingly annual exposures would be calculated that could be lower by several orders of magnitude. The dose rate is finally calculated from the radionuclide concentration in the water by the means of dose conversion factors according to German regulation (Pröhl & Gering 2002). It has to be clearly mentioned that the results presented can only be seen as indicative due to the lack of site-specific data, especially the waste inventory.

Figure 8-15 shows the result from the CLAYPOS simulation using the reference input values given in Table 8-3. The highest exposure value is due to C-14 (approximately 0.16 Sv/y after 1,800 years, the corresponding radionuclide flux is about 10^{10} Bq/y). Other contributors to the dose at early times are Se-79 and I-129 and Cl-36. Those four nuclides are the ones typically found as main contributors to the dose in safety assessments for clay repositories, e.g. (Nagra 2002b) and (Rübel et al. 2007). The reason for this finding is the low sorption value of the anionic or neutral species in the clay formation. However, due to the lack of site-specific sorption data for three of those four radionuclides, the uncertainty of the result is consequently high. The time of the maximum annual radiation exposure occurs earlier than in the safety

assessments mentioned before. One reason is that no significant retention of the radionuclides in the waste matrix is assumed here with a mobilisation time of only 100 years and the other - more relevant - reason is that the assumed diffusion coefficient is comparably high.

After approximately 90,000 years, the maximal annual exposure is caused by the actinides, mainly Ra-226. This is due to the build-up of Radium in the repository by its mother nuclides. While the mother nuclides in the decay chain have a comparably high K_d-values and are therefore only slightly transported, Radium has a low K_d-value and is able to be transported through the clay formation, although the half-live of Ra-266 if rather short.

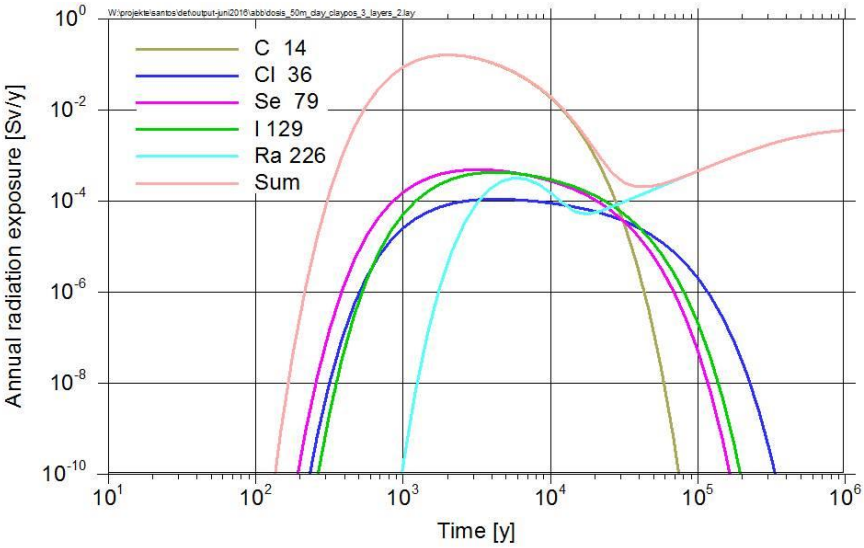

Figure 8-15:
Annual radiation exposure calculated using the CLAYPOS code.

Additional simulations were performed using the code POSA to be able to consider the influence of advective transport in the host rock, too. A direct comparison between the CLAYPOS and the POSA results show that the results from POSA typically yield higher annual radiation exposure values than from CLAYPOS. This effect is among others mainly due to the different outflow boundary conditions considered. Namely, at the end of the transport path a nearly zero nuclide concentration outside the model is considered for CLAYPOS. For POSA without advection the concentration inside the model, i.e. within the last discretized element is maintained constant and equal to the initial concentration leading to not representative concentrations and hence influencing the concentration driven diffusive transport. The maximum POSA exposure for Cl-36, Se-79 and I-129 are approximately five, three and two times higher than the CLAYPOS ones respectively and occur somewhat earlier.

The influence of advection has been analysed in the POSA simulations. Figure 8-16 shows the annual radiation exposure rates for Cl-36, Se-79 and I-129 in the POSA model with and without advection considered. The groundwater filter velocity considered was about $1.75 \cdot 10^{-4}$ m/y which is calculated from a hydraulic conductivity of $5.56 \cdot 10^{-12}$ m^2/s (Kühnlenz & Hammer 2014) and an assumed hydraulic gradient of 1 m/m.

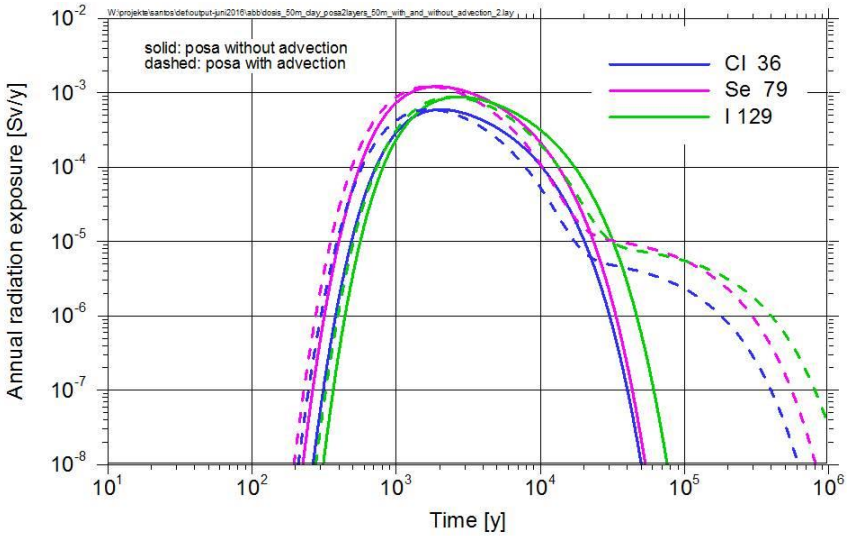

Figure 8-16:
Annual radiation exposures calculated using POSA with and without advection.

It can be seen that the time of occurrence and the value of the maximum radiation exposure is almost not affected by the advection velocity considered. However, the advection leads to a longer tailing of the radiation exposure versus time curve.

8.2.1.2 Probabilistic simulations

Probabilistic simulations have been carried out using CLAYPOS and POSA codes. However, only the CLAYPOS results are shown in the following, since the conclusions drawn are similar for both codes. The goal of a probabilistic analysis is to investigate the effect of parameter uncertainty on the results of the physical model. Specifically, the sensitivity analysis consists of studying the influences of single parameter uncertainties on the physical model and compared among them. The parameters varied as well as the bandwidths considered are shown in Table 8-3. The parameter distribution functions were chosen to be uniform for all parameters since no information about preferential parameter values were available.

The uncertainty analysis gives the variability of the annual radiation exposure due to the variability of the input data. The Monte Carlo probabilistic calculations were performed by means of the CLAYPOS and POSA codes considering 2000 simulations within the bandwidths given. The total annual exposure given by the contribution of all radionuclides was analysed. Figure 8-17 shows the temporal evolution of the mean annual exposure, the maximum, the median, and the quantiles (95% and 5%) for CLAYPOS. The maximum annual exposure (approximately 2.45 Sv/y after 1500 years) is mainly due to the C-14 contribution. The median represents approximately the highest exposure shown in Figure 8-15 whereas the maximum is approximately 15 times higher.

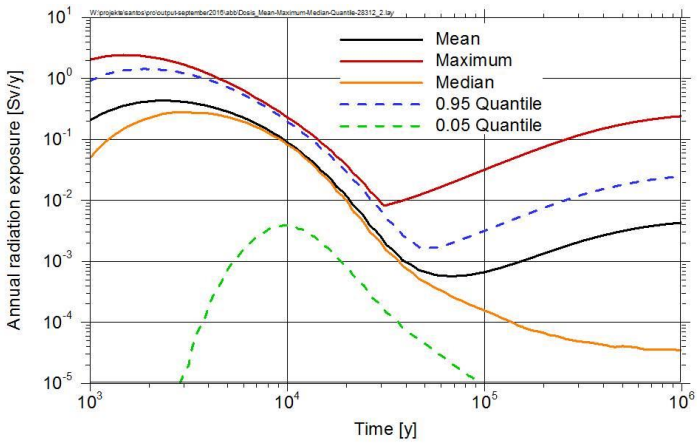

Figure 8-17:
Mean, maximum, median and the quantiles (95% and 5%) of the annual exposure calculated with CLAYPOS.

The difference between the median and the mean increases after approximately 50,000 years suggests a skewed distribution of the data. In such cases the median might be seen as a better estimator than the mean because it is less susceptible to the exceptionally higher or lower values in the data. Figure 8-18 shows the probability distribution of the CLAYPOS maximum annual exposure showing that the largest number of simulations results plots close to the maximum of the annual radiation exposure.

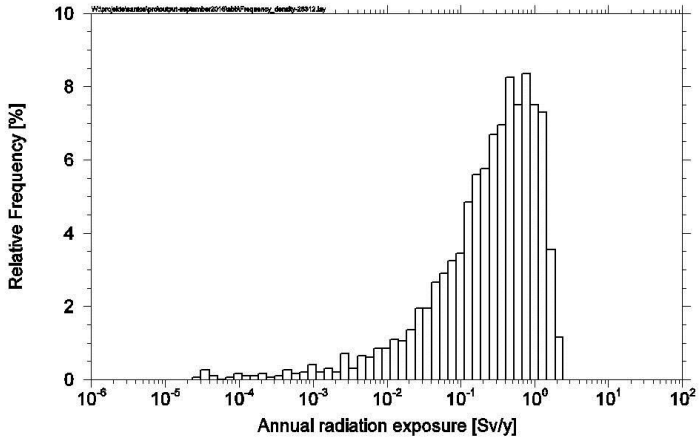

Figure 8-18:
Frequency density of the maximum annual exposure calculated with CLAYPOS.

The sensitivity analysis tries to quantify the contribution of each input parameter variation to the variations of the physical model results. All input parameters are varied at once during the simulations. The analysis methods selected were the “Contribution to the Sample Mean” (CSM) and the “Standardised Rank Correlation Coefficients” (SRRC).

The CSM method is a graphical one that allows a quick assessment and comparison of the sensitivities of a system to variations of different parameters. It provides a good mean for getting a quick visual description of a system. Figure 8-19 shows the contribution of the independent variables to the CSM method for the CLAYPOS model. If the model output does not depend at all on the input variables, the resulting curve corresponds to the diagonal. On the contrary, a CSM curve that deviates significantly from the diagonal indicates a strong sensitivity. Actually, the curvature and not the deviation from the diagonal is the main sensitivity indicator. The sensitivity of the model to variations of input parameters was also analysed by means of the standardised rank correlation coefficients (SRRC) method (see Figure 8-20). For this method, the values of the random variables are replaced by their rank, i.e. by their position in a sorted list of the values. By doing this, the method doesn’t assume a linear relationship between the input parameter variations and their influence on the model allowing the description of complex relationships.

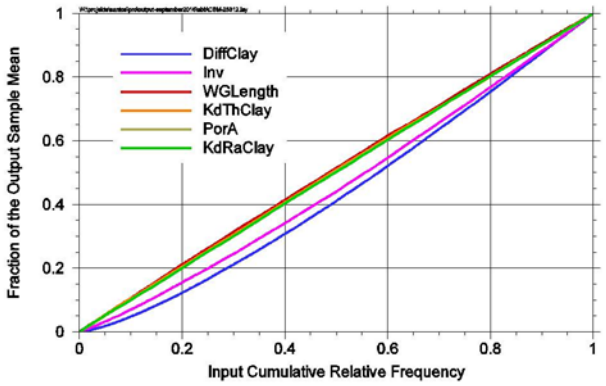

Figure 8-19: Contribution of the independent variables to the CSM method.

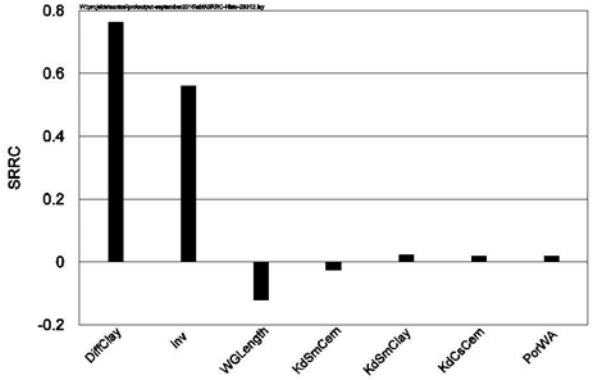

Figure 8-20: Standardised rank correlation coefficients (SRRC) method.

The diffusion coefficients for clay (DiffClay) as well as the radionuclide inventories (Inv) show the highest influence on the maximum annual radiation exposure obtained in the modelling results for both sensitivity methods applied. The rest of the input parameters show a decreasing influence on the maximum annual radiation exposure. The SRRC method allows not only to evaluate the parameters with the highest influence on the annual radiation exposure at the time of its maximum value occurrence, but also for other times as is shown in Figure 8-21. This figure gives the temporal evolution of SRRC and it can be seen that e.g. for late times, the K_d-value of Radium is of high influence on the annual radiation exposure. This finding is in agreement with the observation from the deterministic simulations, that at late times Ra-226 is the main contributor to the dose (see also Figure 8-15).

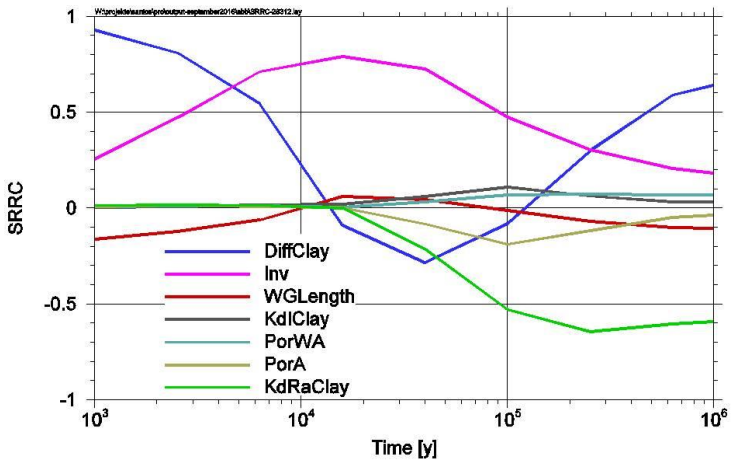

Figure 8-21: Temporal evolution of SRRC for CLAYPOS.

8.2.2 Radionuclide transport in the gas phase

The transport of volatile radionuclides together along with non-active gases is another potential pathway for the release of radionuclides from the repository into the biosphere. A flow of gases occurs along gas pressure gradients in the repository drifts which result from the gas production by the anaerobic corrosion of iron and other metals, but also from the microbial degradation of organic matter leading to a pressure increase in the repository.

C-14 is the most important radionuclide that occurs in volatile form in the repository (either as carbon dioxide or methane) which can lead to a potential radiation exposure in the biosphere. The reason is that a significant amount of C-14 can be in gaseous form and that the half-life of C-14 is long enough not to decay completely on the transport pathway. Other potentially volatile radionuclides are for example Tritium and I-129. While the first one has a comparably short half-life and usually decays during transport, the latter occurs mainly in liquid form and if at all, only has a very small fraction in volatile form.

This section describes simulations with TOUGH2 EOS7R simulating the transport of C-14 from the repository. The simulations are based on those for gas pressure build-up and gas flow presented in section 7.3. Since the EOS7R module used here assumes air as gas instead of hydrogen assumed in the EOS5 module used in section 7.3, the gas production rates were recalculated according to the mole mass of the gases compared to the simulations for the gas pressure build-up. All other parameters were used as presented before. However, since the solubility and volatility of air and hydrogen are different, differences for the evolution of the gas-pressure evolution might occur.

No site specific data is available for the inventory and the potential release of volatile C-14 from the waste forms. Therefore, data for the German ERAM repository for low-level waste was used as basis. For the ERAM east-field emplacement area, a C-14 release of $1.98 \cdot 10^{7}$ Bq per cubic metre of waste is given (Becker et al. 2009), resulting in an amount of $5.23 \cdot 10^{-8}$ kg per cubic metre of emplacement vault volume for the repository concept regarded. The release of the volatile C-14 was assumed to occur within one year into the gas phase of the emplacement vaults resulting in a release rate of $3.32 \cdot 10^{-11}$ kg/s per vault.

The result of the TOUGH2 simulation, which shows the gas flow and the C-14 concentration in the gas at the outer surface of the drift seal is plotted in Figure 8-22. Additionally, the C-14 flux calculated from those two parameters is shown plotted as well. The C-14 flux increases rapidly after about 100 years and reaches a maximum value of about $6 \cdot 10^{8}$ Bq/y. Considering the uncertainty of the underlying input data, this result can be regarded as to be in the same order than the release of C-14 dissolved in the liquid phase. Therefore, the release of volatile C-14 from the repository can potentially contribute significantly to the potential radiation exposure in the biosphere and has to be regarded additionally to the release of dissolved radionuclides through the host rock.

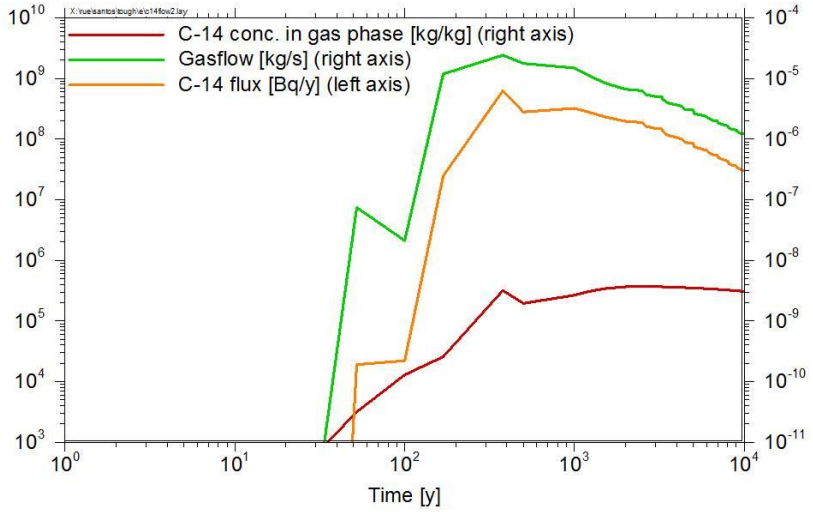

Figure 8-22:
C-14 flux at the outer surface of the drift seal together with the gas flow and the C-14 concentration at the same point.

9 Compilation of FEP

9.1 FEP list

A FEP list gives a summary of features that characterize the initial properties of a repository system at the end of the operational period and gives relevant information on events and processes that may influence the future evolution of the repository system. In the context of a safety assessment, the FEP list is highly relevant as it is the connecting link between the fundamentals (site description, geoscientific long-term prognosis, and radioactive waste inventory), the repository concept, and the system analysis. Apart from the compilation of the most relevant basics, the FEP list reflects the interrelation between the site-specific conditions and the modifications that result from the disposal of radioactive waste. Therefore, it is a sound basis for scenario development, for process analyses, for demonstrating the integrity of geological and geotechnical barriers, and for the analysis of the radiological consequences. For these purposes, it is useful to add relevant data and information and to expand the FEP list to a FEP catalogue that is to describe the entire repository system.

The contents and structure of a FEP list/catalogue are influenced by the intended use in the course of the safety assessment and by the legal requirements (regulations for radiological assessment including provisions for human intrusion scenarios). In the German R&D projects ISIBEL for salt as a host rock (Krone et al. 2013) and ANSICHT for clay as a host rock (Jobmann et al. 2016), a methodology has been developed to systematically derive scenarios from site specific FEP catalogues. To reflect all relevant future evolutions, the FEP list/catalogue has to be as complete as possible to be able to describe the whole repository system. Measures to increase completeness of a FEP list are

- comparison with the international NEA-FEP database, which is a compilation of numerous FEP lists from different host rocks,
- bottom-up and top-down approaches to identify relevant FEP,
- plausibility checks of the sequences and interdependences of the FEP as well as
- consideration of indications from the geoscientific long-term prognosis, the scenario development and the process analyses.

The basis for the FEP list in this project, described below, were state-of-the-art FEP catalogues that have been prepared for a generic HLW repository site in German clay formations (Jobmann et al. 2016) and for the license application for the closure of a German L/ILW repository in salt formations (ERAM, not yet published). The basic principle for all FEP lists (incl. the NEA-FEP-list) is their composition from two major FEP-groups:

- the "features" or "components" that describe all elements of the repository system, and
- the "processes" (and "events") that affect the components and describe the future evolution of the repository system.

With regard to the definition of FEP, there is a broad scope of discretion: e.g. it is possible to describe one component in one FEP or to define each element or each property of the component in an individual FEP. So the NEA-FEP-list is very detailed with a high degree of itemization. In German projects, one intention was to define FEP in such a way that the FEP are clearly separated and that overlaps are avoided. Furthermore, "components" including their properties are completely described in one FEP. Looking at the interaction between the FEP in causal sequences, a direct interaction between two "components" is not possible, but this always runs via connecting "processes". So, a "process" may influence the properties of a "component" and vice versa (e.g. the process "*concrete corrosion*" modifies the chemical, mechanical, and hydraulic properties of the component "*drift seal*" and, conversely, the chemical and hydraulic properties of the "*drift seal*" influence the intensity of "*concrete corrosion*").

For the first draft of the FEP list of this project, the ANSICHT NORTH Clay FEP List has been supplemented with project-specific components and processes of the Leningrad region (Table 9-1). In an iterative process, the completeness of the FEP list has to be checked continuously to see if new site data have been determined or the repository concept modified. Furthermore, two FEP categories, which were excluded from the German FEP lists due to regulatory reasons, have to be added to the this FEP list: "components of the biosphere" and "future human actions". In Germany, the assessment of radionuclide release into the biosphere and the evaluation of potential human intrusion scenarios will be handled by stylized scenarios defined by the regulator. In other countries, these scenarios have to be developed from the FEP list/catalogue and therefore, they have been added here (like in the NEA-FEP-List).

In Germany, a systematic approach to develop scenarios directly from a FEP catalogue is preferred. In a FEP catalogue, comprehensive data that characterize the FEP properties can be compiled. In annex B, there are examples for the description of a component-FEP and a process-FEP. The FEP descriptions may include a definition, general information, a description of the circumstances at the site and site-specific impacts, a classification of the conditional probability of occurrence, information regarding the time frame of action, and the interactions with other FEP. The structure and the contents of the descriptions can be adapted to the intended application in the course of the safety assessment.

Table 9-1: Draft FEP list for a near surface repository in the Kotlin Clay of the Leningrad region (Radon-site).

No.	FEP-Category (grey) and FEP name	Short characterization	NEA-IFEP-Groups
	Components in underground openings	**Describe all relevant, engineered, underground components of the repository mine including the waste packages**	**2.1 Waste Form 2.2 Waste packaging 3.1 Repository characteristics and properties**
1	Waste matrices	Describes the chemical, hydraulic, mechanical and thermal l properties of the waste matrices (Concrete, bitumen, metal) at the time of emplacement.	2.1.2 Waste form characteristics and properties
2	Radioactive waste inventory	Describes the chemical, biological and physical properties of the radioactive waste at the time of emplacement, especially the composition and activity.	2.1.1 Contaminant inventory
3	Disposal containers	Describes the characteristics and chemical, hydraulic, mechanical and thermal l properties of the different waste containers (ZshZK-1/2, NZK-MR: concrete containers, metal drums) at the time of emplacement.	2.2. Waste packaging
4	Backfill	Describes the chemical, hydraulic, mechanical and thermal properties of the backfill (excavated material with additive) at the time of repository closure.	3.1.1 Buffer / Backfill
5	Disposal drift seals	Describes the chemical, hydraulic, mechanical and thermal properties of the drift seal (Asphalt blocks + bitumen, alternative: bentonite (Seal), concrete (abutment)) at the time of sealing.	3.1.2 Room / tunnel seals
6	Access drift seals	Describes the chemical, hydraulic, mechanical and thermal properties of the drift seal (seal: asphalt blocks, bentonite, abutment: concrete) at the time of sealing.	3.1.2 Room / tunnel seals
7	Shaft seals	Describes the chemical, hydraulic, mechanical and thermal properties of the shaft seal (seal: bentonite, bitumen, concrete abutments, gravel column) at the time of sealing.	3.1.3 Shaft/ ramp seals

8	Ramp seal	Describes the chemical, hydraulic, mechanical and thermal properties of the ramp seal (seal: asphalt blocks, bentonite, abutment: concrete) at the time of sealing.	3.1.3 Shaft/ ramp seals
9	Borehole seal	Describes the chemical, hydraulic, mechanical and thermal properties of the borehole seal at the time of sealing.	3.1.4 Other engineered features
10	Technical installations	This FEP compiles all technical equipment remaining in the repository after closure, e.g. rock bolts, cables, support, roadway etc. and summarizes their properties	3.1.4 Other engineered features
11	Drift lining	Describes the chemical, hydraulic, mechanical and thermal properties of the drift lining at the time of installation.	3.1.4 Other engineered features
12	Shaft lining	Describes the chemical, hydraulic, mechanical and thermal properties of the shaft lining at the time of installation.	3.1.4 Other engineered features
13	Void volume	Describes the contour and the fluid fill of void volumes in the repository that cannot assigned to other components, e.g. crotches between disposal containers (no pore volumes or contour zones of barriers).	3.1 Repository characteristics and properties:
14	Excavation damaged zone and unsaturated zone	Tension redistribution in the geosphere results in the disintegration of a rock zone close to the mine openings. Mine ventilation leads to an evaporation of rock water in the near excavation area..	3.1.5 Excavation damaged and disturbed zones
15	Metal corrosion products	The corrosion of waste, waste containers and technical equipment produces corrosion products with different properties than the starting material	3.1 Repository characteristics and properties
16	Concrete corrosion products	The corrosion of waste matrices, waste containers and technical equipment produces corrosion products with different properties than the starting material	3.1 Repository characteristics and properties:
17	Liquids in underground excavations	This FEP describes the quantities and the chemical properties of liquids from waste, from construction material and from inflow the surrounding rocks or via the shafts/ramp	3.1 Repository characteristics and properties
18	Gas in underground excavations	This FEP describes the quantities and the chemical properties of mine air and gas from metal corrosion and microbial degradation of organic matters.	3.1 Repository characteristics and properties
19	Surface exploration drillings	Describes the chemical, hydraulic, mechanical and thermal properties of the surface drillings after borehole sealing..	3.1 Repository characteristics and properties
20	Underground exploration drillings	Describes the chemical, hydraulic, mechanical and thermal properties of the underground drillings after borehole sealing.	3.1 Repository characteristics and properties
	Components in the Geosphere	**Describes all relevant characteristics and properties of the host rock and the adjoining rock formations**	**4.1 Geosphere characteristics and properties**
21	Host rock (Kotlin Clay)	Describes the chemical, hydraulic, mechanical and thermal properties of the host rock at the time of repository closure..	4.1.1 Stratigraphy 4.1.3 Geological resources 4.1.4 Geothermal characteristics 4.1.6 Hydraulic characteristics 4.1.7 Mechanical characteristics 4.1.8 Geochemical characteristics 4.1.9 Biological characteristics
22	Fractures and faults in the host rock	Describes the chemical, hydraulic, mechanical and thermal properties of the fractures and faults..	4.1.2 Large-scale discontinuities
23	Near surface decompression zone of the host rock	Describes the chemical, hydraulic, mechanical and thermal properties of the near surface decompression zone.	4.1.7 Mechanical characteristics
24	Liquids in the host rock	This FEP describes the quantities and the chemical properties of pore water, hydrocarbons and water infiltrating via fractures an faults from the mine or from adjoining rocks.	4.1.6 Hydraulic characteristics and properties

25	Gas in the host rock	This FEP describes the quantities and the chemical properties of free gases, gaseous hydrocarbons and gas infiltrating via fractures an faults from the mine or from adjoining rocks.	4.1.6 Hydraulic characteristics and properties
26	Adjoining rock formations	Describes the chemical, hydraulic, mechanical and thermal properties of the adjoining rock at the time of repository closure..	4.1.1 Stratigraphy 4.1.3 Geological resources 4.1.4 Geothermal characteristics 4.1.6 Hydraulic characteristics 4.1.7 Mechanical characteristics 4.1.8 Geochemical characteristics 4.1.9 Biological characteristics 5.1.3 Soil and sediments
27	Fractures and faults in the adjoining rock formations	Describes the chemical, hydraulic, mechanical and thermal properties of the fractures and faults in the adjoining rocks.	4.1.2 Large-scale discontinuities
28	Liquids in the adjoining rock formations	This FEP describes the quantities and the chemical properties of the water in the aquifers (Lomonosov-Aquifer and Gdovsker-Aquifer) and the pore water in the other rocks.	4.1.6 Hydraulic characteristics and properties 5.1.4 Near-surface aquifers and water-bearing features
29	Gas in the adjoining rock formations	This FEP describes the quantities and the chemical properties of gas in the aquifers (Lomonosov-Aquifer and Gdovsker-Aquifer) and the pores or fractures of the other rocks.	4.1.6 Hydraulic characteristics and properties
	Components in Biosphere	**Describes all relevant characteristics and properties of the biosphere including future human actions**	**5.1 Surface environment**
30	Topography and morphology	The relief and shape of the surface environment and its potential evolution with time	5.1.1 Topography and morphology
31	Soils	Characteristics of soils that overlie the rock and sediments of the geosphere and their potential evolution	5.1.3 Soil and sediments
32	Terrestrial surface water bodies	Characteristics of rivers and lakes and their potential evolution	5.1.5 Terrestrial surface water bodies
33	Sea and Coast	Characteristics of the sea and coast and their potential evolution	5.1.6 Coastal features 5.1.7 Marine features
34	Vegetation	Characteristics of terrestrial and aquatic vegetation and their potential evolution	5.1.9 Vegetation
35	Animals	Characteristics of terrestrial and aquatic animals and their potential evolution	5.1.10 Animals
36	Human characteristics and behaviour	Describes the supposed characteristics and behaviour of future humans	5.2 Human characteristics and behaviour
37	Climate and weather	Characteristics of climate and weather and their potential evolution. Incl. rain, flooding, storm etc.	5.1.11 Climate and weather
	Geological Processes	**Long-term processes arising from the wider geological setting and their effects on the performance and safety of the repository system**	**1.2 Geological factors**
38	Vertical movements of lithosphere	Describes very slow, large-scale epirogenetic movements (up or down-lift) of the lithosphere due to the underlying movement of the crustal plates.	1.2.1 Tectonic movement
39	Orogeny	All processes contributing to mountain building	1.2.2 Orogeny
40	Deformation of geological structures	Describes deformations of geosphere that are not caused crustal plate movements, e.g. isostatic movements	1.2.3 Deformation (elastic, plastic, or brittle)
41	Seismicity	Release of accumulated geologic stress via rapid relative movements in the geosphere.	1.2.4 Seismicity
42	Trench formation	Due to the stretching of lithosphere rift zones develop and trench formations are build.	1.2.3 Deformation (elastic, plastic, or brittle)
43	Magmatic and hydrothermal activity	Magmatic activity includes the intrusion of magma into rock formations. Hydrothermal activity may be associated with magmatic activity.	1.2.5 Volcanic and magmatic activity 1.2.7 Hydrothermal activity

44	Metamorphism	Describes the process of recrystallization of rocks as a consequence of high temperatures and pressures	1.2.6 Metamorphism
45	Diagenesis	Transformation of sediments by compaction, cementation and crystallization.	1.2.9 Diagenesis
46	Erosion	Include processes for destruction of sediments and transport of erosion products.	1.2.8 Regional erosion and sedimentation
47	Sedimentation	Deposition of particles from a transport medium.	1.2.8 Regional erosion and sedimentation
	Climate induced processes and other impacts	**Processes resulting from climate changes and other external impacts**	**1.3 Climatic factors** **1.5 Other external factors**
48	Climate induced heat flow	Temperature fluctuations due to global climatic changes (e.g. ice ages or warm climate periods) affect the temperature in the upper part of geosphere.	1.3.1 Global climate change 1.3.2 Regional and local climate change
49	Precipitation	Summarizes the amount of precipitation	1.3.1 Global climate change 1.3.2 Regional and local climate change
50	Transgression or regression	Offshore or onshore relocation of the coast line.	1.3.3 Seal level change
51	Periglacial processes	Physical processes in cold, but ice-sheet-free environments (e.g. permafrost).	1.3.4 Periglacial effects
52	Effects of glaciers and ice sheets	Include processes like exaration (a glacial erosion process).	1.3.5 Glacial and ice-sheet effects
53	Glacial channelling	Below a glacier, melting water may erode glacial channels.	1.3.5 Glacial and ice-sheet effects
54	Meteor strike	The impact of large extra-terrestrial solid bodies on the earth surface.	1.5.1 Meteorites and human space debris
	Future Human Actions	**Possible future human actions that may affect the performance of the repository system**	**1.4 Future Human Actions**
55	Human influences on climate	The human activities that could affect the change of climate globally and regionally	1.4.1 Human influences on climate
56	Drilling activities	Any type of drilling activity in the vicinity of or within the repository	1.4.5 Drilling activities
57	Mining and other underground activities	Any type of mining or excavation activity carried out in the vicinity of or within the repository	1.4.6 Mining and other underground activities
58	Surface activities	Activities that may be carried out in the surface environment which may affect the engineered and/or geological barriers or the exposure pathways	1.4.8 Surface activities
59	Water management	Groundwater and surface water management (incl. water procurement, reservoirs, dams and river management)	1.4.9 Water management
60	Deliberate human intrusion	Consequences of deliberate intrusion into the repository after closure	1.4.12 Deliberate human intrusion
	Chemical and microbial processes	The chemical and microbial processes affect the repository components and the surrounding rocks, and the overall chemical/microbial evolution of the repository system.	**2.3.4 Chemical processes (waste p.)** **2.3.5 Biological processes (waste p.)** **3.2.4 Chemical processes (repository)** **3.2.5 Biological processes (repository)** **4.2.4 Chemical processes (geosphere)** **4.2.5 Biological processes (geo-**
61	Corrosion of concrete	Describes the chemical degradation of concrete	2.3.4.5 Alteration (waste package) 3.2.4.5 Alteration (repository)
62	Corrosion of metals	Describes the electrochemical reaction of metals with surrounding fluids and resulting gas generation	2.3.4.4 Corrosion (waste package) 3.2.4.4 Corrosion (repository)
63	Hydrogen embrittlement	The intrusion of hydrogen in metal structures results in a modification of the mechanical properties.	2.3.4 Chemical processes (waste pack.) 3.2.4 Chemical processes (repository)
64	Solution, transformation and regeneration of clay minerals	Describes the mineralogical and chemical transformation of clay minerals resulting from changes of hydrochemistry	3.2.4.5 Alteration (repository) 4.2.4.5 Alteration (geosphere)
65	Solution, transformation and regeneration of other minerals	Describes the mineralogical and chemical transformation of minerals like quartz, feldspar and pyrite resulting from changes of hydrochemistry	3.2.4.5 Alteration (repository) 4.2.4.5 Alteration (geosphere)

66	Chemical alteration of organic matters	Describes the alteration of man-made (waste, cables, pipes etc.) and natural organics by chemical processes.	2.3.4.5 Alteration (waste package) 3.2.4.5 Alteration (repository) 4.2.4.5 Alteration (geosphere)
67	Sorption and desorption	Sorption describes the physico-chemical interaction of dissolved species with a solid phase. Desorption is the opposite effect.	2.4.1.4 Sorption and desorption (waste p.) 3.3.1.6 Sorption and desorption (repository) 4.3.1.7 Sorption and desorption (geosphere)
68	Complexation	Impact of complexing agents on the radioactive waste	2.3.4.7 Complexation (waste package)
69	Colloid generation and filtration	Generation of colloids and their filtration during transport	2.3.4.8 Colloid formation (waste pack.) 3.2.4.8 Colloid formation (Repository)
70	Microbial processes	Summarizes all microbial processes in the mine and in the surrounding rocks.	2.3.5 Biological processes (waste pack.) 3.2.4 Biological processes (repository) 4.2.4 Biological processes (geosphere)
	THM processes	**The thermal, hydraulic and mechanical processes in the repository and the surrounding geosphere that may affect the evolution of the repository system.**	**2.3.1 Thermal processes (Waste pack.)** **2.3.2 Hydraulic processes (Waste p.)** **2.3.3 Mechanical processes (Geosphere)** **3.2.1 Thermal processes(Repository)** **3.2.2 Hydraulic processes (repository)** **3.2.3 Mechanical processes (repository)** **4.2.1 Thermal processes (Geosphere)** **4.2.2 Hydraulic processes (Geosphere)** **4.2.3 Mechanic processes (Geosphere)**
71	Swelling and shrinking of clay minerals	Means the adsorption and release of water from the crystal interim layer of clay minerals.	2.3.3 Mechanical processes (waste package): 2.3.3.2 Material volume change 3.2.3 Mechanical processes (repository): 3.2.2.1 Material volume change 4.2.3 Mechanical processes (geosphere)
72	Swelling and shrinking of concrete	Describes not thermal induced volume or pressure changes of concrete.	2.3.3 Mechanical processes (waste pack.): 2.3.3.2 Material volume change 3.2.3 Mechanical processes (repository): 3.2.2.1 Material volume change
73	Convergence	Reduction of void volume by rock deformation.	4.2.3 Mechanical processes (geosphere)
74	Backfilling by rock fall	Describes the backfilling of void volumes of the repository after closure by rock fall.	3.2.2.3 Collapse of openings 4.2.3 Mechanical processes (geosphere)
75	Heat flow	Means the energy transport as a result of temperature differences.	2.3.1 Thermal processes (waste package) 3.2.1 Thermal processes (repository) 4.2.1 Thermal processes (geosphere)
76	Thermal expansion or contraction	Volume change resulting from temperature change.	2.3.1 Thermal processes (waste package) 3.2.1 Thermal processes (repository) 4.2.1 Thermal processes (geosphere)
77	Phase transition	Describes the transition from solid to liquid or from liquid to gas depending from the composition of the material, the pressure and the temperature.	2.3.2 Hydraulic processes (waste pack.) 3.2.2 Hydraulic processes (repository) 4.2.2 Hydraulic processes (geosphere)
78	Mechanical stress changes	Describes the transition of tension resulting from an increase or decrease of tension in the rocks or a component of the repository.	2.3.3 Mechanical processes (waste pack.) 3.2.3 Mechanical processes (repository) 4.2.3 Mechanical processes (geosphere)
79	Fluid pressure change	Describes a change of fluid pressure because of changes of tension in components / rocks or fluid flow processes.	2.3.2 Hydraulic processes (waste pack.) 3.2.2 Hydraulic processes (repository) 4.2.2 Hydraulic processes (geosphere)
80	Liquid flow processes	Describes the liquid flow because of potential gradients.	2.3.2 Hydraulic processes (waste pack.) 3.2.2 Hydraulic processes (repository) 4.2.2 Hydraulic processes (geosphere)
81	Gas flow processes	Describes the gas flow because of potential gradients.	2.3.2 Hydraulic processes (waste pack.) 3.2.2 Hydraulic processes (repository) 4.2.2 Hydraulic processes (geosphere)
82	Bitumen migration	Describes the migration of bitumen from waste packages and seal constructions in surrounding repository components, the EDZ or fractures and faults of the host rock.	2.3.2 Hydraulic processes (waste pack.) 3.2.2 Hydraulic processes (repository) 4.2.2 Hydraulic processes (geosphere)
83	Dispersion	Distribution of dissolved substances by inhomogeneous flow velocities in porous media.	2.4.1 Water-mediated migration (waste f.) 3.3.1 Water-mediated migration (reposi-

			tory) 4.3.1 Water-mediated migration (geosphere)
84	Diffusion	Stirring of different substances by BROWN molecular movements	2.4.1 Water-mediated migration (waste f.) 3.3.1 Water-mediated migration (repository) 4.3.1 Water-mediated migration (geosphere)
85	Radionuclide transport in the liquid phase	Summarizes all kind of transport processes of radionuclides in liquids	2.4 Contaminant migration (waste pack.) 3.3 Contaminant migration (repository) 4.3 Contaminant migration (geosphere)
86	Radionuclide transport in the gas phase	Summarizes all kind of transport processes of radionuclides in gas	2.4 Contaminant migration (waste pack.) 3.3 Contaminant migration (repository) 4.3 Contaminant migration (geosphere)
87	Dissolution and outgassing	Describes the transition of gas between gaseous phase and the dissolved phase	2.4.1 Water-mediated migration (waste f.) 2.4.2 Gas-mediated migration (waste f.) 3.3.1 Water-mediated migration (repository) 3.3.2 Gas-mediated migration (repository) 4.3.1 Water-mediated migration (geosphere) 4.3.2 Gas-mediated migration (geosphere)
88	Gas fracs in host-rock	Generation of fluid pressure induced fractures by exceedance of tensile strength of the host rock.	3.2.2 Hydraulic processes (repository): 3.2.3.4 Gas-induced dilation 4.2.2 Hydraulic processes (geosphere)
89	Deflagration and explosion of gases	A deflagration or explosion resulting from the ignition of a flammable gas mixture in the repository	2.3.3 Mechanical processes (waste package): 2.3.3.5 Gas explosion 3.2.3 Mechanical processes (repository): 3.2.3.5 Gas explosion
90	Displacement of vertical sealing element	Describes the displacement of sealing elements of the shafts or ramp from their installation position by mechanical or hydraulic impacts.	3.2.3 Mechanical processes (repository) 3.2.2 Hydraulic processes (repository)
91	Channelling in backfill	Generation of flow paths by inhomogeneous compaction or swelling or erosion of backfill	3.2.2 Hydraulic processes (repository): 3.2.2.2 Piping/hydraulic erosion
92	Channelling in a sealing element	Generation of flow paths by inhomogeneous compaction or swelling or erosion of bentonite or viscous fingering in asphalt	3.2.2 Hydraulic processes (repository): 3.2.2.2 Piping/hydraulic erosion
93	Failure of waste container	Failure of waste container by chemical, mechanical, hydraulic or thermal impacts.	2.3.1 Thermal processes (waste package) 2.3.2 Hydraulic processes (waste pack.) 2.3.3 Mechanical processes (waste pack.): 2.3.3.4 Stress corrosion cracking 2.3.4 Chemical processes (waste pack.)
94	Early failure of disposal drift seal	Failure of disposal drift seal during the functional lifetime by chemical, mechanical, hydraulic or thermal impacts.	3.2.1 Thermal processes (repository) 3.2.2 Hydraulic processes (repository) 3.2.3 Mechanical processes (repository): 3.2.3.3 collapse of openings, 3.2.3.4 gas-induced dilation 2.3.4 Chemical processes (repository)
95	Early failure of access drift seal	Failure of access drift seal during the functional lifetime by chemical, mechanical, hydraulic or thermal impacts.	3.2.1 Thermal processes (repository) 3.2.2 Hydraulic processes (repository) 3.2.3 Mechanical processes (repository): 3.2.3.3 collapse of openings, 3.2.3.4 gas-induced dilation 2.3.4 Chemical processes (repository)
96	Early failure of shaft seal	Failure of shaft seal during the functional lifetime by chemical, mechanical, hydraulic or thermal impacts.	3.2.1 Thermal processes (repository) 3.2.2 Hydraulic processes (repository) 3.2.3 Mechanical processes (repository): 3.2.3.3 collapse of openings, 3.2.3.4 gas-induced dilation 2.3.4 Chemical processes (repository)
97	Early failure of ramp seal	Failure of ramp seal during the functional lifetime by chemical, mechanical, hydraulic or thermal impacts.	3.2.1 Thermal processes (repository) 3.2.2 Hydraulic processes (repository) 3.2.3 Mechanical processes (repository): 3.2.3.3 collapse of openings, 3.2.3.4 gas-induced dilation 2.3.4 Chemical processes (repository)
98	Early failure of borehole seal	Failure of borehole seal during the functional lifetime by chemical, mechanical, hydraulic or thermal impacts.	3.2.1 Thermal processes (repository) 3.2.2 Hydraulic processes (repository) 3.2.3 Mechanical processes (repository): 3.2.3.3 collapse of openings, 3.2.3.4 gas-induced dilation 2.3.4 Chemical processes (repository)

	Radiological processes	Processes in the repository system that are induced by the emitted radiation from the waste and the radiogenic evolution of the waste packages	**2.3.5 Radiological processes (waste package)** **3.2.5 Radiological processes (repository)** **4.2.5 Radiological processes (geosphere)**
99	Radioactive decay and ionizing radiation	Spontaneous transformation of instable atomic nuclei combined with the emission of characteristic ionizing radiation	2.3.6.1 Radioactive decay and ingrow (waste package) 3.2.6.1 Radioactive decay and ingrow (repository)
100	Radiolysis	Radiolysis of water within a waste package can produce hydrogen, oxygen and hydroxide peroxide.	2.3.6.2 Radiolysis (waste package) 3.2.6.2 Radiolysis (repository)
101	Radionuclide mobilization	The processes that directly affect the mobilization of radionuclides from the waste form once the waste container has failed.	2.4. Contaminant release (from waste form)
102	Radiation induced activation	Generation of radioactive isotopes due to nuclear reaction after absorption of neutrons.	2.3.5 Radiological processes (waste pack.)
103	Criticality	Fissile substances are arranged in such a manner that a self-preserving nuclear reaction can take place.	2.3.6.6 Criticality

10 Conclusions

This report presents first of all the sealing concept developed for a near surface L/ILW repository at the “Radon Site”, taking into consideration the repository concept developed by the Consortium formed by the companies VI POWER ENGINEERING LTD. and AEA TECHNOLOGY in the framework of a TACIS project financed by the European Union (Consortium SGN/IVO/AEA 1997-A).

The repository concept foresees that the radioactive waste will be transported to the repository through a transport tunnel (ramp) that will connect two underground disposal areas with the facilities located on the surface of the site. Moreover two ventilation shafts (fresh and exhausted air shafts) will also connect the underground openings with the surface.

It shall be noted that the mentioned conceptual design was developed about 20 years ago assuming that the repository will be located in the Lower Cambrian “Blue Clay” formation at the “Koporje Site”. However, according to the most recent information the repository will be located in the Kotlin Clay formation at the “Radon Site”. For this reason, it is recommended to review and, if required, to update the repository design in order to ensure that the concept developed 20 years ago is still appropriate. From our point of view, in the course of a potential revision of the repository design it would be meaningful to consider the possibility of increasing the distance between the two shafts and the disposal drifts. In this way, additional storage space for potential gas produced within the disposal drifts will be available and therefore the risk of building up high gas pressure inside the underground openings may be minimised.

In the course of the present project relevant data in regard to the characteristics of Kotlin Clay formation at the “Radon Site” has been already compiled (see the report provided by BGR (Kühnlenz & Hammer 2014). These data have been used to assess the characteristics of the site and therefore to develop the sealing concept proposed in the present document. It shall be noted that at this stage of the project, data in regard to some aspects were not yet available (e.g. characteristics of the EDZ, etc.). In these cases assumptions based on existing data from different sources or conservative assumptions based on expert judgments have been made. These assumptions shall be confirmed in future phases of the project by the results of additional on-site investigations.

Another aspect that shall be considered is the uncertainty in regard to the radioactive waste inventory that will be disposed of in the repository. The current inventory estimate is based on the results of a TACIS project (Consortium DBE/ANDRA/NDA/SKB 2008) carried out in 2008. For this reason it may be checked if the provided estimates in regard to volume, activities and types of containers used to dispose of radioactive waste are still valid or need to be updated. Potential changes on these estimates may have impact on the sealing concept and therefore may need to be considered.

The proposed sealing concept is based on the principle that any fluid coming from the surface shall always pass at least through three seals (shaft or ramp seal, access drift seal and disposal drift seal) before being in contact with the radioactive waste disposed of in the disposal drifts. The same principle is applied to contaminated fluids that may potentially migrate from the disposal drifts to the biosphere. The proposed sealing concept considers redundancy, by using more than one seal of the same kind along the complete underground pathway, as well as diversity by using sealing elements with different materials but with the same functional requirements.

To ensure that the proposed sealing concept for the LILW repository at the “Radon Site” fulfils the long-term containment of the radioactive waste in the repository, the integrity of the following barriers shall be demonstrated. For this reason and in order to exemplify the meth-

odology used to demonstrate the integrity of the sealing elements, the permeability of the ramp seal has been assessed. As already mentioned, it shall be noted that at this stage of the project some of the data in regard to the characteristics and behaviour of the host formation (e.g. EDZ) are not yet available and for this reason the results of the demonstration of the integrity of the ramp seal are based on existing data from different sources or conservative assumptions based on expert judgments that have been made. These assumptions shall be confirmed in future phases of the project by the results of additional on-site investigations.

Finally, it shall be noted that the sealing concept for the repository has been developed assuming that the underground openings (i.e. disposal drifts, access disposal drifts, etc.) will be built according to the above mentioned conceptual design. However, if due to the characteristics of the “Radon Site” the location, the dimensions of underground openings (e.g. disposal drifts, access disposal drifts, etc.) or the repository design need to be modified; the sealing concept presented in the present report may need to be updated.

Specific characteristics of the flow regime in the investigated area could be simulated. The flow is generally directed to the west and shows highest flow velocities in the aquifers, i.e. the Quaternary sands and the Gdovsk aquifer. Lowest flow velocities are observed in the Kotlin Clay layer. With regard to the construction of a potential repository site, it is crucial to know the possible transport paths of contaminants, including a transport to the surface and biosphere. Thus, it seems important to investigate the vertical components of the flow field in more detail. At the time being, transport times from the repository to the surface cannot be reliably simulated due to the lack of sufficient data. In summary, the presented results can be used to increase the system understanding, to indicate tendencies and to plan further geological-geophysical exploration and on-site investigations.

Simulations of the radionuclide release from the repository in the liquid phase show a similar behaviour as obtained for other repositories in clay with C-14, Cl-36, Se-79 and I-129 being the main contributors to the radionuclide release. Since the waste containers were not considered to last in the post-closure phase and the diffusion-coefficients of the radionuclides are comparably high, the maximum of the radionuclide release already occurs after a few thousands of years. The site specific data basis is not sufficient to perform long-term safety assessments that finally give a safety statement for the repository. Probabilistic simulations show a large variation of obtained results as a result of the parameter uncertainty. As largest contributors of uncertainty were identified the diffusion coefficients of radionuclides in the host rock, the radionuclide inventory and the transport path length in the host rock. Simulations about the release of volatile C-14 suggests that the release of C-14 in the gas phase from the repository can potentially contribute significantly to the potential radiation exposure in the biosphere and should be assessed accordingly.

11 References

Alonso, J., García-Siñeriz, J. L., Bárcena, I., Alonso, M. C., Fernández-Luco, L., García, J., et al. (2008). Temporary Sealing Technology. Final Report. ESDRED.

Anderson, E. B., Sawonenkow, W. G. & Schabalev, S. I. (2006). Perspektiven für den Bau untertägiger Endlager für radioaktive Stoffe in den unterkambrischen Tonen der Leningrader Region. In: Arbeiten des Radium-Institutes „Chlopin". XI. Pages 105-132. АНДЕРСОН, Е. Б., САВОНЕНКОВ, В. Г. & ШАБАЛЕВ, С. И. (2006): Перспективы создания подземных могильников РАО в нижнекембрийских глинах Ленинградской области. В: Труды Радиевого института им. В. Г. Хлопина, т. XI, 2006. С. 105-132; Санкт-Петербург.

Anderson, E. B., Sawonenkow, W. G. & Schabalev, S. I. (2011). Perspektiven für den Bau untertägiger Endlager für radioaktive Stoffe in den unterkambrischen Tonen der Leningrader Region. Vortrag. Russisch-deutscher Workshop zum Thema "Umgang mit den schwach- und mittelradioaktiven Abfällen", Sankt-Petersburg. АНДЕРСОН, Е. Б., САВОНЕНКОВ, В. Г., ШАБАЛЕВ, С. И. (2011). Перспективы создания подземных могильников РАО в нижнекембрийских глинах Ленинградской области. Презентация. Российско-германский семинар по обращению с радиоактивными отходами низкого и среднего уровня активности. Санкт-Петербург.

ANDRA (2005). Dossier 2005 Argile, Tome: Architecture and management of a geological repository.

Arand, W., Haas, H. & Steinhoff, G. (1992). Zur Herstellbarkeit, Beständigkeit und Wirksamkeit von Deponiebasisabdichtungen aus Asphalt, Bitumen Magazin, Ausgabe 4/92, Seite 152 – 162.

Ayachit, U. (2015). The ParaView Guide: A Parallel Visualization Application. Middletown (Kitware), 276 p.

Becker, D.-A., Buhmann, D., Mönig, J., Noseck, U., Rübel, A. & Spießl, S. (2009). Endlager Morsleben, Sicherheitsanalyse für das verfüllte und verschlossene Endlager mit dem Programmpaket EMOS. Planfeststellungsverfahren zur Stilllegung des Endlagers für radioaktive Abfälle Morsleben. Verfahrensunterlage P 278.

Barton, N. (1982). Modelling rock joint behaviour from in situ block tests: Implications for nuclear waste repository design. Office of Nuclear Waste Isolation. Columbus, Ohio, ONWI-308.

Bossart, P., Trick, T., Meier, P.M. & Mayor, J.-C. (2004). Structural and hydrogeological characterisation of the excavation-disturbed zone in the Opalinus Clay, Mont Terri Project, Switzerland, Applied Clay Science 26, Pages 429 – 448.

Breidung, K.P. (2002) Schachtverschlüsse für untertägige Deponien in Salzbergwerken. Forschungsvorhaben Schachtverschluss Salzdetfurth – BMBF-gefördertes Vorhaben, FKZ.: 02C0516, Kali u. Salz GmbH.

Burkhardt, G. & Egloffstein, T. (1995). Asphaltdichtungen im Deponienbau, expert Verlag, Renningen-Malmsheim.

Chan, R., Ho, P. & Chan, E. (1999). Report on Concrete Admixtures for Waterproofing Construction. Technical Report. Structural Engineering Branch, Architectural Services Department.

Consortium DBE/ANDRA/NDA/SKB (2008). Concept and programme for the realisation of a radioactive waste repository for short-lived low- and intermediate-level waste in the Leningrad Region Tacis R4.05/04. Task 5 Updating of the repository inventory.

Consortium SGN/IVO/AEA Technology (1997-A). Final Repository of Radioactive Waste for LSK Radon, Description of Plant Concept. Document Reference Number: IVO –

YDIN/RUS-A6-626. TACIS Project Feasibility study for St. Petersburg Waste Management Centre, Project Reference Number: NUCRUS 94 405.

Consortium SGN/IVO/AEA Technology (1997-B). List of Drawings. Document Reference Number: YDIN/RUS-A6-62 M1. TACIS Project Feasibility study for St. Petersburg Waste Management Centre, Project Reference Number: NUCRUS 94 405.

Consortium SGN/IVO/AEA Technology (1997-C). Preliminary Safety Assessment of the Conceptual Design for a Radioactive Waste Disposal Facility for the St Petersburg Waste Management Centre AEAT-2723. Project Reference Number: NUCRUS-94.495.

Cyziene, J., Sliaupa, S., Lazauskiene, J., Baliukevicius, A. & Satkunas, J. (2005). Characterization of the Lower Cambrian Blue Clays for deep geological disposal of radioactive waste in Lithuania. - In: Geologija 2005. T. 52, P. 11-21.

Daschko, R.Ä. & Volkova, R.Ä. (2004). Geomechanische Analyse der Sankt-Petersburger Tone als klüftig-blockiges Medium. - In: Memoiren des Berginstitutes. Moderne Probleme der Geomechanik /Дашко, Р.Э., Волкова, А.В. (2004): Геомеханический анализ коренных глин Санкт-Петербурга как трещиновато-блочной среды. - В: Зап. Горного института. Современные проблемы геомеханики, геотехнологии, маркшейдерского дела и геодезии. Т. 156. С. 118–122.

Daschko, R.Ä. (2005). Besonderheiten der ingenieurgeologischen und geoökologischen Untersuchungen und Bewertungen der Blauen Tone, als Milieu für die Endlagerung der radioaktiven Abfälle. In: Bericht der jährlichen Tagung des Wissenschaftsrates über die Probleme der Geoökologie, Ingenieurgeologie und Hydrogeologie. GEOS. – 2005. Ausg. 7. S. 233-240; Sankt-Petersburg/ Дашко. Р.Э. (2006): Особенности инженерно-геологического и геоэкологического изучения и оценки глинистых пород как среды захоронения радиоактивных отходов. В: Материалы годичной сессии Научного совета РАН по проблемам геоэкологии, инженерной геологии и гидрогеологии. ГЕОС. – 2005. Вып. 7.- с. 233-240; Санкт-Петербург

Daschko, R.Ä. (2006). Ingenieurgeologische und geoökologische Bewertung der unterkambrischen Blauen Tone aus der Sicht der Endlagerung der radioaktiven Abfälle. In: Geoökologie, Ingenieurgeologie, Hydrogeologie, Geokryologie 2006. Nr.3, S. 235-241; Sankt-Petersburg/ Дашко. Р.Э. (2006): Инженерно-геологическая и геоэкологическая оценка нижнекембрийских синих глин как среды размещения радиоактивных отходов. В: Геоэкология, инженерная геология, гидрогеология, геокриология 2006, № 3, 235-241; Санкт-Петербург

Daschko, R. Ä., Alexandrova, O. J., Kotjukov, P. V. & Shidlovskaja, A. J. (2011). Besonderheiten der ingenieurgeologischen Bedigungen von Sankt-Petersburg. In: Entwicklung der Städte und geotechnischer Bau. Ausgabe 1/2011. Sankt-Petersburg. 2011. ДАШКО, Р.Э., АЛЕКСАНДРОВА, О.Ю., КОТЮКОВ, П.В., ШИДЛОВСКАЯ, А.В. Особенности инженерно-геологических условий Санкт-Петербурга. В: Развитие городов и геотехническое строительство. Выпуск 1/2011; Санкт-Петербург.

Dansgaard, W. (1964). Stable isotopes in precipitation. Phys. Lab. II, H.C. Orsted Institute, University of Copenhagen.

DGGT (1997). GDA-Empfehlungen Geotechnik der Deponien und Altlasten.

DIN 1054 (2010). DIN 1054:2010-12. Baugrund – Sicherheitsnachweise im Erd- und Grundbau – Ergänzende Regulungen zu DIN EN 1997-1.

Dueck, A., Johannesson, L.E., Kristensson, O. & Olsson, S. (2011). Report on hydro-mechanical and chemical-mineralogical analyses of the bentonite buffer in Canister Retrieval Test. Technical Report. Clay Technology. SKB.

Eurocode 0 (2010). DIN EN 1990. Eurocode 0: Grundlagen der Tragwerksplanung (Deutsche Fassung EN 1990:2002 + A1:2005 + A1:2005/AC:2010).

Eurocode 2 (2010). DIN EN 1992-1-1. Eurocode 2: Bemessung und Konstruktion von Stahlbeton- und Spannbetontragwerken – Teil 1-1: Allgemeine Bemessungsregeln und Regeln für den Hochbau (Deutsche Fassung EN 1992-1-1:2004 + AC:2010).

Eurocode 7 (2009). DIN EN 1997-1. Eurocode 7: Entwurf, Berechnung und Bemessung in der Geotechnik – Teil 1: Allgemeine Regeln (Deutsche Fassung DIN EN 1997-1:2004 + AC:2009).

Engelhardt, H.J., Jobmann, M. & Müller-Hoeppe, N. (2011). Materialspezifikation für Dichtelemente für die Planung von Schacht- und Streckenverschlüssen. Arbeitspaket 9.1.2, Vorläufige Sicherheitsanalyse für den Standort Gorleben, Rev01, DBE TECHNOLOGY GmbH.

Feistel, R., Weinrebe, S., Wolf, H., Spitzer, P., Adel, B., Nausch, G., Schneider, B., & Wright, D. G. (2010). Density and Absolute Salinity of the Baltic Sea 2006 – 2009. Ocean Sci. 6 (3-24).

Galicia, M. (2002). Thermo-hydro-mechanical characterization of a bentonite from Cabo de Gata – A study applied to the use of bentonite as sealing material in high level radioactive waste repositories. Technical Report. ENRESA.

Gerardi, J. (2005). Barrierewirksame Eigenschaften von Ton und Tonstein: Fachinformationssystem BETTON. - Bundesanstalt für Geowissenschaften und Rohstoffe, Bereich: Geotechnik/Endlagerung, Hannover.

Glaubach, U., Gruner, M. & Hofmann, M. (2008). Material zur Verbesserung der Flüssigkeitsdichtheit einer Bitumen- oder Asphaltdichtung durch wesentliche Verbesserung der Adhäsion bzw. Benetzung in der Kontaktzone zum Salzgestein. Patentschrift DE 10 2008 050 211 B4.

Glaubach, U., Hofmann, M., Gruner, M., Grafe, F., Wilsnack, T., Kudla W., Königer, F., Emmerich, K. & Schumann, R. (2016). Schachtverschlüsse für Endlager für hochradioaktive Abfälle, FuE-Projekt ELSA-Phase-II, Konzeptentwicklung für Schachtverschlüsse und Test von Funktionselementen von Schachtverschlüssen, Teilbericht zum Arbeitspaket 4 Halb-technische Versuche. TU Bergakademie Freiberg, Institut für Bergbau und Spezialtiefbau, Freiberg.

Gruner, M., Rumphorst, K. & Sitz, P. (2008). Design and Emplacement of Bentonite Barriers. International Conference Underground Disposal Unit Design & Emplacement Processes for a Deep Geological Repository.

Guo, R., Kjartanson, B. & Martino, J. (2005). Thermo-hydro-mechanical simulation of the concrete bulkhead during the heating phase of the tunnel sealing experiment. In E. Alonso, A. Ledesma (Hrsg.) Advances in Understanding Engineered Clay Barriers (pages 431-441). Balkema Publishers.

Hansen, J. (2015). DOPAS – Full Scale Demonstration of Plugs and Seals. 6th International Conference “Clays in Natural and Engineered Barriers for Radioactive Waste Confinement”. Brussels, Belgium.

HeidebergCement (2014). Betontechnische Daten, Ausgabe 2014. HeidebergCement AG, Entwicklung & Anwendung, Oberklamweg 6, 69181 Leimen.

Herold, P., Gruner, M., Kudla, W. & Jobmann, M. (2016). Konzeptentwicklung für Schachtverschlüsse im Ton- und Salzgestein, Technischer Bericht, Arbeitspaket 1, FuE-Vorhaben ELSA Phase II, DBE TECHNOLOGY GmbH und TU Bergakademie Freiberg.

Herold, P. & Müller-Hoeppe, N. (2013). Safety demonstration and verification concept – Principle and application examples. Technical Report. DBE TECHNOLOGY GmbH.

Hoth, P., With, H., Reinhold, K., Bräuer, V., Krull, P. & Feldrappe, H. (2007). Untersuchung und Bewertung von Tongesteinsformationen: Endlagerung radioaktiver Abfälle in tiefen geologischen Formationen Deutschland, BGR, Hannover/Berlin.

Hölting, B. & Coldewey, W. (2005). Hydrogeologie. Einführung in die Allgemeine und Angewandte Geologie, 326 p, Spektrum Akademischer Verlag, Heidelberg.

IAEA (2006). Fundamental Safety Principles. IAEA Safety Standards. Safety Fundamentals No. SF-1. Vienna.

Itasca (2012a). FLAC3D Version 5.0 - User's Guide. Itasca Consulting Group Inc., Minneapolis, Minnesota.

Itasca (2012b). FLAC3D Version 5.0 - Constitutive Models. Itasca Consulting Group Inc., Minneapolis, Minnesota.

Jobmann, M. (2002). F+E-Vorhaben Schachtverschluss Salzdetfurth. Hydraulische Modellierungen. Abschlussbericht. DBE TECHNOLOGY GmbH.

Jobmann, M., Amelung, P., Billaux, D., Polster, M., Schmidt, H. & Uhlig, L., (2007). Untersuchungen zur sicherheitstechnischen Auslegung eines generischen Endlagers im Tonstein in Deutschland. Projekt GENESIS, Abschlussbericht, DBE Technology GmbH, Peine.

Jobmann, M. (2014). Zusammenstellung messtechnischer Ergebnisse zu den hydraulischen Verhältnissen im Bereich der Auflockerungszone im Ton und Tonstein. Technischer Bericht. FuE-Vorhaben Schachtverschlüsse für Endlager für hochradioaktive Abfälle – ELSA Phase II. DBE TECHNOLOGY GmbH.

Jobmann, M. & Lommerzheim, A. (2015). Endlagerkonzept sowie Verfüll- und Verschlusskonzept für das Endlagerstandortmodell SÜD. Projekt ANSICHT: Methodik und Anwendungsbezug eines Sicherheits- und Nachweiskonzeptes für ein HAW-Endlager im Tonstein. Technischer Bericht TEC-26-2015-TB. DBE TECHNOLOGY GmbH.

Jobmann, M. (2016). Mikrostrukturelle Untersuchungen an Salzgrus-Ton-Gemischen und Bitumen-Steinsalz Proben, Technischer Bericht, FuE-Projekt ELSA-Phase-II, DBE TECHNOLOGY GmbH, Peine.

Jobmann, M., Burlaka, V., Meleshyn, A. & Rübel, A. (2016). Spezifische Prozessanalysen. Projekt ANSICHT: Methodik Anwendungsbezug eines Sicherheits- und Nachweiskonzeptes für ein HAW-Endlager im Tonstein, Technischer Bericht TEC-13-2016-B, DBE TECHNOLOGY GmbH, BGR, GRS. Peine, Hannover, Braunschweig.

Jobmann, M., Bebiolka, A., Jahn, S., Lommerzheim, A., Maßmann, J., Meleshyn, A., Mrugalla, S., Reinhold, K., Rübel, A., Stark, L. & Ziefle, G. (2017). Sicherheits- und Nachweismethodik für ein Endlager im Tongestein in Deutschland - Synthesebericht -. Projekt ANSICHT: Methodik Anwendungsbezug eines Sicherheits- und Nachweiskonzeptes für ein HAW-Endlager im Tonstein. Synthesebericht, DBE TECHNOLOGY GmbH, BGR, GRS. Peine, Hannover, Braunschweig.

JRC & DG-ENTR (2008). The Eurocodes: Implementation and use. Booklet B1.

Karnland, O., Olsson, S. & Nilsson, U. (2006). Mineralogy and sealing properties of various bentonites and smectite-rich clay materials. Technical Report. SKB.

Kiefer, D. (1997). Sicherheitskonzept für Bauten des Umweltschutzes. DAfStb-Heft 481.

Kreyenmeyer et al. (2008). ISIBEL. AP5 Nachweiskonzept zur Integrität der einschlusswirksamen technischen Barrieren. DBE TECHNOLOGY GmbH, Peine.

Kröhn, K.-P. (2004). Modelling the re-saturation of bentonite in final repositories in crystalline rock. Technischer Bericht. GRS mbH. Braunschweig.

Krone, J., Bollingerfehr, W., Filbert, W., Keller, S., Lommerzheim, A., Mönig, J., et al. (2013). Status of the safety concept and safety demonstration for a HLW repository in salt. Summary Report. DBE TECHNOLOGY GmbH, BGR, GRS.

Kudla, W., Dahlhaus, F., Glaubach, U., Gruner, M., Haucke, J., Hofmann, M. & Wasowiecs, B. (2009). Diversitäre und redundante Dichtelemente für langzeitstabile Verschlussbauwerke. Bericht im Auftrag des Bundesministeriums für Bildung und Forschung 02C1124. Hg. v. Institut für Bergbau und Spezialtiefbau, TU Bergakademie Freiberg.

Kühnlenz, T. & Hammer, J. (2014). Zusammenstellung der Kenntnisse zu den Tonformationen am Standort Sosnovyi Bor (Nähe St. Petersburg), Zwischenbericht B3.1/B50112-36/2013-0002/001, BGR, Hannover.

Lux, K.-H. (2005). Endlagerstandortsuche, Gebirgsmechanische Beurteilung von Tongesteinsformationen im Hinblick auf die Endlagerung radioaktiver Abfälle, Abschlussbericht, TU Clausthal.

Madsen, F. T. (1998). Clay mineralogical investigations related to nuclear waste disposal Clay Minerals, 33, p. 1009-1029.

Martino, J., Dixon, D., Holowick, B. & Kim, C.-S. (2011). Enhanced Sealing Project (ESP): Seal Construction and Instrumentation Report. Technical Report. Atomic Energy of Canada Limited (AECL).

Merkel, A. (2017). Klimadaten für Städte weltweit. https://de.climate-data.org/location/21451/, last access February 27, 2017.

Mönig, J. (1998). Gaserzeugung durch Radiolyse und Wärmeeinwirkung. In: Erzeugung und Verbleib von Gasen in einem Endlager für radioaktive Abfälle: Bericht über den GRS-Workshop vom 29. und 30. Mai 1996 in Braunschweig/ zsgest. von Ingo Müller-Lyda. – Köln [u.a.] – (1997), S. A-29 – A-41.

Müller, K., Kreutz, H., Ziegenmeyer, H. & Meier, G.-A. (1987). Probenuntersuchungen an Lagerbegrenzungsbohrungen der Schachtanlage Konrad (TA 2219.29). - Abschlussbericht der TU Clausthal: 194 S.; Clausthal-Zellerfeld.

Müller-Hoeppe, N., Buhmann, D., Czaikowski, O., Engelhardt, H.-J., Herbert, H.-J., Lerch, C., Linkamp, M., Wieczorek, K. & Xie, M. (2012). Integrität geotechnischer Barrieren - Teil 1: Vorbemessung. Bericht zum Arbeitspaket 9.2, Vorläufige Sicherheitsanalyse für den Standort Gorleben. GRS-287, GRS mbH.

Müller-Hoeppe, N. & Krone, J. (1999). Ein neuer Ansatz zur Bewertung der Wirksamkeit von Barrieren im Endlager. Tech. rep. DBE TECHNOLOGY GmbH.

Nagra (2002a). Projekt Opalinuston. Synthese der geowissenschaftlichen Untersuchungsergebnisse. Entsorgungsnachweis für abgebrannte Brennelemente, verglaste hochaktive sowie langlebige mittelaktive Abfälle. Technischer Bericht NTB 02-03, Wettingen.

Nagra (2002b). Project Opalinus Clay: The long-term safety of a repository for spent fuel, vitrified high-level waste and long-lived intermediate-level waste sited in the Opalinus Clay of the Züricher Weinland. Nagra, NTB 02-05, Wettingen.

Nagra (2008). Effects of post-disposal gas generation in a repository for low- and intermediate-level waste sited in the Opalinus Clay of Northern Switzerland. NTB 08-07, Wettingen.

Nikulenkov, A.M. (2011). Experimentelle Begründung der Migrationsparameter in sandig-tonigen Ablagerungen des Unterkambriums und Obervendium für die Sicherheitsbewertung des Betriebes von Endlagern für schwach- und mittelradioaktive Abfälle (Sosnovyi Bor, Leningrader Region). – Autoreferat zur Promotion; Sankt-Petersburg. www.spmi.ru (Zugriff 15.07.2013)/ Никуленков, А.М. (2011): Эксперементальное обоснование миграционных параметров песчано-глинистых отложений нижнего кембрия и верхнего венда для оценки безопасности

эксплуатации хранилищ низко- и среднефктивных отходов (г. Сосновый Бор, Ленинградская область). - Автореферат; Санкт-Петербург. www.spmi.ru (Обращение 15.07.2013)

Nirex (2001). Generic Phased Disposal System Documentation. Nirex Reports No: N/025 to N/031.

NEA (2012). Cementitious Material in Safety Cases for Geological Repositories for Radioactive Waste; Role, Evolution and Interaction. Nuclear Energy Agency, RWM/R(2012)/3/REV.

Pereverzeva, S.A., Rumynin, W.G., Tokarev, I.V., Sapozhnikov, B.G., Sindalovskii, L.N., Nikulenkov, A., Varnakova, J. (2008). Untersuchungen der ingenieurgeologischen und hydrogeologischen Eigenschaften der vendischen Tone mit dem Ziel der Durchführung der hydrogeologischen Arbeiten zur Entwicklung und Weiterführung des Monitorings des Untertagezustandes auf dem Industriegebiet des Leningrader Spezialkombinats „Radon".Sankt-Petersburg. Переверзева С.А., Румынин В. Г., Токарев И.В., Сапожников Б.Г., Синдаловский Л.Н., Никуленков А., Варнакова Ю. (2008) Изучение инженерно-геологических и гидрогеологических свойств вендских глин с целью проведения геологических работ по созданию и ведению мониторинга состояния недр на промплощадке ФГУП ЛСК «Радон»; Санкт-Петербург.

Petrov, O.V., Morozov, A.F. & Lebedev, A.V. (2010). Atlas der geologischen und ökogeologischen Karten der Ostseeregion Russlands. VSEGEI, 78 S.; Sankt-Petersburg/ Петров О.В, Морозов А.Ф, Лебедев А.В. (2010): Атлас геологических и эколого-геологических карт Российского сектора Балтийского моря. Изд-во ВСЕГЕИ, 78 с.; Санкт-Петербург

Plechkova, I.L. (1997). Ingenieurgeologische Analyse und Bewertung der unterkambrischen Blauen Tone der Vorglint-Zone von Sankt-Petersburg. Autoreferat zur Promotion. 19 S.; Sankt-Petersburg/ Плечкова, И.Л.: Инженерно-геологический анализ и оценка синих нижнекембрийских глин предглинтового района г. Санкт-Петербург. Автореферат. 19 с.; Санкт-Петербург

Pröhl, G. & Gering, F. (2002). Dosiskonversionsfaktoren zur Berechnung der Strahlenexposition in der Nachbetriebsphase von Endlagern nach dem Entwurf der Allgemeinen Verwaltungsvorschrift zu §47 Strahlenschutzverordnung in Anlehnung an die Vorgehensweise im Rahmen des Planfeststellungsverfahrens des geplanten Endlagers Konrad. GSF-Forschungszentrum für Umwelt und Gesundheit, Neuherberg.

Pruess, K., Oldenburg, C. & Moridis, G. (2012): TOUGH2 User's Guide, Version 2. LBNL-43134, Earth Sciences Division, Lawrence Berkeley National Laboratory, Berkley.

Reiche, T. (2016). RepoTREND – Das Programmpaket zur integrierten Langzeitsicherheitsanalyse von Endlagersystemen, GRS-416, Gesellschaft für Anlagen- und Reaktorsicherheit (GRS) gGmbH, ISBN 978-3-944161-95-2, Braunschweig.

Reiter, S. (2017). Grid Generation for Scientific Computations. http://promesh3d.com/, accessed February 27, 2017.

Rübel, A., Becker, D.-A. & Fein, E. (2007). Radionuclide transport modelling to assess the safety of repositories in clays, GRS-228, Gesellschaft für Anlagen und Reaktorsicherheit (GRS) mbH, Braunschweig.

Rumynin, V.G., Mironova, A.V., Pankina, E.B., Vhernomorova, N.V. & Mysik, S.G. (2003). A study of diffusion and sorption properties of Cambrian clays using radioactive tracers (36 Cl and 90 Sr). In: Radiochemistry, Vol. 46, No. 4. P.391-397.

Rumynin, V.G. (2011). Site characterisation of the Kotlin clay and model development with respect to the UR design and safety assessment. Speech. Russisch-deutscher Workshop zum Thema "Umgang mit den schwach- und mittelradioaktiven Abfälllen". St. Petersburg.

Scheider, A. (Ed.) (2016). Modelling of Data Uncertainties on Hybrid Computers (H-DuR). Final report, FKZ 02 E 11062A (BMWi), Gesellschaft für Anlagen- und Reaktorsicherheit (GRS) gGmbH, GRS-392, 2016.

Schnier, H. (1986a). Ergebnisse der festigkeitsmechanischen Laboruntersuchungen an Gesteinsproben aus dem Hangend- und Liegend-Bereich der Grube Konrad. – BGR-Bericht, Archiv-Nr.: 99 467/ I: 18 S., 17 Abb., 14 Tab., 8 Anl.; Hannover.

Schnier, H. (1986b). Ergebnisse der festigkeitsmechanischen Laboruntersuchungen an Proben aus den Schachtwiderlagerbohrungen im Schacht Konrad 2. – BGR-Bericht, Archiv-Nr. 99 467 / II: 8 S., 3 Abb., 3 Tab., 2 Anl.; Hannover.

Schönenberg, R. & Neugebauer, J. (1987). Einführung in die Geologie Europas.- 5. Auflage, 294 S., Rombach, Freiburg.

Schulze, O. (2009). Steinsalz und Tonstein - Untersuchung von Endlager relevanten Eigenschaften. - In: DMV & IGCM (Hrsg.): Tagungsband Energie und Rohstoffe 2009 - Sicherung der Energie- und Rohstoffversorgung - 6. – 12. September 2009, Goslar, 409-424, Clausthal-Zellerfeld.

Schumann, R., Emmerich, K., Kemper, G., Königer, F., Kudla, W., Gruner, M., et al. (2009). Verschluss mit Äquipotenzialsegmenten für die untertätige Entsorgung (UTD und ELA) gefährlicher Abfälle zur Sicherstellung der homogenen Befeuchtung der Dichtelemente und zur Verbesserung der Langzeitstabilität. Tech. Rep. Kompetenzzentrum für Materialfeuchte (CCM), Karlsruher Institut für Technologie.

Shaw, R.P. (Ed.) (2013). Gas Generation and Migration, International Symposium and Workshop, 5th to 7th February 2013, Luxembourg, Proceedings, Forge Report D0.09.

Singh, B. & Goel, R. K. (1999). Rock Mass Classification – A Practical Approach in Civil Engineering, Elsevier Science Ltd.

Sitz, P. (1981). Querschnittsabdichtungen untertätiger Hohlräume durch Dämme und Pfropfen. VEB Deutscher Verlag für Grundstoffindustrie.

Tang, A. M., Cui, Y. J., Li, X. L., Gedeon, M. & Rumynin, V. G. (2010). Hydro-mechanical characterization of Vendian clay from Russia. In: Clay in natural and engineered barriers of radioactive waste confinement proceedings of the meeting “Nantes 2010”. Pages 89-129.

Teichmann, L., Neydek, J. & Manthee, F. (2002). FuE-Vorhaben Schachtverschluss Salzdetfurth, Geotechnische Messungen, Untersuchungen zur Schottersäule Schacht 1. Tech. rep. DBE TECHNOLOGY GmbH.

Van Geet, M., Bastaiens, W., Volckaert, G., Weetjens, E., Sillen, X., Maes, N., et al. (2009). RESEAL II A large-scale in-situ demonstration test for repository sealing in an argillaceous host rock – Phase II. Final Report. Office for Official Publications of the European Communities.

Vogel, A., Reiter, S., Rupp, M., Nägel, A. & Wittum, G. (2013). UG 4: A novel flexible software system for simulating PDE based models on high performance computers. Computing and Visualization in Science 16 (4), 165-179.

Wagner. K. (2005). Beitrag zur Bewertung der Sicherheit untertätiger Verschlussbauwerke im Salinargebirge. Dissertation, Fakultät für Geowissenschaften, Geotechnik und Bergbau der Technischen Universität Bergakademie Freiberg.

Weetjens, E., Perko, J., Yu, L. (2009): Final report on gas production and transport. PAMINA Report M 3.2.16, SCK CEN, Mol. http://www.ip-pamina.eu/downloads/pamina.m3.2.16.pdf

Wieczorek, K., Behlau, J., Heemann, U., Masik, S., Müller, C., Raab, M. & Kuate Simo, E. (2014). VIRTUS - Virtuelles Untertagelabor im Steinsalz, Technischer Bericht, GRS-354, Gesellschaft für Anlagen- und Reaktorsicherheit (GRS) gGmbH, Braunschweig.

Witherspoon, P., Wang, J., Iwai, K. & Gale, J. (1980). Validity of Cubic Law for Fluid Flow in a Deformable Rock Fracture, Water Resources Research. 16 (6). Pages 1016-1024.

Wittke, W. (1991): Endlager Konrad, Schachtverfüllung/ Alte Bohrungen, Teil 1: Ergebnisse des Untersuchungsprogramms im Bereich der Unterkreide (343 m-Sohle). - Bericht A I., Unveröff. Textbd. XIII u. 2 Abbildungsbd.: 173 S., 1 Abb. / 141 Abb.; Aachen.

Wolf, M. (1989). Mikrobieller Abbau von Bitumen. Technischer Bericht, NTB 89-14, Nagra, Wettingen, Schweiz.

Yildizdag, K., Herklotz, M., Jobmann, M., Polster, M., Schonebeck, M., & Uhlig, L. (2008). Investigation on the THM Behavior of a Heated Bentonite Barrier by Measurements and Numerical Calculations. Final Report, DBE TECHNOLOGY GmbH, Peine.

Zhang, C. L. (2012). Investigations of excavated claystone as backfill / seal material- Clays in Natural and Engineered Barriers for Radioactive Waste Confinement, 5th International meeting. Montpellier, France.

ANNEX

Annex A: Results of flow simulations

Annex B: Examples for FEP-descriptions in FEP catalogue

Annex A: Results of flow simulations

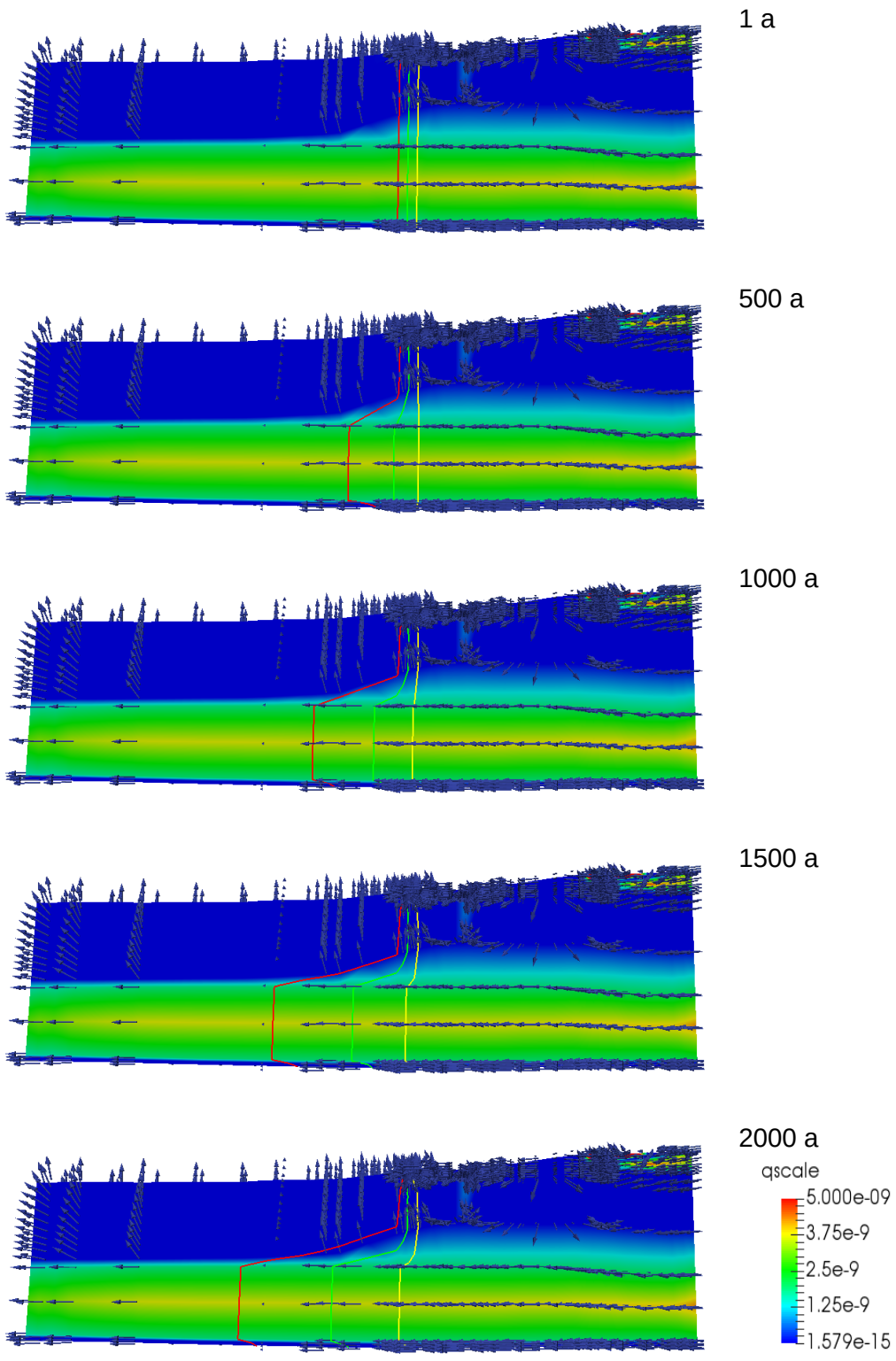

Fig. A-01: Cross-section at 400 m to the north boundary (y = 6,636,500 m, location a in Figure 8-9) for a model time t = 1 year, 500 years, 1000 years, 1500 years and 2000 years. The color shows the magnitude of the velocity ("qscale", [m s^{-1}]), the arrows show the flow direction. The red, green, yellow lines show the iso-lines for c_{rel} = 0.9, 0.5 and 0.1, respectively.

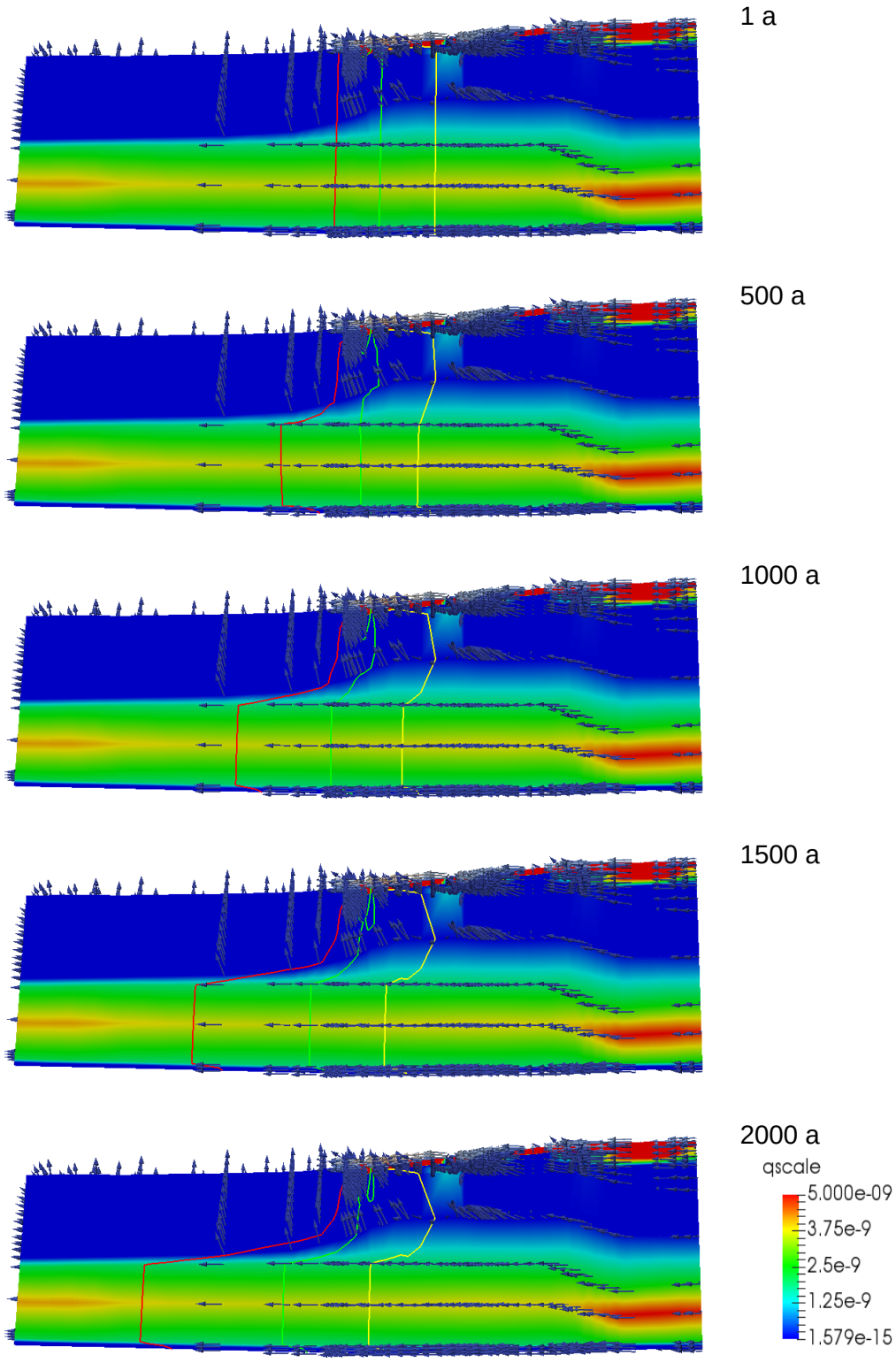

Fig. A-02: Cross-section at 1,100 m to the north boundary (y = 6,635,800 m, location b in Figure 8-9) for a model time t = 1 year, 500 years, 1000 years, 1500 years and 2000 years. The color shows the magnitude of the velocity ("qscale", [m s^{-1}]), the arrows show the flow direction. The red, green, yellow lines show the iso-lines for c_{rel} = 0.9, 0.5 and 0.1, respectively.

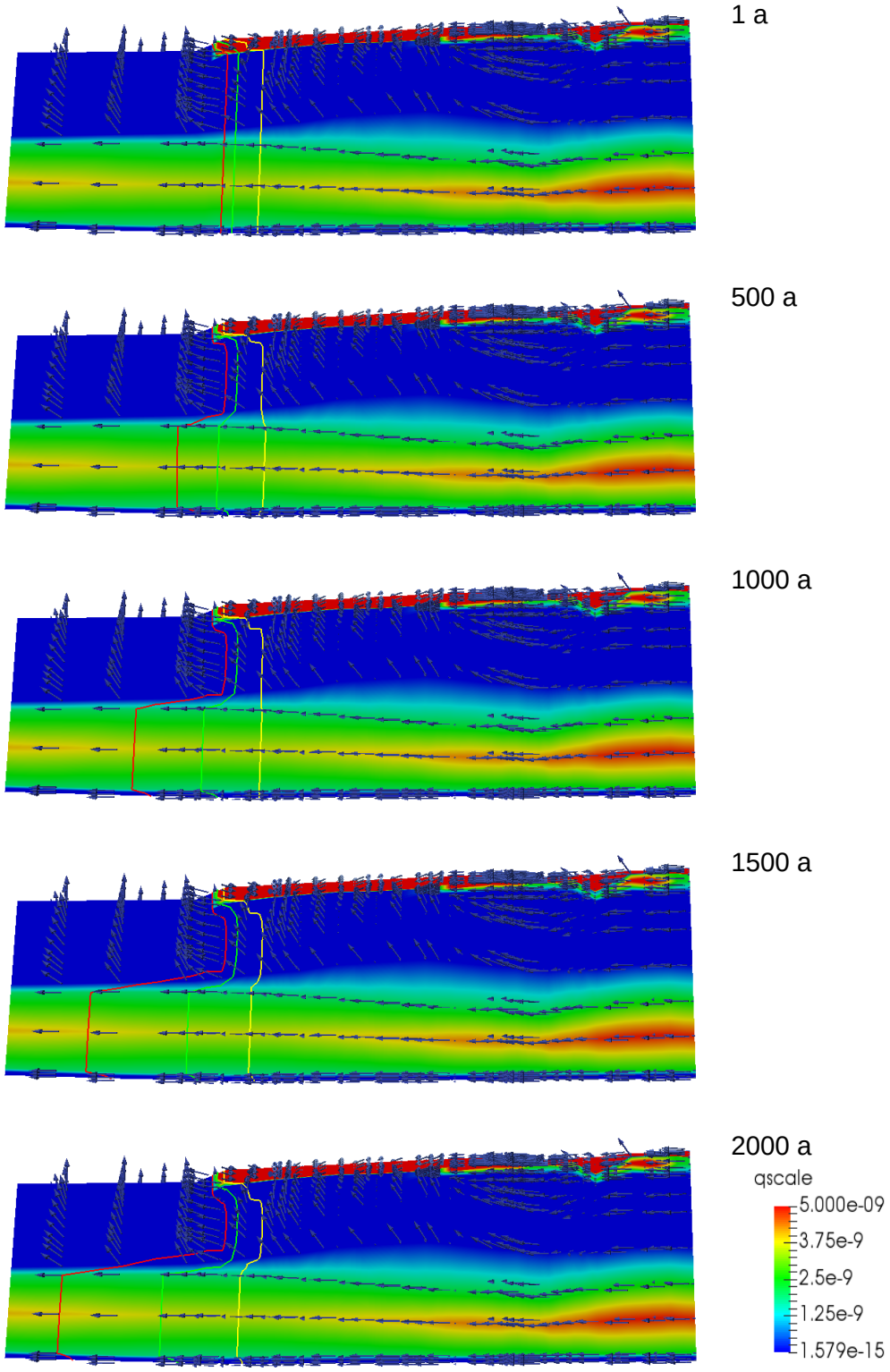

Fig. A-03: Cross-section at 2200 m to the north boundary and to the south boundary (y = 6,634,700 m, location c in Figure 8-9) for a model time t = 1 year, 500 years, 1000 years, 1500 years and 2000 years. The colour shows the magnitude of the velocity ("qscale", [m s^{-1}]), the arrows show the flow direction. The red, green and yellow lines show the isolines for c_{rel} = 0.9, 0.5 and 0.1, respectively.

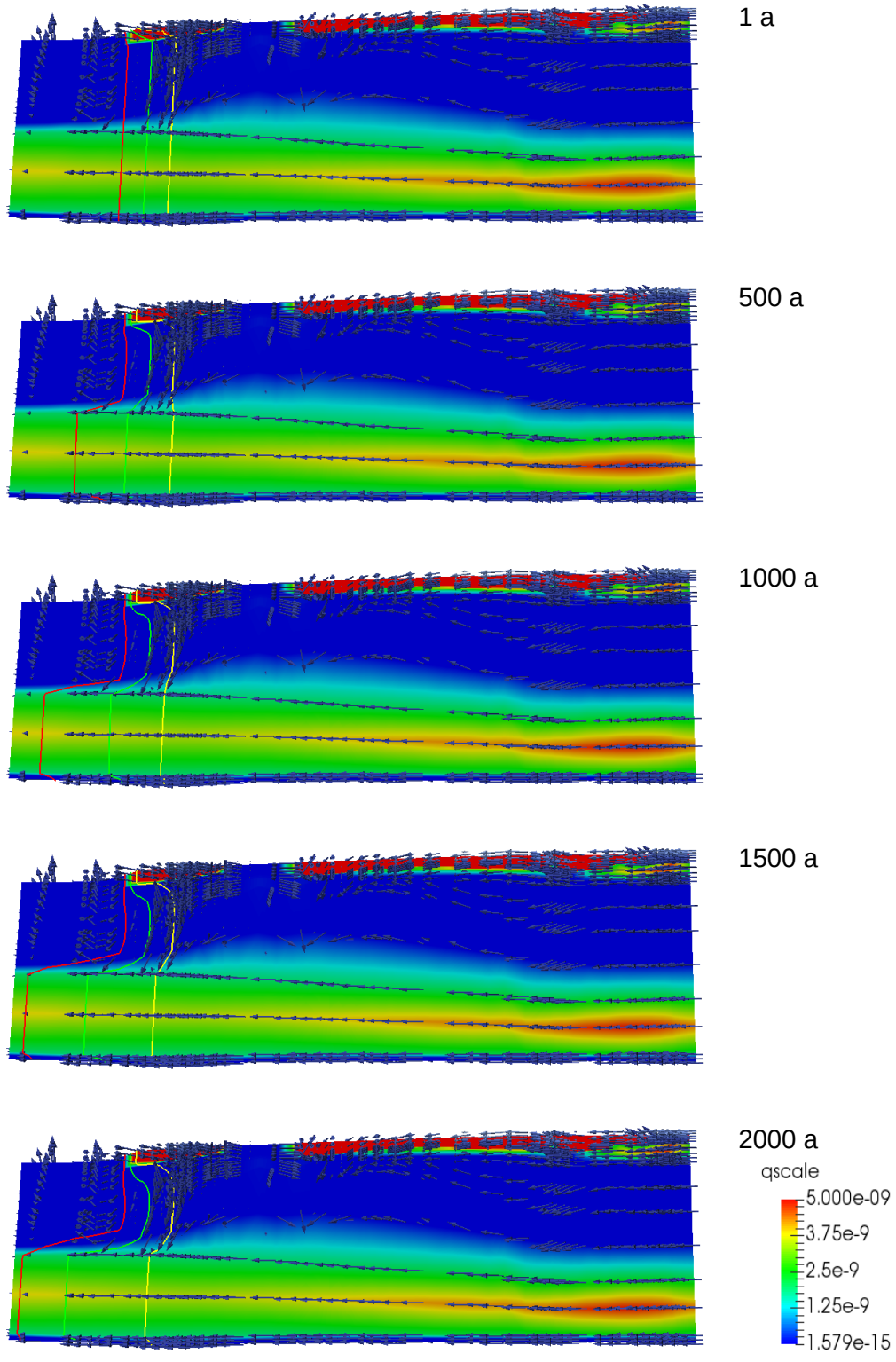

Fig. A-04: Cross-section at 1100 m to the south boundary (y = 6,633,600 m, location d in Figure 8-9) for a model time t = 1 year, 500 years, 1000 years, 1500 years and 2000 years. The colour shows the magnitude of the velocity ("qscale", [m s^{-1}]), the arrows show the flow direction. The red, green, yellow lines show the iso-lines for c_{rel} = 0.9, 0.5 and 0.1, respectively.

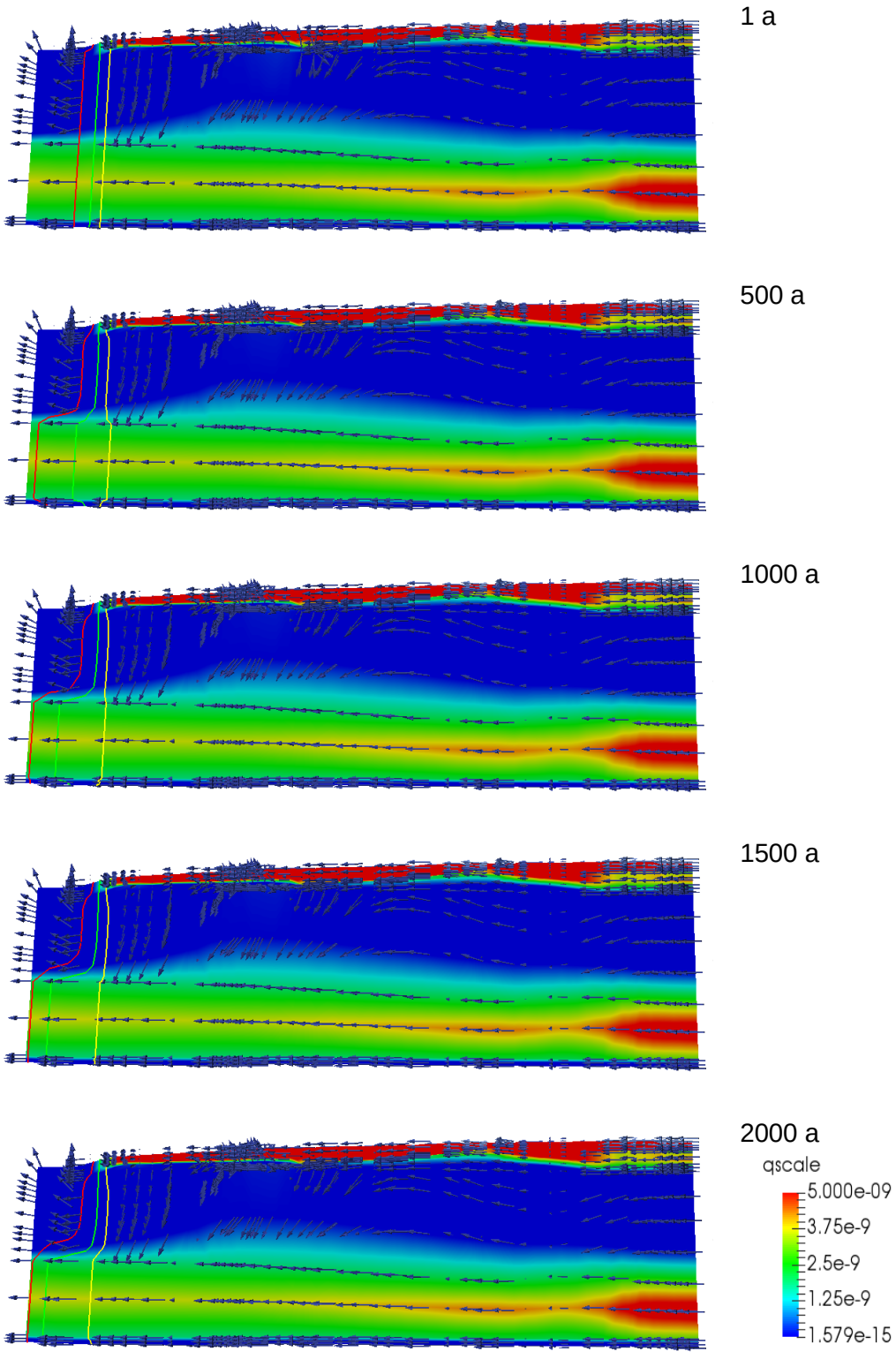

Fig. A-05: Cross-section at 400 m to the south boundary (y = 6,632,900 m, location e in Figure 8-9) for a model time t = 1 year, 500 years, 1000 years, 1500 years and 2000 years. The colour shows the magnitude of the velocity ("qscale", [m s^{-1}]), the arrows show the flow direction. The red, green, yellow lines show the iso-lines for c_{rel} = 0.9, 0.5 and 0.1, respectively.

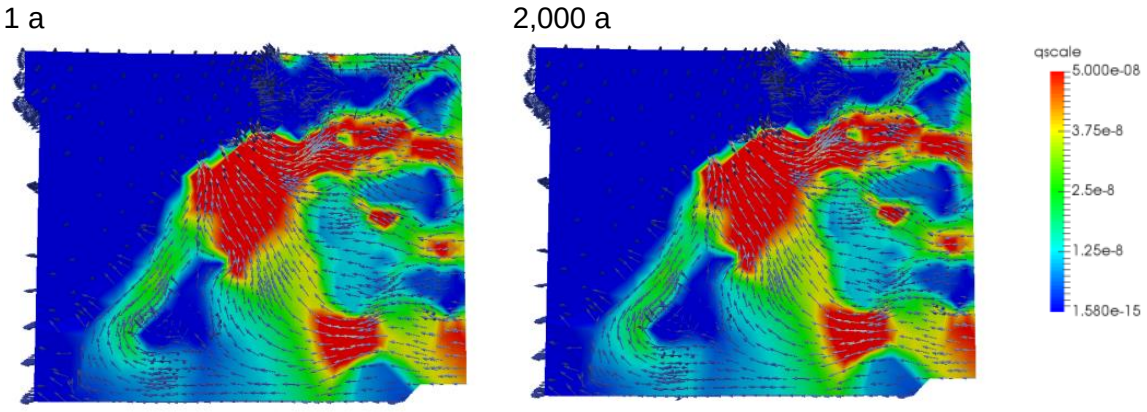

Fig. A-06: Model surface at a time = 1 year and 2000 years. The colour shows the magnitude of the velocity ("qscale", [m s^{-1}]), the arrows show the flow direction.

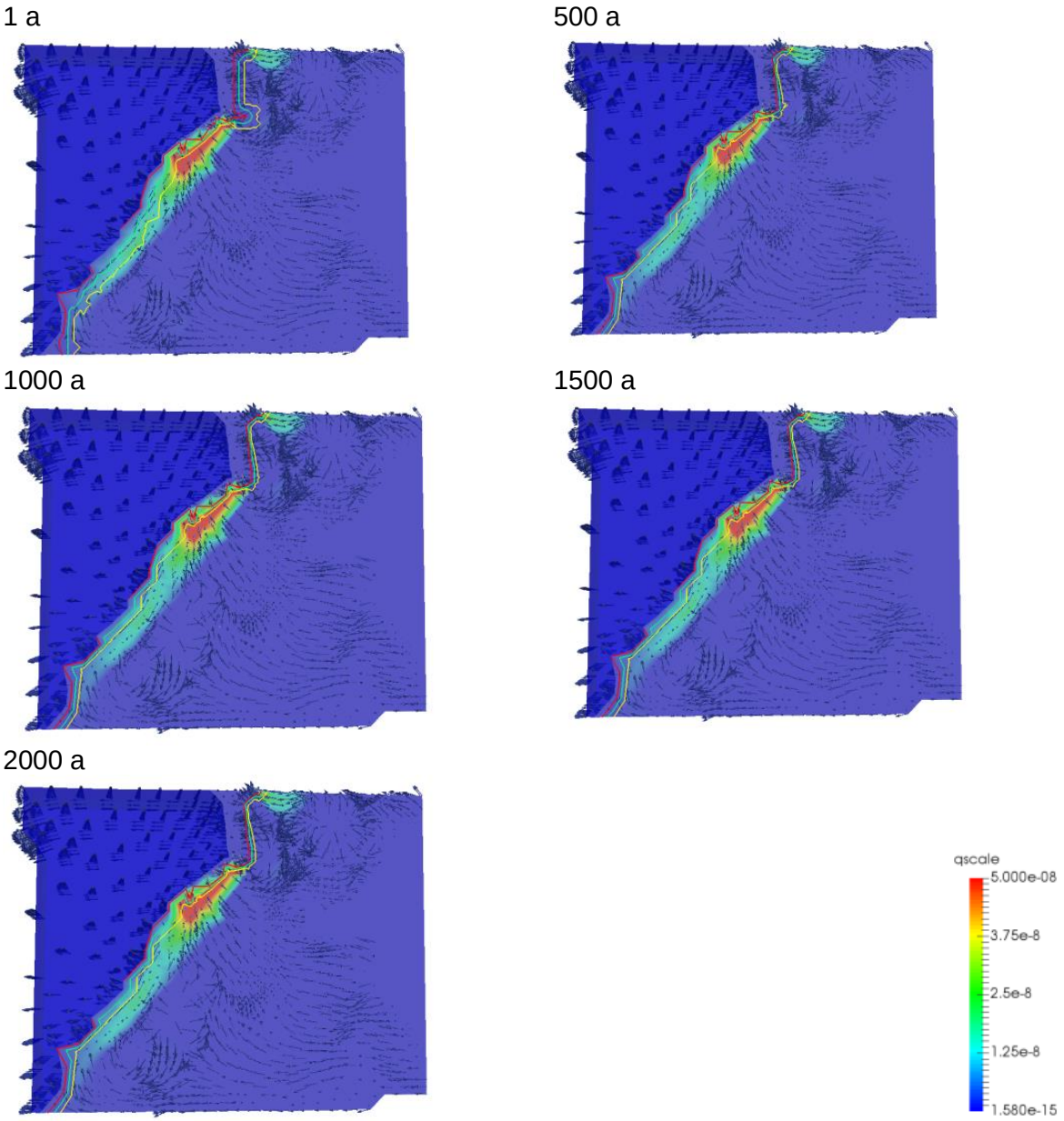

Fig. A-07: Cross-section at z = -5 m (location f in Figure 8-9) for a model time t = 1 year, 500 years, 1000 years, 1500 years and 2000 years. The colour shows the magnitude of the velocity ("qscale", [m s^{-1}]), the arrows show the flow direction. The red, green, yellow lines show the isolines for c_{rel} = 0.9, 0.5 and 0.1, respectively. The transparent white plane in the figure for z = -5 m shows the area, where the model was cut off. The blue region is lower than z = -5 m.

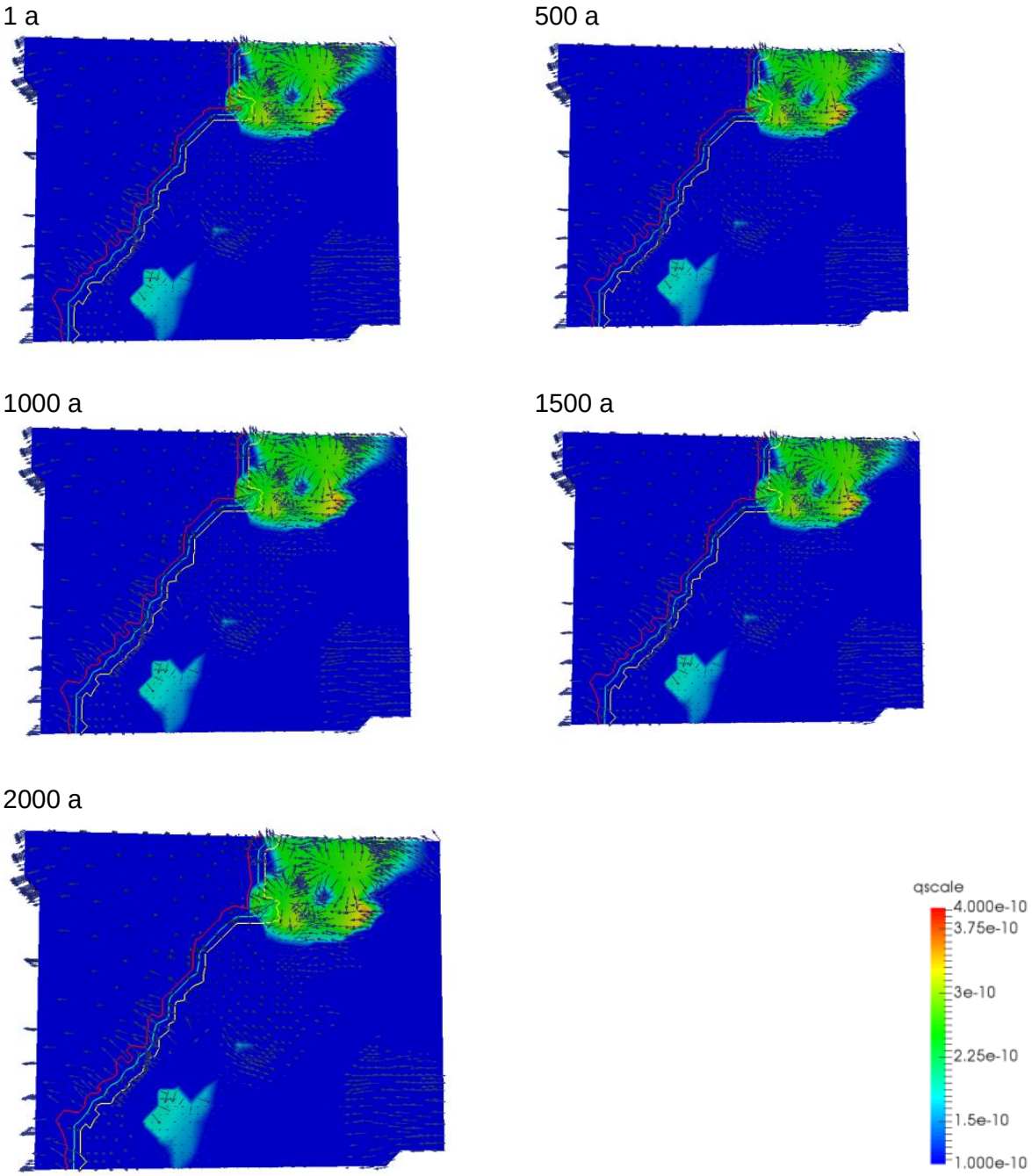

Fig. A-08: Cross-section at z = -50 m (location g in Figure 8-9) for a model time t = 1 year, 500 years, 1000 years, 1500 years and 2000 years. The colour shows the magnitude of the velocity ("qscale", [m s^{-1}]), the arrows show the flow direction. The red, green, yellow lines show the isolines for c_{rel} = 0.9, 0.5 and 0.1, respectively.

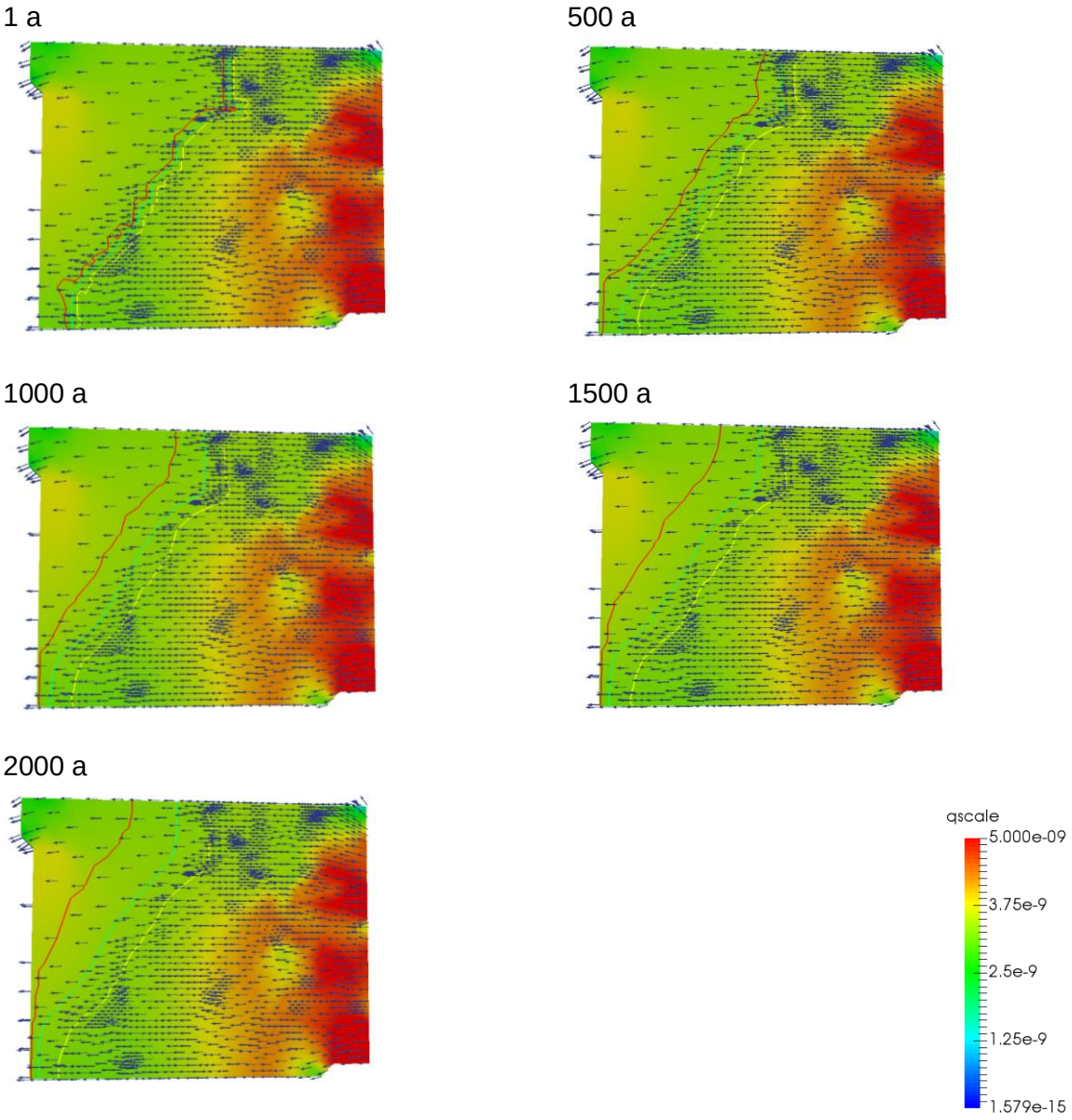

Fig. A-09: Cross-section at z = -120 m (location h in Figure 8-9) for a model time t = 1 year, 500 years, 1000 years, 1500 years and 2000 years. The colour shows the magnitude of the velocity ("qscale", [m s^{-1}]), the arrows show the flow direction. The red, green, yellow lines show the isolines for c_{rel} = 0.9, 0.5 and 0.1, respectively.

Annex B: Examples for FEP-descriptions in FEP catalogue

FEP-Name: ***Disposal Drift Seals***
FEP-type: **component** **NEA-IFEP-Group No**: 3.1.2

Short description / Definition

The disposal drift seals will be arranged close to the transition from the disposal drifts to the access drifts. Their main function is to minimize the potential migration of fluids from and to the disposal drifts. This function shall be fulfilled at least until the corresponding access drift seal completely fulfils its sealing functions. The FEP describes the mechanic, hydraulic, thermal and chemical properties of the barrier components and their construction materials as well as their behavior towards external impacts and the contact with the host rock.

General information and examples

Drift and shaft seals are basic elements of every safety concept and the resulting repository closure concept. In the course of the Preliminary Safety Analysis for the Gorleben Site (VSG), a drift sealing system was dimensioned (Herold & Müller-Hoeppe 2012, Müller-Hoeppe et al. 2012b). In Germany, detailed technical functional demonstrations have only been carried out for shaft seals or are under development (Müller-Hoeppe et al. 2012a). Furthermore, the development of suitable sealing systems will be done in the course of the R&D project ELSA (Kudla et al. 2013).

For Belgian, French and Swizz repository concepts for clay formations, detailed drift seal designs already exist. They consist of bentonite sealing elements and concrete abutments (ANDRA 2005a,b; ONDRAF-NIRAS 2001; NAGRA 2002a). There are differences with regard to the selected bentonite types (Ca-bentonite vs. Na-bentonite) and the procedure of barrier construction (highly compacted moulded bricks vs. pellets und powder). Each concept includes a reduction of the EDZ prior to the construction of the drift seal. Existing fractures will be sealed by injection material.

In all underground research laboratories in-situ tests of drift seals are projected or already done to test and optimize the constructability and the functionality of the barrier concepts. Few years ago, the large R&D project DOPAS (Full scale demonstration of plugs and seals) was started by the European Commission (http://www.igdtp.eu/index.php/european-projects/dopas). 14 European waste management agencies contribute to the project and in four European URLs in-situ tests of sealing construction will be performed in 1:1 scale.

Existing sealing concepts prefer bentonite as sealing material, because the material properties are well investigated and the favourable sealing properties are scientificly proven. So thermal parameters and expansion coefficients of bentonite and other clays are investigated by Yildizdag et al. (2008), Jobmann et al. (2013) und Jobmann et al. (2007).

Permeability as a function of swelling pressure and indirectly from saturation level has been investigated by Jobmann (2002). Conclusion on the initial saturation level of bentonite sealing elements of the Gorleben shaft seal have been given by Engelhardt & Müller-Hoeppe (2011). More material specifications have been described by Engelhardt et al. (2011) and Sitz et al. (1999). An overview on microbial activities in claystones are included in Meleshyn (2011, 2014) To ensure the correct positioning and restraint of the sealing elements, they are fixed by concrete abutments. Data on the durability of concrete and the thermo-mechanical properties are given by Thienel (2011) and Huismann (2010). Kadhim el-Tornachi (2005) give indications on surface roughness (Kudla et al. 2009).

Description of components

The backfilled disposal drifts are to be closed by drift seals to minimize the potential migration of fluids from and to the disposal drifts (Jobmann et al. 2016). This function is to be fulfilled at least until the corresponding access drift seal completely fulfils its sealing functions. The disposal drift seals are to be designed in compliance with the following requirements:

- Hydraulic requirements: The sealing elements are to effectively seal the disposal drifts against any fluids (gases and liquids), thus delaying the potential migration of fluids from and to the disposal drifts.
- Mechanical requirements: The sealing elements are to be stable under the expected pressure caused by the rock mass and by potential fluids.
- Chemical requirements: The sealing elements are to be chemically stable during their entire functional period, i.e. at least 300 years.
- Biological requirements: The sealing elements are to be sufficiently resistant to microbial degradation at least during the functional lifetime of the barrier.

The disposal drift seals will consist of two sealing elements made of asphalt and will surround an element made of bitumen. Moreover, these sealing elements will be fixed by two abutments made of high-strength, non-reinforced concrete. The bitumen elements will have a slot along the drift contour with a depth of about 1 m, which will be filled with the corresponding bitumen. The slots will interrupt the liner, will divide potential fluid pathways, will create hydraulic cut-offs and will thus allow minimizing the migration of the fluids in axial direction along the EDZ. The depth of the slots depends on the predicted EDZ and on the sealing and healing properties of the host rock. The EDZ is characterized by cracks and fractures that increase the hydraulic conductivity. However, in clay as well as in most rock formations, these cracks and fractures close over time.

After completion of the drift seal construction, the abutment will be enlarged at the access drift side and fill the whole cross-section of the access drift. This concrete construction forms a second abutment.

For further safety assessments, the potential gas production and fluid pressure development within the disposal galleries will be estimated. If the fluid pressure may lead to a failure of either the disposal drift seal or the surrounding host rock, the asphalt-bitumen module will be replaced by bentonite-sand seals. They are tight against water but permeable to gas.
The seal will have a total length of approximately 5 m. The abutments located in the disposal drifts will have a length of approximately 1 to 2 m; 1 m is planned for each asphalt element and between 0.5 and 1 m for the element made of bitumen.

If the alternative option is implemented, the length of the plugs consisting of a bentonite-sand mixture is estimated to be approximately of 3 m. These dimensions have been estimated in an initial design step, taking into account the geometry of the repository concept and the characteristics of the site. Detailed engineering calculations are to be carried out to demonstrate the integrity of the proposed disposal drift sealing elements and to thus demonstrate that the function of the seals will be fulfilled.

Site-specific consequences

The disposal drifts are important elements of the closure concept. They minimize the potential migration of fluids from and to the disposal drifts. As long as the repository system is static, all components are in equilibrium. On their own, components do not modify the system evolution. Modifications result from the impact of processes and their interaction with the properties of the components.

Chronological limits

The disposal drift seal is to fulfil its function at least until the corresponding access drift seal completely fulfils its sealing functions. As a first approach, the functional life time of the disposal drift seals has been estimated to be at least 300 years. The necessary life time will have to be verified by process analyses.

Conditional probability of occurrence

[x] probable
[ ] less probable
[ ] not to be considered

Direct dependencies

Affecting FEP (only processes can affect a component)
Seismicity
Drilling activities
Mining and other underground activities
Deliberate human intrusion
Corrosion of concrete
Solution, transformation and regeneration of clay minerals
Solution, transformation and regeneration of other minerals
Chemical alteration of organic matters
Sorption and desorption
Colloid generation and filtration
Microbial processes
Swelling and shrinking of clay minerals
Swelling and shrinking of concrete
Convergence
Heat flow
Thermal expansion and contraction
Mechanical stress change
Fluid pressure change
Bitumen migration
Deflagration and explosion
Channelling in a sealing element (*low probability of occurrence*)
Early failure of a disposal drift seal (*low probability of occurrence*)

Affected FEP (by the properties of the component)
Drilling activities
Mining and other underground activities
Deliberate human intrusion
Corrosion of concrete
Solution, transformation and regeneration of clay minerals
Solution, transformation and regeneration of other minerals
Chemical alteration of organic matters
Sorption and desorption
Colloid generation and filtration
Microbial processes
Swelling and shrinking of clay minerals
Swelling and shrinking of concrete
Convergence
Heat flow
Thermal expansion and contraction

Mechanical stress change
Fluid pressure change
Bitumen migration
Liquid flow process
Gas flow process
Dispersion
Diffusion
Deflagration and explosion
Channelling in a sealing element (*low probability of occurrence*)
Early failure of a disposal drift seal (*low probability of occurrence*)

Open Questions

- detailed design with construction material specifications
- functional lifetime

References

ANDRA (2005a). Dossier 2005: Argile Tome: Architecture and management of a geological repository. Tech. rep., Andra.

ANDRA (2005b): Référentiel des matériaux d'un stockage de déchets à haute activité et à vie longue. – Rapport Andra: n° C.RP.ASCM.04.0015.

Engelhardt, H., & Müller-Hoeppe, N. (2011). Ermittlung der anfänglichen Porenraumsättigung vom Salzbeton Typ Asse und vom Sorelbeton A1 und Ca-Bentonit Typ Salzdetfurth (Arbeitspaket 9.1.2). Technischer Bericht, DBETEC, Peine.

Herold, P. & Müller-Hoeppe, N. (2012): Konstruktiver Entwurf der Streckenverschlüsse – Grundlagen für die hydraulische Auslegung (Variante B1 und Variante A). Memo im Arbeitspaket 9.1.2, Vorläufige Sicherheitsanalyse für den Standort Gorleben, DBE TECHNOLOGY GmbH: Peine.

Herold & Jobmann (2014). Konzeptentwicklung für Schachtverschlüsse im Tongestein, Technischer Bericht, Stand 26.11.2014, DBE TECHNOLOGY, Peine.

Huismann, S. (2010). Materialverhalten von hochfestem Beton unter thermomechanischer Beanspruchung. Thesis, Technischen Universität Wien Fakultät für Bauingenieurwesen.

Jobmann, M. (2002). Hydraulische Modellierungen, F+E-Vorhaben Schachtverschluss Salzdetfurth. Technischer Bericht, DBETEC, Peine.

Jobmann, M. et al. (2016): SANTOS - Sealing concept for a LILW repository at the "Radon-Site".- FKZ 02S8234, DBE TECHNOLOGY GmbH, Peine.

Jobmann, M., Breustedt, M., Li, S., Polster, M., & Schirmer, S. (2013). Investigations on THM effects in buffer, EDZ and argillaceous host rock. Final Report - FKZ: 02E10086, DBE TECHNOLOGY GmbH, Peine.

Jobmann, M., Polster, M., & Schonebeck, M. (2007). Investigation on thermal expansion effects in clay formations. Final Report - FKZ: 02E9531, DBE TECHNOLOGY GmbH, Peine.

Kadhim El-Tornachi, M. (2003). Rauheit von Betonoberflächen, 3D-Laser-Messung und Beschreibung der Rauheit von Betonoberflächen, Reibung und Kraftübertragung zwischen Alt- und Neubeton unter nicht ruhender Belastung. Thesis, Fakultät Bauwesen der Universität Dortmund.

Kudla, W., Dahlhaus, F., Glaubach, U., Gruner, M., Haucke, J., Hofmann, M., et al. (2009). Diversitäre und redundante Dichtelemente für langzeitstabile Verschlussbauwerke. Abschlussbericht, TU BAF Institut für Bergbau und Spezialtiefbau, Freiberg.

Kudla, W., Schreiter, F., Gruner, M., Jobmann, M., Bollingerfehr, W., Müller-Hoeppe, N., et al. (2013). Schachtverschlüsse für Endlager für hochradioaktive Abfälle – ELSA Teil

1–. Abschlussbericht, TU Bergakademie Freiberg Institut für Bergbau und Spezialtiefbau & DBE TECHNOLOGY GmbH, Freiberg, Peine.

Meleshyn, A. (2011). Microbial processes relevant for the long-term performance of radioactive waste repositories in clays. Final Report, GRS-291, FKZ 02E10548, GRS, Braunschweig.

Müller-Hoeppe, N., Buhmann, D., Czaikowski, O., Engelhardt, J., Herbert, H.-J., Lerch, C., et al. (2012a). Integrität geotechnischer Barrieren - Teil 1 Vorbemessung. Technischer Bericht, GRS-287, DBE TECHNOLOGY GMbH, GRS, Peine, Braunschweig.

Müller-Hoeppe, N., Breustedt, M., Wolf, J., Czaikowski, O., Wieczorek, K. (2012b). Integrität geotechnischer Barrieren, Teil 2, Vertiefte Nachweisführung, Bericht zum Arbeitspaket 9.2 Vorläufige Sicherheitsanalyse für den Standort Gorleben, GRS-288, DBE TECHNOLOGY GMbH, GRS, Peine, Braunschweig.

NAGRA (2002): Project Opalinus Clay, Safety Report, Demonstration of disposal feasibility for spent fuel, vitrified high-level waste and long-lived intermediate-level waste (Entsorgungsnachweis). – Nagra: Technical Report 02-05; Wettingen, Switzerland.

ONDRAF/NIRAS (2001): Technical overview of the SAFIR 2 report. – NIROND 2001-05 E, December 2001.

Thienel, K.-C. (2011). Werkstoffe des Bauwesens, Dauerhaftigkeit von Beton. Tech. rep., Universität der Bundeswehr München Institut für Werkstoffe des Bauwesens Fakultät für Bauingenieur- und Vermessungswesen.

Yildizdag, K., Herklotz, M., Jobmann, M., Polster, M., Schonebeck, M., & Uhlig, L. (2008). Investigation on the THM Behavior of a Heated Bentonite Barrier by Measurements and Numerical Calculations. Final Report, DBE TECHNOLOGY GmbH, Peine.

FEP-Name: **Mechanical stress change**
FEP-type: component **NEA-IFEP-Group No:** 3.1.2

Short description / Definition

Mechanical stress changes describe an increase or decrease of stresses in a structure area of the mine with reversible deformations by mechanically-, hydraulically- or chemically-mineralogically-induced loads.

General information and examples:

Generally, every stress difference in the mine / geosphere system results in stress changes. The general stress status results from the effective stress in the geosphere, the fluid pressure in the pores and the mine openings, volume changes of construction materials, e.g. by metal corrosion or hydration of concrete, thermally-induced stresses as well as stresses resulting from the transformation and regeneration of clay minerals or other minerals (e.g. pyrite) in the geosphere. Dynamic stress changes by seismic impact are described in the FEP *Earthquake*.

Different characteristics can result in stress changes, e.g. material properties (deformations, fracture mechanics), modifications of the mine openings (drifting or backfilling of excavations) or modifications of the external or internal load impacts.

Loads may result from mechanical impacts, e.g. superimposed loads, proper weight or dynamic seismologically-induced loads. But loads can also result from each other process that is linked to the mechanical behaviour of a material. So, temperature change can produce thermally-induced stresses (cf. *FEP Thermal expansion or contraction*), saturation changes attributed to the hydraulic process class can cause fluid pressure changes (cf. FEP *Liquid flow processes* and *Gas flow processes*), and volume changes resulting from phase transitions due to chemical processes can also change the stress field (cf. FEP *Swelling and shrinking of concrete* and *Swelling and shrinking of clay minerals)*.

Naturally, in virgin rock formations, there is a primary stress field, which will be disturbed by the mining activities. From excavations, a deviatory stress field results that will be compensated by the mechanical properties of the rock at the mine opening contour. Depending on the magnitude of the stress deviator and the solidity properties of the rock, the stresses can be compensated without crack by convergence, i.e. not exceeding the dilatancy limit. Otherwise, if the stability / dilatancy limits are exceeded, the stress changes result in an excavation damaged zone (EDZ). In clay formations, the EDZ may be closed because of the swelling properties of the clay minerals and the convergence. Due to the drift lining, convergence causes supporting pressure in disturbed contour areas, so fractures can be closed. The stress changes und redistribution are completed when convergence has led to the state of stress equilibrium.

Description of the process:

The primary stress field in the host rock is close to the depth-depending lithostatic pressure (100 m). The lithostatic pressure is also decisive for the secondary stress field, which develops after completion of mine construction. Experience in clay mining has shown that after drifting of mine openings, secondary stresses will occur at the cavity contour. These will lead to stress redistribution with exceedance of the dilatancy limit and development of an EDZ (cf. FEP *Excavation damage zone*) with fractures. Furthermore, convergence-induced deformations of the cavity contour will occur.

In shafts and the ramp, the thermomechanical stresses will arise due to climate impacts. Furthermore for future site evolution, the impact of hydraulic loads (fluid pressure) on the host rock and geotechnical barriers has to be taken into account for the evaluation of the stress field.

In future site evolution, stress changes may result from modified superimposed loads (glaciers, sedimentation, erosion). An evaluation of the consequences of these impacts has to be done by model calculations.

During the future system evolution, stress changes and stress redistribution will occur in all technical and geotechnical components of the repository and the surrounding rock.

Waste packages
In radioactive waste, corrosion and alteration processes resulting in dissolution of elements or a regeneration of minerals, cause stress changes due to volume changes. Gas generation by metal corrosion or degradation of organic components may provoke fluid pressure changes in the waste containers. After failure of the waste container, a direct mechanical impact on the waste is possible, e.g. load of other waste containers or backfill, or lithostatic pressure after creeping of the rock. Corresponding to the low temperatures due to radioactive decay, thermomechanical stresses are of low relevance.

With regard to the waste containers, there were only requirements with regard to operational safety. So the containers are designed for the load of other stacked containers or for accident scenarios (container drop), but not for the lithostatic pressure. Therefore, the stresses in the containers can exceed the breaking strength after load by the rock. Furthermore corrosion products with a significantly larger volume result from the corrosion of the steel drums and cause stresses in the concrete overpacks. As long as the containers are tight, gas generation by metal corrosion can provoke an increase of fluid pressure and stresses in the waste containers.

Backfill
In order to limit the deformations of the host rock, the mine openings will be completely backfilled with excavated rock. To reduce the permeability of the backfill material, additives, like high performance concrete and self-compacting concrete, or pozzolanic admixtures, like silica fume, are to be included. Hydration heat of the backfill material will induce thermomechanical stresses. After compaction of the backfill, the material has a supporting function and will stabilize the contour or the lining of the mine opening. In mine openings without lining, the support pressure of the backfill will stabilize the EDZ and stimulate the closure of fractures.

Geotechnical barriers
The shaft, drift, ramp, and borehole seals consist of sealing components (bentonite, asphalt), which are fixed by concrete abutments. The barrier structures will be designed to comply with site-specific mechanical, hydraulic, and chemical requirements. After closure of the contact zone at the cavity contour, the lithostatic pressure and the swelling pressure of the bentonite

components will be carried by the barrier structure. The barrier design also covers the site-specific earth quake. Furthermore, the barrier will stabilize the EDZ and stimulate the closure of fractures.

Depending on the chemistry / mineralogy of the construction material, swelling and shrinking of the concrete can occur and cause stresses and fractures in the structure. Alteration processes can have similar consequences. Because of the exothermal hydration reaction of the concrete, thermomechanical stresses will arise during the early post-closure phase. For the shafts and the ramp, thermomechanical stresses may also result from climate impacts.

Technical installations

Technical installations like drift lining, abutments of technical equipment, and railways will influence the stress distribution in the backfilled mine. The lithostatic pressure may affect these installations and can result in fracturing of the concrete structures in the long-term. In addition, material-specific volume changes and alterations may affect the integrity of the concrete structures. For steel constructions, the volume increase by the corrosion products may result in stresses.

Excavation damaged zone

The EDZ results from the disturbance of the primary stress field in the host rock by the mining activities. The characteristics of the EDZ depend on the geological boundary conditions, which are not yet known. The stability of the EDZ is significantly decreased during the operational and the early post-closure phase. After creeping of the rock on the barrier constructions and drift lining / backfilled drifts, stress balancing between rock and mine starts. The EDZ may be closed because of the swelling properties of the clay and of convergence. Convergence results in supporting pressure in disturbed contour areas, so fractures can be closed. The stress changes are completed when convergence has led to a state of stress equilibrium. Then, the stability of the EDZ increases and stresses can be absorbed.

In hydraulically effective fractures of the EDZ, mineral transformations may result in volume changes, which results in stresses. If they exceed the stability of the rock, new fractures may be formed. During the early post-closure phase, the hydration heat of the concrete backfill may cause thermomechanical stresses in the EDZ.

Site specific consequences

Effective rock stresses, volume changes of construction materials due to chemical-mineralogical processes, and thermomechanical stresses due to hydrate heat of concrete or climate impacts are the most important boundary conditions for the future stress development at the site. Furthermore, seismic impacts and changing loads at the earth's surface (e.g. glaciers, sedimentation, erosion) have to considered.

The stress development in the closed repository mine depends on the geotechnical barriers and the backfill. Due to creeping of the rock (convergence), the roof gap of the barrier will be closed and the barrier will be loaded. This is decisive for the efficiency of the sealing function. Additionally, the fractures of the EDZ will be closed by the supporting pressure of the barrier.

Furthermore, stresses can induce fractures as fluid pathways in the waste matrix, in disposal containers and in barriers. This can cause corrosion of the respective component on the one hand, and influence radionuclide mobilization and transport on the other hand.

If gas generation causes high fluid pressures that exceed the tensile strength of the host rock, fractures may be induced in the host rock.

Chronological limitation

No limitation, the process has to be considered for the whole assessment period.

Conditional probability of occurrence

[x] probable
[ ] less probable
[ ] not to be considered

Direct dependencies

Affecting FEP (only components can affect a process)
Waste matrices
Disposal containers
Backfill
Disposal drift seals
Access drift seals
Shaft seals
Ramp seals
Borehole seals
Technical installations
Drift lining
Void volume
Excavation damaged zone
Metal corrosion products
Concrete corrosion products
Liquids in underground excavation
Gas in underground excavation
Surface exploration drillings
Underground exploration drillings
Host rock
Fractures and faults in host rock
Near surface decompression zone of the host rock
Liquids in the host rock

Gas in the host rock
Adjoining rock formations
Fractures and faults in adjoining rock formations
Liquids in adjoining rock formations
Gas in adjoining rock formations

Affected FEP (by intensity of the process)
Waste matrices
Disposal containers
Backfill
Disposal drift seals
Access drift seals
Shaft seals
Ramp seals
Borehole seals
Technical installations
Drift lining
Void volume
Excavation damaged zone
Metal corrosion products
Concrete corrosion products
Liquids in underground excavation
Gas in underground excavation
Surface exploration drillings
Underground exploration drillings
Host rock
Fractures and faults in host rock
Near-surface decompression zone of the host rock
Liquids in the host rock
Gas in the host rock
Adjoining rock formations
Fractures and faults in adjoining rock formations
Liquids in adjoining rock formations
Gas in adjoining rock formations

Open Questions:

- Evolution of the mechanical system at the different engineered barriers
- Evolution of the fluid pressure within the complete shaft sealing system including the influence of climate changes
- Are there any requirements to be stated for engineered barriers with regard to earthquakes?